FORMING OF ADHESIVE BONDED STEEL SHEETS

A Thesis Submitted in Partial Fulfillment of the Requirements

for the Degree of

DOCTOR OF PHILOSOPHY

by

SATHEESHKUMAR V

(Roll No. 10610311)

Department of Mechanical Engineering

Indian Institute of Technology Guwahati

Guwahati – 781039

INDIA

April 2015

Department of Mechanical Engineering
Indian Institute of Technology Guwahati
Guwahati-781039 INDIA

CERTIFICATE

It is certified that the work contained in the thesis entitled "**FORMING OF ADHESIVE BONDED STEEL SHEETS"** submitted by **Mr. SATHEESHKUMAR V** to the Indian Institute of Technology Guwahati for the award of the degree of Doctor of Philosophy has been carried out under my supervision in the Department of Mechanical Engineering, Indian Institute of Technology Guwahati. This work has not been submitted elsewhere for the award of any other degree or diploma.

(Dr. R. Ganesh Narayanan)
Associate Professor
Department of Mechanical Engineering
Indian Institute of Technology Guwahati
Guwahati-781039
INDIA

Dedicated to

My Mother Mrs.V.Saradha,

My Elder Sister Dr.Mrs.S.V.Aruna,

My Father Mr.K.Veerasamy,

My Teacher (late) Mr.V.Rajaram,

and

All My Teachers

ACKNOWLEDGEMENT

At foremost, I express my deepest gratitude to my supervisor, Dr. R. Ganesh Narayanan for his invaluable guidance, and immense support throughout my PhD work. His innovative ideas, and guidance in doing systematic and constructive research with a focused mind are remarkable. His personal approach combined with professional ethics, providing full freedom in doing research, focus in smart work, and the presence of mind will remain be a source of inspiration for the rest of my life.

I am thankful to my Doctoral Committee members, Prof. U.S. Dixit, Dr. S. Pal, and Dr. Arbind Kr. Singh, for their insightful comments and valuable suggestions during my progress of research work. I would like to express my sincere thanks to Prof. D. Chakraborty, Prof. P. Mahanta, Prof. Anoop K. Das, Department Head, Prof. P.S.Robi, and all other faculty members of the Department of Mechanical Engineering for their support.

I am extremely grateful to Prof. Abu Taleb Khan, Chemistry department, IIT Guwahati, and Mrs. Nivethitha Laskar, Divisional Officer, District Magistrate Office, Guwahati for their invaluable help during my foreign conference trip. I am thankful to DST-SERB for the financial support to attend the foreign conference.

Special thanks to Dr.S.Kanagaraj, Department of Mechanical Engineering, IIT Guwahati, for his support and providing full privilege to utilize the Advanced Materials Science laboratory facilities. I enjoyed with all lab facilities during my research works.

Special thanks to Dr.K.S.R.Krishnamurthy, Department of Mechanical Engineering, IIT Guwahati for providing facilities in Strength of Materials laboratory in a right time always.

Special thanks to Dr.S.Senthilvelan, Department of Mechanical Engineering, IIT Guwahati for providing testing facilities in the Tribology laboratory.

Special thanks to Dr.Deepak Sharma, Department of Mechanical Engineering, IIT Guwahati for his support during my research work.

Special thanks to Dr.G.Pugazhenthi, Department of Chemical Engineering, and Dr.Prabhu Venkataraman, Department of Humanities and Social Studies, IIT Guwahati for their invaluable moral support.

I thank IIT Guwahati and department of Mechanical Engineering administration for providing all facilities. I thank very much the technical staffs Dr. D.K. Sharma, Mr. N.K. Das, Mr. J. Basumatary, Mr. Sanjib Sarma, Mr. Rituraj Sakia, Mr. C. Banikya, Mr. S. Ahmed, Mr. Nip Bora, Mr. D. Chetri, Mr. M.K. Bhaishya, Mr. Gohain, Mr. Medhi, Mr. Mrinal Sarma, Mr. Khaklary, and all office bearers for their help and support through my research works.

I am very much thankful to Dr.C.Shyam Anand, and Dr.Mrs. Padam Priyal for their constant support in all the ways.

I thank very much Dr.A.Satheesh, Dr.C.Subramanian, Dr.R.Anantharaj, Dr.T.Kannan, Dr.P.Janaki Ramulu, and Dr.S.P.Sakthivel for their constant support and help in all the ways. I thank Dr. Biswajit Nayak, and Mr.Chandrahas Patel for their invaluable support.

The company of my beloved friends and their support at IIT Guwahati made my four years of stay enjoyable. Especially, Dr.S.Anbarasu, Dr.S.Murugavel, Dr.M.Eswaran, Dr.P.Saravanan, Mr.A.Paventhan, Mr.Manish Kumar, Dr.Gowri Shankar, Mr.Ravi Kant, Mr.Jagadish, Mr.N.Prabhakaran, Mr.Rathakrishnan, Mr.V.Thamarai Selvan, Mr.Muthu Sivarama Pandiyan, Mr.Rajesh, Mr,Vijay, Mr.Sathyaraj, Mr.Narendran, Mr.Gopi Chandran, Mr.N.Vijayan, Mr.D.Thyagarajan, Mr.M.S.Aravinda Kumar, Dr.C.Shravan Kumar, Mr.N.Sivaramakrishnan, Mr. Sengoden, Mr.Balaji, Mr.G.Murugavel, Mr.Muthuraj, Mr.Baskar, Mr.A.Johnney Mertens, Mr.Avanish Verma, Mr.R.Vignesh Babu, Mr.Vignesh, Mr.M.Charan, Mr.Balasubramanian, Mr.Kodeesawaran, Dr.Ratnakar Das, Mr.Dhamodharan, Mr.Varma, Mr.Vivek Selvan, Mr. G.N.Shelke, Mr.Vinod Yadav, Mr.Ravichandra Rao & family, Mr.Aravind Agrawal, Mr.Tinu, Mr.Pritham, Mr.Biswajit Parida, Mr.N.Yadhaiah, Mr.S.Sajit, Mr.Rupesh Singh, Mr.Anil Kumar Deepati, Mr.Arpan Kr. Mandal, Mr.P.Ramesh Babu, Dr.Ravikumar Peetala, Mr.Deepak Yadhuwanshi, Mr. Bipul Das, Mr.Prakash Kr. Sahu, Mr.Jagannath Sardar, Mr.Amitava Gatak, Mr.Purnendu Mandal, Mr.Panjol Paul, Mr.R.Kalidasan, Mr.P.V.S.S. Sridhar, Mr. Sathisha, Mr.Sumit Agrawal, Mr.Rasmi Ranjan, Mr.Anil Das, Mr.Sanjib Das, and Mr.Gobhindo Biswas. Each of them deserves special thanks.

I am very much grateful to my beloved friends Mr.R.Someswaran, Dr.R.Sidhick Basha, Mr.A.Muthuraja, Dr.S.Chockalingam, and I am happy to thank Mr.R.Vinoth Kumar, IIT Guwahati for their invaluable support and joyful life.

I am very much thankful to my beloved friends Mr.V.Ananda Kumar, and Mr.S.Arun Kumar for their invaluable support during my studies.

I am very much grateful to the important persons in my life Dr.C.J.Thomas Renald, Mr.K.Karthikeyan, Mr.M.Thiagarajan, department of Mechanical Engineering, Sri Ramakrishna Engineering College, Coimbatore for their invaluable support. I am thankful to Mr.G.K.Sathiya Manoj, and Mr.S.Balasanthosh, Sri Ramakrishna Engineering College, Coimbatore for their kind support and help.

I am thankful to Dr.S.P.Jesumathy, NIT Trichy, Dr.Mrs.N.Shanmuga Priya, and Ms.N.Sharmila, IIT Guwahati for their constant support.

I am very much happy to thank my beloved friend Mr.S.Arun, IIT Guwahati for the enjoyable company, and immense support in my all critical situations.

Special thanks to my brother-in-law Mr.D.R.Rajan for his constant support in all the ways. I am very much thankful to my uncles Mr.R.Sekar, Mr.R.Kumar, Mr.A.Balakrishnan, Mr.A.Elumalai, and all my relations for their constant support and encouragement throughout my endeavour.

Last but not least, I am very much happy to thank my younger brother Mr.V.Jagadeesh who supported me a lot, made me to stay at IIT Guwahati comfortably, and took care our family in place of me also.

Satheeshkumar V

Abstract

Adhesive bonding technology proves its efficiency and effectiveness in the joining process of dissimilar materials including metals and non-metals. The adhesive bonded blanks categorized under tailor made blanks (TMBs) are widely used in the construction of aircraft and automobile body structures mostly as formed parts. The adhesive bonding technology is also used in almost all manufacturing sectors with the main advantages of eliminating stress concentrations caused by the mechanical fastening methods, and high temperature involved welding methods. It also exhibits the advantages over the requirements such as different mechanical properties, material properties, surface attributes, weight reduction, and design flexibility. The mechanical properties of adhesive bonded blanks are mainly influenced by the quality of adhesive and its properties. Since adhesive imparts adhesion force between adherends, most of the modelling of adhesive bonded blanks and their mechanical performance prediction studies focused on intact locking at the interface between adhesive layer and adherends or direct modelling of interface bonding between adherends rather than considering appropriate properties of adhesives. But the adhesion force and the performance characteristics are dependent on the adhesive properties. Since most of the parts in the manufacturing sectors are formed parts and the adhesive bonding technique is more advantageous, it is mandatory to study the forming behaviour of adhesive bonded sheets at varying adhesive properties.

The main objectives of the present thesis is to investigate the role of adhesive properties on the forming behaviour of adhesive bonded sheets, and predicting the adhesive bonded sheet forming behaviour with the aim of representing adhesive. In the experimental investigations, the adhesive properties in the bonded sheets are changed by varying hardener/resin ratios at different levels, by generating artificial defects in the adhesive, by filling carbon black nano sized powder at varying wt.% and by reinforcing high ductile wires in the adhesive at different levels. The forming behaviour of adhesive bonded sheets is evaluated through tensile test, in-plane plane-strain (IPPS) formability test, and deep drawing. The results like failure pattern, stress-strain behaviour, % elongation at failure, and limit strains of base materials constituting adhesive bonded sheets are monitored during tensile and IPPS formability tests. The deformation pattern, load-stroke behaviour, cup height, and wrinkling of cups are monitored during deep process of

adhesive bonded sheets. The results show that the formability of adhesive bonded sheets, forming limit strains of base materials constituting adhesive bonded sheets, and deep drawability of adhesive bonded blanks increase with increase in hardener/resin ratio of adhesives, due to improved ductility of adhesive layer with hardener rich formulation improves the plasticity of adhesive bonded sheets and base material constituents. In the case of presence of artificial defects in the adhesive layer at different aspect ratios and shapes, the formability of adhesive bonded sheets and the forming limits of base material constituents decrease with increase volume of defects as compared to the without defect case of adhesive bonded sheets. This is due to the early failure of adhesive layer by which the strain is concentrated critically at the defects location reduces the ductility of adhesive.

In the case of carbon black nano powder filled adhesive bonded sheets at different wt.%, the formability of adhesive bonded sheets and forming limits of base material constituents, and deep drawability of adhesive bonded sheets improve up to a certain level (2 wt.% in the present work), and then decrease with excessive addition of carbon black. This is due to filling of carbon black up to a certain level increase the ductility of adhesive, and thereby improves the formability of adhesive bonded sheets.

In the case of high ductile wire reinforcement in the epoxy adhesive which is low ductile comparatively, the ductility of adhesive bonded sheets, forming limits, and deep drawability improves up to a certain number of reinforcement, and then decreases with excessive reinforcement of adhesive. During finite element simulation, wires are not modelled individually; instead many wires were equivalently modeled as continuous sheet with a finite width having mechanical properties of *Cu* wire in order to understand the forming behaviour of adhesive bonded sheets when low ductile adhesive is reinforced with high ductile material. It is conceptualized during prediction that the high ductile material reinforcement in low ductile adhesive improves the formability of adhesive bonded sheets.

The forming behaviour of adhesive bonded sheets is predicted by finite simulation using PAM STAMP 2G®, an elasto-plastic explicit dynamic finite element code. The forming behaviour of adhesive bonded sheets is predicted with the influence of adhesive properties at varying hardener/resin ratio, and carbon black weight during tensile test, IPPS formability test, and deep drawing process. The stress-strain behaviour, forming limit strains of base material constituents, and deep drawability of adhesive bonded sheets are predicted by incorporating

mechanical properties of base materials and adhesive without modelling interface bonding between base materials and adhesive layer, and validated with experimental results. During forming limit strain prediction, two different necking criteria namely effective strain rate based necking criterion (ESRC), and thickness gradient based necking criterion (TGNC) are used. The results show that there is a good agreement in the overall stress-strain behaviour of adhesive bonded sheets with experimental results. The forming limits results show a moderate agreement with the experimental results predicted by using both necking criteria. The deep drawability results also show a moderate agreement with the experimental results. This is due to absence of interface bonding between the base materials and the adhesive layer during simulations. But there is a good agreement in the deformation patterns, and wrinkling pattern between finite element simulation and experimental results.

Further, the true stress-strain behaviour of adhesive is evaluated by rule of mixture concept from adhesive bonded sheets at varying hardener/resin ratio, and different carbon black wt.%. It is believed that the true stress-strain behaviour evaluated by rule of mixtures is the constitutive behaviour of adhesive and interface bonding. The forming behaviour of adhesive bonded sheets is predicted by incorporating adhesive properties evaluated by direct tensile testing of adhesive, and by rule of mixtures during finite element simulation. The tensile test, IPPS formability test, and deep drawing tests are simulated. The results show that there is not much difference in forming limit strains of base materials constituting adhesive bonded blanks by both the ways of incorporation of adhesive properties during prediction. There is also not much variation in the load-stroke behaviour and cup height results of adhesive bonded sheets.

In addition, the maximum drawing load during deep drawing of adhesive bonded sheets at varying hardener/resin ratio, and with different carbon black wt.% is estimated by three simple equations that are available in the literature. Generally, these equations are used to estimate maximum drawing load of unbonded sheets. The estimated drawing loads during deep drawing of adhesive bonded sheets are validated with experimental results, and it is found to be in good agreement. An attempt is made to predict the load-stroke behaviour of adhesive bonded sheets in the deep drawing process by proposing a set of equations which are simply as function of maximum drawing load and punch-stroke to overcome the difficulties in the incorporation of adhesion properties of adhesive. The maximum drawing load evaluated from experiment, finite element simulation, and estimation are utilized during prediction of load-stroke behaviour by

proposed equations. There is a good agreement in load-stroke behaviour predicted and experimental results except few cases.

Based on the basic understanding from the forming behaviour of adhesive bonded sheets at varying adhesive properties, and difficulties in the incorporation of adhesion properties during prediction, the equivalent forming behaviour of adhesive bonded sheets is predicted by using geometrical heterogeneities in the base materials without using any adhesive properties, and thus adhesive is represented. The thickness heterogeneity factor of geometrical heterogeneities designed in the base materials are varied, and the equivalent forming limit strains in the tensile test and cup height results in the deep drawing process are predicted with the effect of varying adhesive properties. The predicted results validated with experimental results are found to be in good agreement.

Further, the forming behaviour of adhesive bonded blanks is predicted by neural network with the influence of adhesive properties. The results such as forming limit strains of base materials constituting adhesive bonded blanks in the tensile test, and the final cup height of adhesive bonded blanks during cup deep drawing are predicted neural network, compared with the numerically predicted results, and validated with the experimental results. The predicted results are found to be in good agreement with the experimental results and numerical predictions during validation.

Finally, an expert system involving neural network, numerical simulation, and material modeling is proposed to predict the formability of adhesive bonded sheets at the design stage. This will help us to choose appropriate adhesives, reinforcements, and additives for acceptable formability.

ABBREVIATIONS

ABB	Adhesive bonded blanks
IPPS	In-plane plane-strain
H/R	Hardener/resin ratio
CB	Carbon black
Wt.%	Weight %
BHF	Blank holding force
FLC	Forming limit curve
FLD	Forming limit diagram
FE	Finite element
ESRC	Effective strain rate base necking criterion
TGNC	Thickness gradient based necked criterion
TMB	Tailor made blank
TWB	Tailor welded blank
Eq.	Equation

Nomenclature

σ	True stress in MPa
ε	True strain
K	Material strength coefficient in MPa
n	Strain hardening exponent
r	Plastic strain ratio
r_0, r_{45}, r_{90}	Plastic strain ratio in 0º, 45º, and 90º to the rolling direction of the sheets
t_A and t_B	thickness in the groove region and thickness in the bulk region of the sheet metal
f	Thickness heterogeneity factor
μ	Coefficient of friction
R	Normal anisotropy

CONTENTS

ABSTRACT.....vii

ABBREVIATIONS.....xi

NOMENCLATURE.....xii

CONTENTS.....xiii

List of Figures.....xxi

List of Tables.....xxviii

Chapter 1: Introduction, Literature review, Significance and Objective of work

1.1 Introduction.....1

1.2 Literature review.....3

1.2.1 Introduction to adhesive bonding technology.....3

1.2.2 Adhesion theories.....3

1.2.3 Advantages of adhesive bonds.....5

1.2.4 Disadvantages.....5

1.2.5 Applications.....6

1.2.6 Influencing parameters of adhesives on mechanical properties.....6

1.2.7 Influencing parameters of bonded blanks on mechanical properties.....8

1.2.8 Modeling and simulation of adhesive bonded sheets.....13

1.2.9 Formability Analysis.....14

1.2.9.1 Introduction to formability of sheet metals.....14

1.2.9.2 Prediction of formability of sheet metals by neural networks.....20

1.2.9.3 Forming behavior of adhesive bonded sheets.....22

1.2.9.4 Formability prediction of adhesive bonded sheets.....24

1.3 Significance of work.....26

1.4 Objectives of thesis.....27

1.5 Organization of Thesis.....27

Chapter 2:Investigation on the influence of adhesive properties on the formability of adhesive bonded steel sheets

2.1 Methodology 29
2.1.1 Experimental materials and mechanical properties 29
2.2 Evaluation of tensile properties of the adhesive systems 33
2.3 Testing of adhesive bonded steel sheets 35
2.4 Results and discussion 36
2.4.1 Influence of hardener/resin ratio on the tensile properties of adhesive systems 36
2.4.2 Failure pattern of adhesive bonded steel sheets 38
2.4.3 Effect of adhesive properties on the tensile behaviour of adhesive bonded blanks
2.4.3.1 Comparison between double sheet and adhesive bonded blanks 40
2.4.3.2 Comparison between single sheet and adhesive bonded blanks 42
2.4.3.3 Comparison between adhesive bonded sheets having different hardener/resin ratios 43
2.4.3.4 Comparison of engineering stress – strain behaviour of adhesive bonded blanks and single sheets 44
2.4.3.5 Strain hardening exponent (n) of adhesive bonded blanks 48
2.4.4 Effect of adhesive properties on the limit strain of adhesive bonded steel sheets 50
2.4.5 Uncertainty in limit strain measurement 53
2.4.6 Influence of interfacial bonding between adhesive layer and base materials on the formability of adhesive bonded steel sheets 54
2.4.7 Suggestions for the selection of adhesive bonded sheets 55
2.5 Influence of adhesive properties on in-plane plane-strain formability of adhesive bonded steel sheets 56
2.5.1 Optimizing the sample geometry for plane-strain condition 56
2.5.2 Testing of adhesive bonded steel sheets using IPPS formability sample 58
2.6 Results and discussion 60
2.6.1 Comparison of stress-strain behaviour between double sheet and adhesive bonded blanks 60
2.6.2 Comparison of stress – strain behaviour of adhesive bonded blanks and single sheet 62
2.6.3 Comparison of stress – strain behaviour of adhesive bonded blanks with different hardener/resin ratios 63

2.6.4 Comparison of strain hardening exponent (n) between single sheets, double sheets and adhesive bonded blanks....66

2.6.5 Effect of adhesive properties on limit strain of adhesive bonded blanks in plane-strain condition....68

2.6.6 Uncertainty in limit strain measurement....70

2.7 Conclusions....71

Chapter 3:Formability of adhesive bonded steel sheets with artificial adhesive defects

3.1 Experimental Methodology....73

3.2 Testing of adhesive bonded blanks and formability evaluation....73

3.3 Results and discussion....77

3.3.1 Failure pattern of adhesive bonded blanks with finite defects in the adhesive....77

3.3.2 Effect of aspect ratio and shape of adhesive finite defect on the tensile behaviour and IPPS formability of adhesive bonded blanks....80

3.3.2.1 Load – extension behaviour of adhesive bonded blanks....80

3.3.3 Limit strain of adhesive bonded blanks....81

3.3.4 Comparison of strain hardening exponent (*n*) between adhesive bonded blanks with adhesive finite defects and without defect....83

3.3.5 Comparison of strain gradient between adhesive bonded blanks with and without adhesive finite defects....84

3.3.6 Effect of number of adhesive finite defects on the tensile behaviour of adhesive bonded blanks....85

3.3.6.1 Influence on the load-extension behaviour....85

3.3.7 Influence on the limit strain of adhesive bonded blanks with increase in number of adhesive finite defects....87

3.3.8 Comparison of strain hardening exponent (*n*) with increase in number of adhesive finite defects in adhesive bonded sheets....89

3.3.9 Influence of volume of adhesive finite defect on the forming behaviour of adhesive bonded blanks....89

3.3.10 Effect of location of adhesive finite defects on the tensile behaviour of adhesive bonded blanks....91

3.3.10.1 Influence on the load-extension behaviour....91

3.3.11 Influence on the limit strain of adhesive bonded blanks....93

3.3.12 Comparison of strain hardening exponent (*n*) with different locations of adhesive finite defects in adhesive bonded blanks....94

3.3.13 Failure pattern of adhesive bonded blanks with and without infinite adhesive defects 95

3.3.14 Effect of orientation of infinite defect in the adhesive layer on the tensile behaviour of adhesive bonded blanks 97

3.3.14.1 Comparison of tensile behaviour between adhesive bonded blanks with and without defects 97

3.3.15 Influence of orientations of infinite defect in the adhesive layer on the limit strain of adhesive bonded steel sheets 100

3.3.16 Comparison of strain hardening exponent (n) between with and without infinite defects in adhesive bonded blanks 101

3.4 Conclusions 103

Chapter 4:Prediction of formability of adhesive bonded steel sheets with the influence of hardener/resin ratio of adhesive and experimental validation

4.1 Methodology 107

4.2 Experimental evaluation of forming of adhesive bonded blanks 107

4.3 Predicting the forming behaviour of adhesive bonded blanks with different hardener/resin ratios 107

4.3.1 Prediction of stress-strain behaviour of adhesive bonded sheets 110

4.3.2 Prediction of limit strains of adhesive bonded sheets: Necking criteria 112

4.3.2.1 Effective strain rate based criterion (ESRC) 112

4.3.2.2 Thickness gradient based necking criterion (TGNC) 113

4.4 Results and discussion 113

4.4.1 Failure of adhesive bonded blanks at different hardener/resin ratios: Experiment and prediction 113

4.4.2 Experimental evaluation and prediction of tensile behaviour of adhesive bonded sheets 116

4.4.3 Forming limit strain prediction of adhesive bonded blanks with effect of hardener/resin ratio 121

4.5 Conclusions 125

Chapter 5:Evaluation of adhesive mechanical properties by rule of mixtures and its application in necking prediction

5.1 Methodology 127

5.2 Approach 1: Experimental evaluation of adhesive properties 127

5.3 Approach 2: Rule of Mixtures 127

5.4 Prediction of limit strains of adhesive bonded sheets 129

5.5 Results and discussion 129

5.5.1 Comparison of limit strains of base materials constituting adhesive bonded sheets through approach-1 and approach-2 129

5.6 Conclusions 132

Chapter 6:Experimental evaluation and prediction of formability of carbon black filled adhesive bonded steel sheets

6.1 Methodology 135

6.2 Testing of carbon black filled epoxy adhesive 136

6.3 Forming of carbon black filled adhesive bonded blanks: Experiment 136

6.4 Forming behaviour of carbon black filled adhesive bonded blanks: Prediction 137

6.5 Results and discussion 137

6.5.1 Tensile behaviour of epoxy adhesive filled with different wt.% of carbon black 137

6.5.2 Failure of adhesive bonded sheets at different CB wt.%: Experiment and prediction 138

6.5.3 Experimental evaluation and prediction of tensile behaviour of adhesive bonded sheets 140

6.5.4 Forming limit strain of adhesive bonded blanks with effect of wt.% of CB –Prediction 143

6.6 Conclusions 147

Chapter 7:Improving the formability of adhesive bonded sheets through wire reinforcement

7.1 Methodology 149

7.2 Experimental evaluation of formability of wire reinforced adhesive bonded sheets 150

7.3 Prediction of forming behaviour of wire reinforced adhesive bonded sheets 153

7.4 Results and discussion 155
7.4.1 Failure pattern of wire reinforced adhesive bonded sheets 155
7.4.2 Influence of longitudinal wire reinforcement on the stress-strain behaviour of adhesive bonded sheets 157
7.4.3 Effect of longitudinal wire reinforcement on the limit strains of adhesive bonded sheets 161
7.5 Numerical evaluation of forming behaviour of high ductile wire reinforced in the epoxy adhesive bonded sheets 165
7.6 Effect of transverse wire reinforcement on the forming limit strain of adhesive bonded sheets 166
7.7 Influence of wire reinforcement on deep drawability of adhesive bonded sheets 167
7.7.1 Deformation pattern 168
7.7.2 Wrinkling behaviour during deep drawing of wire reinforced adhesive bonded sheets 171
7.8 Conclusions 172

Chapter 8:Experimental evaluation and prediction of deep drawability of adhesive bonded blanks

8.1 Methodology 175
8.2 Experimental evaluation of adhesive mechanical properties 175
8.3 Evaluation of deep drawability of adhesive bonded blanks – Experiment 175
8.4 Numerical prediction of deep drawability of adhesive bonded blanks 176
8.5 Estimation of maximum drawing load in cup drawing using simple analytical models 177
8.6 Prediction of drawing load (P_d) – punch stroke (x) behaviour during deep drawing .. 182
8.7 Results and discussion 183
8.7.1 Tensile behaviour of epoxy adhesive 183
8.7.2 Deformation pattern of adhesive layer constituting adhesive bonded blanks 184
8.7.2.1 Delamination and thinning 184
8.7.2.2 Wrinkling behaviour of adhesive bonded blanks 187
8.7.2.3 Deep drawability prediction of un-bonded and adhesive bonded blanks 189
8.7.3 Comparison of estimated maximum drawing load from analytical equations ... 193

8.7.4 Prediction of load – progression behaviour through maximum load estimation 195
8.8 Conclusions 197

Chapter 9:Estimation of formability and deep drawability of adhesive bonded sheets using equivalent geometrical heterogeneities

9.1 Methodology 199
9.2 Prediction of forming behaviour of adhesive bonded blanks using geometrical heterogeneities 199
9.2.1 Prediction of forming behaviour of adhesive bonded blanks during tensile test 200
9.2.2 Deep drawability prediction of adhesive bonded blanks 201
9.3 Results and discussion 204
9.3.1 Prediction of limit strains of base materials constituting the adhesive bonded sheets 204
9.4 Conclusions 216

Chapter 10:Prediction of formability of adhesive bonded sheets by neural network and its validation

10.1 Methodology 219
10.2 Tensile test and forming limit strain evaluation 219
10.3 Deep drawability and cup height evaluation 219
10.4 Artificial Neural Network (ANN) modelling 220
10.4.1 Learning rule 221
10.4.2 Activation function 222
10.4.3 Data selection 222
10.4.4 Back propagation algorithm 223
10.4.5 Network performance 223
10.5 Neural network model 225
10.6 Prediction of formability of adhesive bonded sheets using geometrical heterogeneities 228
10.6.1 Prediction of forming behaviour during tensile test and deep drawing process 228
10.7 Results and discussion 228
10.7.1 Prediction of forming behaviour of adhesive bonded blanks by ANN 229

10.7.1.1 Prediction of limit strains of base materials constituting adhesive bonded blanks in tensile test 229

10.7.1.2 Prediction of deep drawability of adhesive bonded blanks 234

10.7.2 Validation of tensile test results with numerical prediction and experimental data 236

10.7.3 Validation of deep drawability with numerical prediction and experimental data 238

10.8 Proposed expert system.....238

10.9 Conclusions.....241

Chapter 11:Conclusions and scope of future work

11.1 Conclusions.....243

11.2 Scope of future work.....247

References.....249

List of Publications.....259

List of Figures

Fig. 1.1 Schematic of plane-strain specimen geometry……19
Fig. 2.1 Schematic of testing specimens…. 31
Fig. 2.2 Load-extension behaviour of (a) DDQ steel sheets, and (b) SS 316L sheets, (c) Epoxy bonded sheets with H/R 0.6:1 and (d) Epoxy bonded sheets with H/R 1:1 32
Fig. 2.3 (a) Evaluation of tensile properties from engineering stress-strain curve, and (b) Evaluating *n, K* values from true stress-true strain data..... 32
Fig. 2.4 Load-extension behaviour for different hardener/resin ratios: (a) epoxy adhesive, and (b) acrylic adhesive 37
Fig. 2.5 Failure pattern of adhesive bonded blanks 40
Fig. 2.6 Comparison of load – extension behaviour of single sheets of DDQ steel and SS 316L, double sheet without adhesive, (a) epoxy bonded blanks with different H/R ratios, and (b) acrylic bonded blanks with different H/R ratios 41
Fig. 2.7 Comparison of engineering stress – strain behaviour of single sheet made of DDQ steel and SS 316L, double sheet without adhesive, (a) epoxy adhesive bonded blanks with different H/R ratios, and (b) acrylic adhesive bonded blanks with different H/R ratios..... 45
Fig. 2.8 Comparison of engineering stress – strain behaviour (a) epoxy adhesive bonded blanks with different H/R ratio, (b) acrylic adhesive bonded blanks with different H/R ratio 47
Fig. 2.9 Comparison of limit strain in DDQ steel specimen from double sheet without adhesive, single DDQ steel sheet, (a) DDQ steel specimen from epoxy adhesive bonded blanks for different H/R ratios, (b) DDQ steel specimen from acrylic adhesive bonded blanks for different H/R ratios……51
Fig. 2.10 Comparison of limit strain in SS 316L specimen from double sheet without adhesive, single SS 316L sheet, (a) SS 316L specimen from epoxy adhesive bonded blanks for different H/R ratios, and (b) SS 316L specimen from acrylic adhesive bonded blanks for different H/R ratios 51
Fig. 2.11 Comparison of maximum strain 52
Fig. 2.12 Comparison of limit strain from DDQ steel and SS 316L sheets in which three layer unbonded and bonded by epoxy adhesive with, a) H/R ratio of 0.6:1, and b) H/R ratio of 1:1 54
Fig. 2.13 A typical geometry of in-plane plane-strain specimen..... 56
Fig. 2.14 Different strain paths and optimized plane-strain path 57
Fig. 2.15 Optimized IPPS test geometry. 58
Fig. 2.16 Failure pattern of in-plane plane-strain forming specimens as single sheet: (a) DDQ steel, and (b) SS 316L 58
Fig. 2.17 Geometry of in-plane plane-strain formability testing specimen (a) adhesive bonded sheets, and (b) double sheet 59

Fig. 2.18 Comparison of engineering stress – strain behaviour of single sheet made of DDQ steel and SS 316L, double sheet without adhesive and (a) epoxy adhesive bonded blanks with different H/R ratios, and (b) acrylic adhesive bonded blanks with different H/R ratios 61
Fig. 2.19 Comparison of engineering stress-strain behaviour (a) epoxy adhesive bonded blanks with different H/R ratios, and (b) acrylic adhesive bonded blanks with different H/R ratios 64
Fig. 2.20 Comparison of total elongation of different regions of epoxy bonded sheets from IPPS formability test and tensile test with different H/R ratios 65
Fig. 2.21 Comparison of total elongation of different regions of acrylic bonded sheets from IPPS formability test and tensile test with different H/R ratios. 65
Fig. 2.22 Method of grid measurement (a) before deformation, and (b) after deformation 68
Fig. 2.23 Comparison of limit strain in DDQ steel specimen from double sheet, single DDQ sheet, (a) DDQ steel specimen from epoxy adhesive bonded blanks for different H/R ratios, (b) DDQ steel specimen from acrylic adhesive bonded blanks for different H/R ratios 69
Fig. 2.24 Comparison of limit strain in SS 316L specimen from double sheet, single SS 316L sheet, (a) SS 316L specimen from epoxy adhesive bonded blanks for different H/R ratios, (b) SS 316L specimen from acrylic adhesive bonded blanks for different H/R ratios 69
Fig. 3.1 Tensile sample made of adhesive bonded blanks showing geometry of adhesive defects, (b) showing geometry of increase in number of defects, (c) showing geometry for different locations of defects, (d) geometry of IPPS adhesive bonded formability testing specimen showing different shapes and aspect ratios of adhesive finite defects; Magnified view of adhesive finite defects with (e) $a/b = 1$, (f) $a/b = 0.5$, and (g) $a/b = 1.5$ 76
Fig. 3.2 (a) Tensile sample made of adhesive bonded steel sheets showing different orientations of adhesive infinite defects, and (b) Geometry of IPPS adhesive bonded formability testing specimen showing different orientations of adhesive infinite defects. 77
Fig. 3.3 Failure pattern of adhesive layer in adhesive bonded blanks with different aspect ratios ... 78
Fig. 3.4 Failure pattern of adhesive layer in the adhesive bonded blanks with different numbers and location of adhesive defects 79
Fig. 3.5 Comparison of load – extension behaviour of adhesive bonded blanks with and without adhesive finite defect 80
Fig. 3.6 Decrease in extension at failure % in different deforming regions A, B, and C 81
Fig. 3.7 Comparison of limit strain of base materials constituting adhesive bonded blanks with influence of different aspect ratios of adhesive finite defect in tensile test, (a) DDQ steel specimen, and (b) SS 316L specimen 82
Fig. 3.8 Comparison of limit strain of base materials constituting adhesive bonded blanks with influence of different aspect ratios of adhesive finite defect in IPPS forming test, (a) DDQ steel specimen, and (b) SS 316L specimen 83
Fig. 3.9 Comparison of strain gradient of DDQ steel sheet in adhesive bonded blanks between with and without adhesive finite defect till failure of DDQ steel from tensile test with different aspect ratios 85

Fig. 3.10 Comparison of load – extension behaviour of adhesive bonded blanks with increase in number of adhesive finite defects from tensile test 87
Fig. 3.11 Comparison of limit strain of base materials in adhesive bonded blanks with increase in number of adhesive finite defects at different aspect ratios 88
Fig. 3.12 Comparison of load-extension behaviour between increasing number of adhesive defects from 1 to 3 combined as a single defect for an equivalent volume in adhesive bonded blanks 90
Fig. 3.13 Comparison of limit strain between increasing number of adhesive defects combined as a single defect for an equivalent volume in adhesive bonded blanks (a) DDQ steel specimen, and (b) SS 316L specimen 91
Fig. 3.14 Comparison of load – extension behaviour of adhesive bonded blanks with different locations of adhesive finite defects 92
Fig. 3.15 Comparison of limit strains of base materials in adhesive bonded blanks with different locations of adhesive defects at different aspect ratios 94
Fig. 3.16 Failure pattern of adhesive layer with different orientations of infinite defect in adhesive bonded blanks 96
Fig. 3.17 Gripping of adhesive bonded specimens in the presence of 45° oriented infinite defect in the adhesive layer 97
Fig. 3.18 Comparison of load – extension behaviour of adhesive bonded blanks with and without transverse oriented defect (a) tensile tested epoxy bonded blanks, and (b) IPPS formability tested epoxy bonded blanks 99
Fig. 3.19 Comparison of decrease in percentage of total extension of DDQ steel sheets and SS 316L sheets in adhesive bonded blanks in the presence of infinite defect with respect to the adhesive bonded blank without infinite defect, (a) adhesive bonded tensile specimens, and (b) adhesive bonded IPPS specimens 100
Fig. 3.20 Comparison of limit strains of adhesive bonded blanks with influence of different orientations of infinite defect from tensile test, (a) DDQ steel, and (b) SS 316L 101
Fig. 3.21 Comparison of limit strains of adhesive bonded blanks with influence of different orientations of infinite defect from IPPS formability test, (a) DDQ steel, and (b) SS 316L 101
Fig. 4.1 FE model and boundary conditions of tensile adhesive bonded blanks in the simulation: (a) before deformation, and (b) after failure 108
Fig. 4.2 FE model and boundary conditions of IPPS adhesive bonded blanks in the simulation: (a) before deformation, and (b) after failure 109
Fig. 4.3 Schematic of load sharing in adhesive bonded blank during tensile test showing different deforming regions 111
Fig. 4.4 Limit strains of DDQ steel and SS 316L tensile tested as single sheet with different mesh size during FE simulation 114
Fig. 4.5 Comparison of true stress-strain behaviour of base materials between experimental and prediction: (a) DDQ steel, and (b) SS 316L 114

Fig. 4.6 Comparison of tensile behaviour of adhesive bonded blanks with different hardener/resin ratios: (a) Experiments, (b) Simulations, (c) H/R = 0.6:1, (d) H/R = 0.7:1, (e) H/R = 0.8:1, (f) H/R = 0.9:1, and (g) H/R = 1:1 118
Fig. 4.7 Comparison of percentage elongation (true strain) of adhesive bonded blanks with different hardener/resin ratios between experiment and predicted results: (a) Tensile test, and (b) IPPS formability test 120
Fig. 4.8 Variation of effective strain rate ratio with true major strain in bulk in base materials in adhesive bonded blanks with different H/R ratios: (a) DDQ steel, and (b) SS 316L 121
Fig. 4.9 Comparison of experiment and prediction of base materials limit strain: (a) tensile test, and (b) IPPS forming test 122
Fig. 4.10 Comparison of limit strains base materials in adhesive bonded blanks with different H/R ratios between experiments and predictions in tensile test 123
Fig. 4.11 Comparison of limit strains base materials in adhesive bonded blanks with different H/R ratios between experiments and predictions in IPPS forming test: (a) H/R = 0.6:1-DDQ steel, (b) H/R = 0.6:1-SS 316L, (c) H/R = 0.8:1-DDQ steel, (d) H/R = 0.8:1-SS 316L, (e) H/R = 1:1-DDQ steel, and (f) H/R = 1:1-SS 316L 124
Fig. 5.1 Schematic of load sharing by adhesive bonded sheets during tensile test 128
Fig. 5.2 Comparison of true stress-strain behaviour of epoxy adhesive obtained by approach-1 and approach-2 with different hardener/resin ratios: (a) H/R = 0.6:1, and (b) H/R = 1:1 130
Fig. 5.3 Comparison of limit strain results of adhesive bonded sheets with different H/R ratios between experiments and predictions during tensile test 131
Fig. 5.4 Comparison of limit strain results of adhesive bonded blanks with different H/R ratios between experiments and predictions during IPPS formability test: (a) H/R = 0.6:1-DDQ steel, (b) H/R = 0.6:1-SS 316L, (c) H/R = 1:1-DDQ steel, and (d) H/R = 1:1-SS 316L 132
Fig. 6.1 (a) TEM photograph of CB nano sized powder and (b) diffraction pattern of carbon black nano sized powder 135
Fig. 6.2 Engineering stress-strain behaviour of adhesive samples with different CB wt.% 137
Fig. 6.3 Comparison of true stress-strain behaviour of adhesive bonded blanks with different CB wt.% from tensile test: (a) Experimental result, (b) Predicted result, (c) CB – 1 wt.%, (d) CB – 2 wt.%, (e) CB – 3 wt.%, (f) CB – 4 wt.%, (g) CB – 5 wt.%, and (h) CB – 6 wt.% 142
Fig. 6.4 Elongation results (true strain) with different wt.% of carbon black in adhesive bonded . 143
Fig. 6.5 Comparison of experimental limit strain results of adhesive bonded sheets with different CB wt.% from tensile test: (a) DDQ steel, and (b) SS 316L 143
Fig. 6.6 Comparison of experimental limit strain results of adhesive bonded sheets with different CB wt.% from IPPS formability test: (a) DDQ steel, and (b) SS 316L 144
Fig. 6.7 Comparison of limit strain results of adhesive bonded sheets with different CB wt.% between experiments and predictions in tensile test 145
Fig. 6.8 Comparison of limit strain results of adhesive bonded sheets with different CB wt.% between experiments and predictions in IPPS formability test: (a) CB wt.% = 2–DDQ steel,

(b) CB wt.% = 2–SS 316L, (c) CB wt.% = 4–DDQ steel, (d) CB wt.% = 4–SS 316L, (e) CB wt.% = 6–DDQ steel, and (f) CB wt.% = 6–SS 316L..... 146
Fig. 6.9 Comparison of limit strain results of DDQ steel and SS 316L sheets constituting adhesive bonded sheets with different thickness values of adhesive layer at 2 wt.% of CB in the adhesive. 146
Fig. 7.1 Engineering stress-strain behaviour of Cu and Al wires..... 149
Fig. 7.2 Wire reinforced adhesive bonded sheets with different orientations..... 151
Fig. 7.3 (a) Wire reinforced adhesive bonded circular sheets, and (b) Schematic of deep drawing tools used in experiment..... 151
Fig. 7.4 Finite element (FE) model of adhesive bonded sheets during tensile test..... 154
Fig. 7.5 FE model of middle layer with different cases: (a) only epoxy layer, (b) more epoxy and less Copper width, (c) less epoxy and more Copper width, and (d) Only Copper sheet..... 154
Fig. 7.6 Failure pattern of wire reinforced adhesive bonded sheets during tensile test: (a) failure of adhesive layer, (b) failure of DDQ steel, and (c) failure of SS 316L..... 155
Fig. 7.7 Failure pattern of longitudinally wire reinforced adhesive layer constituting adhesive bonded sheets..... 156
Fig. 7.8 Failure pattern of transversely wire reinforced adhesive layer constituting adhesive bonded sheets..... 157
Fig. 7.9 Engineering stress-strain behaviour of wire reinforced adhesive bonded sheets with different numbers of wire from tensile test: (a) Cu wire, and (b) Al wire..... 158
Fig. 7.10 Engineering stress-strain behaviour of wire reinforced adhesive bonded sheets with different numbers of wire from IPPS formability test: (a) Cu wire and (b) Al wire..... 159
Fig. 7.11 Elongation trend of Cu and Al wire reinforced adhesive bonded sheets in regions A, B and C with different numbers of wire during tensile test..... 160
Fig. 7. 12 Elongation trend of Cu and Al wire reinforced adhesive bonded sheets in regions A, B and C with different numbers of wire during IPPS formability test..... 160
Fig. 7.13 Limit strains in base materials constituting wire reinforced adhesive bonded blanks in tensile test..... 161
Fig. 7.14 Limit strains in base materials constituting wire reinforced adhesive bonded blanks in IPPS formability test..... 162
Fig. 7.15 Comparison of true stress-strain behaviour of unreinforced and *Cu* reinforced adhesive bonded sheets from numerical prediction..... 165
Fig. 7.16 Limit strains in base materials constituting transverse wire reinforced adhesive bonded sheets with different numbers of wires from tensile test: (a) DDQ steel, and (b) SS 316L..... 167
Fig. 7.17 Deformation pattern of Cu wire reinforced adhesive layer constituting adhesive bonded sheets: (a) Unreinforced, (b) 4 wires (c) 8 wires, (d) 16 wires, and (e) 40 wires..... 169
Fig. 7.18 (a) Deep drawing behaviour of Cu wire reinforced adhesive bonded sheets with different number of wires, and (b) Comparison of cup height at maximum load..... 170
Fig. 7.19 Wrinkling behaviour of adhesive bonded sheets with different numbers of Cu wire reinforcements..... 171
Fig. 8.1 FE model: (a) deep drawing tools, (b) adhesive bonded blanks, and (c) deformed cup.... 176

Fig. 8.2 Schematic representation of cup drawing of adhesive bonded blanks 178
Fig. 8.3 General deep drawing behaviour of a sheet taken into consideration 182
Fig. 8.4 Comparison of true stress-strain behavior of epoxy adhesive obtained by approach-1 and approach-2 with different wt.% of CB 183
Fig. 8.5 Mesh sensitive analysis: (a) Limit strains – tensile test of DDQ steel, and (b) Cup height – deep drawing test of SS 316L 184
Fig. 8.6 Deformation pattern of adhesive layer constituting adhesive bonded blanks 186
Fig. 8.7 Comparison of wrinkling of adhesive bonded blanks from experiment 188
Fig. 8.8 Comparison of wrinkling of adhesive bonded blanks from FE simulation 188
Fig. 8.9 Comparison of load-progression behaviour of base materials between experiment and prediction 189
Fig. 8.10 Load-stroke behaviour of adhesive bonded blanks from experiment 190
Fig. 8.11 Comparison of load-stroke behaviour of adhesive bonded blanks between experiment and prediction 191
Fig. 8.12 Comparison of cup height at maximum load between experiment and prediction 192
Fig. 8.13 Comparison of maximum drawing load between experiment, estimation and numerical simulation 194
Fig. 8.14 Comparison of deep drawing behaviour between experiment and proposed model with max. load from experiment, numerical prediction and by estimation 196
Fig. 9.1 FE models with (a) rectangular-infinite groove in region *'a'* (initial infinite geometrical heterogeneity), (b) square hole in region *'a'* (initial infinite geometrical heterogeneity), and (c) square-finite groove in region *'a'*, (initial finite geometrical heterogeneity) 201
Fig. 9.2 FE model of circular blank showing the initial finite heterogeneity (circular-finite groove) in region *'a'* 202
Fig. 9.3 Methodology followed during prediction of forming behaviour of adhesive bonded blanks using geometrical heterogeneities 203
Fig. 9.4 FE models with different geometrical heterogeneities in the base materials showing necking at region *'a'* after deformation 205
Fig. 9.5 Variation of effective strain rate ratio with true major strain in bulk in DDQ steel sheet different initial geometric heterogeneities during tensile test 206
Fig. 9.6 The range of *'f'* for predicting the limit strains with different rectangular-infinite groove widths (w) during tensile test: (a) w= 0.5 mm, and (b) w= 3 mm 207
Fig. 9.7 Predicted limit strains of DDQ steel with the effect of different hardener/resin ratios of adhesive with the equivalent *'f'* at different rectangular-infinite groove width (w) in tensile test: (a) w = 0.5 mm, (b) w = 1 mm, (c) w = 1.5 mm, (d) w= 2 mm, and (e) w= 2.5 mm 208
Fig. 9.8 (a) The range of *'w'* of square hole for predicting the limit strains, and (b) Predicted limit strains of DDQ steel with the effect of different hardener/resin ratios of adhesive with the equivalent 'w' of square hole 209
Fig. 9.9 The range of *'f'* for predicting the limit strains with different square-finite groove size (w): (a) w= 0.5 mm, and (b) w= 3.5 mm 210

Fig. 9.10 Predicted limit strains of DDQ steel with the effect of different hardener/resin ratios of adhesive with the equivalent *'f'* at different square-finite groove size (*w*): (a) *w* = 0.5 mm, (b) *w* = 1 mm, (c) *w* = 1.5 mm, (d) *w*= 2 mm, (e) *w*= 2.5 mm, and (f) *w*= 3 mm.....211
Fig. 9.11 Comparison of cup height result with different radius at region '*a*' in circular blank at different *'f'* values.....213
Fig. 9.12 (a) Cup height of adhesive bonded blanks with different hardener/resin ratios during experiment, and (b) The range of *'f'* for predicting the cup height at d_1 = 60 mm in the region *'a'* (circular-finite groove).....214
Fig. 9.13 Load-stroke behaviour at different *'f'* values during deep drawing process.....215
Fig. 9.14 Predicted cup height results by circular-finite groove in region '*a*' of SS 316L circular blank with the effect of different hardener/resin ratios of adhesive with equivalent *'f'* values…...215
Fig. 10.1 Neural network architecture developed for predicting the forming behaviour of adhesive bonded blanks in tensile test…….226
Fig. 10.2 Neural network architecture developed for predicting the forming behaviour of adhesive bonded blanks in deep drawing process……...227
Fig. 10.3 Comparison of limit strains of base materials of adhesive bonded blanks between experiment and ANN output.....231
Fig. 10.4 Comparison of intermediate levels of limit strains of base materials of adhesive bonded blanks between experiment and ANN output……...233
Fig. 10.5 Comparison of cup height results of adhesive bonded blanks: (a) different H/R ratios of adhesive, (b) different CB wt.% in adhesive, and (c) various numbers of wire reinforcement.....235
Fig. 10.6 Comparison of cup height results of adhesive bonded blanks for intermediate levels.....236
Fig. 10.7 Comparison of limit strains between experiment, ANN prediction and geometrical heterogeneity prediction during tensile test: (a) rectangular infinite-groove (Groove-A), and (b) square finite-groove (Groove-B)……237
Fig. 10.8 Comparison of cup height results between experiment, ANN prediction, and geometric heterogeneity prediction……...238
Fig. 10.9 Proposed expert system for prediction of formability of adhesive bonded sheets……...240

List of Tables

Table 2.1 Nominal chemical composition of DDQ steel and SS 316L sheets in weight % 30

Table 2.2 Mechanical properties of DDQ steel sheets..... 33

Table 2.3 Mechanical properties of SS 316L sheets..... 33

Table 2.4 Details of epoxy adhesive and acrylic adhesive obtained from the suppliers..... 33

Table 2.5 Five levels of different hardener/resin ratios 34

Table 2.6 Mechanical properties of epoxy adhesive and acrylic adhesive 38

Table 2.7 Comparison of increase in percentage of total extension of DDQ steel sheets and SS 316L sheets in adhesive bonded blanks with respect to double sheet 42

Table 2.8 Comparison of increase in percentage of total extension results of DDQ steel and SS 316L single sheet and adhesive bonded blanks..... 43

Table 2.9 Comparison of increase in total elongation results of DDQ steel sheets and SS 316L sheets in adhesive bonded blanks with respect to single sheet..... 46

Table 2.10 Comparison of percentage of elongation results at region A, B and C of adhesive bonded blanks with different hardener/resin ratios 47

Table 2.11 Strain hardening exponent (n) in region 1 and region 2 of double sheet..... 49

Table 2.12 Strain hardening exponent (n) value in regions A, B and C of adhesive bonded blanks..... 49

Table 2.13 Comparison of increase in strain hardening exponent (n) in region B and region C of adhesive bonded blanks with respect to region 1 and region 2 of double sheet..... 49

Table 2.14 Comparison of increase in elongation of DDQ steel and SS 316L sheets in adhesive bonded blanks with respect to double sheet..... 62

Table 2.15 Comparison of improvement in total elongation of DDQ steel sheets and SS 316L sheets in adhesive bonded blanks with respect to single sheet..... 63

Table 2.16 Strain hardening exponent (n) value in regions 1 and 2 of double sheet..... 67

Table 2.17 Strain hardening exponent (n) value in regions A, B and C of adhesive bonded blanks..... 67

Table 3.1 Uncertainty measurement of limit strain 83

Table 3.2 Strain hardening exponent (n) in regions A, B and C of adhesive bonded blanks without pregenerated adhesive finite defect from tensile and IPPS formability tests 84

Table 3.3 Strain hardening exponent (n) in regions A, B and C of adhesive bonded blanks with different aspect ratios (a/b) of adhesive finite defect from tensile and IPPS formability tests 84

Table 3.4 Strain hardening exponent (n) in regions A, B and C of adhesive bonded blanks with increase in number of adhesive finite defects at a/b = 0.5, 1, and 1.5..... 89

Table 3.5 Strain hardening exponent (n) in regions A, B and C of adhesive bonded blanks with different locations of adhesive defect for a/b = 0.5, 1 and 1.5..... 95

Table 3.6 Strain hardening exponent (n) in region A, B and C of adhesive bonded steel sheets without infinite defect in the adhesive layer 102

Table 3.7 Strain hardening exponent (*n*) in region 1 and region 2 of adhesive bonded steel sheets characterised by adhesive separation 102

Table 3.8 Strain hardening exponent (*n*) in regions A, B and C of adhesive bonded steel sheets characterised by adhesive failure 103

Table 3.9 Uncertainty measurement of limit strain 103

Table 4.1 Density of epoxy adhesive with different hardener/resin ratios 107

Table 4.2 Prediction of progression at failure of adhesive bonded blanks with different H/R ratios in tensile test 115

Table 4.3 Prediction of progression at failure of adhesive bonded blanks with different H/R ratios in IPPS formability test 115

Table 6.1 Density of epoxy adhesive with different CB wt.% 136

Table 6.2 Prediction of progression at failure of adhesive bonded blanks with different CB wt.% in tensile test 138

Table 6.3 Prediction of progression at failure of adhesive bonded blanks with different CB wt.% in IPPS formability test 139

Table 7.1 Uncertainty measurement of limit strain 163

Table 7.2 Strain hardening exponent (*n*) in regions A, B and C of wire reinforced adhesive bonded sheets from tensile test 164

Table 7.3 Strain hardening exponent (*n*) in regions A, B and C of wire reinforced adhesive bonded sheets from IPPS formability test 164

Table 8.1 Normal anisotropy of adhesive bonded blanks 181

Table 8.2 Strain hardening exponent (*n*) and strength coefficient (*K*) of adhesive bonded blanks 182

Table 10.1 Optimization of network with different activation functions in the hidden layer and output layer for tensile test 224

Table 10.2 Optimization of network with different ANN structures, learning rules with different μ and α, and different training algorithms for tensile test 224

Table 10.3 Optimization of network with different ANN structures for deep drawing test 225

Table 10.4 Input parameters and different levels 229

Table 10.5 Percentage of error range of limit strains 231

Table 10.6 Input parameters and different levels used during intermediate level prediction 232

Table 10.7 Percentage of error range in limit strains 233

Table 10.8 Input parameters and different levels during training of network corresponding to the target data 234

Table 10.9 Percentage of error range in cup height results 235

Table 10.10 Input parameters and different levels used during intermediate level prediction 235

Chapter 1

Introduction, Literature review, Significance and Objective of work

1.1 Introduction

The adhesive bonding technology is well accepted technology in the manufacturing sectors in order to eliminate stress concentrations at the location of joints caused by the conventional mechanical fastening methods, and also eliminates high temperature involved joining processes like conventional welding methods. The adhesive bonded sheets categorized under tailor made blanks (TMB) are mainly used in the construction of aircraft and automotive body structures. The main advantages of using adhesive bonded blanks in the manufacturing sectors are usage of light weight materials after joining can save excessive fuel, utilization of different mechanical properties, surface attributes and loading conditions, exploring different material thickness and properties combination towards cost reduction without compromising the quality, and component design flexibility [Pocius, 2002; Katsiropoulos *et al.,* 2012].

Most of the parts in the construction of aircraft and automotive body structures are formed parts. The general mechanical behaviour and forming behaviour of adhesive bonded sheets are influenced by the quality of adhesives. The strength of an adhesive bond resulting from chemical interactions at the metal surface or the energies of adhesion; chemical or physical interactions at the interface show a significant influence on the adhesion strength [Brockmann *et al.,* 1982]. The bonding process is influenced by the properties of the adhesive such as viscosity, surface energy, strength, modulus of elasticity and specific density changing with time and ambient conditions. Adhesives in structural applications are applied as liquids and exhibit their strength as solids after curing. The major factors influencing bonding performance are surface and bulk properties of the adhesive, surface and bulk properties of the substrate, residual stress at the interface, environmental conditions and contaminants, joint geometry, and type of external loads applied [Gutowski, 1987].

There are numerous studies on the modelling of adhesive bonded blanks mainly following tying nodes at the interface of two components, cohesive zone theory for adhesive layer in bonded blanks, mesh refinement strategy at the interface between adhesive and substrates, representation of bonded blanks as single component during prediction of mechanical properties and forming behaviour. These methods mainly focus on intact locking between adherends in the rather than considering the adhesive properties during deformation which is not actual case in the experiments.

The main objectives of the present work is to investigate the influence of adhesive properties on the forming behaviour of adhesive bonded sheets, and predicting forming behaviour of adhesive bonded sheets with the aim of representing the adhesive. In this work, the adhesive properties are changed by varying hardener/resin ratio of adhesives, by pregenerating artificial defects in the adhesive, by filling carbon black nano sized powder in the adhesive at varying wt.%, by reinforcing high ductile wires in the low ductile adhesive. Based on the understanding from the results during these investigations, the adhesive is represented in the base materials using geometrical heterogeneities without using any adhesive properties. The forming behaviour of adhesive bonded sheets is also predicted by neural networks. These prediction works are carried out to overcome the difficulties involved during incorporation of adhesion properties, selection of suitable instability conditions, and predicting the forming behaviour of adhesive bonded blanks at varying adhesive properties.

Literature review, significance of the work, objectives of the work, and tasks involved are presented in Chapter 1. The experimental investigations on the influence of adhesive properties varying hardener/resin ratio, and adhesive defects generated artificially on the formability of adhesive bonded sheets are presented in Chapter 2 and 3. The forming behaviour of adhesive bonded steel sheets with the effect of hardener/resin ratio of adhesive is predicted through finite element simulations in Chapter 4. The evaluation of adhesive mechanical properties by rule of mixtures, and the importance of interfacial bonding between base materials and adhesive on the formability of adhesive bonded sheets is demonstrated in Chapter 5. The influence of carbon black filled adhesive on the forming behaviour of adhesive bonded sheets is investigated and predicted in Chapter 6. The influence of low ductile adhesive reinforced with high ductile wires on the formability of adhesive bonded sheets is investigated and predicted in Chapter 7. The influence of adhesive properties on the deep drawability of adhesive bonded blanks is analysed in Chapter 8. The estimation of formability and deep drawability of adhesive bonded sheets using equivalent

geometrical heterogeneities is demonstrated and hypothesized in Chapter 9. The formability of adhesive bonded sheets is predicted by neural network in Chapter 10.

1.2 Literature review

1.2.1 Introduction to adhesive bonding technology

An adhesive may be defined as a material which when applied to surfaces of materials can join them together and resist separation. The adhesive must be a liquid at the time of application, in order to make intimate molecular contact with the adherends (substrates) by wetting the surfaces. Then the adhesive gets harden (cure) to a cohesive solid. Once hardened, the polymer in an adhesive can be linear or cross linked. The act of cross linking renders polymers insoluble and infusible, and greatly reduces creep. All structural adhesives are cross linked. Curing (hardening) takes place within the bulk of the adhesive, and adhesion occurs at the interface (Adams, 2010).

1.2.2 Adhesion theories

There are different types of adhesion theories such as mechanical interlocking, diffusion, adsorption, chemical bonding, electrostatic and wetting theory (Adams, 2010).

(a) Mechanical Theory

The adhesion occurs by the penetration of adhesives into pores, cavities, and other surface irregularities on the surface of the substrate. The adhesive displaces the trapped air at the interface (Pocius, 2000).

(b) Theory of diffusion

This theory requires that both the adhesive and adherend are polymers, which are mutually compatible and miscible. The diffusion theory is primarily applicable when both the adhesive and the adherend are polymers with relatively long-chain molecules capable of movement. The diffusion theory attributes adhesion of polymeric materials to the inter-penetration of chains at the interface. The major driving force for polymer autohesion and heterohesion is due to mutual diffusion of polymer molecules across the interface (Ebnesajjad, 2008).

(c) Adsorption theory

The adsorption theory states that adhesion results from intimate intermolecular contact between two materials, and involves surface forces that develop between the atoms in the two surfaces. The most common surface forces that form at the adhesive-adherend interface are van der Waals forces (Pertrie, 2000).

(d) Chemical bonding mechanism

The chemical bonding theory of adhesion enables the formation of covalent, ionic or hydrogen bond or Lewis acid-base interactions across the interface (Adams, 2010).

(i) Covalent bonds

Covalent bonds are formed with silane coupling agents that they chemically react with both substrate and adhesive, so forming covalent bonds across the interface which is both strong and durable (Adams, 2010).

(ii) Ionic bond

In ionic bond, the chemical bonds form through an electrostatic attraction between two oppositely charged ions. Ionic bonds are formed between a cation, usually a metal, and an anion, usually a nonmetal. The bonds with partially ionic and partially covalent character are called polar covalent bonds. Ionic bonding is a form of noncovalent bonding (Johnson, 2002).

(iii) Hydrogen bond

A hydrogen bond is the attractive interaction of a hydrogen atom with an electronegative atom, such as nitrogen, oxygen or fluorine that comes from another molecule or chemical group. A special type of dipole – dipole interaction that occurs when a hydrogen atom that is bonded to a small, highly electronegative atom (most commonly F, O, N, or S) is attracted to the lone electron pairs of another molecule (Ebnesajjad, 2008).

(e) Electrostatic (Electronic) theory

The electrostatic theory exhibits the adhesion due to electrostatic effects between the adhesive and the adherend. An electron transfer is taken place between the adhesive and the adherend. The electrostatic forces in the form of an electrical double layer form at the adhesive and adherend interface (Pertrie, 2000).

(f) Wetting theory

The adhesive must first wet the surface or it must be applied in the liquid form to achieve bonding between the adhesive and the substrate. A measure for the wettability of a surface is the angle of contact that forms between a drop of liquid and a substrate surface which depends on the surface tension and the viscosity of the adhesive, and also on the texture of the surface (Pocius, 2002).

1.2.3 Advantages of adhesive bonds

The adhesive bonds do not exhibit high stress concentrations during assembly of components, whereas the mechanical fasteners pierce the components during joining and cause high stress concentrations. It also eliminates the high temperature involved joining process like conventional welding methods. Thus, adhesive bonds enable the properties of the components for utilization. Adhesive joint prevents crevice corrosion, and it is useful in bonding of dissimilar materials. It exhibits its special advantages in bonding of heat-sensitive materials. Adhesive bonds take a vital role in weight saving and recycling of primary materials which is more advantage in automotive sectors in order to save fuel consumption. It distributes tension uniformly in bonded areas and provides high vibration damping. Many adhesives do not require input of mechanical energy to affect an assembly. Hence, shock-sensitive materials can be easily made into an assembly. Especially, the adhesive not only form a joint, but also it acts as a sealing agent and acting as an insulator in the assemblies. Adhesives also allow galvanically dissimilar materials to adhere to one another without accelerating corrosion. The adhesive bonds show their efficiency and importance in joining processes of steel and aluminum components, and metal and non-metal surfaces (Pocius, 2002; Katsiropoulos *et al.*, 2012; Taib *et al.*, 2006; Zadpoor *et al.,* 2009).

1.2.4 Disadvantages

The primary disadvantage of adhesive bonding is that it relies on adhesion for the transfer of load through the assembly. An adherend with an improper surface could lead to lower joint strengths. Adhesive bonds do require a much larger area of contact between the adherends and the adhesive in order to carry the same load as a mechanical fastener. Adhesives are internal to the joint in nature, which makes difficult to examine the joint quality without destructing the joints. But in the recent researches, numerous non-destructing have been brought for testing adhesive joints. In adhesive

bonded joints, strength is dependent on the condition of the adherend surface and durability in adverse environments affected by surface condition. Adhesive joints are difficult to rework and some adhesive have a limited shelf life, toxic components and poor resistance to crack propagation (Pocius, 2002).

1.2.5 Applications

Adhesive bonds are used in a wide array of applications. The main applications of structural adhesive bonds are discussed here. In the tailor-made blanks (TMBs) technology, the sheet metals used for production of the structural parts of ground and air vehicles do not need to be uniform in thickness, nor do they have to be composed of one single material, or even bear the same type of coating. These tailor-made blanks are sheet metal assemblies are mostly achieved by adhesive bonding techniques (Zadpoor *et al.,* 2009). In addition adhesives have been used in a number of repair and maintenance operations (Ning *et al.*, 1992). The aerospace industry uses adhesive bonding to great advantage in the construction of many components. It is easy to see that mush of the fuselage, the wing structure, and the engine housing are at least partially adhesively bonded. Military applications initiated the use of adhesive bonded advanced composites. The bonded polymer matrix composite laminates at wing skins and control surfaces applications can be found on many types of commercial aircrafts with the aim of reduced weight assemblies (Katsiropoulos *et al.,* 2011). Adhesive bonded sandwich structures are used in refrigerated transportation containers, pleasure boats and commercial vessels, building panels, etc. (Karlsson and Astrom, 1997).

1.2.6 Influencing parameters of adhesives on mechanical properties

In an adhesive bonded blank, the adhesive which is used for bonding of base metals drives the efficiency of bonding. While analysing the influencing factors of an adhesive, Wake, 1978 reviewed mainly about the theories of adhesion, joint strength, surface properties of substrates, fracture mechanics of structural adhesives and adhesive properties. It was mentioned that the joint strength widely depends on the mechanical properties of the adhesive rather than on its behaviour at the interface. The influence of adhesive joints with different types of acrylic adhesives and different surface preparation methods on lap shear strength and fracture energy. The results showed that the increase in lap shear strength and the fracture energy depends on the surface preparation methods irrespective of adhesives (Allen *et al.,* 1984; 1985). d'Almeida and Monteiro, 1996 investigated the

influence of different resin/hardener ratios of the epoxy monomer, diglycidyl ether of bisphenol-A (DGEBA), with an aliphatic amine, triethylene tetramine (TETA) on mechanical properties by compression test. It was observed that the epoxy rich systems showed brittle behaviour which is associated with the development of a rigid macromolecular structure and the hardener rich systems showed fracture behaviour with a large deformation. Later, d'Almeida and Monteiro, 1997 also investigated the effects of different hardener/resin matrix of diglycidyl ether of bisphenol-A (DGEBA), with triethylene tetramine (TETA) on the mechanical properties in the fabrication of glass microspheres (GM) composites and chopped-glass fiber (CGF) composites by tensile and flexural tests. The results showed that ultimate strength and percentage of ultimate strain increase with increase in hardener/resin ratio, while Young's modulus decreases.

Detwiler and Lesser, 2010 investigated on the network formation and the physical properties of amine-cured epoxy resins. It was suggested that physical ageing is inherent in epoxy network formation, and the resulting strain localization degrades the mechanical integrity of epoxy resins in the partially cured state apart from the curing conditions. Saleh *et al.,* 2011 carried out a study on the mechanical properties of the epoxy resin diglycidyl ether of bisphenol-A (DGEBA) with the aliphatic and aromatic amine hardeners. The results showed that the formulation above stoichiometry ratio of both types of adhesive system increase the total elongation, while ultimate tensile strength and Young's modulus showed a decreasing trend. d'Almeida *et al.,* 2003 carried out a study on the room temperature ageing of DGEBA/TETA with different epoxy formulations and showed that the epoxy rich mixtures have their inherent brittleness increased by the ageing treatment due to recrystalization of the unreacted epoxy monomers, while the amine rich mixtures exhibit an increase on the deformability. Ma *et al.,* 2010 investigated the mechanical and thermal properties of epoxy resin and carbon black (CB) composites through modified methods of silicone coupling agent to improve the dispersion of CB in epoxy resin. The results showed the maximum improvement in tensile strength, elongation, flexural strength and impact strength with the mass fraction of CB was 2%. The use of modified CB significantly enhanced the mechanical properties of the composites than that of the direct mixing method. It was observed that the tensile fracture surface of the composite filled with 2 wt.% modified CB held more micro cracks than that of 5 wt.% modified CB, and the formed micro cracks could consume more energy of rupture to have better tensile strength. Novak *et al.,* 2003 investigated electrical conductivity and elongation at break of epoxy filled with electro conductive carbon black, graphite or with silver-coated basalt

particles or fibres. The percolation concentrations were found to be 14 vol.% for epoxy/carbon black composites, 22 vol.% for epoxy/graphite composites, 28–29 vol.% for both epoxy/silver coated basalt particles and fibres. Sumfleth *et al.,* 2011 carried out combined rheological and electrical analysis on epoxy nano composite suspensions including multi-wall carbon nanotubes (MWCNTs) and CB. The results showed that multi-filler (MWCNTs and CB) suspensions exhibit a similar rheological behaviour as the binary MWCNT suspensions. For both types of suspensions a rheological percolation threshold of around 0.2 and 0.25 wt% was determined. Prasse *et al.,* 2010 examined the chemical interaction of non-oxidised carbon black and an epoxy resin in the non-cured state. It was found that the amine hardener-epoxy content on the charge transfer to the CB resulting electrically induced agglomeration of the particles.

From these studies, it is understood that the mechanical properties of adhesives are more influenced by the hardener/resin ratio, and filling of nano sized powder particles.

1.2.7 Influencing parameters of bonded blanks on mechanical properties

The mechanical behaviour of adhesive bonded sheets is influenced by quality of adhesives. The important studies are described here. Deb *et al.,* 2007 studied the mechanical behaviour of adhesively bonded joints made from dual phase steel bonded with epoxy adhesive at a high temperature and found greater degree of strain rate sensitivity with a reduction in joint strength. Zadpoor *et al.,* 2010 carried out an experimental study on the mechanical behaviour of adhesive bonded blanks with different sheet thicknesses and evaluated the mechanical properties for both transverse and longitudinal joint orientations. It was found that the tensile load at the onset of damage decreases as thickness ratio increases. Grant *et al.,* 2009 investigated the tensile behaviour and three point bending behaviour of adhesive bonded sheets. The mechanical testing was carried out at -40°C, +20°C and +90°C using lap joint and T-joint configurations. It was realized that the failure load is higher at -40°C than at +20°C and +90°C for thin adhesive bonding. But for thick bonding, the failure load is independent of the temperature. Borsellinoa *et al.,* 2009 used four different types of resins such as two types of polyester resins, vinylester resin and epoxy resin for bonding of aluminium AA6082 sheets. More tensile strength was observed for epoxy adhesive system and larger percentage of total elongation was noted for vinylester resin. Shin *et al.,* 1999 examined the tensile properties of aluminum/polypropylene/aluminum (Al/PP/Al) sandwich sheets at room and elevated temperatures. The results showed better tensile strength in the sandwich sheet

with hard skin and low volume fraction of the polypropylene core than the sandwich sheet with soft skin and high volume fraction of the polypropylene core. It was found that the influence of temperature on tensile strength of the sandwich sheet with high volume fraction of polypropylene core is higher than that with low volume fraction of polypropylene core.

Berry and d'Almeida, 2002 carried out an experimental study about the influence of size of circular cantered defects on the bonded area of a carbon–epoxy bonded single lap joint on mechanical properties. The results showed reduced stiffness of the adhesive layer, favouring the deformation of the single lap joint. Although the defects reduce the fracture load, the maximum tear stress acting at the joint is reduced with increase in the defect size. Melander *et al*., 1999 studied the effect of different types and size of artificial bond defects such as reduced degree of bond filling, bonds with a channel without adhesive, zig-zag-shaped bond edges, and finally bond areas with smooth corners. From the results of fatigue testing, it was found that the fatigue strength was found to differ for different bond defects. Apart from this, the stiffness was also measured for the bonds and was found to vary with defect type and size. Moreover, it was addressed that weak bonds do affect the structural load response of the bondline in a number of ways. This effect is due to the reduction in bondline stiffness (Heslehurst, 1999). Llopart *et al.,* 2010 investigated the effect of imperfect bonding, owing to partial lack of adhesive, on the strength of composite non-crimp fabric (NCF) double-lap shear (DLS) joints. The results showed a significant decrease in strength of the imperfect bonded specimens. The lack of adhesive causes the development of shear stress concentration, there by debonding initiates early failure of the joint. Chadegani and Batra, 2011 analyzed stresses in two layers bonded with an adhesive including a void within the adhesive and the specimen was divided into several regions depending upon the number of notches and voids. The results showed that there is not much influence on the stress distribution due to presence of the void in single-notch and double-notch specimens near the free edge of the adhesive/substrate interface. Lin and Hui, 2004 carried out a study on the growth and failure of small crack-like defects in elastomers under hydrostatic tension. It was brought forth that strain hardening has important effect on the determination of the critical pressure for crack initiation. It was also demonstrated using a fracture mechanics approach that small crack-like cavities fail at higher hydrostatic tension than large crack-like defects, as long as there is sufficient strain hardening.

Karachalios *et al.,* 2013 investigated the effect of increasing size of artificial rectangular and circular defects located in the middle of the single lap joint on joint strength. Two different

adhesives, one strong and ductile and the other weak and brittle, and three different types of steel were used to fabricate single lap joints in a variety of configurations. In the case of a toughened structural adhesive, a linear decrease in joint strength was observed with increase in defect area. In the case of the brittle adhesive, the reduction in strength was noticed with increase in defect size as the case with a ductile adhesive, but it is not proportional for small defect sizes. It was also concluded that in the case where failure is dominated by the bonded area, the size of the defect influence more on the strength, but not shape of the defect.

The work done by Perton *et al.,* 2011 describes a new method involving the propagation of high amplitude ultrasonic waves to evaluate the adhesive bond strength at high strain rate. The resulting tensile forces normal to the interface were used to estimate the delamination inside the laminates. The same was used to evaluate the bond strength. The effect of surface roughness on the bonding strength of adhesives like epoxy and cyanoacrylate was studied by Uehara and Sakurai, 2002. It was found that the optimum value of roughness is in the range of 3-6 μm with respect to tensile strength of the adhesion. There is no clear relationship observed between the peel strength and the surface roughness for different types of adhesives. Pereira *et al.,* 2010 investigated the effect of surface treatment and adhesive thickness on the shear strength behaviour of aluminium alloy adhesive lap joints. The lap joints were fabricated by using a high strength epoxy adhesive. The surface treatments using sodium dichromate–sulphuric acid etch and abrasive polishing showed improved joint shear strength as compared to caustic etch, and Tucker's reagent etch. The shear strength of single lap joints was found to be increased with decrease in surface roughness, increase in base sheets thickness and overlap length.

The presence of defects in the adhesive layer increases the peak stress levels around the defects and the joint may fail at the ultimate stress or it may fail under cyclic loading where local debonding near the flaw can develop. Analytical studies on the influence of through gaps which may be called as a debond or a void in single-lap adhesive joints subjected to combined axial and bending loads show high peel stresses at the free edges created by the gap. It was also shown that there is a difference of the order of 20% in maximum shear stress occurred in the presence of central void size of up to 70% of the overlap length which is very close to the overlap ends (Olia and Rossettos, 1996; Rossettos *et al.,* 1994). The presence of strip defect affects slightly the specific strength of the single lap joint and there is no effect of size of the defect on specific strength of the joints. The maximum load decreases with increase in size of the defect (de Moura *et al.,* 2006).

Srivatsan *et al.,* 1999 reported the impact toughness properties of fine steel wire-longitudinally reinforced polymer matrix composites and then bonded by an epoxy adhesive on the surface of the base metal. Impact test was performed on the longitudinally reinforced polymer with 8 and 16 number of wires at different temperature of 30 °C, 0 °C, -70 °C, and -190 °C. The results showed that the impact toughness of the polymer composites and the base material degraded with a decrease in test temperature. The impact toughness of the 16 wires reinforced polymer matrix was lower than the impact toughness of the 8 wires reinforced polymer matrix at 0 °C and 30 °C with no difference at the lowest temperature of -190 °C. Forte *et al.,* 2000 investigated the influence of glass fiber reinforced adhesive on the fracture behaviour by analytical and experimental methods. A plane strain analysis was used to determine the energy-release rates for mid-plane cracking in aluminum-bonded specimens with different amounts of adhesive reinforcement. During modeling, the adhesive layer and the mid-plane traction free crack was developed using the large radius axisymmetric damage model (LRAM). The LRAM was developed as a convenient way to approximate the thermo-elastic stress field and energy release rates of laminated bodies subjected to various idealized cracks. The results showed that there was an increase in extension and shear moduli with increase in fiber volume, while Poisson's ratio showing decreasing trend.

Cheng *et al.,* 2007 described the contribution of the active composite layer to the reduction of stress concentrations in the adhesive layer during the design and analysis of a shape memory alloy (SMA) reinforced joint. The first-order shear deformation theory was employed to conduct stress analyses of the joint system, and the state-space method was used to obtain the final analytic solutions, including the peel and shear stresses in the adhesive layer. The results showed that the active composite layer reduces stress concentrations at the joint edges. It was shown that increasing the processing temperature and/or increasing the volume fraction of the embedded SMA fiber/wire could reduce the maximum peel and shear stresses in the adhesive layer.

Khalili *et al.,* 2008 investigated on the chopped glass fibres and micro-glass powder reinforced epoxy adhesive in single lap joints subjected to tensile, bending, impact and fatigue loads. The adherends were glass reinforced composite laminates. The adhesive region was analysed with different fibre orientations (0°, 45° and 90°) at a constant volume fraction and different micro-glass powder volume fractions in the joints. The results showed that 0° and 45° orientations of glass fibres in the adhesive increase the joint strength, while 90° shows a decreasing trend. The use of optimum volume fraction of micro-glass powder reinforced in the adhesive showed the significant

improvement in performance. Zhang *et al.,* 2011 developed a carbon fiber reinforced adhesive for fabricating carbon/carbon composites. It was found that the strength of adhesive was a cubic function of the volume fraction of carbon fiber. It was concluded that the carbon fiber could bridge the adhesive matrix and as a result of bridging effect the extension of micro-crack is inhibited.

Hufenbach *et al.,* 2012 investigated the effect of surface preparation of steel wires reinforced in the Magnesium metal matrix composites. It was observed that the impact resistance of magnesium improves by the steel mesh reinforcement. Aboubakr *et al.,* 2014 reported the creep of epoxy–nano clay composite at the FRP interface. It was recommended that epoxy creep at the FRP interface could be reduced by filling about 10% clay content. Nam *et al.,* 2014 investigated the influence of Polyurethane (PU) adhesive reinforced with chopped glass fibers in double-cantilever-beam joints composed of stainless steel and aluminum adherends on fracture toughness at cryogenic temperature. An optimal reinforcement method was suggested for the appreciable performance of PU adhesive at cryogenic temperatures.

Vietri *et al.,* 2014 developed adhesive formulations based on epoxy/nanostructured carbon for preparing toughened epoxy aeronautic adhesives. Different types of nanofillers were dispersed into an epoxy matrix. It was found that the nanofiller of carbon in the epoxy adhesive exhibits a significant improvement in the relevant mechanical performance and bond strength of the joints as the weight fraction of carbon nano-fillers increased from 1.37 to 5 wt.%. Takano *et al.,* 2001 carried out an experimental study and developed a microstructure-based process analysis on knitted fibre reinforced thermoplastics in deep drawing process. The homogenization theory was applied to analyse the micro-macro coupled behaviour of the knitted fabric composite material during large deformation in the deep-drawn product. Behrens *et al.,* 2010 investigated on the effects of hydro-mechanically deep-drawn parts with local reinforcements. The localized reinforcement was accomplished by the bonded blanks technology, where base sheets are locally joined with reinforcement of sheets made of different materials by adhesive bonding. The results showed that the optimization of the used reinforcement improved the formability. Nakamura, 2009 carried out a study on the tensile deformation and deep drawing of the green composites reinforced with ramie woven fabrics at high temperature. Several conditions to cause more deformability of the green composites were found. The results showed that the fracture strain at high temperature increases significantly as compared to that of room temperature, and initial deformation resistance of the composites seen at room temperature, was not seen at high temperature.

From the above discussion, it is perceived that the adhesive properties influence the mechanical properties of the adhesive bonded blanks significantly. Further, the mechanical behaviour of adhesive bonded blanks is also influenced by adhesive defects, nano fillers, and various reinforcements. Most of the works on adhesive bonded blanks present the delamination behaviour, strength analysis, and wrinkling, rather the formability issues.

1.2.8 Modeling and simulation of adhesive bonded sheets

In the modelling of adhesive bonded blanks, Crocombo, 1989 stated that the term global yielding, which applies when a path of adhesive along the overlap region reaches the state in which it can sustain no further significant increase in applied load. It was found that global yielding gives accurate joint strengths during prediction. Kim *et al.,* 2011 introduced the superimposed meshing technique in the finite element method for adhesive bonded joints to overcome difficulties in manual meshing technique. A cohesive zone model was used to model the interface between substrates and adhesive layer. It was found that the simulation of adhesive joints shows accurate results with the superimposed finite element discretization method. In the analysis of adhesive bonded floor beam with the aim of reducing weight and implementing in the aircraft structures, the two metal parts and the adhesive layer were assembled together by tying the nodes during finite element simulation. The FE models and the tests used during this study show a reduction in weight of 12.5% for Al-2024 and 37% for Al-7075 (Monaco *et al.,* 2009).

Nassar *et al.,* 2012 proposed a damage model for analysing the deformation and interfacial failure behaviour of an epoxy resin bonded single-lap thick joint with the effect of adhesive overlap length, thickness, and plasticity. It was concluded that increased plastic deformation of the adhesive makes the interfacial stress distribution more uniform, while there is no considerable effect of adhesive thickness. Nishimura, 1993 proposed a new method for analyzing stress intensity factors of pre-existing multiple cracks at different locations of base sheets in an adhesively bonded metallic sandwich sheet in the presence of adhesive debond. It was found that the stress intensity factor of multiple cracks in a sandwich sheet is slightly larger than that of a single crack. The combined effect of multiple cracks in the same sheet was not so large, but for cracks in different sheets the effect was greater. The effect of adhesive debonding on the stress intensity factor was greater than that of the multiple cracks in the base sheets of adhesive bonded blanks.

Czamocki and Piekarski, 1986 predicted the joint strength of adhesive bonded joint by finite element method. Four different criteria including maximum normal stress criterion, modified distortion energy criterion and two criteria for polymers in biaxial state of stress were used in the prediction. The results showed that there is about 10% difference in joint strength between experiment and predictions. May *et al.,* 2014 introduced a rate-dependent constitutive law for cohesive interface elements for the adhesive considering both the rate dependency of the initiation stress and the rate dependency of the fracture toughness. The material model was validated by comparing finite element predictions showing good agreement to the experimental data. It was demonstrated that the use of developed rate dependent cohesive zone models is suitable for modelling the response of adhesively bonded metallic structures subjected to crash loading. Most of the studies on adhesive bonded blanks are mainly aimed on predicting the joint strength and fracture mechanisms.

From these analyses, it is found that the adhesive bonded blanks are modelled by various techniques such as global yielding concept, cohesive zone model for adhesive layer, tying the nodes at the interface of substrates. It is perceived that all these adhesive bonded blanks modelling methodologies are mainly focused on intact locking at the interface of base materials rather considering the inherent properties of adhesives.

1.2.9 Formability Analysis

1.2.9.1 Introduction to formability of sheet metals

The formability is a measure of the ability of the sheets to deform plastically during a forming process in order to produce a desired component with definite requirements on mechanics, dimension and appearance, being mainly limited by the occurrence of flow localization or instability.

In the sheet metal forming processes, the major failure modes are localized necking, wrinkling and fracture. The localized necking occurs due to the excessive stretching which causes plastic instability. Generally, the formability of sheet metals is evaluated using the concept of forming limit diagrams (FLDs). The limits of the formability of metals are commonly represented by forming limit curves (FLCs), which indicate the magnitudes of strain at the onset of localized necking in different strain paths (Hasan *et al.,* 2014). The forming limits were initially developed by Keeler and Backhofen, 1964, and Goodwin, 1968 provided a useful empirical gauge of forming limits in

stamping processes, which relates the major and minor strains in the surface of a sheet where plastic flow localization or failure occurs.

It is generally understood that both localized macroscopic defects and distributed microscopic defects where localised plastic deformation takes place result in the failure of 'as received' materials. These defects influence the subsequent deformation and mechanical behaviour of the bulk material significantly. The conventional fracture mechanics deals mostly with the influence of a major crack which is assumed to be present in a defect free continuum. The damage mechanics widely deals with the collective effect of distributed microscopic defects without a major crack (Wang and Kuang, 1996). Related to this context, Marciniak and Kuczynski (M–K) (1967) predicted the limit strains of the sheet metal as a function of the initial geometrical inhomogeneity of the sheet metal, strain-hardening exponent, coefficient of normal anisotropy, initial plastic strain, and strain at which the fracture occurs. The loss of stability was analysed by a groove in a direction perpendicular to the larger principal stress, where local strains begin to concentrate gradually during biaxial tension of sheet metal. The physical inhomogeneity was reduced to the equivalent geometrical inhomogeneity and thus expressed by the coefficient *'f'*. The initial inhomogeneity of the material, $f = t_B/t_A$ (where t_B – thickness in the groove region and t_A – thickness in the bulk region of the sheet metal) exhibits significant influence on the limit strain. For the fully homogeneous material, $f = 1$, the strain attains a large value. The results showed that the value of the limit strain increases as the inhomogeneity of the material reduces, or the coefficient *'f'* increases. Marciniak *et al.,* 1973 predicted limit strains in sheet metal subjected to biaxial tension based on the assumption of initial inhomogeneity of the material with the considerations of strain-rate sensitivity, and planar anisotropy. It was concluded that the limit strain and shape of the FLC are influenced by the coefficient of inhomogeneity of sheet metal, strain-rate sensitivity exponent, and strain hardening exponent. By the influence of planar anisotropy, the results showed two different branches of limit strain curve for sheet metal in the direction of rolling and normal to it, which are intersected asymmetric to the common strain line. It was concluded that it is necessary to draw both branches of the strain curve in the direction of rolling and normal to it, for complete representation of the forming limit of sheet metal.

Parmar and Mellor, 1978 followed the M-K model to predict the limit strains in frictionless in-plane stretching. This analysis is particularly useful for describing the plastic behaviour of materials with the plastic strain ratio (*r*-values) less than unity. Further, Parmar *et al.,* 1977 proposed that the

effective thickness of a plastically deformed sheet metal decreases with increase in surface roughness which occurs with increasing strain so that a tensile instability condition occurs at surface strains smaller than those predicted results. The limit strains were predicted with the assumption that the localised necking develops into a groove at the instability condition. Al-Qureshi *et al.,* 2005 analysed the influence of surface roughness that is related directly to the grain size to the onset of plastic instability and necking conditions in the stretch forming of thin sheet metals. The roughness was represented by the modified sinusoidal nonlinear model thickness variation, and the limit strains were evaluated based on the modified Al-Qureshi/Bressan theoretical model considering surface asperities. The results showed that the plastic instability strains decrease in all cases as thickness to grain size ratio decreases.

Bate and Wilson, 1984 analysed the development of strain localisation in a biaxially stretched sheet of work hardening material which contains a regular array of axisymmetric defects model, and long groove model by the finite element method. It was concluded that the strains developed in the defects at stages of deformation close to localisation failure are much higher in the axisymmetric defect model than in the corresponding long groove model. Ghazanfari and Assempour, 2012 made an attempt to eliminate the requirement of experimental data for determining the FLD with the M–K model in order to find the initial inhomogeneity coefficient and calibrate the diagram. The geometrical inhomogeneity was replaced with material inhomogeneity. The advantage of assuming material inhomogeneity like strength inhomogeneity (K), anisotropy inhomogeneity (R), and strain hardening inhomogeneity (n), rather than geometrical inhomogeneity is to derive an empirical law to predict a value of $N= n^a/n^b$ (n^a and n^b – strain hardening exponent in the bulk region and groove region, respectively) for different materials. The empirical law for evaluating the value of N resulted in FLDs to be in good agreement with experimental diagrams.

Evangelista *et al.,* 2002 introduced a modification of the M-K method by using finite element method, and a modified homogeneity factor which is defined as the ratio of the strength constants in the material constitutive equation, for the two regions such as bulk region and groove region of the M-K model. The FLDs were predicted well using modified M-K method. Rocha *et al.,* 1984-1985 analysed the occurrence of plastic instabilities of a rate-sensitive anisotropic material through modified M-K analysis. The plastic flow was analyzed using a two-zone model in which heterogeneity in the sheet metal was described in terms of a groove inclined at an angle to the principal minor stress direction as one zone, and the homogenous region as bulk zone. The influence

of the anisotropic behaviour of the sheet was analysed using Hill's theory of plastic anisotropy. The FLDs were evaluated for proportional loading, and for non-proportional loading through uniaxial tension and biaxial stretching. It was observed that the hypothesis of normality between the groove and the major principal stress axis is not valid in the case of anisotropic materials for proportional loading under biaxial stress states. The results showed that the critical limiting strains are dependent on the initial band orientations.

Banabic and Dannenmann, 2001 analyzed the influence on the FLDs by using the parameter *'a'* (the ratio of the uniaxial yield stress and biaxial yield stress) during bi-axial stretching of a sheet metal. The yield criterion by Hill (1993) was used for evaluating the limit strains with the Swift's instability condition for diffuse necking, and also by using the M-K analysis. It was found that the increase of parameter *'a'* causes a significant increase in the limit strains. In the case of the M-K theory, the parameter '*a*'significantly influences the shape and position of the FLDs. Further, Banabic, 1999 proposed a more realistic model for predicting FLDs by using an extra parameter $t=\sigma_1/\sigma_b$ (where σ_1 – principal stresses, and σ_b – yield stress obtained by the bulge test) with the plastic function in the yield criterion by Hill (1993) and validated.

Tang and Tai, 2000 carried out a study on the evolution of preferred grain orientation, its effect on plastic deformation, and mechanical properties based on crystallographic theory, and the continuum mechanics of textured polycrystals (CMTP) technique. The mechanical damage due to microdefect development was also studied using continuum damage mechanics (CDM). The forming limit strains in biaxially-stretched textured sheet were predicted using the M-K model. The results showed that the proposed method could reduce the over-estimation of limit strains in the biaxial stretching state. It was concluded that the most important factors influencing the forming limits are the plastic damage, crystal texture and initial surface roughness of the metal sheet. During prediction of forming limit strains of the sheet metal using M-K model, the inhomogeneity factor *'f'* varies from 0.99 to 0.95.

Ragab and Saleh, 2000 predicted the forming limit diagram assuming that necking is initiated due to the presence of initial heterogeneous distribution of void-like defects in the sheet metal at which the strain grows unstably. A modified constitutive model for voided materials based on Green's yield function was developed to predict the forming limit diagram with the consideration of work-hardening exponent, strain-rate sensitivity, and normal anisotropy of the sheet metal. The results showed that the consideration of void growth into a model to predict forming limits shows

good agreement with the experiments. Butuc *et al.,* 2011 analysed the sheet metal formability using the physically-based hardening model considering the evolution of the anisotropic work-hardening induced by the microstructural evolution at large strains. The onset of localized necking was simulated based on the M–K analysis, with the phenomenological anisotropic yield criterion, Yld2000-2d. It was concluded that the transient hardening effects are not the main factor influencing the formability. The microstructural hardening model proves to capture very well the hardening behaviour of the sheet, including strain induced anisotropy. Stoughton and Yoon, 2012 proposed the polar effective plastic strain forming limit diagram (PEPS FLD) in reference to its polar nature, and its radial variable defined by the effective plastic strain. The primary advantages of the PEPS FLD over other diagrams based on variables with stress dimensions is the lack of dependence on the stress-strain relation, and any saturation or softening that could be included in the material model.

Further, the plane-strain formability test provides useful information about the mechanical behaviour of sheet material, such as yield function shape and work hardening parameters. This test can be used in strain-path dependency studies and forming limit diagram characterization in a critical strain condition for real stamped parts (Floresa *et al.,* 2010). Wagoner, 1980 developed a technique for measurement of plane-strain work hardening which eliminates the experimental uncertainties of large strain gradients, friction, and out-of-plane bending inherent in the usual plane-strain deformation mode. From the test results of 2036-T4 aluminum alloy with different types of plane-strain specimens by modifying the dimensions of specimen shown in Fig. 1.1(a), it was found that the work-hardening rate in plane-strain is lower than that in uniaxial tension. The results also showed that there is no considerable effect of varying root radius and notch angle on strain distributions with the fracture strain variation between 0.09 and 0.11, while the plane-strain region is 75-80% of total width at the notch. When maximizing plane-strain region to 90% of total width, the fracture strain from 0.08 to 0.10 was observed. As a result of further effort by increasing notch radius and also plane-strain region to 80% of total width, the specimen fails at centre and showed strain between 0.14 and 0.18. This specimen geometry was chosen for further analysis.

Further, Wagoner, 1981 extended tensile tests and plane-strain tests on an aluminum-killed steel and a cold-rolled dual-phase steel. Two types of plane-strain specimen configurations were tested as shown in Fig. 1.1(a, b). After critical analysis, the specimen geometry shown in Fig. 1.1(b) was chosen for further analysis. The results showed that beyond the uniform strain, there are indications

that the uniaxial tension work-hardening rate exceeds the work-hardening rate in plane-strain. The thicknesses mentioned in the figure are for different materials.

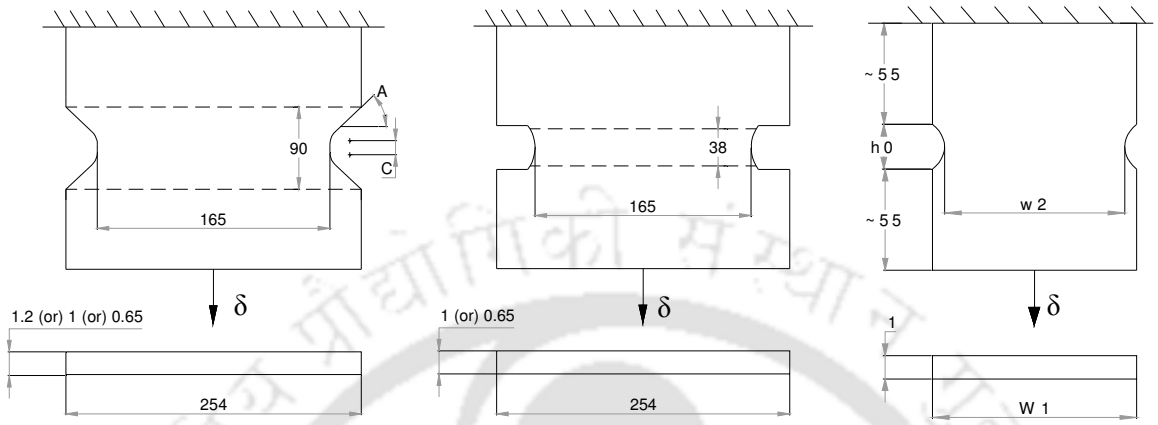

Fig. 1.1 Schematic of plane-strain specimen geometry (a) IPPS-Type 1 (Wagoner, 1980), (b) IPPS-Type 2 (Wagoner, 1981), and (c) IPPS-Type 3 (Holmberg *et al.,* 2004); (where δ - displacement) All dimensions in mm.

Holmberg *et al.,* 2004 developed in-plane plane-strain sample geometry as shown in Fig. 1.1(c) for determining the forming limit of sheet metals and tested with mild steel and high strength steel materials. Since an exact plane strain condition is difficult to achieve, the results showed a minor strain of about 2–4% occurred during the test. It was concluded that the specimen free length should be as small as possible and width should be as per convenience and the width of the wedges to get a condition as close to plane-strain in the middle region of the specimen. Mukesh *et al.,* 2013a and Mukesh *et al.,* 2013b carried out a study on the influence of friction stir welding process parameters and external flash on the formability of friction stir welded blanks in the plane-strain condition. The optimized in-plane plane-strain sample showed a minor strain of about 2–5% during the test. Branco *et al*., 2014 developed the plane strain specimen geometries at a controlled level by introducing U-shaped and V-shaped grooves in the standard middle-cracked tension specimen to reduce the size of the plane stress surface regions. A plane strain state criterion was proposed and less severe plane strain state criteria were also established from which alternative specimen geometries were obtained.

From these studies, the general forming behaviour studies and their predictions by numerical and analytical methods are understood.

1.2.9.2 Prediction of formability of sheet metals by neural networks

Apart from the numerical and analytical approaches of prediction of forming limits sheet metals, while focusing on the soft computing applications especially on neural network method in the sheet metal forming process to overcome the difficulties arise during mathematical modelling of conventional and typical materials behaviour, Wang *et al.,* 2000 introduced a model based on a feed forward back propagation artificial neural network to predict the critical geometrical criteria for wrinkling of formed sheet components. The geometrical features of various formed parts were generalized and correlated with surface behaviour whether wrinkled or wrinkle-free. It was found that the developed network could predict a large portion of the occurrence of wrinkling based on the given information on the geometrical features of points. Shahin and Elchalakani, 2008 investigated the feasibility of using artificial neural networks (ANNs) for developing accurate and simple-to-use models for predicting the ultimate pure bending of steel circular tubes. Multilayer feed-forward neural networks that were trained with the back-propagation algorithm using four design parameters such as tube thickness, tube diameter, yield strength of steel and modulus of elasticity of steel as network inputs and the ultimate pure bending as the output. The results showed that ANNs outputs are in good agreement with the experimental results. Elangovan *et al.,* 2010 introduced feed forward back propagation neural network (BPNN) to predict forming limit diagram of perforated sheet with a set of geometrical variables as its inputs and the safe strains as its output. The activation function tan-sigmoid and purelin were used in hidden layer and output layer, respectively. Levenberg–Marquardt algorithm was used chosen for training the network, and the performance of the network was calculated by mean squared error (MSE) performance function. The results showed that the BPNN with two hidden layers having eight neurons trained with Levenberg–Marquardt algorithm was found to be the optimum network model.

Kotkunde *et al.,* 2014 investigated the influence of punch speed, blank holder pressure (BHP) and temperature on forming limit diagram (FLD) of a Ti-6Al-4V alloy. Taguchi technique was used to identify the influence of input parameters on major strain and minor strain. The output data was generated through finite element model of deep drawing process. The major and minor strain values were predicted using a feed forward back propagation based ANN model with the input parameters used in the finite element simulation. The results showed that there is a good agreement between ANN prediction and actual output data.

Gisario *et al.,* 2011 estimated the springback of aluminium sheets during laser bending by measuring the difference between the nominal bending angles. Neural network solutions were proposed to improve the correlation between experimental and numerical data, with the multi-layer perceptrons trained by back-propagation algorithm. The inputs such as starting deflection, power, scan- speed, passes and spot area were considered and the bending angle was considered as response. Only one hidden layer was considered, and the hyperbolic tangent function was used as activation function both in the hidden layer and output layer. The mean squared error value was calculated for judging the performance of the network. It was concluded that neural network solutions could be very useful in predicting, controlling and managing springback of sheets.

Abbassi *et al.,* 2013 proposed an approach based on GTN finite element-ANN hybrid model in order to evaluate the ductile damage and fracture phenomena with a minimized computing time compared with the classical inverse identification method. The neural network model was trained by back propagation algorithm using the finite element results of notched tensile test with varying of the damage parameters. The developed ANN model showed its better performance with well predicted results.

Veera Babu *et al.,* 2009 developed an ANN model based on feed forward back propagation algorithm to predict the tensile behavior of tailor welded blanks (TWB) made of steel grade and aluminium alloy base materials with the effect of thickness ratio, strength ratio, and weld conditions. The optimized neural network structure holds 2 hidden layers with tan-sigmoid and linear activation functions. Finite element simulation was carried out to generate output data for training the ANN model. The validated results showed acceptable prediction errors. An expert system framework was proposed using the trained ANN for designing TWB conditions.

Patel *et al.,* 2012 developed a cellular automata finite element–artificial neural network (CAFEANN) hybrid model to predict the evolution of grain size and yield strength during friction stir welding. The output data generated from the finite element model with the effect of different weld conditions were trained by the developed feed forward neural network back propagation ANN model. Levenberg Marquardt algorithm was used to train the network. The sigmoid activation function was used for calculating the outputs, and MSE function was used to judge the performance function of the network. It was concluded that the developed CAFE-ANN hybrid model could be used to predict, and analyze the effect of welding parameters on the grain size and yield strength evolution.

Tiryaki *et al.,* 2014 developed a feed forward and back propagation multilayer ANN model for predicting an optimum bonding strength of heat treated woods. The input parameters such as grain orientation, time, feed, temperature, wood species, and adhesive types were considered. The ANN results were compared with the results of multiple linear regression (MLR) model. Two hidden layers were used in the ANN model. The hyperbolic tangent sigmoid transfer function in the hidden layers and linear transfer function in the output layer as the activation function were preferred. The Levenberg–Marquardt algorithm was used as the training algorithm. The gradient descent with a momentum back propagation algorithm was used as the learning rule. MSE was calculated in order to judge the performance of the network. It was shown that the ANN model having good agreement with MLR model in all cases. The results also indicated that the developed model is an effective tool for optimizing the effects of heat treatment conditions on bonding strength of wood.

From these studies, it is understood that neural network approach has been widely used in sheet metal forming behaviour prediction. It is found that the neural network approach is not used for predicting general sheet metal forming behaviour, but also it is used for predicting various results of welded sheets, and bonded joints.

1.2.9.3 Forming behavior of adhesive bonded sheets

In this section, the some of the important studies on formability of adhesive bonded sheets and some relevant studies are discussed. Parsa *et al.,* 2010 carried out a study on the forming behaviour of sandwich sheets made of Al3105/polypropylene/Al3105 (Al/PP/Al) using thin film hot melt adheres with different thickness ratios by monitoring limiting drawing ratios (LDRs) in the experiment. It was found that the limiting drawing ratio decreases with increase in polymer core thickness. It was observed that the interface remains almost intact during conventional sheet metal forming processes. Morovvati *et al.,* 2010, 2011 carried out a study on the wrinkling behaviour of single layer and two layer sheets bonded using polyurethane adhesive during deep drawing process. The results showed that increase in blank holding force (BHF) decreases wrinkling in the deep drawing of bonded sheets. For a given blank diameter, increase in punch diameter tends to decrease BHF and for a given punch diameter, increase in blank diameter decreases BHF. Aghchai *et al.,* 2008 carried out a study on the formability of a two layer metallic sheet (Al1100/St12) bonded by polyurethane adhesive. It was concluded that the two layer sheet improves the formability of a low formable constituent.

Weiss *et al.,* 2007 investigated the influence of temperature on the forming behaviour of A1/PP/Al sandwich sheet through shear and tensile tests, four-point bend and channel tests. It was concluded that the core material properties influence on the forming behaviour of metal/polymer laminates in some, but not all, forming processes. Kee *et al.,* 2009 applied aluminum sandwich sheets with polypropylene core for an automotive hood part with the aim of reducing weight after conducting in-plane stretching and out-of-plane stretching tests. The fabricated sandwich hood was 65% lighter than the steel sheet and 30% lighter than an aluminum alloy sheet.

D'Urso and Maccarini, 2012 carried out a study on the formability of aluminum foam sandwich (AFS) panels through three-point and four-point bending tests. It was found that foam density resulted to be the most significant parameter affecting formability, lower density foams led to a remarkable reduction of defect rate. The quality of foam-skin joining resulted to be another significant parameter affecting the formability. The significant debonding and fatigue damage could cause failure of lap joint that will finally lead to structural failure of vehicles.

Takiguchi and Yoshida, 2001; 2003 analysed the plastic bending of adhesive-bonded sheet metals through V-bending experiments. The specific increase of shear strain, as well as of the punch load which related directly to the change of the die-sheet contact boundary conditions was analysed. The condition of deforming sheet at the initial stage supported by two edges of die was so called 'air-bending condition'. It was recommended that the air-bending operation for adhesive-bonded sheet metals for suppressing the shear deformation of the adhesive layer to within an acceptable limit. Further, the same authors proposed a new technique of plastic bending of adhesive-bonded sheet metals. The effect of forming speed on the deformation characteristics of adhesively bonded aluminium sheets was analysed through V-bending experiments and numerical simulations using a rate-dependent constitutive model of plasticity for the adhesive. It was found that the large shear deformation and the geometrical imperfection caused by large transverse shear deformation occurring in the adhesive layer are suppressed by high-speed forming since the deformation resistance becomes higher at high strain rate.

Liu and Xue, 2013 carried out an experimental study on the formability of sandwich sheets with different thicknesses of polyethylene (PE) core. The results showed that the forming limit of sandwich sheet increases with increase in the thickness of polyethylene core and it is higher than the monolithic metal sheet. In the cup drawing of Aluminum/Polypropylene/Aluminum (AA/PP/AA) sandwich sheets, it has been revealed that springback could be reduced by forming at higher

temperature. The decreasing strength of the core material with increasing process temperature increases unwanted wrinkling in the heated cup drawing tests (Weiss *et al.,* 2007). Specifically, in the formability evaluation of AA/PP/AA sandwich sheet for automotive hood, it was shown that the sandwich sheet could reduce the weight and maintain the flexural rigidity as compared to the steel sheet (Kim *et al.,* 2010). Sokolovan *et al.,* 2012 carried out a study on the formability of 316L/PP–PE/316L sandwich sheets with the influence of sample size and core thickness in the deep drawing process. It was found that the forming behaviour of the sandwich sheets is significantly influenced by the geometry of the punch and the core thickness. It was also observed that thicker the core, the more resistive is the outer sheet to drawing. The loading of inner sheet for sandwich with thicker core could be damped by the elastic core.

Oya *et al.,* 2010 investigated the formability of polymer cored multilayered steel sheets fabricated by hot and cold rolling to accomplish interface bond between polymer core and steel sheets. In tensile test, the elongation of the high-strength materials constituting multilayered sheet beyond the original fracture strain limit was observed. The observations after V-bending tests and hemming tests through scanning electron microscope confirmed that no delamination occurred at interfaces. The rule of mixtures was adopted to obtain the flow curve of the constituent high-strength material, and there was a good agreement with experimental results.

From this section, it is observed that even though the formability of adhesive bonded sheets has been investigated, the influence of adhesive layer properties has not been addressed in these studies.

1.2.9.4 Formability prediction of adhesive bonded sheets

In this prediction of adhesive bonded sheets forming behaviour and relevant studies are discussed. Parsa *et al.,* 2010 carried out a predicted the forming behaviour of sandwich sheets made of Al3105/polypropylene/Al3105 with different thickness ratios by monitoring limiting drawing by finite element simulation. During simulation, the interface bonding between polymer core and base materials was done by using cohesive zone model which combines aspects of strength-based analysis and energy based fracture mechanics, in order to simulate the macroscopic damage along polymer-steel interface by specifying a traction-separation response. After deformation also the sandwich sheet was observed to be intact which is not always actual in the experiments. Kim *et al.,* 2003 analysed the formability of the hot roll bonded sandwich sheet AA/PP/AA. The FLD was constructed based on the modified M–K theory employing Hill's 1948 and Barlat's 2000 yield

functions. It was found that the greater thickness is the main cause of the higher formability of the sandwich sheet as compared to that of the skin sheet. It was predicted that the FLD of the sandwich sheet is better than that of the unbonded base sheet. It was suggested that it is necessary to develop a better yield function of the sandwich sheet, considering the mechanical properties of each component of the sandwich sheet to improve the prediction of accurate FLD. Aghchai *et al.,* 2008 studied formability of a two layer metallic sheet (Al1100/St12) in two methods. In the first method, the two-layer sheet was assumed as an equivalent to a one-layer sheet by deriving equivalent mechanical parameters. In the other method, the mechanical properties of each layer were separately utilized to the two-layer sheet. It was found that the method in which the mechanical properties of each layer incorporated separately in the formability of two layer sheet prediction shows good agreement with the experimental results.

Cherouat and Borouchakic, 2009 proposed two approaches to simulate the deep drawing of composite fabrics, such as geometrical and mechanical approaches. The behaviour of the resin was assumed to be isotropic viscoelastic and the behaviour of the fibre was supposed as elastic during numerical simulations. A good correlation between experiment and the proposed approaches were demonstrated. Parsa *et al.,* 2010 carried out spring back evaluation of AA3105/polypropylene/AA3105 sandwich sheet materials after being subjected to double-curvature forming. It was found that the increase of tool radius in one direction not only decreased the spring back in that particular direction but also reduced the spring back in right angular direction.

Liu *et al.,* 2012 investigated the influence of interfacial adhesion strength between skin sheet and core polymer on the formability of AA5052/polyethylene/AA5052 sandwich sheets. The interface conditions between base sheet and core materials were modelled for simulating the forming process of sandwich sheet. The results showed that the interface stress could suppress the increase in void volume fraction and delays the fracture of base sheets. It was concluded that the FLD of sandwich sheet shifts higher with the increase in interfacial adhesion strength.

From these studies, it is understood that the interfacial bonding between two base materials takes a vital role in the forming behaviour prediction of bonded blanks. But the influence of varying adhesive properties on the forming behaviour of bonded sheets has not been addressed, which is the actual occurrence in the practical cases. So, it is mandatory to investigate study the role of adhesive at varying properties on the forming behaviour of adhesive bonded sheets, and its accurate prediction.

1.3 Significance of work

There has been numerous studies on the performance of adhesive joints, mainly focusing on the bond strength, durability, failure investigations, stress distributions, fracture toughness, peel strength of bonds, delamination of adhesives with adherends, fatigue life of adhesives, geometrical effects of substrates on adhesive bonding, spring back of adhesive bonds, defects formation in joints, bonding mechanisms, curing characteristics, temperature of bonding, amount of enforcement pressure, duration of bonding, pre-treatment of adhesive, blend morphology of adhesive, hybrid adhesive properties, and microstructural changes, and a few studies on the forming behaviour of bonded sheets. The following discussion highlights some of the important results revealing the performance of adhesive bonded sheets. Both experimental and modelling results are presented.

The forming of adhesive bonded blanks is influenced by the bonding width, adhesive thickness, and surface roughness of base materials on the tensile behaviour [Ravi and Ganesh Narayanan, 2012]. It is found that the engineering stress attained in forming the bonded blank for the same amount of strain is greater if the surface roughness is greater. There was no effect due to adhesive thickness on the elongation at the break point of the bonded blank. The cohesive zone model is used to model the interface between substrates and adhesive layer during modelling of adhesive bonded sheets, and the simulation of adhesive joints shows accurate results [Parsa *et al.*, 2010; Kim *et al.*, 2011]. Moreover, the metal parts and the adhesive layer assembled together by tying the nodes during finite element simulation [Monaco *et al.*, 2009] is another simple modelling strategy to take care of bonding. In the forming studies of bonded sheets, the wrinkling behaviour of single layer and two layer sheets bonded with adhesive during deep drawing process decreases with increase in increase in blank holding force [Morovvati *et al.*, 2011]. During the formability analysis two layer adhesive bonded metallic sheet the two layer sheet improves the formability of a low formable constituent [Aghchai *et al.*, 2008], but the influence of adhesive layer properties was not addressed in these studies [Aghchai *et al.*, 2008; Morovvati *et al.*, 2011].

The formability of sandwich sheets is influenced the interfacial adhesion strength between skin sheet and polymer core. The FLD of sandwich sheet in the presence of interfacial bonding is higher than the sandwich sheets in the absence of interfacial bond. Moreover, the interfacial adhesion strength shifts the FLD of sandwich sheet to higher level [Liu *et al.*, 2012]. It is also found by da Silva and Adams that the mixing of brittle adhesive and ductile adhesive increases the joint strength of brittle adhesive [da Silva and Adams, 2007]. From these studies, it is perceived that all the

approaches for modelling the adhesive bonded blanks focus on intact interface locking or adhesion between the sheets during deformation which are not actual during experiments. The adhesion force or adhesion strength offered by the adhesive is mainly dependent on the adhesive properties, functional groups, and bonding mechanisms [Brockmann *et al.*, 1982; Gutowski, 1987; da Silva and Adams, 2007]. From these studies, it is found that there is a scope for analysing the role of adhesive properties on the forming behaviour of adhesive bonded blanks, and to resolve the difficulties arise during incorporation of adhesion properties and the instability conditions in the forming behaviour prediction of adhesive bonded blanks.

1.4 Objectives of thesis

The main objective of the present thesis is two fold – (i) Analysing the influence of adhesives on the formability of adhesive bonded sheets, and (ii) Predicting the formability of adhesive bonded sheets with an aim of accurate representation of adhesive during modelling.

The subtasks involved to achieve the main objective are

(i) Investigating the influence of hardener/resin ratio on the formability of adhesive-bonded sheets.
(ii) Studying the formability of adhesive bonded sheets having artificial adhesive defects.
(iii) Analysing the influence of filler in adhesive on the formability of adhesive bonded sheets.
(iv) Exploring the effects of high ductile wire reinforcements in the low ductile adhesive layer on the formability of adhesive bonded blanks.
(v) Predicting the forming behaviour of adhesive bonded blanks without adhesive bonding.
(vi) Prediction through geometrical heterogeneities in the base material.
(vii) Predicting the formability of adhesive bonded blanks by neural network.

1.5 Organization of Thesis

The thesis consists of eleven chapters, which are organized as follows:

- The first chapter has provided an introduction and literature review of adhesive bonding process, significance and objectives of the present work.
- Chapter 2 investigates the influence of adhesive properties at varying hardener/resin ratio on forming behaviour of adhesive bonded sheets.

- Chapter 3 presents the effect of artificially generated adhesive defects on the formability of adhesive bonded sheets.
- In Chapter 4, the formability of adhesive bonded steel sheets with the influence of hardener/resin ratio of adhesive is predicted through finite element simulations and validated with experimental results.
- Chapter 5 demonstrates the evaluation of adhesive mechanical properties by rule of mixtures, and the importance of interfacial bonding between base materials and adhesive on the formidability of adhesive bonded sheets is discussed.
- Chapter 6 presents the experimental evaluation and prediction of formability of carbon blank filled adhesive bonded steel sheets. In this study, the influence of carbon black nano sized powder is filled in the adhesive with different wt.% is investigated and predicted.
- Chapter 7 demonstrates the improvement in the formability of adhesive bonded sheets when low ductile adhesive is reinforced with high ductile wires by experiment and finite element simulation.
- Chapter 8 presents the experimental evaluation and prediction of deep drawability of adhesive bonded blanks at varying adhesive properties. In this study, the adhesive properties are changed by varying hardener/resin ratio and by filling carbon black powder with different wt.%.
- In Chapter 9, the estimation of formability and deep drawability of adhesive bonded sheets using equivalent geometrical heterogeneities is demonstrated and hypothesized. In this analysis, the thickness heterogeneity factor is varied in the base material at varying dimensions of the geometrical heterogeneities in order to predict the equivalent forming behaviour at varying adhesive properties.
- In Chapter 10, the formability of adhesive bonded sheets is predicted by neural network and validated with experimental results.
- Conclusions from the thesis work are presented in Chapter 11 followed by scope for future work and references.

Chapter 2

Investigation on the influence of adhesive properties on the formability of adhesive bonded steel sheets

2.1 Methodology

In this section, the base materials and the adhesives used in the experiment, the evaluation of mechanical properties, testing of adhesive bonded sheets are discussed.

2.1.1 Experimental materials and mechanical properties

Two dissimilar materials namely deep drawing quality (DDQ) cold rolled steel and stainless steel (SS 316L) sheets were used as base materials in the preparation of adhesive bonded blanks. The thickness of base materials is 0.6 mm each. Table 2.1 shows the nominal chemical composition of two base materials as obtained from the suppliers. Before determining the mechanical properties of both base materials, about 40 tensile specimens were cut at different locations in the sheet materials along the rolling direction of the sheets through CO_2 laser cutting machine to test the repeatability of mechanical properties of the base materials. Fig. 2.1(a) shows the dimensions of the tensile specimen according to ASTM E646-07e1 standard. The tensile tests were performed at a nominal cross-head speed of 1 mm/min, at room temperature of 25 °C on the INSTRON 8801 machine (Capacity = 100 kN) and the load-extension behaviour was recorded for all specimens. Fig. 2.2 (a, b) shows the load-extension behaviour of DDQ steel and SS 316L sheets, respectively. From these results, a good repeatability of mechanical behaviour is observed for both DDQ steel and SS 316L sheets. Out of 40 samples of DDQ steel and SS 316L specimens tested, about 4 or 5 samples showed different results. But most of the base material samples show the elongation of 39±2 % and 60±1 % for DDQ steel and SS 316L as shown in Table 2.2 and 2.3, respectively. Among the most populated results, one curve was chosen for both base materials randomly for further comparison. Followed by, the tensile specimens made of both base materials were cut in different directions with respect to rolling direction of the sheets like 0°, 15°, 30°, 45°, 60°, 75°, 90°. After tensile testing of 3 specimens in each direction to check the repeatability, the load-extension behaviour of all 21 specimens was obtained from

the INSTRON 8801 machine data. The load-extension behaviour was converted into engineering stress–strain behaviour, and the mechanical properties such as yield strength, ultimate tensile strength, uniform elongation, total elongation were evaluated. The engineering stress–strain behaviour of all specimens was converted into true stress-strain behaviour to evaluate the strain-hardening exponent (n) and strength co-efficient (K) by following Hollomon's power law ($\sigma = K\varepsilon^n$). Similarly, Fig. 2.2(c, d) shows the repeatability results of epoxy adhesive bonded blanks tested with hardener/resin ratio of 0.6:1 and 1:1. The methodology for evaluating these properties is schematically described in Fig. 2.3. The plastic strain ratio (r) values were evaluated as per ASTM E517-10 standard and the parallel strips were cut along different directions with respect to rolling direction by using power shearing machine as shown in Fig. 2.1(b). The rectangular strips shown in Fig. 2.1(b) were deformed till 20% strain and the longitudinal, transverse and thickness strains were evaluated for finding plastic strain ratios in seven rolling directions. The mechanical properties of DDQ steel and SS 316L sheet materials are listed in Table 2.2 and Table 2.3, respectively. The adhesive systems used in this study were (i) commercially available Bisphenol-A-Epicholorhydrin type epoxy resin (Araldite-AW106→Part A) and Polyamidoamine type hardener (Araldite-HV953IN→Part B), and (ii) two component acrylic structural adhesive (My-T-Bond 1001 (Part A & B)). The details about two adhesive systems obtained from the suppliers are listed in Table 2.4.

Table 2.1 Nominal chemical composition of DDQ steel and SS 316L sheets in weight % (Tata steel, 2012; MTLS, 2012)

Materials	C %	Si %	Mn %	S %	P %	Cr %	Ni %	Mo %	Cu %	Co %	Ti %	V %	Fe %
DDQ steel	0.100	0.12	0.600	0.035	0.040	-	-	-	-	-	-	-	Remaining
SS 316L	0.016	0.335	1.209	0.002	0.024	16.413	10.222	2.164	0.405	0.032	0.012	0.034	69.070

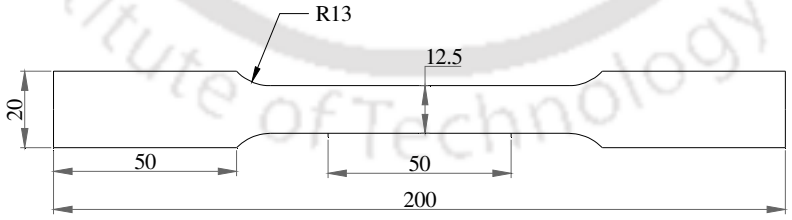

(a)

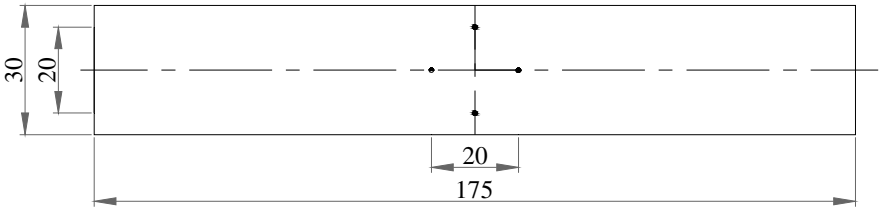

(b)

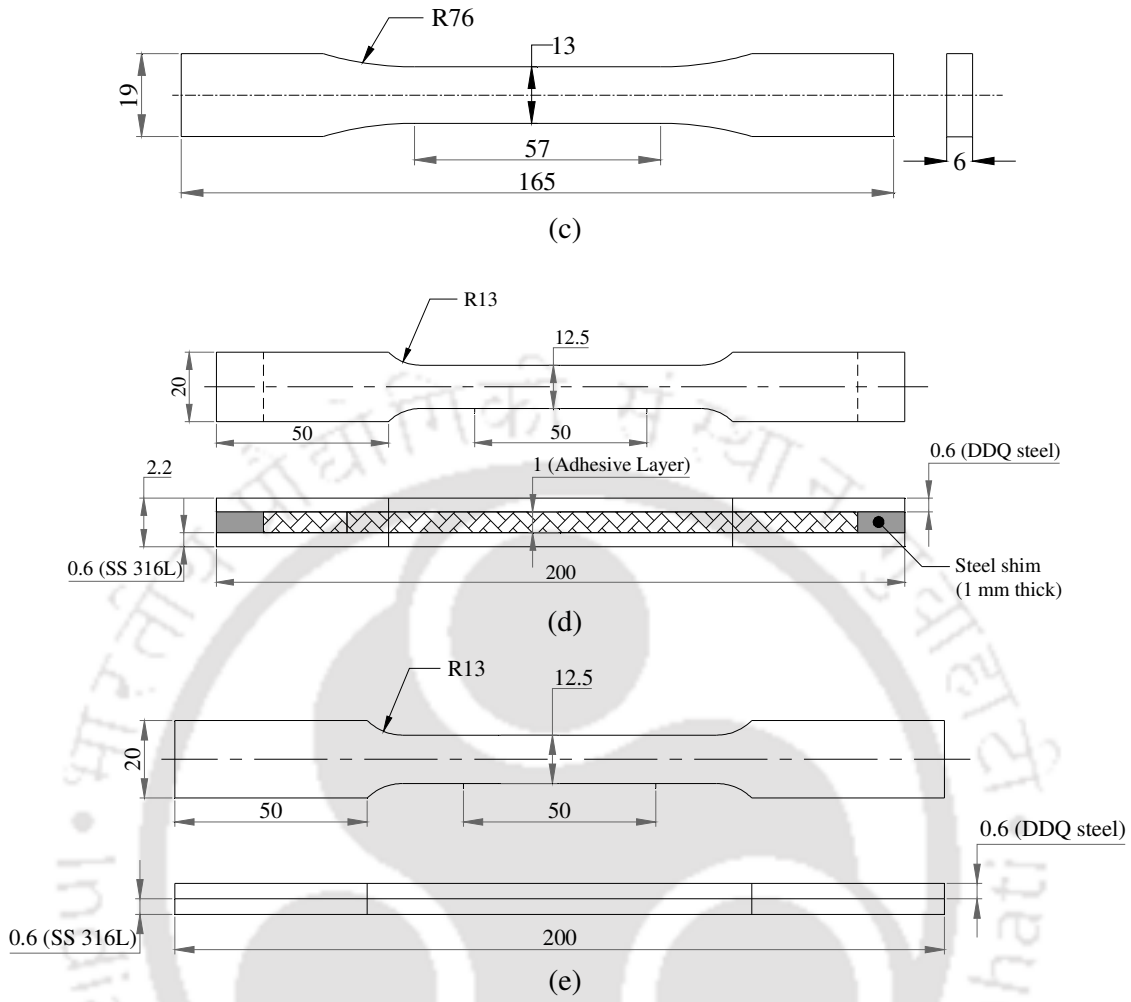

Fig. 2.1 Schematic of testing specimen (a) tensile specimen as per ASTM E 646-98 standard, (b) rectangular specimen used for plastic strain ratio evaluation as per ASTM E517, (c) tensile specimen made of adhesive as per ASTM D 638-I standard, (d) tensile sample made of adhesive bonded steel sheets as per ASTM E 646-98 standard, and (e) double sheet as per ASTM E 646-98 standard (All dimensions in mm)

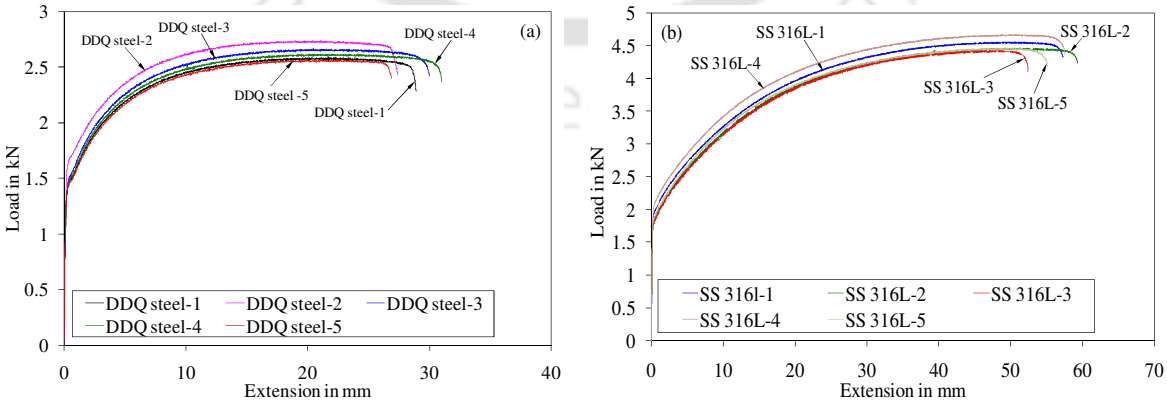

(Error variation obtained from about 50 tensile tests: in maximum load = ±0.06 kN, and in extension = ±1.5 mm)

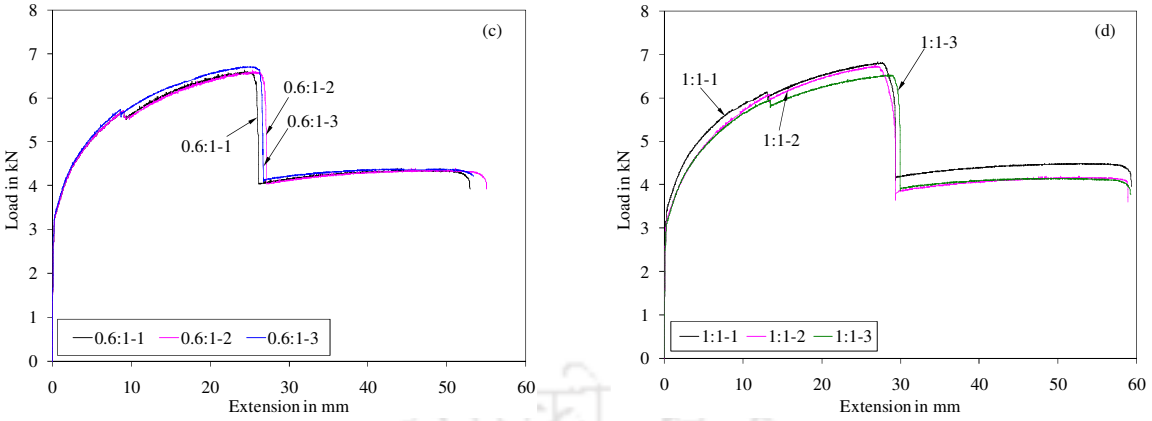

(Error variation obtained from 3 tensile tests: in maximum load = ±0.15 kN, and in extension = ±1 mm)

Fig. 2.2 Load-extension behaviour of (a) DDQ steel sheets, and (b) SS 316L sheets, (Note: Error variation obtained from about 50 tensile tests: maximum load = ±0.06 kN, and extension at failure = ±1.5 mm) (c) Epoxy bonded sheets with H/R 0.6:1 and (d) Epoxy bonded sheets with H/R 1:1 (Note: Error variation obtained from 3 tensile tests: maximum load = ±0.15 kN, and extension at failure = ±1 mm).

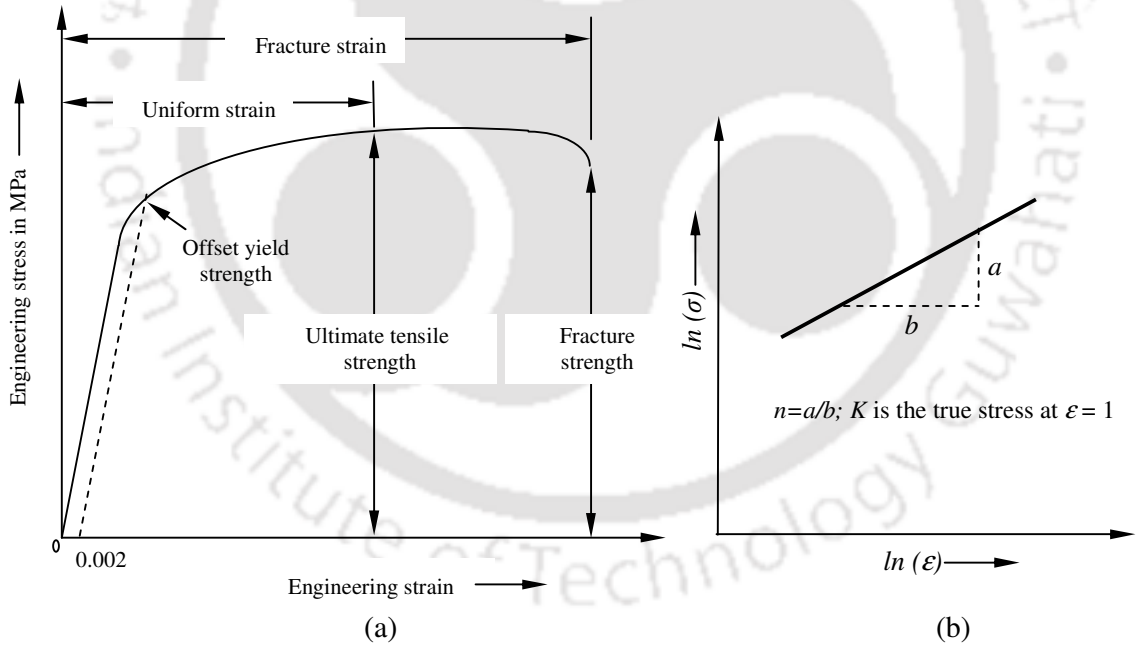

Fig. 2.3 (a) Evaluation of tensile properties from engineering stress-strain curve, and (b) Evaluating *n, K* values from true stress-true strain data

Table 2.2 Mechanical properties of DDQ steel sheets

Rolling direction	Yield strength (MPa)	Ultimate tensile strength (MPa)	Uniform elongation (%)	Total elongation (%) (at 50 mm gauge length)	Strain hardening exponent, *n*	Strength coefficient, *K* (MPa)	Plastic strain ratio, *r*
0°	199±10	352±5	25±1	39±2	0.31	725±25	1.32
15°	185±10	352±4	31±2	35±1	0.30	674±10	1.45
30°	184±3	350±1	34±0.5	36±1	0.29	663±5	1.44
45°	186±5	343±4	32±1	36±1	0.28	646±10	1.13
60°	184±2	347±2	29±3	35±1	0.29	660±3	1.02
75°	176±2	344±2	31±1	35±0.5	0.29	650±10	1.51
90°	182±2	348±5	36±4	35±0.5	0.30	672±10	1.58

Table 2.3 Mechanical properties of SS 316L sheets

Rolling direction	Yield strength (MPa)	Ultimate tensile strength (MPa)	Uniform elongation (%)	Total elongation (%) (at 50 mm gauge length)	Strain hardening exponent, *n*	Strength coefficient, *K* (MPa)	Plastic strain ratio, *r*
0°	229±5	610±5	58±1	60±1	0.57	1760±15	1.32
15°	249±3	609±3	60±1	63±1.5	0.57	1820±20	1.55
30°	243±10	645±5	53±1	61±3	0.56	1740±15	1.48
45°	245±10	583±5	59±2	60±2	0.58	1742±10	1.54
60°	275±10	627±10	61±2	63±2	0.60	1492±20	1.47
75°	263±5	603±5	63±1	67±1	0.61	1464±10	1.62
90°	258±3	610±5	63±0.5	66±1	0.61	1458±10	1.66

Table 2.4 Details of epoxy adhesive and acrylic adhesive obtained from the suppliers (Huntsman, 2012; Metlok, 2012)

Adhesive	Resin/hardener	Appearance	Viscosity at 25°C (cP)	Mix ratio by weight	Pot life in minute	Curing time in hr	Curing temperature in °C
Epoxy	Resin	White opaque paste	30000-50000	1	100	24	25
	Hardener	Brownish yellow, clear to slightly hazy liquid	20000-40000	0.8			
Acrylic	Resin	White opaque paste	5000-7000	1	60	24	25
	Hardener	Yellowish	5000-7000	1			

2.2 Evaluation of tensile properties of the adhesive systems

The adhesive tensile specimens made of epoxy and acrylic adhesive systems with different hardener/resin ratios were prepared according to ASTM D638-10 standard as shown in Fig. 2.1(c) by moulding process. The five different hardener/resin (H/R) ratios were chosen as shown in Table 2.5 depending on the mixing ratio of hardener/resin of both adhesive systems. It is observed

from the supplier sheet that the stoichiometric mixing ratios are 0.8:1 and 1:1 for epoxy and acrylic adhesive, respectively. Hence, two different ratios are considered above and below the stoichiometric mixing ratio as given in Table 2.5.

Table 2.5 Five levels of different hardener/resin ratios (by weight %)

Adhesive system	Levels of hardener/resin ratio				
	1	2	3	4	5
Epoxy	0.6:1	0.7:1	0.8:1	0.9:1	1:1
Acrylic	0.8:1	0.9:1	1:1	1.1:1	1.2:1

Four adhesive tensile specimens were prepared for each hardener/resin ratio with the help of a setup fabricated for the present work. A perspex sheet with 6 mm thickness was cut to make moulds of tensile specimen shape using CO_2 laser cutting machine. The resin and hardener of epoxy adhesive were taken in a beaker with above mentioned ratios measured by using the balancing machine (Make: Sartorius, weighing range from 0.1 mg to 250 g) and stirred with a new spatula every time until ensuring a homogeneous mixture. The adhesive mixture was poured into the mould which is fixed on the setup and the extra adhesive was wiped out with the help of wiping slider in the setup. A thin film of oil was applied at the walls of each mould to avoid bonding between walls and adhesive specimens. The adhesive specimens were allowed to cure for more than 24 hr at room temperature before testing. Since the perspex mould is made of acrylic composition, problems were faced during preparation of acrylic adhesive specimens due to sticking between wall of mould and specimens even after applying grease at the wall. It is suggested that using perspex sheets is not a suitable method for preparing acrylic adhesive specimen and so the expendable moulds made of plaster of paris were prepared by using same dimensions of the mould. Then mixture of hardener and resin of acrylic adhesive was poured into the moulds with above mentioned hardener/resin ratios. Shrinkage was observed more in the case of acrylic adhesive system and more care was taken to maintain uniform thickness. To avoid air bubbles in the adhesive systems, the defoamer namely BYK N066 with weight % of 0.3-0.4 was added during mixing of hardener and resin. The dimensions of each specimen were measured and ensured for dimensional accuracy. The thickness of specimens was measured at five locations in the gauge length and the average thickness of specimens was found to be 6.0±0.05 mm.

All tensile tests on the adhesive specimens were tested through INSTRON 8801 machine with a cross-head speed of 1 mm/min at room temperature. After the completion of each test, the load-extension behaviour data was obtained from the computer system which is interfaced with

testing machine and correspondingly converted manually into engineering stress-strain behaviour of the specimens. Three specimens were tested for each case to check the repeatability and if the repeatability was not sufficient, the fourth specimen was tested. The mechanical properties of adhesive specimens were evaluated as per the methodology schematically described in Fig. 2.3(a).

2.3 Testing of adhesive bonded steel sheets

The adhesively bonded tensile specimens were prepared according to ASTM E646-98 standard by using two types of adhesive systems such as epoxy and acrylic adhesive systems with different hardener/resin ratios (by weight) as given in Table 2.5. Fig. 2.1(d) shows the dimensions of the adhesive bonded specimen. The tensile specimens made of DDQ steel and SS 316L were washed in the soap bath and then cleaned gently in the acetone bath to make surface of the specimens free from contaminants. After drying all the specimens by using dryer, circular grids were printed on the surface of the base material specimens by using rubber stamp and the diameter of circular grids was measured by using profile projector (Make: Optomech PP400TE, accuracy = 1 micron). About 400 circular grids were measured to obtain an average diameter that will be used for limit strain evaluation. The average diameter of circular grids was calculated as 2.8±0.05 mm. The homogeneous mixture with different hardener/resin ratios of epoxy and acrylic adhesive systems were applied on the base materials surface smoothly with the help of the setup. The uniform adhesive thickness was maintained between the two sheets by using appropriate mould and shims between the base materials. Though curing time for both adhesive systems is 24 hr, the adhesively bonded specimens were allowed to cure for more than 24 hr at a constant temperature of 25 °C in oven. Shrinkage was observed more in the case of acrylic adhesive system and care was taken to maintain uniform thickness. To avoid air bubbles in the adhesive systems, the defoamer namely BYK N066 with weight % of 0.3-0.4 was added during mixing of hardener and resin. To ensure the uniform thickness of adhesive layers in the adhesive bonded blanks, about 10 adhesive layers were separated from adhesive bonded blanks after completion of curing and thickness was measured along the centre axis of the adhesive layers at five locations in the gauge region by using digital micrometer. The average thickness of adhesive layers in adhesive bonded blanks was found to be 1±0.015 mm.

All the tensile tests on adhesively bonded specimens were carried out in INSTRON 8801 machine with a cross-head speed of 1 mm/min at room temperature. Also two tensile specimens made up of DDQ steel and SS 316L were placed one above other as shown in Fig. 2.1(e), but without any adhesive, like a double sheet (herein after called as double sheet), and tensile tests

were carried out. After the completion of tensile tests, the load–extension behaviour of all bonded blanks was obtained from the machine data and converted into engineering stress–strain behaviour and true stress – strain behaviour. Further, the limit strain values were evaluated by measuring the length of major and minor axes of the deformed circular grids at the failure region of the tested blanks by using profile projector. The limit strains were measured for both base materials constituting adhesive bonded sheets. Three specimens were tested in each case to check the repeatability, and if the repeatability is not good, fourth test was performed in all the experimental works carried out in the present thesis work.

2.4 Results and discussion

2.4.1 Influence of hardener/resin ratio on the tensile properties of adhesive systems

Before analysing the influence of adhesive properties on the tensile behaviour of adhesive bonded blanks, the influence of different hardener/resin ratios on the tensile properties of both adhesive systems (only adhesive without base materials) are discussed in this section. Fig. 2.4(a, b) shows the load-extension behaviour for different hardener/resin ratios of epoxy and acrylic adhesive systems, respectively. From Fig. 2.4(a), it is noticed that the increase in hardener/resin ratio increases the extension of the epoxy adhesive specimens. About 3.5 mm total extension is observed for the epoxy adhesive specimen with the hardener/resin ratio of 0.6:1. With respect to the extension observed in the adhesive specimen with hardener/resin ratio of 0.6:1, the increase in percentage of total extension is calculated as 5.7%, 28.6%, 74.3% and 82.9% for the specimens with hardener/resin ratio of 0.7:1, 0.8:1, 0.9:1 and 1:1, respectively. A large deformation is observed for the epoxy adhesive specimen with hardener/resin ratio of 1:1. This is due to the excess amount of hardener molecules not finding enough resin molecules to accomplish cross-links. The non-reacted amine groups turn the specimen into plastic in nature. The networks are able to accommodate larger strain due to the amine rich formulation having more cross-link density, indicating improvement in elongation. But in the case of hardener/resin ratio of 0.6:1, relative excess of resin monomer would not find enough hardener molecules which leads less cross-link density, and turns the adhesive specimen into brittle and causes the low deformation capacity. The epoxy adhesive specimens with resin rich formulation would then behave as weak spots like voids in its polymeric structure from where cracks may be originated (d'Almeida and Monteiro, 1996; Saleh *et al.,* 2011). The same phenomena can also be observed with the load–extension behaviour of acrylic adhesive system with different hardener/resin ratios

which is shown in Fig. 2.4(b). It is noticed that the sample with rich acrylic resin formulation with hardener/resin ratio of 0.8:1 shows low deformation.

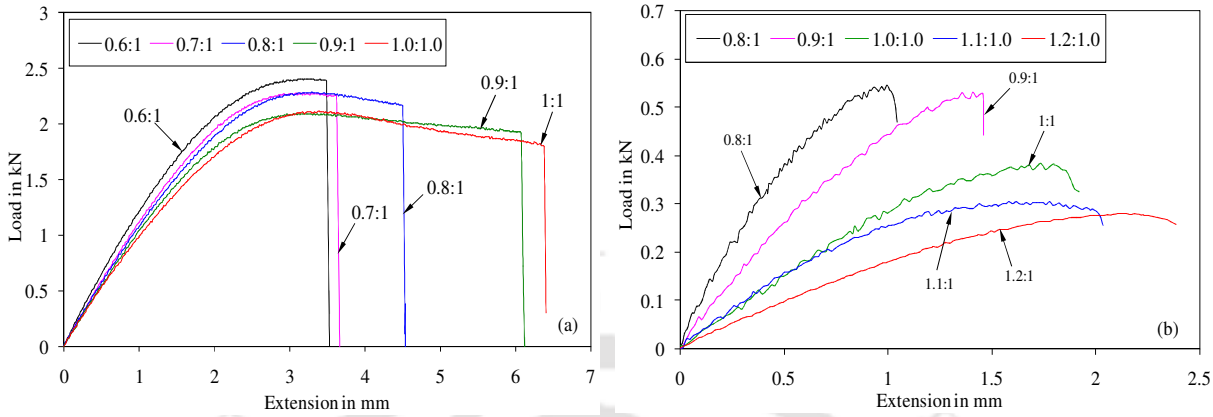

Fig. 2.4 Load-extension behaviour for different hardener/resin ratios: (a) epoxy adhesive, and (b) acrylic adhesive (Error variation in maximum load = ±0.04 kN)

A higher extension is observed for the acrylic adhesive specimen with hardener/resin ratio of 1.2:1 indicating larger deformation of hardener (amine groups) rich formulation case. On an average, 1.1 mm total extension is observed for the acrylic adhesive specimen with the hardener/resin ratio of 0.8:1. With respect to the extension of 0.8:1 case, the increase in total extension is calculated as 32.7%, 72.7%, 81.8% and 118.2% for the specimens with hardener/resin ratio of 0.9:1, 1:1, 1.1:1 and 1.2:1, respectively. The mechanical properties of epoxy and acrylic adhesive systems were then evaluated from engineering stress-strain curves and are listed in Table 2.6. From these results, a decrease in Young's modulus and ultimate tensile strength is observed with increase in hardener/resin ratio from 0.6:1 to 1:1 in the case of epoxy adhesive system and from 0.8:1 to 1.2:1 in the case of acrylic adhesive system, while total elongation shows an increasing trend. These results indicate that the brittle material (resin rich formulated specimens) would exhibit higher Young's modulus, ultimate tensile strength, but lower elongation than the hardener rich formulated specimens.

Similar results were obtained by Saleh *et al.,* 2011 from the tensile testing of adhesive samples by using two part epoxy adhesive systems namely diglycidyl ether of bisphenol A (DGEBA) type resin and two types of hardeners namely diamino diphenylmethane (DDM) and triethylene tetramine (TETA). d'Almeida and Monteiro, 1996 carried out an investigation on the variation of the mechanical properties through compression tests on the epoxy adhesive system (diglycidyl ether of bisphenol-A(DGEBA), with an aliphatic amine, triethylene tetramine (TETA)) formulated with eight resin/hardener ratios which covered a range of epoxy rich and

hardener rich, as well as stoichiometric composed samples. The results of both investigations showed that the epoxy rich systems showed brittle behaviour that is associated with the development of a rigid macromolecular structure. The hardener rich systems showed fracture behaviour characteristic of materials with large deformation. Though d'Almeida and Monteiro, 1996 had conducted compression tests and not tensile tests, some of their test behaviour agrees with the tensile test results of the present work.

Table 2.6 Mechanical properties of epoxy adhesive and acrylic adhesive

Adhesive system	H/R ratio	Young's Modulus (GPa)	Ultimate tensile strength (MPa)	Uniform elongation (%)	Total elongation (%) (at 57 mm gauge length)
Epoxy based	0.6:1	0.995±0.0055	34±3	5.508±0.1	6±0.1
	0.7:1	0.872±0.0055	30±0.5	5.596±0.05	6±0.2
	0.8:1	0.867±0.0055	30±0.5	5.705±0.03	8±0.5
	0.9:1	0.840±0.0055	28±0.2	5.720±0.29	10.5±0.25
	1:1	0.839±0.019	28±0.5	6.093±0.2	11±1.5
Acrylic based	0.8:1	1.870±0.001	26±2	1.9±0.05	2±0.1
	0.9:1	1.400±0.005	25±1	2.47±0.01	2.5±0.02
	1:1	1.150±0.005	20±3	3.05±0.03	3.2±0.1
	1.1:1	0.966±0.002	19±2	3.15±0.03	3.5±0.2
	1.2:1	0.750±0.0065	19±1	3.69±0.05	4.2±0.1

From the above results, it is clear that varying the hardener/resin ratio not only changes the degree of the hardener/resin reaction in the adhesive systems, but also controls structural changes, consequently affecting the forming behaviour.

2.4.2 Failure pattern of adhesive bonded steel sheets

The failure pattern during the tensile testing of the adhesive bonded steel sheets is proposed as follows. Fig. 2.5(a-d) presents the failure pattern of different layers of adhesive bonded sheets like epoxy adhesive, acrylic adhesive, DDQ steel sheet and SS 316L sheet.

(a) Failure of adhesive layer

During tensile testing of the adhesive bonded blanks, all three layers such as adhesive layer, DDQ steel and SS 316L sheet are deformed simultaneously. Till the failure of adhesive layer, the adhesive bonded blank behaves as a global specimen. During failure of adhesive layer (both epoxy and acrylic), a mixed failure including cohesive and adhesive failure was observed. The failure of adhesive layer occurs due to its less ductility when compared to the base materials which can be termed as cohesive failure. Later, the interfacial layer and bonding between adhesive layer and base materials have failed due to relative motion between adhesive layer and

base materials during deformation and this failure can be seen as adhesive failure. The failure of adhesive layer at a location was observed in the case of epoxy adhesive for different hardener/resin ratios as shown in Fig. 2.5(a) and the failure at multiple locations is noticed in the case of acrylic adhesive for different hardener/resin ratios (Fig. 2.5(b)). Elsewhere, Ravi and Ganesh Narayanan, 2012 investigated the influence of sheet surface roughness, adhesive thickness, and bonding width on the forming behaviour of adhesive bonded blanks by bonding interstitial free (IF) steel sheets using Bisphenol-A-Epicholorhydrin type epoxy resin and polyamidoamine type hardener. In their results, during the tensile testing of epoxy adhesive bonded blanks with adhesive thickness of 2.4 mm, a mixed (cohesive and adhesive) failure of adhesive layer was observed at multiple locations for the epoxy adhesive with same functional group. This failure of epoxy adhesive layer at multiple locations may be because of larger thickness of adhesive.

(b) Failure of DDQ steel sheet

After failure of adhesive layer, DDQ steel and SS 316L sheets bear the tensile load and behave as a double sheet. Since the formability of DDQ steel is lesser than SS 316L sheet as observed from Table 2.2 and 2.3, the failure of DDQ steel sheet is noticed after the failure of adhesive layer. Fig. 2.5(c) shows the failure of DDQ steel in the adhesive bonded blank and the location of failure is observed in the gauge region.

(c) Failure of SS 316L sheet

Fig. 2.5(d) shows the failure of SS 316L sheet from the adhesive bonded blank which fails after the failure of DDQ steel specimen. The same failure pattern of adhesive bonded blanks was observed for both epoxy adhesive and acrylic adhesive systems with different hardener/resin ratios.

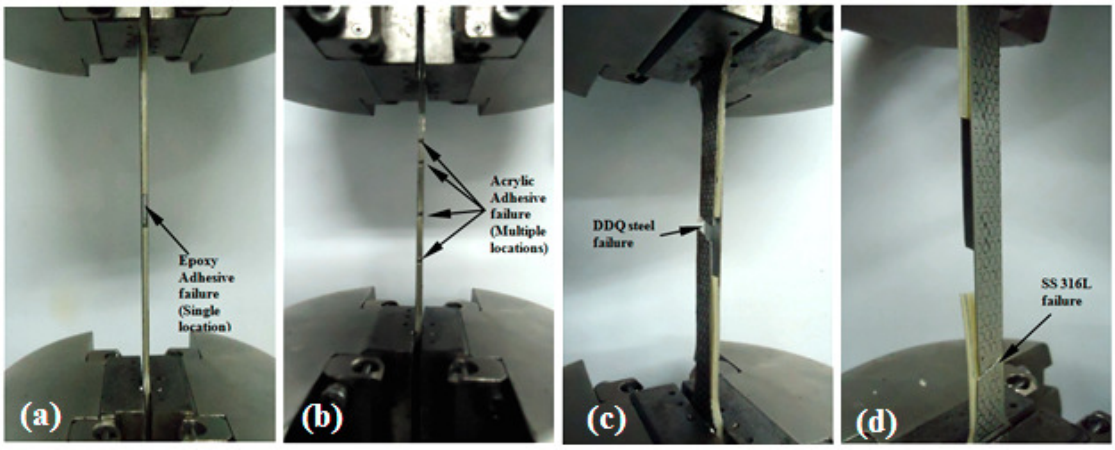

Fig. 2.5 Failure pattern of adhesive bonded blanks (ABB) (a) failure of epoxy adhesive in ABB, (b) failure of acrylic adhesive in ABB, (c) failure of DDQ steel specimen in ABB, and d) failure of SS 316L specimen in ABB

2.4.3 Effect of adhesive properties on the tensile behaviour of adhesive bonded blanks

2.4.3.1 Comparison between double sheet and adhesive bonded blanks

Fig. 2.6(a, b) shows the comparison of load – extension behaviour between single sheet made of DDQ steel and SS 316L, double sheet without adhesive and two types of adhesive bonded blanks made of epoxy and acrylic adhesives having different hardener/resin ratios. While comparing the load–extension behaviour of double sheet without adhesive and adhesive bonded blanks, an increase in extension is observed for both types of adhesive bonded blanks till the failure of DDQ steel specimens. The extension results of SS 316L in adhesive bonded blanks are also compared with the SS316L in double sheet.

The total extension of about 26.5 mm and 53.75 mm is found from the load–extension behaviour of double sheet till failure of DDQ steel and SS 316L sheets, respectively. With respect to these total extension values, the increase in total extension is calculated between double sheet and adhesive bonded blanks which is shown in Table 2.7. It is noticed in general that increase in hardener/resin ratio of both adhesive systems improves the extension or deformation of base materials considerably except in some of the cases. When comparing the load-extension behaviour of single DDQ steel and SS 316L sheet with double sheet, no significant increase in extension (about 1.9% with respect to DDQ steel sheet) is noted in general. This lesser amount of increase in extension is because of the contribution of SS 316L sheet in the double sheet forming behaviour.

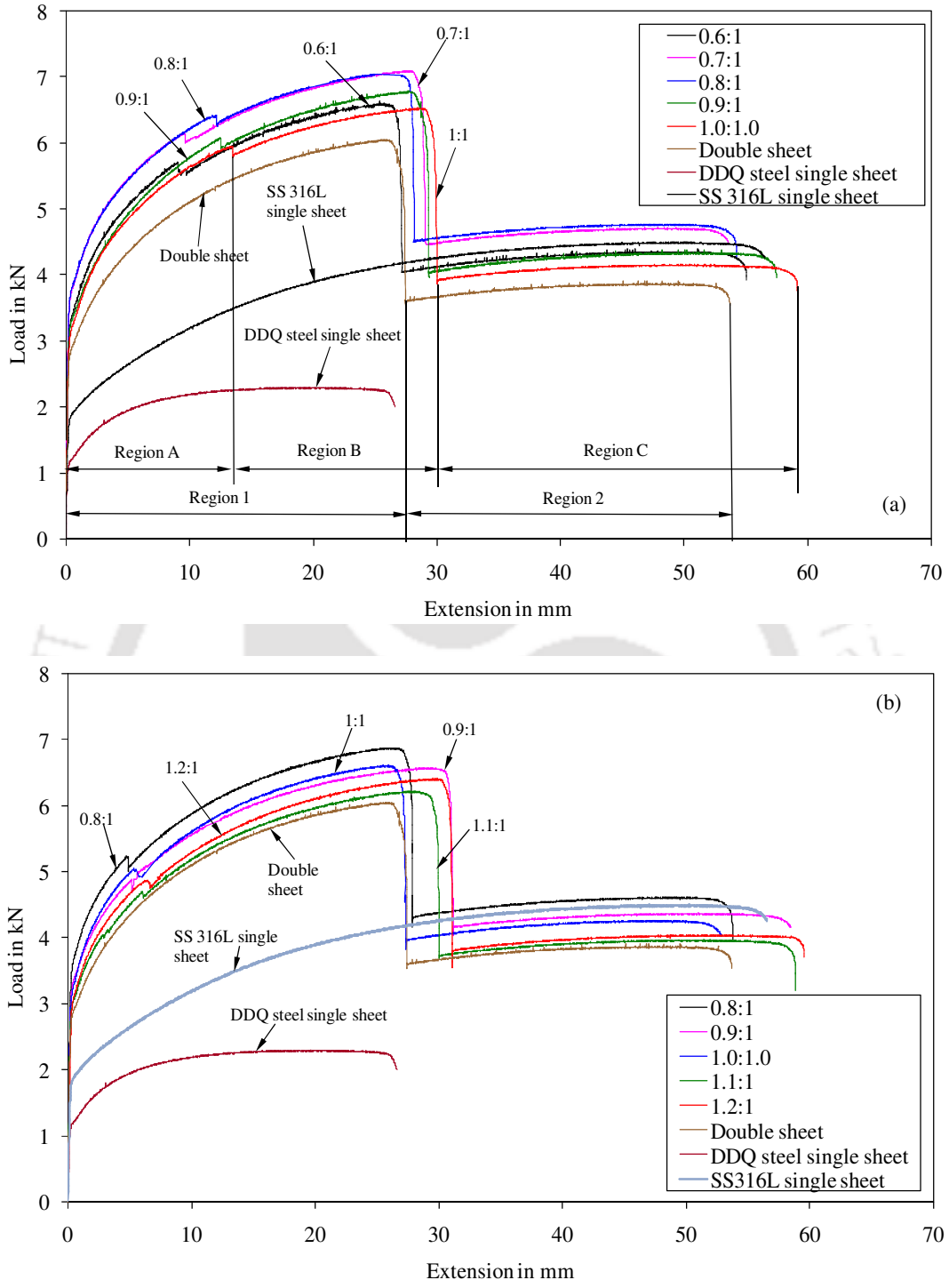

Fig. 2.6 Comparison of load – extension behaviour of single sheets of DDQ steel and SS 316L, double sheet without adhesive, (a) epoxy bonded blanks with different H/R ratios, and (b) acrylic bonded blanks with different H/R ratios (where Region A → tensile behaviour of global adhesive bonded blank, DDQ steel sheet and SS316L sheet, Region B → tensile behaviour of DDQ steel sheet and SS316L sheet of adhesive bonded blank, Region C → tensile behaviour of SS 316L sheet of adhesive bonded blank, Region 1→ tensile behaviour of DDQ steel sheet and SS316L sheet in the case of double sheet and Region 2→ tensile behaviour of SS316L sheet of double sheet)

Table 2.7 Comparison of increase in percentage of total extension of DDQ steel sheets and SS 316L sheets in adhesive bonded blanks with respect to double sheet

Adhesive bonded blank (ABB)	H/R ratio	Increase in total extension (%)	
		Till failure of DDQ steel sheet	Till failure of SS 316L sheet
Epoxy based	0.6:1	1.7	0.5
	0.7:1	6.7	0.5
	0.8:1	6.7	0.5
	0.9:1	10.4	4.2
	1:1	12.3	9.8
Acrylic based	0.8:1	3.1	0.1
	0.9:1	17.0	8.8
	1:1	3.1	1.8
	1.1:1	12.5	9.4
	1.2:1	17.0	10.9

Note: Increase in total extension % = (Extension of ABB till failure of DDQ steel sheet or SS 316L sheet – extension of double sheet till failure of DDQ steel sheet or SS 316L sheet) / (Extension of double sheet) ×100

Elsewhere, Aghchai *et al.,* 2008 investigated the formability limits of a two-layer sheet through analytical models and an experimental approach. The formability of the two layer sheet was compared with the formability of its components. They concluded that the FLD of the two-layer sheet is better than the lower formable component and two layer sheet improves the formability of a sheet that has a low formability. Polyurethane adhesive was applied to join the two layers together (Aghchai *et al.,* 2008), but the influence of adhesive properties on the overall formability was not addressed which plays a critical role during the forming of bonded sheets.

2.4.3.2 Comparison between single sheet and adhesive bonded blanks

In the comparison of load – extension behaviour of DDQ steel single sheet and SS 316L single sheet with adhesive bonded blanks, a significant increase in total extension is encountered. The total extension of about 26 mm and 55 mm is found for DDQ steel and SS 316L single sheets, respectively. The increase in percentage of total extension between single sheets and adhesive bonded blanks for minimum and maximum hardener/resin ratios is given in Table 2.8. A significant increase in percentage of total extension for DDQ steel sheet in both types of adhesive bonded blanks is observed. The percentage increase in total extension increases with increase in hardener/resin ratio. Negligible increase in percentage of total extension is detected for SS 316L sheet in both types of adhesive bonded blanks for the lower level (0.6:1 and 0.8:1) of

hardener/resin ratios. But a considerable increase in percentage of total extension is seen for SS 316L sheet in both types of adhesive bonded blanks for higher level of hardener/resin ratios. This is due to the added extension caused by the adhesive layer with appreciable plasticity during global behaviour (deformation of all the three regions) of adhesive bonded blanks is preserved in the base materials till their failures which is not present in the case of single sheet made of DDQ steel and SS 316L tensile behaviour.

Table 2.8 Comparison of increase in percentage of total extension results of DDQ steel and SS 316L single sheet and adhesive bonded blanks

Adhesive bonded blank (ABB)	H/R ratio	Increase in total extension (%)	
		Till failure of DDQ steel sheet	Till failure of SS 316L sheet
Epoxy based	0.6:1	1.9	1.7
	1:1	14.4	7.3
Acrylic based	0.8:1	5.0	2.4
	1.2:1	19.2	8.4

Note: Increase in total extension % = (Extension of ABB till failure of DDQ steel sheet or SS 316L sheet – extension of single sheet of DDQ steel sheet or SS 316L till failure) / (Extension of single sheet) ×100

2.4.3.3 Comparison between adhesive bonded sheets having different hardener/resin ratios

Fig. 2.6(a, b) presents the comparison of load – extension behaviour for different hardener/resin ratios of epoxy and acrylic adhesive bonded blanks, respectively. In Fig. 2.6(a), it is noted that there is an increase in extension with increase in hardener/ratio of the epoxy adhesive bonded blanks from 0.6:1 to 1:1. Even in the case of acrylic adhesive bonded blanks, the extension of bonded blanks increases with increase in hardener/ratio from 0.8:1 to 1.2:1 that can be observed from Fig. 2.6(b). The total extension of about 9 mm and 4.8 mm is found for hardener/resin ratio of 0.6:1 and 0.8:1 of epoxy and acrylic adhesive bonded blanks till the failure of adhesive layer, respectively.

With respect to these extension values, the increase in percentage of total extension is calculated as 2.9%, 35.6%, 38.9% and 53.3% for the epoxy adhesive bonded blanks with hardener/resin ratios of 0.7:1, 0.8:1, 0.9:1 and 1:1, respectively. About 14.6%, 15.4%, 18.8% and 37.9% increase in total extension is observed in the case of acrylic adhesive bonded blanks with hardener/resin ratio of 0.9:1, 1:1, 1.1:1 and 1.2:1, respectively. This increase in percentage of total extension is due to the increase in plasticity of the adhesive layer which is controlled by rich hardener formulation as discussed in the results of deformation of adhesives with different

hardener/resin ratios (Section 2.3.1). This increase in percentage of extension causes delay of failure and thus improves the formability of the base materials. In addition, while comparing the increase in percentage of total extension between two adhesive systems, epoxy adhesive bonded blanks show better results than acrylic adhesive bonded blanks for all chosen hardener/resin ratios.

2.4.3.4 Comparison of engineering stress – strain behaviour of adhesive bonded blanks and single sheets (DDQ and SS 316L)

Figs. 2.7(a) and 2.7(b) show engineering stress – strain behaviour of epoxy adhesive bonded blanks and acrylic adhesive bonded blanks, respectively. The stress – strain behaviour of single sheet made of DDQ steel and SS 316L, double sheets without adhesive are also shown in the same Figures. From these results, the percentage elongation at the failure region of DDQ steel and SS 316L in both types adhesive bonded blanks is calculated with respect to the total elongation of DDQ steel, SS 316L single sheets having 32% and 68%, respectively. Figs. 2.8(a) and 2.8(b) present the engineering stress – strain behaviour of epoxy adhesive bonded blanks and acrylic adhesive bonded blanks for different hardener/resin ratios, respectively.

From Table 2.9, it is noticed that there is a significant increase in total elongation of DDQ steel in both types of adhesive systems in most of the cases, while no considerable increase in total elongation is observed in SS 316L sheets except at higher levels of hardener/resin ratios. To identify the function of adhesive layer, the total elongation in different regions such as region A, B and C of adhesive bonded blanks with different hardener/resin ratios is shown in Table 2.10. In the case of epoxy adhesive bonded blanks, there is a significant increase of about 5% in total elongation at the region A of global behaviour of epoxy bonded blanks with different hardener/resin ratios. Though there is not much difference in the total elongation at the region A of global behaviour of acrylic bonded blanks, only 3% improvement is observed, an increasing trend is observed with different hardener/resin ratios. While comparing the total elongation at the region B, a considerable increase is noted with increase in hardener/resin ratio for both types of adhesive bonded blanks except in one or two cases of acrylic adhesive bonded blanks. There is about 4% improvement in region B.

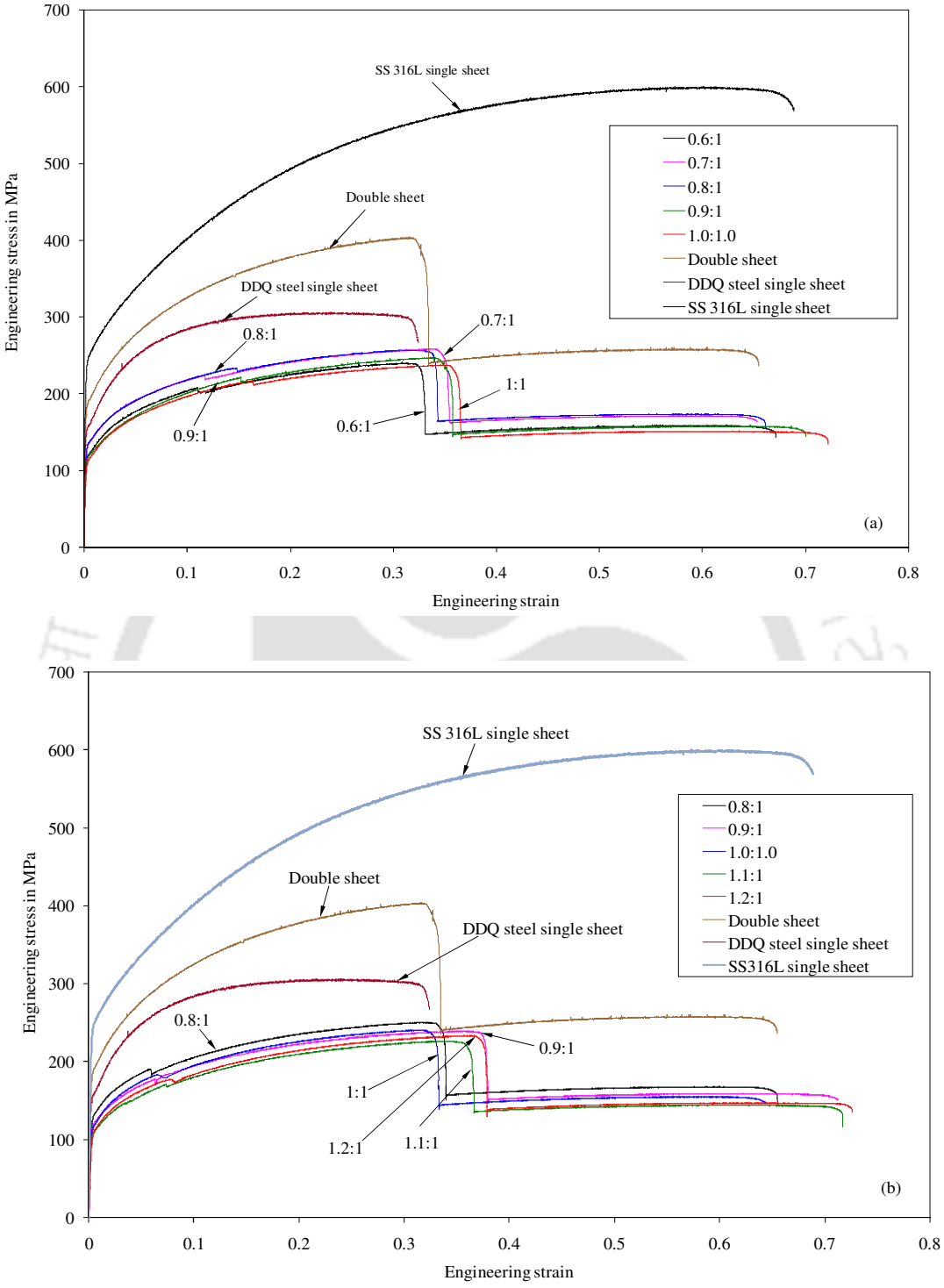

Fig. 2.7 Comparison of engineering stress – strain behaviour of single sheet made of DDQ steel and SS 316L, double sheet without adhesive, (a) epoxy adhesive bonded blanks with different H/R ratios, and (b) acrylic adhesive bonded blanks with different H/R ratios.

Table 2.9 Comparison of increase in total elongation results of DDQ steel sheets and SS 316L sheets in adhesive bonded blanks with respect to single sheet

Adhesive bonded blank (ABB)	H/R ratio	Increase in total elongation (%) (at 82 mm gauge length)	
		DDQ steel sheet	SS 316L sheet
Epoxy	0.6:1	0.7	0
	0.7:1	2.4	0
	0.8:1	1.7	0
	0.9:1	2.5	2.5
	1:1	3.6	4.1
Acrylic	0.8:1	1.2	0
	0.9:1	5.0	3.0
	1:1	1.0	0
	1.1:1	4.0	3.0
	1.2:1	5.0	5.0

Note: Increase in % of total elongation = (Elongation of ABB till failure of DDQ steel sheet or SS 316L sheet – elongation of single sheet of DDQ steel sheet or SS 316L till failure) ×100

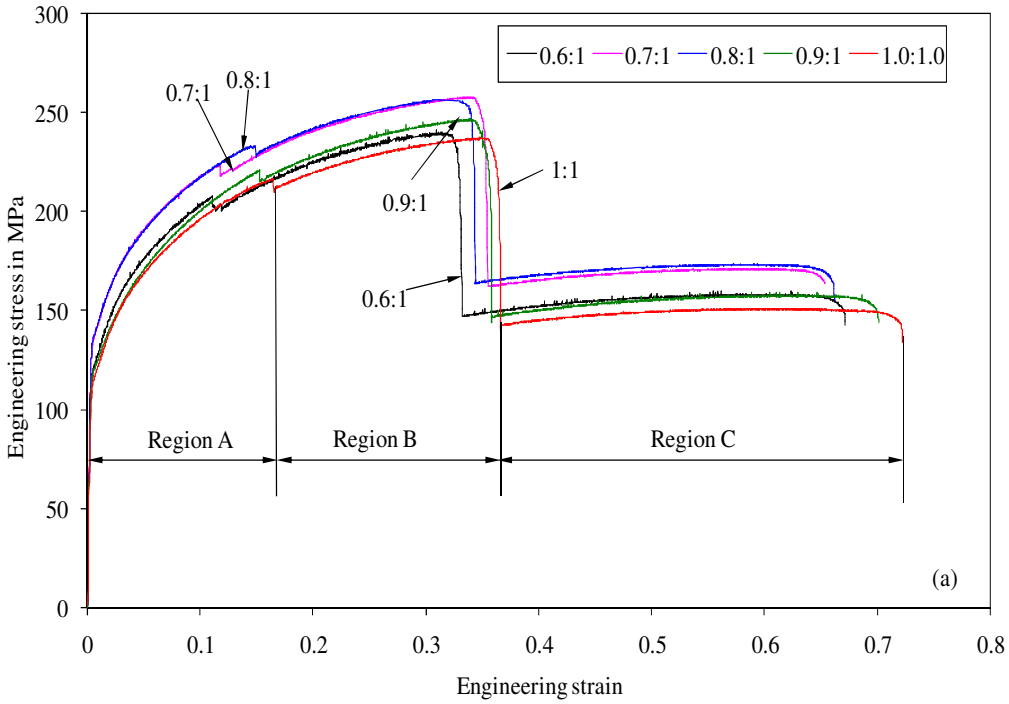

Error variation in ultimate tensile strength = ±8 MPa, and in total elongation = ±1 %

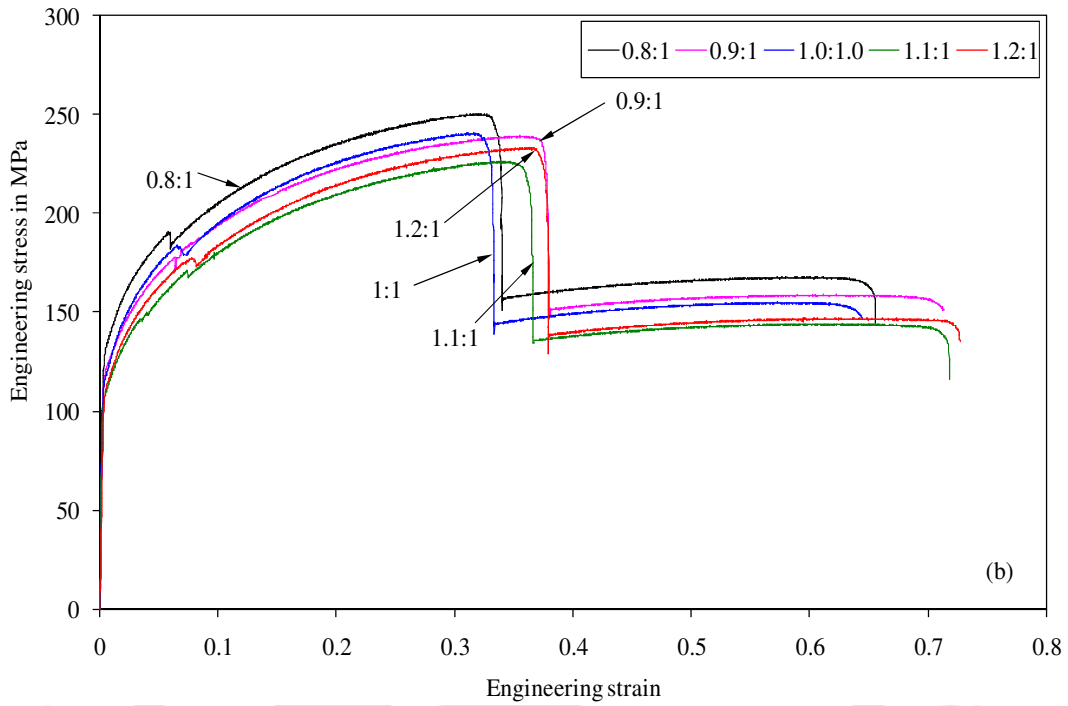

Error variation in ultimate tensile strength = ±10 MPa, and in total elongation = ±0.8 %

Fig. 2.8 Comparison of engineering stress – strain behaviour (a) epoxy adhesive bonded blanks with different H/R ratios (Note: Error variation in ultimate tensile strength = ±8 MPa, and in total elongation = ±1 %), (b) acrylic adhesive bonded blanks with different H/R ratio (Note: Error variation in ultimate tensile strength = ±10 MPa, and in total elongation = ±0.8 %)

Table 2.10 Comparison of percentage of elongation results at region A, B and C of adhesive bonded blanks with different hardener/resin ratios

Adhesive bonded blank (ABB)	H/R ratio	Total elongation (%) (at 82 mm gauge length)		
		Region A	Region B	Region C
Epoxy based	0.6:1	11.27	32.72	67.13
	0.7:1	12.05	34.26	66.00
	0.8:1	14.86	33.83	66.00
	0.9:1	15.24	34.45	69.79
	1:1	16.43	35.69	72.09
Acrylic based	0.8:1	5.92	33.13	64.98
	0.9:1	6.16	37.77	71.17
	1:1	6.75	32.07	64.62
	1.1:1	6.77	36.02	71.68
	1.2:1	8.07	37.77	72.64

Even though a considerable increase in total elongation is observed at the region C, which characterizes the behaviour of SS 316L sheets, for lower and higher level of hardener/resin ratios, the influence is negligible in between them. An improvement of 4–8% is observed in both the adhesive systems in region 'C' between the lower and higher hardener/resin ratio. From these

results, it is conceivable that because of increase in elongation with increase in hardener/resin ratio in the global behaviour of adhesive bonded blanks, *i.e*., at region A, both the base materials show improvement in the total elongation. This confirms that increase in total elongation at region B and C is due to the improvement in plastic deformation caused by the rich hardener formulated adhesive layer in both types of adhesive bonded blanks.

2.4.3.5 Strain hardening exponent (*n*) of adhesive bonded blanks

The engineering stress – strain behaviour of both types of adhesive boned blanks is converted into true stress – strain behaviour and the strain hardening exponent value (*n*) which decides the formability of a sheet material is calculated in (i) the region A at which three materials (adhesive layer, DDQ steel and SS 316L) deform together, (ii) the region B at which DDQ steel and SS 316L are deforming after initial adhesive failure, and (iii) region C at which SS 316L is deforming after failure of DDQ steel sheet. Also the strain hardening exponent value is calculated from stress-strain behaviour of double sheet in, (i) the region 1 at which two base materials (DDQ steel and SS 316L) deform together and (ii) the region 2, at which SS 316L deforms after failure of DDQ steel sheet. Table 2.11 shows the calculated strain hardening exponent values in region 1 and 2 of stress-strain behaviour of double sheet. The strain hardening exponent value in the regions A, B and C of stress-strain behaviour of adhesive bonded blanks is given in Table 2.12. While comparing the strain hardening exponent (*n*) of double sheet at region 1 (Table 2.11) and adhesive bonded blanks at region B (Table 2.12) till failure of DDQ steel sheets, a significant increase in *n*-value is found for all the adhesive bonded blanks. At region 1, the strain hardening exponent is 0.327 for double sheet, while the improved '*n*' values in region 'B' is in between 0.37 and 0.394 for epoxy based, and between 0.347 and 0.387 for acrylic based adhesive. The improvement in '*n*' values in region 'B' and region 'C' of adhesive bonded blank is given in Table 13 with respect to region 1 and region 2 of double sheet.

When comparing the *n*-value calculated till failure of DDQ (region 1) of double sheet (Table 2.11) and DDQ steel single sheet (Table 2.2), a sufficient increase in *n*-value is noted which makes clear that the two layer sheet improves the formability of the DDQ steel sheet which follows the results of Aghchai *et al.,* 2008. In the comparison of *n*-value among adhesive bonded blanks, an appreciable increasing trend of *n*-value in region A is found with increase in hardener/resin ratio of both types of adhesive bonded blanks. A significant increasing fashion of n-value in region B is also observed with increase in hardener/resin ratio. Though there is not much difference in the *n*-value of region C, still an increasing trend of *n*-value with increase in hardener/resin ratio is noted.

Table 2.11 Strain hardening exponent (*n*) in region 1 and region 2 of double sheet

Material	Region 1	Region 2
Double sheet	0.327	0.494

Error variation in *n*-value in region 1 = ±0.007, and region 2 = ±0.001

Table 2.12 Strain hardening exponent (*n*) value in regions A, B and C of adhesive bonded blanks

Adhesive bonded blank	H/R ratio	Region A	Region B	Region C
Epoxy based	0.6:1	0.232	0.370	0.496
	0.7:1	0.237	0.372	0.496
	0.8:1	0.239	0.372	0.496
	0.9:1	0.284	0.392	0.515
	1:1	0.287	0.394	0.517
Acrylic based	0.8:1	0.184	0.347	0.507
	0.9:1	0.195	0.352	0.507
	1:1	0.218	0.368	0.511
	1.1:1	0.221	0.371	0.511
	1.2:1	0.223	0.387	0.512

Error variation in *n*-value in region A = ±0.002, region B = ±0.001, and region C = ±0.001

Table 2.13 Comparison of increase in strain hardening exponent (*n*) in region B and region C of adhesive bonded blanks with respect to region 1 and region 2 of double sheet

Adhesive bonded blank	H/R ratio	Increase in *n*-value (%)	
		Region B with respect to region 1	Region C with respect to region 2
Epoxy based	0.6:1	13.2	0.4
	0.7:1	13.8	0.4
	0.8:1	13.8	0.4
	0.9:1	19.9	4.3
	1:1	20.5	4.7
Acrylic based	0.8:1	6.1	2.6
	0.9:1	7.6	2.6
	1:1	12.5	3.4
	1.1:1	13.5	3.4
	1.2:1	18.3	3.6

From these results, it is comprehended that the combined behaviour of adhesive layer and SS 316L improves the overall formability of global behaviour of adhesive bonded blanks and also improves the formability of DDQ steel sheet. This can be understood from the increase in *n*-value in the double sheet behaviour at region 1 which is more than DDQ single sheet. Also the increasing trend of *n*-value in region B is more than region 1 which makes clear that the combined behaviour of adhesive layer and SS 316L sheet improves the *n*-value of DDQ steel sheet. Moreover, increase in hardener/resin ratio which increases the plasticity of the adhesive

layer improves the *n*-value of global behaviour of adhesive bonded blanks and thus improves the *n*-value of DDQ steel and SS 316L sheets.

2.4.4 Effect of adhesive properties on the limit strain of adhesive bonded steel sheets

In this section, the influence of adhesive properties on the formability of adhesive bonded blanks are discussed through limit strains by measuring the length of major and minor axes of deformed circular grids at the failure region of DDQ steel and SS 316L sheets in adhesive bonded blanks. The limit strains are measured for single sheets of SS 316L and DDQ steel sheets and both the base materials constituting double sheet.

Figs. 2.9(a) and 2.9(b) present the comparison of limit strains of DDQ steel sheet specimen from epoxy adhesive bonded blanks and from acrylic adhesive bonded blanks with different hardener/resin ratios, respectively. The limit strains in DDQ steel specimen from double sheet and single sheet of DDQ steel are also shown. Similarly, Figs. 2.10(a) and 2.10(b) show the comparison of limit strains in SS 316L sheet specimen from epoxy adhesive bonded blanks and from acrylic adhesive bonded blanks with different hardener/resin ratios, respectively. The limit strains in SS 316L specimen from double sheet and single sheet of SS 316L are also shown. There is an increasing trend of forming limit strain with increase in hardener/resin ratio for both types of adhesive bonded blanks and base materials. This increasing fashion of limit strain observed for both DDQ steel and SS 316L specimens is larger than the limit strain observed for DDQ steel and SS 316L sheets in double sheet and single sheets. The maximum forming limit strain is observed in both base materials for the larger hardener/resin ratio, and the minimum forming limit strain is noticed for the lower hardener/resin ratio in both adhesive bonded steel sheets. The DDQ steel sheet from double sheet shows a significant increase in limit strain as compared to DDQ steel single sheet. Even though the forming behaviour of two layer sheet improves the formability of the sheet which has low formability, there is a small improvement in limit strain of SS 316L sheet in double sheet as compared to SS 316L single sheet.

To draw the reason for improvement of limit strain observed in all adhesive bonded blanks as compared to double sheet and single sheets, the limit strain can be related to the *n*-value calculated in the regions A, B and C and in the regions 1 and 2 of the stress-strain behaviour of adhesive bonded blanks and double sheet, respectively. The global behaviour of double sheet show larger *n*-value in region 1 than single DDQ steel specimen. This makes clear that the DDQ steel sheet specimen in double sheet has been deformed plastically more than the single DDQ steel sheet which has caused the increase in limit strain in DDQ steel specimen in the double sheet.

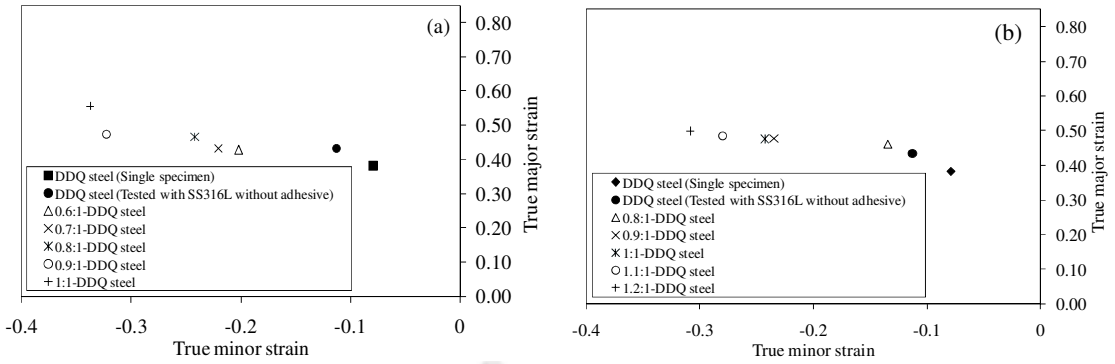

Fig. 2.9 Comparison of limit strain in DDQ steel specimen from double sheet without adhesive, single DDQ steel sheet, (a) DDQ steel specimen from epoxy adhesive bonded blanks for different H/R ratios, (b) DDQ steel specimen from acrylic adhesive bonded blanks for different H/R ratios

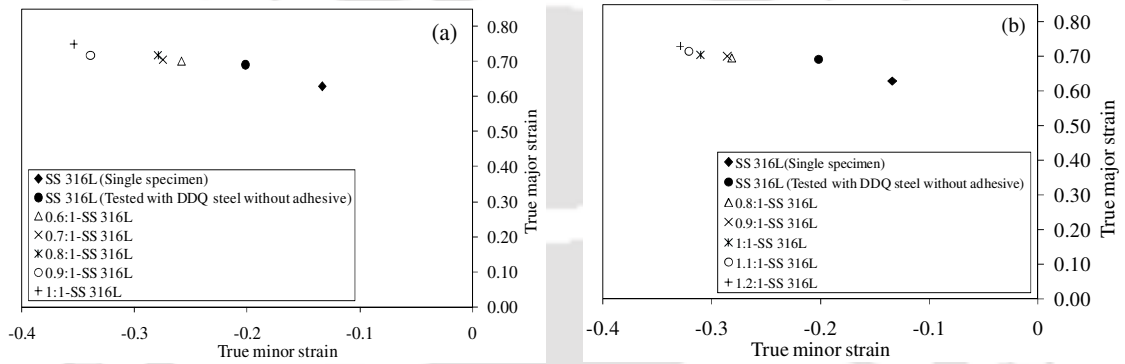

Fig. 2.10 Comparison of limit strain in SS 316L specimen from double sheet without adhesive, single SS 316L sheet, (a) SS 316L specimen from epoxy adhesive bonded blanks for different H/R ratios, and (b) SS 316L specimen from acrylic adhesive bonded blanks for different H/R ratios

Similarly, while comparing *n*-value in the region B of adhesive bonded blanks, the global behaviour of two base materials in adhesive bonded blanks show larger *n*-value than single DDQ steel sheet and DDQ steel sheet from double sheet. This is because of the plastic deformation caused by the global behaviour of adhesive bonded blanks which has increased the limit strain in both base materials by delaying the failure of base materials. The plastic deformation caused by the global behaviour of adhesive bonded blanks in region 1 is governed by the rich hardener formulation of adhesive.

To confirm the increase in limit strain observed in base materials which is caused by the plasticity of adhesive layer, three sets of adhesive bonded blanks each with hardener/resin ratios of 0.6:1, 0.8:1 and 1:1 in the case of epoxy adhesive bonded blanks and 0.8:1, 1:1 and 1.2:1 in the case of acrylic adhesive bonded blanks were prepared. Tensile tests were carried out till the failure of adhesive layer in adhesive bonded blanks and test was stopped. The extension at the failure of adhesive layer in adhesive bonded blanks was noted for all cases of hardener/resin

ratios. The double sheet and single sheets of DDQ steel and SS 316L were also elongated up to the corresponding extension noted for each hardener/resin ratio of adhesive bonded blanks. After the tensile test, the circular grid which has got the maximum strain was identified by measuring major and minor strains of all the grids along the centre axes of the DDQ steel and SS 316L sheets in both types of adhesive bonded blanks, double sheet and single sheet. Fig. 2.11(a-f) shows comparison of maximum strain evaluated from DDQ steel and SS 316L sheets of adhesive bonded sheets till the failure of adhesive layer, and corresponding maximum strain evaluated from DDQ steel and SS 316L specimens of double sheet and single sheet.

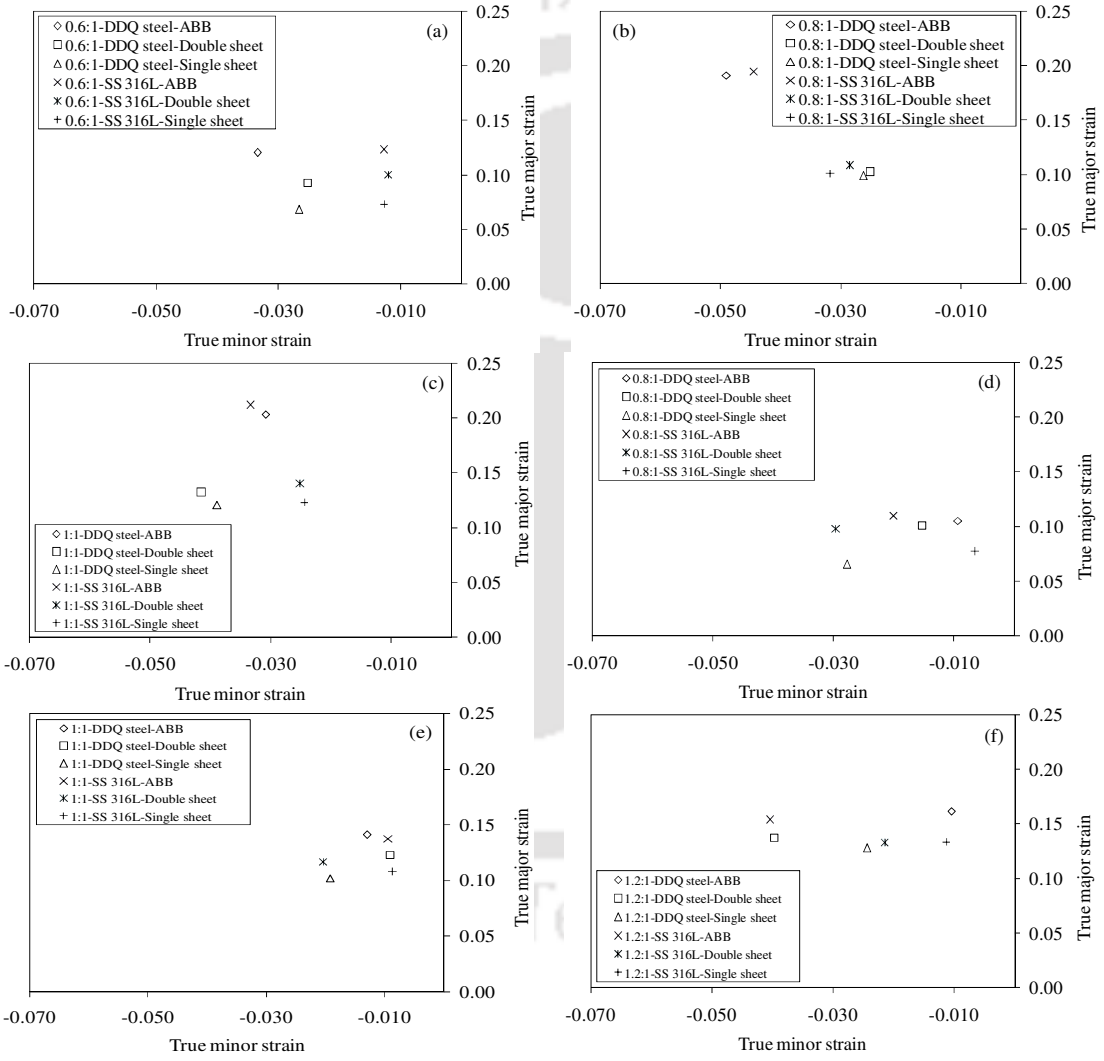

Fig. 2.11 Comparison of maximum strain from DDQ steel and SS 316L sheets of adhesive bonded blanks till failure of adhesive layer and corresponding maximum strain from DDQ steel and SS 316L sheet specimens from double sheet and single sheets: (a) epoxy adhesive bonded blanks with H/R ratio of 0.6:1, (b) epoxy adhesive bonded blanks with H/R ratio of 0.8:1, (c) epoxy adhesive bonded blanks with H/R ratio of 1:1, (d) acrylic adhesive bonded blanks with H/R ratio of 0.8:1, (e) acrylic adhesive bonded blanks with H/R ratio of 1:1, and (f) acrylic adhesive bonded blanks with H/R ratio of 1.2:1.

Figs. 2.11 (a-c) and 2.11 (d-f) present the comparison of maximum strain for epoxy and acrylic adhesive bonded sheets, respectively. It is observed from the Figures that the maximum strain of DDQ steel and SS 316L sheets of adhesive bonded blanks increases with increase in hardener/resin ratio. A considerable increase in maximum strain is noticed. There is about 3–9% improvement in maximum major strain of DDQ steel sheet and about 2–9% in maximum major strain of SS 316L sheet with respect to maximum major strain of single sheets.

From these results, it is understood that the increase in maximum strain of DDQ steel and SS 316L sheets is because of improvement in plastic deformation caused by the adhesive layer and global behaviour of adhesive bonded blanks. This improvement in maximum strain of adhesive bonded sheets with respect to double sheet and single sheet before adhesive failure is preserved till the failure of individual sheets and hence improvement in limit strain is witnessed as presented in Fig. 2.11 (a-f). Moreover, while comparing the limit strain values of two types of adhesive bonded blanks, epoxy adhesive bonded blanks show larger limit strain than acrylic adhesive bonded blanks, showing better formability.

2.4.5 Uncertainty in limit strain measurement

In the testing of bonded sheets, three specimens were tested for each case to check the repeatability in limit strain and if the repeatability was not observed, the fourth specimen was tested. In the case of single DDQ steel sheet, about 10 samples were tested for checking the repeatability in limit strain results. The diameter of circular grids in all samples was measured before testing and the average diameter of circular grids was measured as 2.8±0.05 mm. After testing of blanks, length of major axis and minor axis of the deformed grids at the failure region was measured through digitized profile projector. From the measurement of deformed grids, true limit strains were calculated. Though a good agreement in the repeatability of the tensile behaviour was observed, some of the results were unclear and manual measurement may introduce errors. So it is mandatory to check the measurement uncertainty in limit strains. The standard deviation results reported in the present work is sample standard deviation which provides a better estimation than population standard deviation.

The standard deviation of true major limit strain ranges from 0.002 to 0.049 and the standard deviation of true minor strain ranges from 0.002 to 0.095 for DDQ steel sheets. Similarly, the standard deviation of true major limit strain ranges from 0.003 to 0.032 and the standard deviation of true minor strain ranges from 0.015 to 0.072 for SS 316L sheets. These error variations are much smaller than the limit strain improvement among different adhesive bonded samples with different hardener/resin ratios. Hence, these results confirm an inherent

improvement in the limit strain rather than falling within the standard deviation range found in the case on single sheets.

2.4.6 Influence of interfacial bonding between adhesive layer and base materials on the formability of adhesive bonded steel sheets

The epoxy adhesive strips with 1 mm thickness were prepared as per the dimensions shown in Fig. 2.1(d) with higher and lower levels of hardener/resin ratio of 0.6:1 and 1:1, respectively. The cured adhesive strip was introduced between base materials made of DDQ steel and SS 316L sheets and tensile test was carried out. It should be noted here that the base material and adhesive layer are unbonded. The thickness of adhesive layer in unbonded and in bonded blanks was found to be 1±0.015 mm.

The limit strain results were evaluated for DDQ steel and SS 316L sheets in three layered unbonded and bonded blanks and compared in Fig. 2.12(a, b). It is confirmed that there is an improvement of limit strains of DDQ steel and SS 316L sheets constituting bonded sheets as compared to unbonded sheets with increase in hardener/resin ratio.

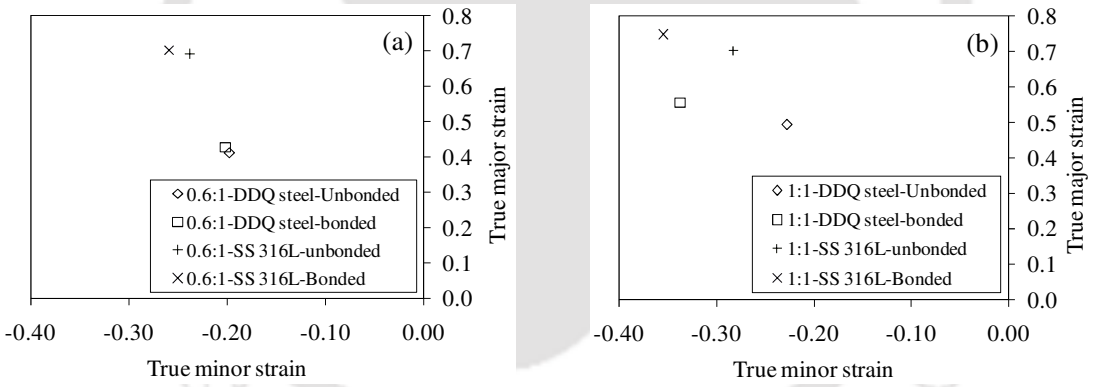

Fig. 2.12 Comparison of limit strain from DDQ steel and SS 316L sheets in which three layer unbonded and bonded by epoxy adhesive with, a) H/R ratio of 0.6:1, and b) H/R ratio of 1:1

It is believed that the effect of adhesive bonding on the formability will remain same for acrylic adhesive bonded sheets. There is a slight improvement in limit strains in the case of 0.6:1 ratio, while a considerable improvement of about 5% in limiting major strain is observed in 1:1 ratio. The improvement in limit strain of bonded sheets as compared to unbonded sheets is mainly due to the delay in necking phenomenon by the presence of interface bonding between the adhesive and steel sheets. Even in unbonded case, adhesive with 1:1 hardener/resin ratio shows larger limit strain as compared to 0.6:1 ratio (Fig. 2.12(a, b)) for DDQ steel sheet.

2.4.7 Suggestions for the selection of adhesive bonded sheets

Just to summarize the work, it has been shown that by increasing the hardener/resin ratio of the adhesive, the formability (like elongation, limit strain) of adhesive bonded blank can be improved. It has been demonstrated that not only the strength of adhesive and adhesive bonded blank are important, but also their formability. Most of the work in the literature demonstrates the strength variation of adhesives and delamination during plastic deformation. Generally the hardener/resin ratio for any practical application is decided based on strength of the adhesive and the joint. But this could be just a sufficient condition. There are other properties like formability of adhesive bonded blank which should be considered while designing a sheet component. The optimum hardener/resin ratio requirement depends on such final property requirements and end application. For instance, if strength is the desired quantity, then probably the hardener/resin ratio of 0.6:1 is suitable in the case of epoxy adhesive, while the hardener/resin ratio of 1:1 is suitable if formability is the requirement. Similarly, if a good fatigue performance is desired, then some other ratio would be suitable. Hence, some engineering knowledge about sheet forming is mandatory for selecting hardener/resin ratio in adhesive bonded blank applications. An important suggestion could be to classify the adhesive bonded blank applications depending on strength, or formability, or fatigue or corrosion etc., as the final requirement and select/use hardener/resin ratio according to that. Even if adhesive bonded blanks are not used, one good idea would be to use adhesives between two steel sheets, so that formability is improved and later the adhesive can be removed for using the remaining single sheet components for automotive applications. The selection of adhesive for an application not only depends on the structural requirement like thickness, but also on the hardener/resin ratio. The strength and formability of adhesive bonded blanks that can be achieved by changing the thickness can also be achieved by changing the hardener/resin ratio for same thickness. By doing so, the adhesive defects can be minimized as thickness is maintained constant. Moreover, choosing the best adhesive for an application depends on many factors including hardener/resin ratio. For instance, if an epoxy adhesive based bonded sheet with hardener/resin ratio of 1:1 shows good formability as compared to the hardener/resin ratio of 1.2:1 of acrylic adhesive, then it is appropriate to choose the epoxy adhesive for adhesive bonded blanks applications. Probably, some other ratio will decide the selection of adhesive if strength is the requirement. Finally computing the formability of adhesive bonded blanks with appropriate adhesive properties for different hardener/resin ratio would definitely help in selecting adhesives, hardener/resin ratio, structural dimensions etc., for any end application.

2.5 Influence of adhesive properties on in-plane plane-strain formability of adhesive bonded steel sheets

2.5.1 Optimizing the sample geometry for plane-strain condition

Fig. 2.13 shows a typical geometry of in-plane plane-strain (IPPS) specimen. It was concluded that insufficient clamping of the specimen affects the localisation and fracture at the desired middle region of the specimen where plane strain conditions apply. The free length and notch size of the specimen should be as small as possible in order to get a condition as close to plane-strain as possible in the middle region of the specimen. With reference to the procedure quoted for the in-plane plane-strain formability test in (Holmberg *et al.,* 2004), CAD models of the specimens were generated with different dimensions of w_1, w_2, R and x by using Pro-E® software and imported into PAM STAMP 2G®, an elasto-plastic finite element code for preprocessing, solving and post processing. All the finite element simulation studies were carried in the environment of PAM STAMP 2G® throughout the present thesis work.

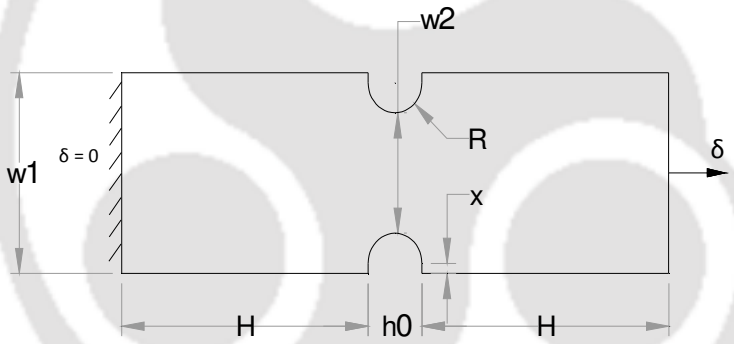

Fig. 2.13 A typical geometry of in-plane plane-strain specimen (where w_1 – specimen width, w_2 – length between two notches, h_0 – notch length, H – free length, R – notch radius, x – free length at the notch and δ – displacement).

The meshing of CAD model was done with quadrilateral shell elements of the Belytschko–Tsay formulation, with five through-thickness integration points. The average mesh size of about 1 mm was kept throughout the specimen. The base material properties given in Tables 2.1 and 2.2 were incorporated during simulations. Hollomon's power law ($\sigma = K\varepsilon^n$; where, K – strength co-efficient and n – strain-hardening exponent) was used to describe the strain-hardening behaviour of base materials. Hill's 1948 isotropic hardening yield criterion (Banabic, 2010) was used as the plasticity model for DDQ steel and SS 316L materials. Displacement boundary conditions (Fig. 2.13) are applied to in-plane plane-strain sample such that one end of the specimen is fixed and the other end is given some finite displacement with a

velocity of 1 mm/min. About 150 formability tests with different dimensions and geometries were simulated and strain paths were predicted. Some of the results of strain paths for DDQ steel sheet and SS 316L sheet are shown in Fig. 2.14(a, b).

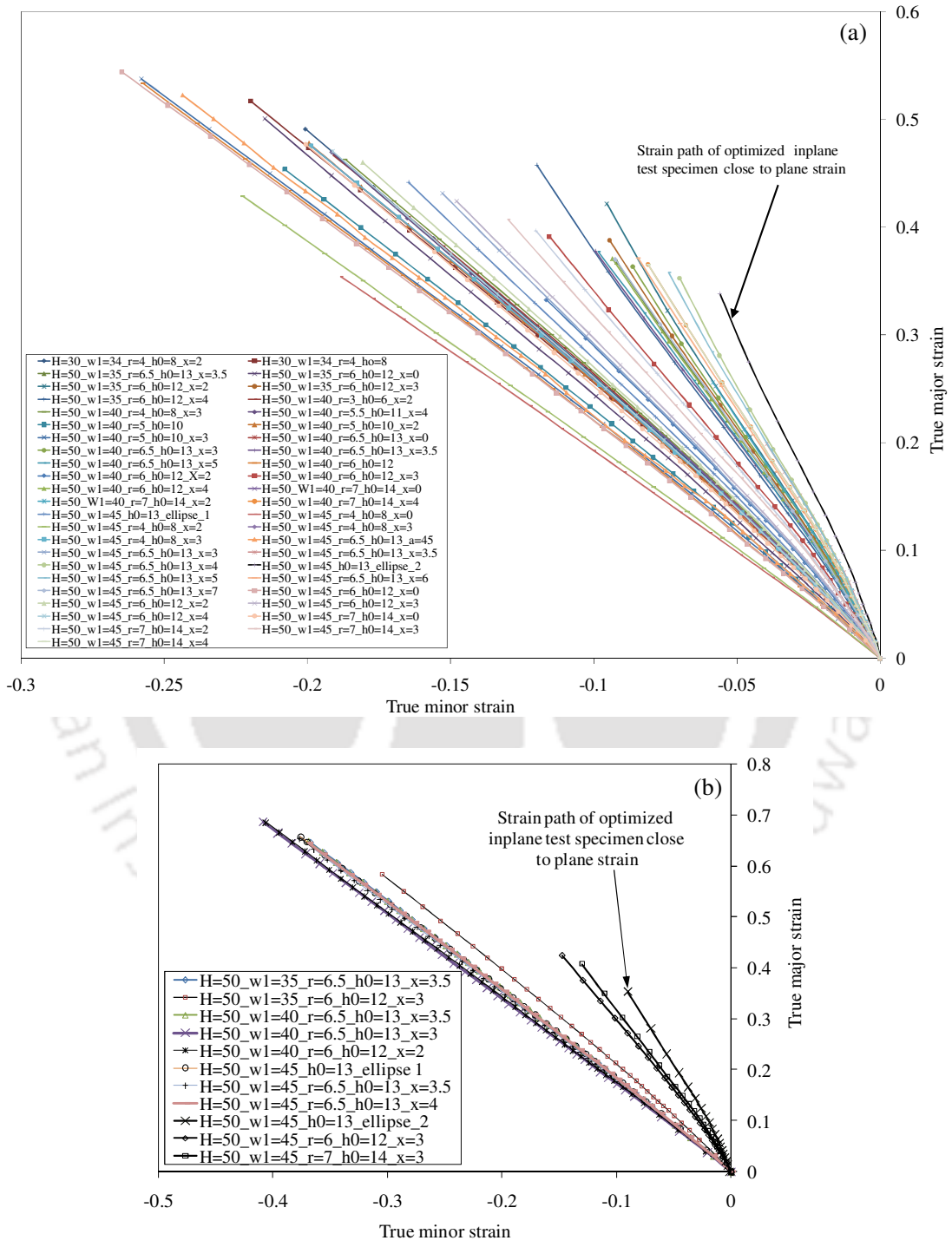

Fig. 2.14 Different strain paths and optimized plane-strain path: (a) DDQ steel sheet, and (b) SS 316L sheet

Since determining exact plane-strain condition is difficult for different materials, the optimized IPPS geometry was decided based on less formable material, DDQ steel. The IPPS sample geometry with DDQ steel was checked for SS 316L sheet, which also exhibits plane-strain condition. The same geometry was used for adhesive bonded sheets during experiments.

The optimized geometry of the IPPS specimen which is close to plane-strain deformation mode is shown in Fig. 2.15. The IPPS forming test samples were made to check the strain path experimentally, and it was found to be close to plane-strain condition. Fig. 2.16(a, b) presents the failure pattern of IPPS samples made of DDQ steel sheet and SS 316L sheets which are failing at the centre region of the specimen.

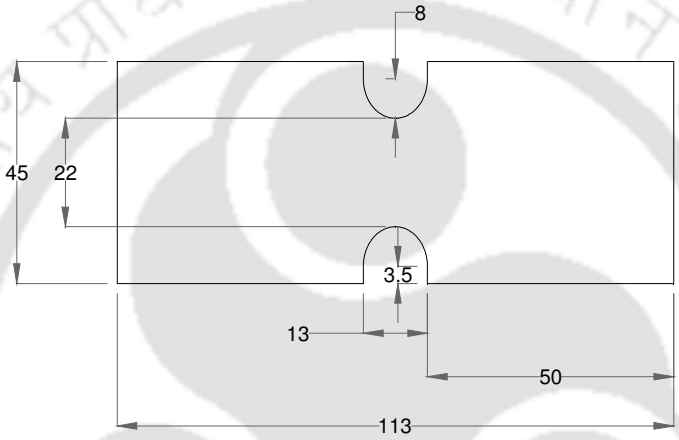

Fig. 2.15 Optimized IPPS test geometry; All dimensions in 'mm'.

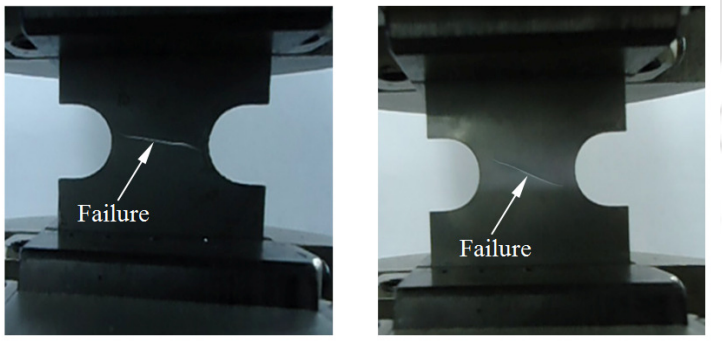

(a) (b)

Fig. 2.16 Failure pattern of in-plane plane-strain forming specimens as single sheet: (a) DDQ steel, and (b) SS 316L

2.5.2 Testing of adhesive bonded steel sheets using IPPS formability sample

The adhesive bonded IPPS specimens were prepared by following the experimental methods as discussed in Section 2.3. Fig. 2.17(a) shows the dimensions of the adhesive bonded IPPS specimen. The average thickness of adhesives in adhesive bonded blanks was found to be 1±0.013 mm. The thickness of the adhesive bonded blanks was measured and the average thickness was found to be 2.2±0.025 mm. All in-plane plane-strain formability tests on the adhesively bonded specimens were carried out with a cross-head speed of 1 mm/min at room temperature. Also two tensile specimens made up of DDQ steel and SS 316L were placed one above other as shown in Fig. 2.17(b), but without any adhesive, like a double sheet, and formability tests were carried out. After completion of the IPPS formability test, the results were monitored as discussed in Section 2.3.

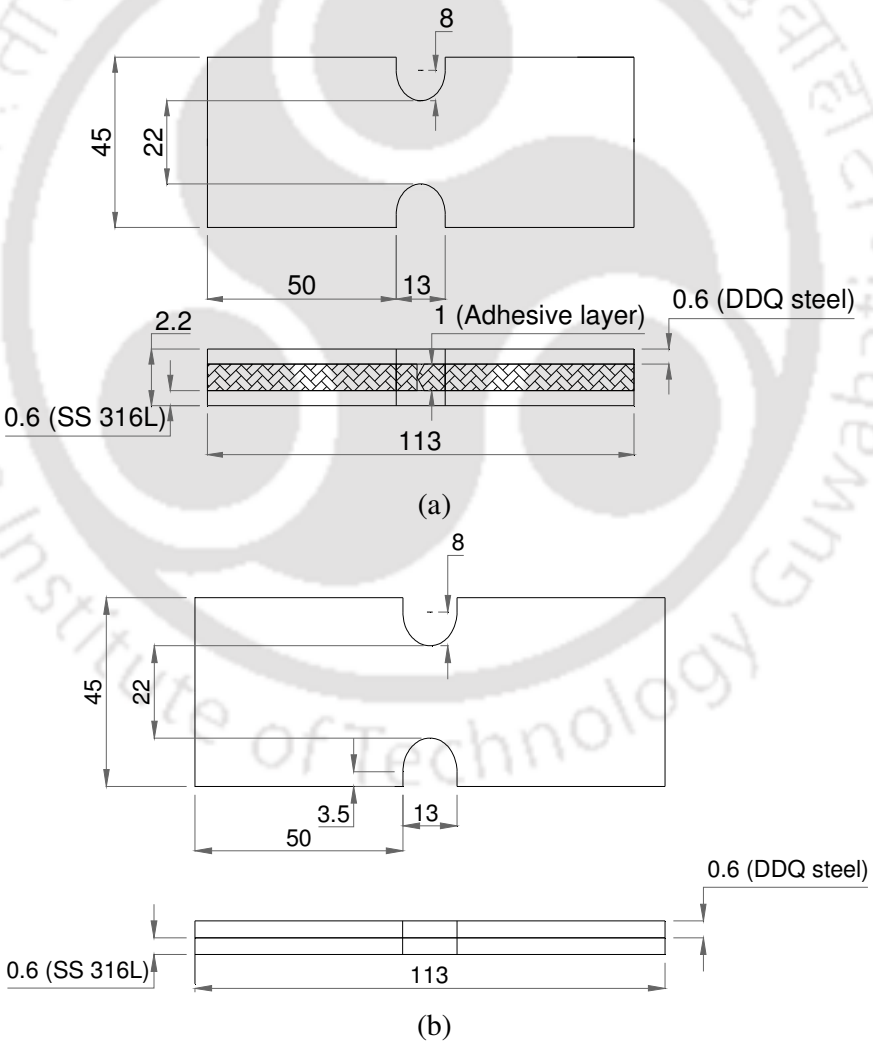

Fig. 2.17 Geometry of in-plane plane-strain formability testing specimen (a) adhesive bonded sheets, and (b) double sheet; All dimensions in mm

2.6 Results and discussion

2.6.1 Comparison of stress-strain behaviour between double sheet and adhesive bonded blanks

The comparison of engineering stress–strain behaviour of epoxy adhesive bonded blanks and acrylic adhesive bonded blanks is shown Fig. 2.18(a, b). The comparison of tensile behaviour of single sheets and double sheet is also included. During IPPS testing of the adhesive bonded blanks, all three layers (adhesive layer, DDQ steel and SS 316L sheets) are deformed together. The forming behaviour that includes the deformation of all three layers is named as region A. In the region A, the adhesive bonded blank behaves as a global specimen till the failure of adhesive layer. A mixed failure including cohesive and adhesive failure was observed in both the epoxy and acrylic adhesives. The cohesive failure of adhesive layer occurs due to its less ductility when compared to the base materials. Subsequently, the bonding between adhesive layer and base materials have failed due to relative motion between adhesive layer and base materials during deformation which is termed as adhesive failure. The failure of adhesive layer at a location was observed in both types of adhesives with different hardener/resin ratios. After failure of adhesive layer, DDQ steel and SS 316L sheets bear the deformation which then behave as a double sheet. Since the ductility of DDQ steel is lesser than SS 316L sheet as observed from elongation given in Tables 2.2 and 2.3, the failure of DDQ steel sheet is noticed after the failure of adhesive layer. The forming behaviour that includes the deformation of DDQ steel and SS 316L constituting adhesive bonded blanks is named as region B till DDQ steel failure. The SS 316L sheet failed after the failure of DDQ steel specimen. The forming behaviour of SS 316L constituting adhesive bonded blanks deformation is named as region C till its failure. The same failure pattern of adhesive bonded blanks is observed for both the epoxy and acrylic adhesive systems with different hardener/resin ratios. During deformation of double sheet, the global forming behaviour (DDQ steel and SS 316L sheets together) is named as region 1 till failure of DDQ steel sheet. The forming behaviour of SS 316L constituting double sheet till its failure is named as region 2.

While comparing the stress-strain behaviour of double sheet without adhesive and adhesive bonded blanks, the increase in elongation can be seen clearly in both the types of adhesive bonded blanks till the failure region of DDQ steel specimens. The elongation results of the SS 316L sheet in adhesive bonded blanks are also compared with the SS 316L in double sheet. The total elongation of about 36.2% and 67.5% is observed from the stress-strain behaviour of double sheet till failure of DDQ steel and SS 316L sheets, respectively.

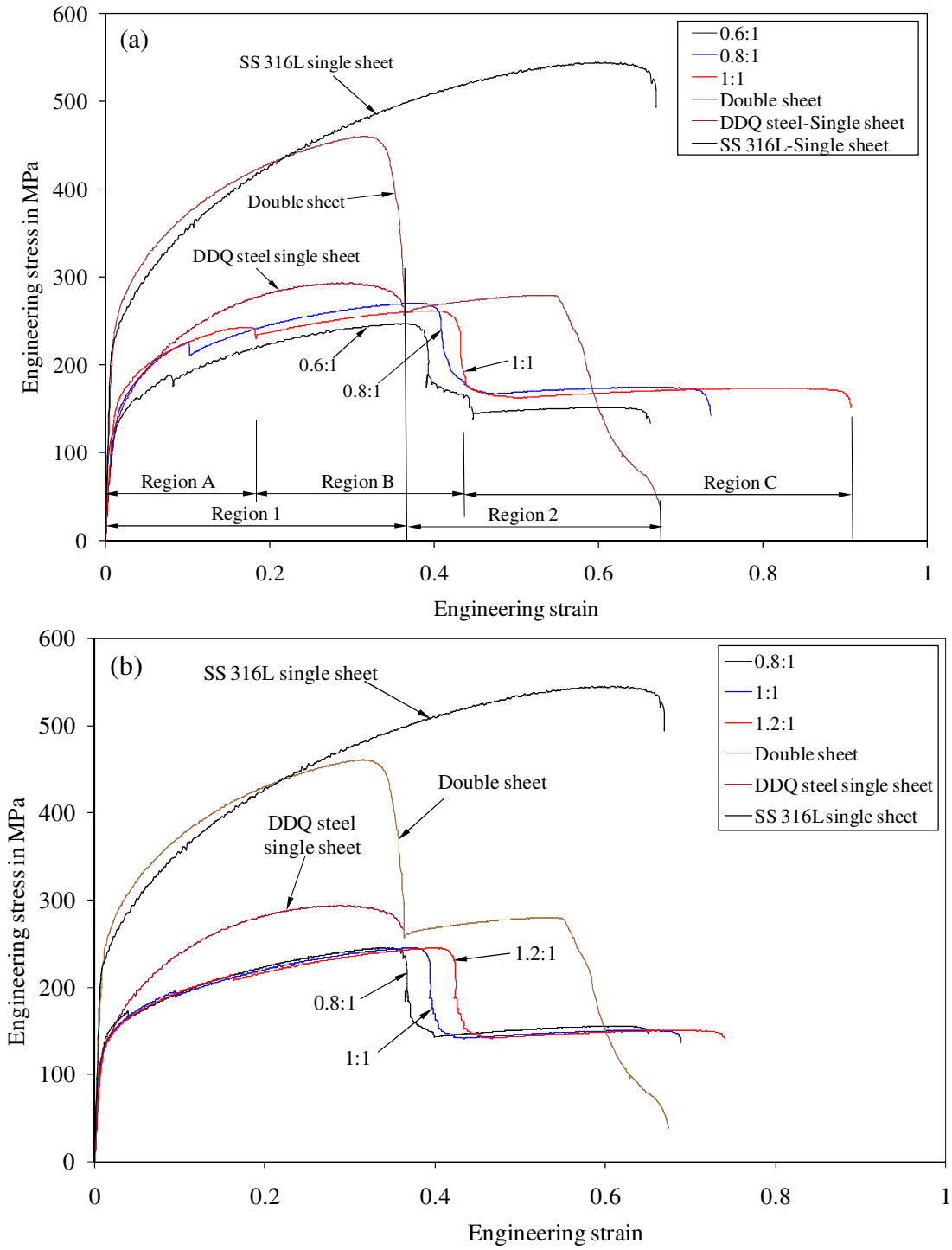

Fig. 2.18 Comparison of engineering stress – strain behaviour of single sheet made of DDQ steel and SS 316L, double sheet without adhesive and (a) epoxy adhesive bonded blanks with different H/R ratios, and (b) acrylic adhesive bonded blanks with different H/R ratios (where Region A→ global forming behaviour of adhesive bonded blanks (i.e., three layers (adhesive layer + DDQ steel sheet + SS316L sheet) together), Region B → forming behaviour of DDQ steel sheet and SS316L sheet in adhesive bonded blanks (ABB), Region C → forming behaviour of SS316L sheet in ABB, Region 1→ global forming behaviour of double sheet (DDQ steel sheet and SS316L sheet), and Region 2→ forming behaviour of SS316L sheet in double sheet)

With respect to these total elongation percentage, the increase in percentage of total elongation is calculated between double sheet and adhesive bonded blanks as shown in Table 2.14. It is noticed that increase in hardener/resin ratio of both adhesive systems improves the elongation or plastic deformation of both base materials in both types of adhesive bonded blanks considerably. While comparing the stress-strain behaviour of single DDQ steel and the DDQ steel sheet from double sheet, an increase in elongation of about 0.7% is noted. Since this increase in elongation is observed in the plane-strain case which is a critical strain path, this can be a considerable increase in percentage of elongation between DDQ steel as a single sheet and in double sheet. The increase in elongation of DDQ steel is caused by SS 316L during the global behaviour of double sheet which follows the similar result of Aghchai *et al.,* 2008. Similarly, in the case of adhesive bonded blanks, the plasticity of adhesive layer and SS 316L together with DDQ steel sheet has imparted improvement in the elongation of adhesive bonded blanks.

Table 2.14 Comparison of increase in elongation of DDQ steel and SS 316L sheets in adhesive bonded blanks with respect to double sheet

Adhesive bonded blank (ABB)	H/R ratio	Increase in total elongation (%)	
		DDQ steel sheet	SS 316L sheet
Epoxy based	0.6:1	3.1	0
	0.7:1	5.1	0
	0.8:1*	5.1	6.6
	0.9:1	6.7	6.6
	1:1	7.5	23.1
Acrylic based	0.8:1	0.9	0
	0.9:1	1.9	0
	1:1*	3.2	1.6
	1.1:1	5.9	3.5
	1.2:1	6.3	6.5

*Note:*Optimum ratios; Increase in % of total elongation = (Elongation of ABB till failure of DDQ steel sheet or SS 316L sheet – elongation of double sheet of DDQ steel sheet or SS 316L till failure) ×100*

2.6.2 Comparison of stress – strain behaviour of adhesive bonded blanks and single sheet

From Fig. 2.18(a, b), the increase in total elongation at the failure region of DDQ steel and SS 316L in both the types of adhesive bonded blanks is calculated as given in Table 2.15. The elongation is calculated with respect to the total elongation of DDQ steel and SS 316L single sheets of about 35.51% and 66.12%, respectively.

It is observed that there is a substantial increase in total elongation of DDQ steel in both the adhesive systems. There is a little increase in elongation of SS 316L sheets except in maximum levels of hardener/resin ratios. From the observation of a slight increase in total elongation of DDQ steel in double sheet, it is confirmed that the increase in total elongation obtained from DDQ steel sheet of adhesive bonded blanks is contributed by both adhesive layer and SS 316L sheet. The global behaviour of adhesive bonded blanks also increases the elongation in SS 316L sheets in the case of maximum levels of hardener/resin ratios.

Table 2.15 Comparison of improvement in total elongation of DDQ steel sheets and SS 316L sheets in adhesive bonded blanks with respect to single sheet

Adhesive bonded blank (ABB)	H/R ratio	Increase in total elongation (%) (13 mm gauge length)	
		DDQ steel sheet	SS 316L sheet
Epoxy based	0.6:1	3.49	0.18
	0.7:1	5.49	0.58
	0.8:1	5.49	7.48
	0.9:1	6.49	7.88
	1:1	7.49	24.88
Acrylic based	0.8:1	0.49	0.00
	0.9:1	1.99	0.00
	1:1	3.49	2.88
	1.1:1	5.49	4.88
	1.2:1	6.49	7.88

Note: Increase in % of total elongation = (Elongation of ABB till failure of DDQ steel sheet or SS 316L sheet – elongation of single sheet of DDQ steel sheet or SS 316L till failure) ×100

2.6.3 Comparison of stress – strain behaviour of adhesive bonded blanks with different hardener/resin ratios

Fig. 2.19(a, b) presents the engineering stress – strain behaviour of epoxy adhesive bonded blanks and acrylic adhesive bonded blanks. From the Fig. 2.19(a, b), increase in % elongation is calculated in the regions A, B and C, and shown in Figs. 2.20(a-c) and 2.21(a-c) for epoxy bonded and acrylic bonded sheets, respectively. A significant increase in % elongation at the region A (till adhesive failure) of global behaviour of adhesive bonded blanks with different hardener/resin ratios is observed. While comparing the total elongation at the region B, a substantial increase is noted in elongation with increase in hardener/resin ratio for both types of adhesive bonded sheets.

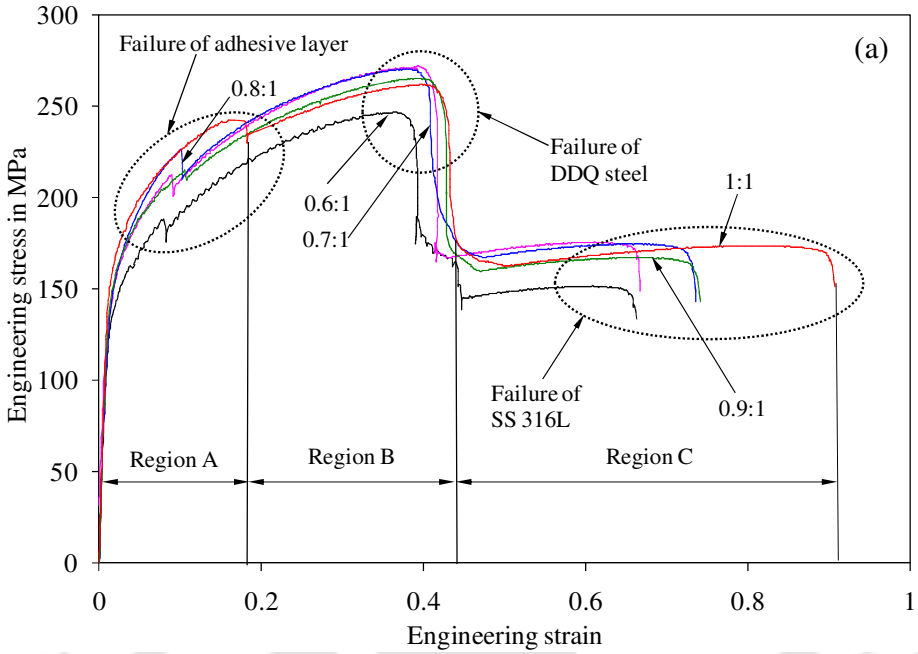

Error variation in ultimate strength = ±5 MPa and % of total elongation = 0.3 %

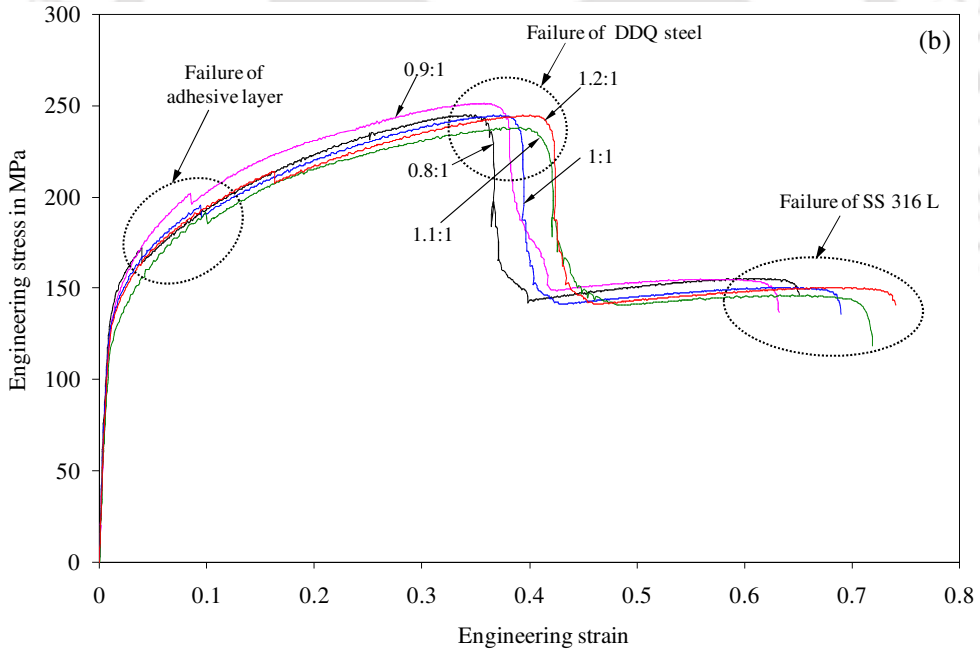

Error variation in ultimate strength = ±5 MPa and % of total elongation = 0.2 %

Fig. 2.19 Comparison of engineering stress-strain behaviour (a) epoxy adhesive bonded blanks with different H/R ratios, and (b) acrylic adhesive bonded blanks with different H/R ratios

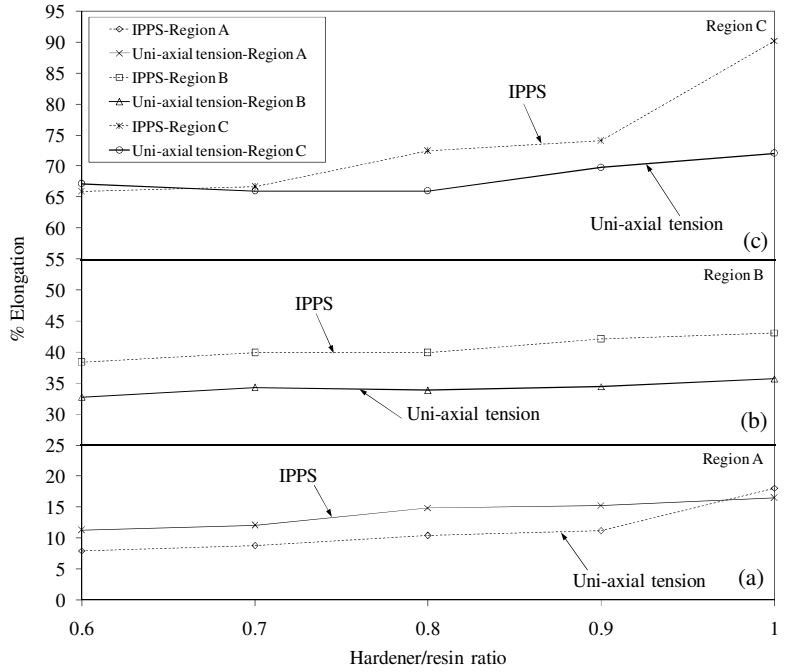

Fig. 2.20 Comparison of total elongation of different regions of epoxy bonded sheets from IPPS formability test and tensile test with different H/R ratios (a) Region A, (b) Region B, and (c) Region C. (Note: Total elongation at 13 mm gauge length for IPPS test and 82 mm for tensile test)

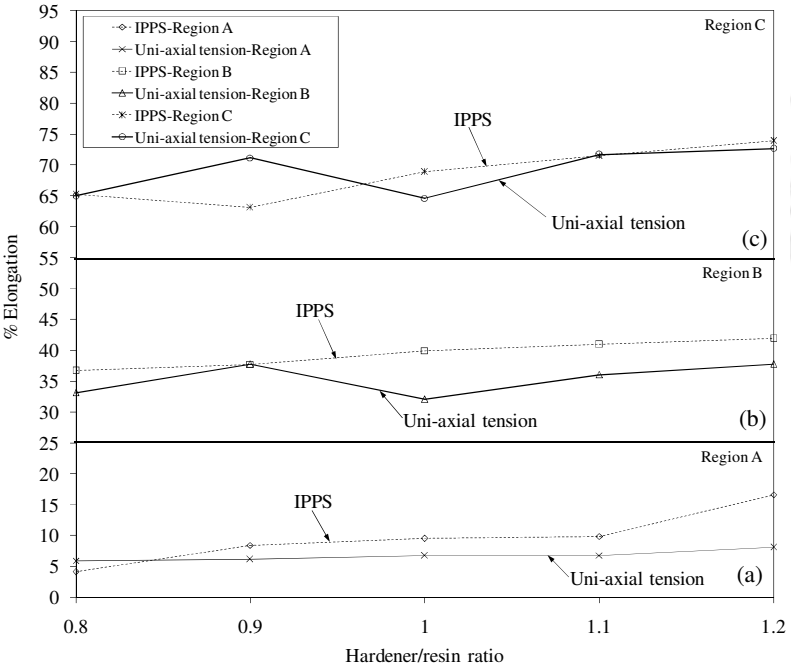

Fig. 2.21 Comparison of total elongation of different regions of acrylic bonded sheets from IPPS formability test and tensile test with different H/R ratios (a) Region A, (b) Region B, and (c) Region C. (Note: Total elongation at 13 mm gauge length for IPPS test and 82 mm for tensile test)

A considerable increase in total elongation is also observed at the region C of SS 316L sheets while performing IPPS formability test. Even though an improvement in total elongation in adhesive bonded blanks (region A and B) was observed in our previous investigation, the trend of total elongation at the region C of SS 316L sheets in adhesive bonded blanks were not clear. Figs. 2.20(a-c) and 2.21(a-c) also present the comparison of total elongation obtained in the regions A, B and C of epoxy and acrylic bonded sheets, respectively, with different hardener/resin ratios in the tension test and IPPS formability test. It is clear that the total elongation of region C of SS 316L sheet also increases with increase in hardener/resin ratio.

From these results, it is confirmed that because of increase in total elongation with increase in hardener/resin ratio in region A of global behaviour of adhesive bonded blanks, and since the improvement is preserved, both base materials showed improvement in the total elongation. This proves that the increase in total elongation at region B and C is due to the improvement in plastic deformation caused by the hardener rich formulated adhesive layer in both types of adhesive bonded blanks.

2.6.4 Comparison of strain hardening exponent (*n*) between single sheets, double sheets and adhesive bonded blanks

The strain hardening exponent (*n*) is calculated in the region A at which three materials are deforming, the region B in which DDQ steel and SS 316L are deforming after initial adhesive failure, and region C in which SS 316L is deforming after failure of DDQ steel. The strain hardening exponent (*n*) is also calculated for double sheet in the region 1 at which two base materials are deforming and the region 2 where SS 316L is deforming. The *n*-values of DDQ steel and SS 316L single sheets is determined as 0.381 and 0.536, respectively.

Table 2.16 shows the strain hardening exponent values in region 1 and 2 of stress-strain behaviour of double sheet. The strain hardening exponent values in the regions A, B and C of stress-strain behaviour of adhesive bonded blanks is tabulated in Table 2.17. While comparing the strain hardening exponent (*n*) value of double sheet in region 1 (Table 2.16) and adhesive bonded blanks (Table 2.17) till failure of DDQ steel sheets in region B, a significant increase in *n*-value is found for all the adhesive bonded blanks. A considerable difference in the *n*-values of region 2 and region C of SS 316L in double sheet and epoxy adhesive bonded blanks is also observed specifically at higher levels of hardener/resin ratio for both types of adhesive bonded blanks. When comparing the *n*-value till failure of DDQ steel from the stress-strain behaviour of double sheet (region 1 in Table 2.16) and DDQ steel single sheet, a substantial increase in *n*-value is

noted. It makes clear that the two layer sheet improves the formability of the DDQ steel sheet that correlates with the results of Aghchai *et al.,* 2008. In the comparison of *n*-value among both types of adhesive bonded blanks, an appreciable increasing trend of *n*-value is found with increase in hardener/resin ratio of global behaviour (region A). A considerable increase in *n*-values in regions B and C are also observed with increase in hardener/resin ratio.

Table 2.16 Strain hardening exponent (*n*) value in regions 1 and 2 of double sheet

Material	Region 1	Region 2
Double sheet	0.389	0.566

Table 2.17 Strain hardening exponent (*n*) value in regions A, B and C of adhesive bonded blanks

Adhesive bonded blank	H/R ratio	Region A	Region B	Region C
Epoxy based	0.6:1	0.244	0.404	0.579
	0.7:1	0.265	0.405	0.582
	0.8:1	0.288	0.409	0.586
	0.9:1	0.290	0.412	0.594
	1:1	0.291	0.425	0.663
Acrylic based	0.8:1	0.221	0.356	0.572
	0.9:1	0.246	0.404	0.579
	1:1	0.248	0.405	0.582
	1.1:1	0.267	0.406	0.584
	1.2:1	0.272	0.412	0.605

From these results, it is confirmed that the combined behaviour of adhesive layer and SS 316L improves the overall formability (global behaviour) of adhesive bonded blanks and also improves the formability of DDQ steel. This can be observed from the increase in *n*-value in the global double sheet behaviour (region 1) which is more than DDQ single sheet. Also the increasing trend of *n*-value in region B is more than region 1 of double sheet. This makes clear that the combined behaviour of adhesive layer and SS 316L improves the *n*-value of DDQ steel. Moreover, there is a significant improvement in '*n*' values in all the three regions of adhesive bonded blanks deformation with increase in hardener/resin ratio. This improvement finally has contributed to the improvement in elongation of adhesive bonded blanks as shown in Section 2.5.3.

2.6.5 Effect of adhesive properties on limit strain of adhesive bonded blanks in plane-strain condition

In this section, the influence of adhesive properties on the formability of adhesive bonded blanks is discussed through limit strains. The limit strains are evaluated by measuring the length of major and minor axes of deformed circular grids at the failure region of DDQ steel and SS 316L sheets constituting adhesive bonded blanks. Fig. 2.22(a, b) shows the method of measuring circular grids printed on the surface of base materials before and after deformation, during IPPS formability tests with photographs.

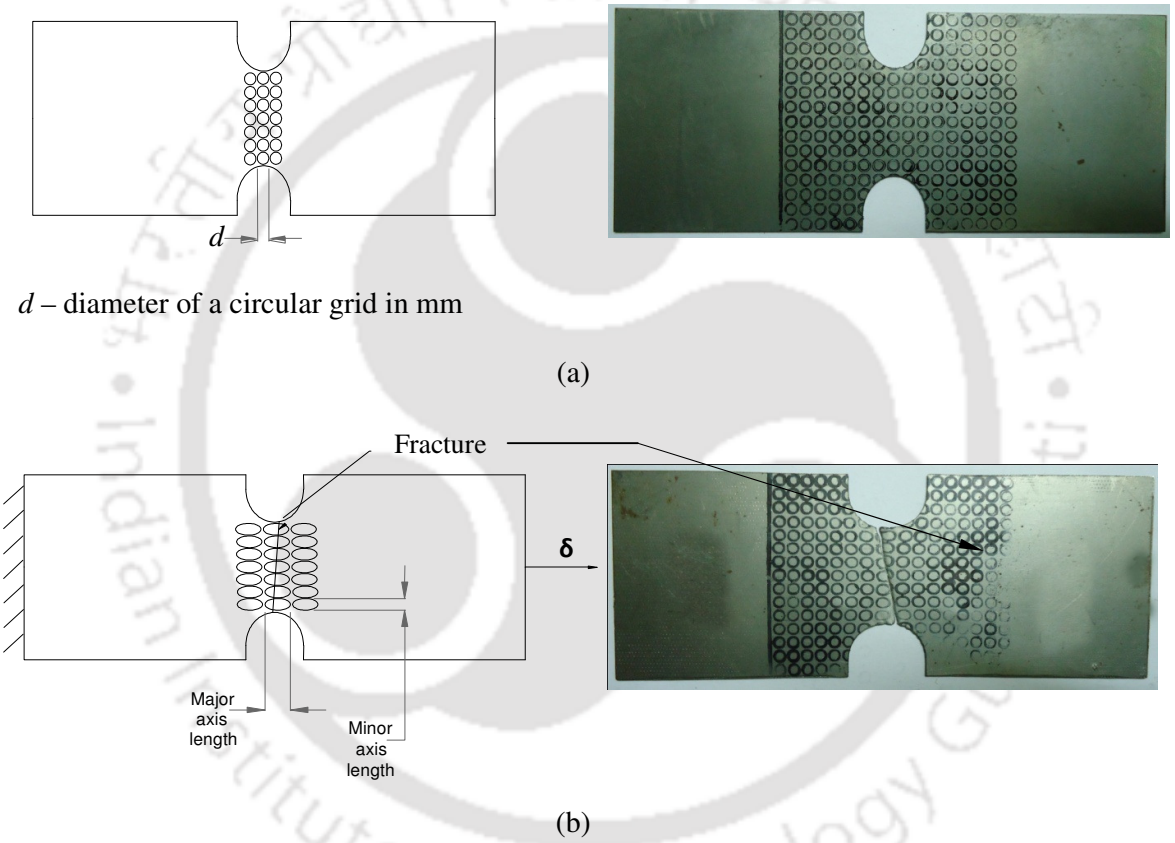

Fig. 2.22 Method of grid measurement (a) before deformation, and (b) after deformation

Fig. 2.23(a, b) shows the comparison of limit strains in DDQ steel sheet of epoxy adhesive bonded blanks and DDQ steel sheet of acrylic adhesive bonded blanks with different hardener/resin ratios, respectively. The limit strains in DDQ steel sheet of double sheet and single sheet of DDQ steel specimen are also included. Similarly, Fig. 2.24(a, b) shows the comparison of limit strain in SS 316L sheet of epoxy adhesive bonded blanks and SS 316L sheet of acrylic adhesive bonded blanks with different hardener/resin ratios, respectively. The limit strains in SS 316L sheet of double sheet and single sheet of SS 316L are also shown.

There is an improvement in forming limit strain with increase in hardener/resin ratio in case of both the types of adhesive bonded blanks and base materials. The limit strain of adhesive bonded blanks is larger than the limit strain observed for DDQ steel and SS 316L sheets in double sheet and monolayer sheets. The maximum forming limit strain is observed for the hardener/resin ratio of 1:1, and the minimum forming limit strain is noticed for 0.6:1 ratio in the case of epoxy adhesive bonded blanks. Similarly, the maximum forming limit strain is noted for 1.2:1 ratio, and the minimum forming limit strain is noticed for the hardener/resin ratio of 0.8:1 in the case of acrylic adhesive bonded blanks. The DDQ steel sheet of double sheet shows a significant increase in limit strain as compared to single sheet.

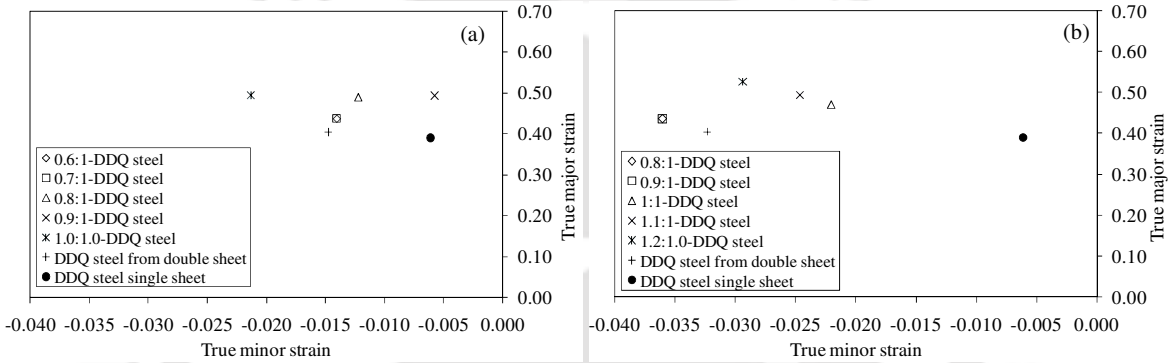

Fig. 2.23 Comparison of limit strain in DDQ steel specimen from double sheet, single DDQ sheet, (a) DDQ steel specimen from epoxy adhesive bonded blanks for different H/R ratios, (b) DDQ steel specimen from acrylic adhesive bonded blanks for different H/R ratios

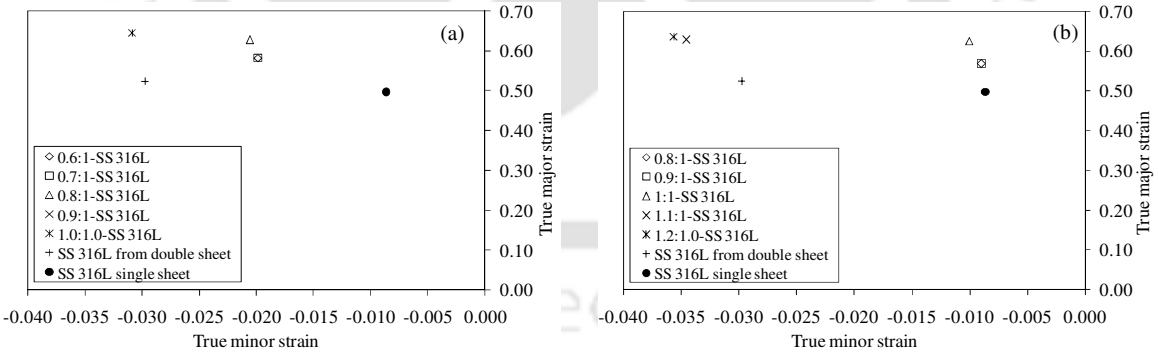

Fig. 2.24 Comparison of limit strain in SS 316L specimen from double sheet, single SS 316L sheet, (a) SS 316L specimen from epoxy adhesive bonded blanks for different H/R ratios, (b) SS 316L specimen from acrylic adhesive bonded blanks for different H/R ratios

There is about 5%–10% improvement in major limit strain of DDQ steel sheet and about 8.5%–15% in major limit strain of SS 316L sheet in epoxy bonded sheets, while about 4.5%–13.5% improvement in major limit strain of DDQ steel, and about 7% –13.5% in major limit

strain of SS 316L sheet in acrylic bonded sheets with respect to major limit strain of monolayer sheets. Both the acrylic and epoxy adhesive bonded sheets show almost equal amount of improvement in limit strain with increase in hardener/resin ratio.

There is a change in strain path away from the plane strain with increase in hardener/resin ratio is observed. The maximum variation in true minor strain is about 0.5–3.75% (Figs. 2.23 and 2.24). Elsewhere, Holmberg *et al.,* 2004 developed in-plane plane-strain sample geometry for determining the forming limit of sheet metals and tested with mild steel and high strength steel sheet materials. The results showed a minor strain of about 2–4% occurred during the test. Since an exact plane strain condition is difficult to achieve and the variation in true minor strain is smaller in range, this variation in strain path can be acceptable and it will not affect the overall results reported in the present study.

Generally, limit strain is directly proportional to strain hardening exponent (n), and improvement in the strain hardening exponent is an indication of improvement in forming limit strain. To illustrate the cause for improvement of limit strain observed in all adhesive bonded sheets as compared to double sheet and single sheets, the limit strain can be related to the n-value calculated in the regions A, B and C and in the regions 1 and 2 of the stress-strain behaviour of adhesive bonded blanks and double sheet, respectively, and adhesive properties. The global behaviour of double sheet shows larger n-value in region 1 (Table 2.16) than single DDQ steel sheet. This makes clear that the DDQ steel sheet specimen in double sheet has been deformed plastically more than the single DDQ steel sheet which has caused the increase in limit strain in DDQ steel specimen in the double sheet. Similarly, while comparing n-value in the region B (Table 2.17) of adhesive bonded blanks, the global behaviour of two base materials in adhesive bonded blanks shows larger n-value than single DDQ steel sheet and DDQ steel from double sheet. This is because of the improved plastic deformation caused by the global behaviour of adhesive bonded blanks which has increased the limit strain in both base materials by delaying the failure of base materials. The plastic deformation caused by the global behaviour of adhesive bonded blanks in region 1 is controlled by the rich hardener formulation of adhesive as discussed in Section 2.3.1.

2.6.6 Uncertainty in limit strain measurement

The standard deviation of true major limit strain ranges from 0.001 to 0.035 and the standard deviation of true minor strain ranges from 0.001 to 0.021 for DDQ steel sheets. Similarly, the standard deviation of true major limit strain ranges from 0.004 to 0.058 and the standard deviation of true minor ranges from 0.005 to 0.025 for SS 316L sheets. From the evaluation of

standard deviation, a considerable difference in limit strains between all cases of DDQ steel and SS 316L sheets including bonded and single sheet cases is checked. These results confirm an inherent improvement in the limit strain and not just the data variation because of experimentation.

2.7 Conclusions

The following conclusions are drawn from this Chapter.

- The epoxy and acrylic adhesives show improved elongation with increase in hardener to resin ratio. This is mainly due to the changeover of resin rich formulation to hardener rich formulation turning the sample more ductile. This is qualitatively agreeing with literature results.
- The adhesive bonded sheets exhibits a typical failure pattern: First the lower ductile adhesive fails, then DDQ steel fails, and finally SS316L sheet fails because of larger elongation as compared to DDQ steel.
- The adhesive bonded blanks showed improved elongation as compared to double sheet, which is due to the effect of presence of adhesive delaying the onset of necking. In the same manner, the elongation of adhesive bonded sheets is better than single sheets, DDQ and SS316L. This is due to the improved elongation in the region of deformation of three layers which is preserved during failure of individual sheets of adhesive bonded blanks.
- With increase in hardener to resin ratio, the elongation of individual sheets has improved. This is true in both the adhesive systems. This is due to the improvement in elongation of adhesives with increase in hardener to resin ratio. This indicates formability improvement with increase in hardener to resin ratio.
- The strain hardening exponent (n) of adhesive bonded blanks has increased with increase in hardener to resin ratio in all the regions of deformation. The region of three layer deformation (before adhesive failure) and two layer deformation (after adhesive failure, but before DDQ steel failure) show sufficient increase in 'n' value, while the last region (before SS316L failure) show small improvement. The improvement in 'n' value of bonded blanks is an indication of formability improvement. The adhesive bonded blanks have larger 'n' value as compared to double sheet in the corresponding regions of deformation.
- The limit strain of DDQ and SS316L sheets constituting bonded blanks show improvement with increase in hardener to resin ratio of both the adhesives, which again implies that formability has improved. This is due to the plasticization of adhesives at higher hardener to

resin ratios. The epoxy adhesive bonded blanks show larger limit strain than acrylic adhesive bonded blanks, showing better formability.

- The adhesive bonded blanks with interface bonding exhibit better formability (limit strain) as compared to the case without interface bonding.
- The novelty of this work lies not only on showing the effect of adhesive properties on the forming of metal sheets constituting adhesive bonded blanks, but also on the sample geometry used for such formability analyses. An in-plane plane-strain formability sample is specifically designed for this purpose using finite element simulations and used in the present work.
- During IPPS formability tests of actual adhesive bonded steel sheets, the total elongation is found to be improved with increase in hardener/resin ratio. Increase in hardener/resin ratio of adhesive systems increases the forming limit strains in adhesive bonded blanks. This has been confirmed in the formability of adhesive bonded sheets in plane-strain strain-path.
- In the global behaviour of adhesive bonded blanks, the material which has high formability (SS 316L) and adhesive layer together improves the formability of DDQ steel which possesses low formability.

Chapter 3

Formability of adhesive bonded steel sheets with artificial adhesive defects

3.1 Experimental Methodology

In this section, the method of artificial adhesive defects generation in the adhesive bonded sheets, and the formability evaluation are discussed. The mechanical properties of base materials and epoxy adhesive are already discussed in Chapter 2 in Sections 2.1.1 and 2.4.1, respectively.

3.2 Testing of adhesive bonded blanks and formability evaluation

In this work, two different types of adhesive defects like finite and infinite defects were pregenerated in the adhesive layer constituting adhesive bonded blanks. Here adhesive finite defect refers to the defect which is surrounded by adhesive in all the directions except in the thickness direction, whereas the adhesive infinite defect is not surrounded by adhesive in one of the directions (width or length direction), and the absence of adhesive in the thickness direction remain same.

The adhesive bonded tensile specimens and IPPS formability test specimens were prepared by using epoxy adhesive with constant hardener/resin ratio of 1:1, for which the total elongation is higher as given in Table 2.6, and also larger formability was observed for the adhesive bonded blank in Chapter 2. In the case of adhesive finite defect, the shape and the aspect ratios (a/b) of defect, locations, and number of defects were varied during tensile test. Fig. 3.1(a) shows the geometry of the adhesive bonded tensile specimen showing different aspect ratios of finite defects in the adhesive layer in the same sample. Similarly, Figs. 3.1(b) and 3.1(c) show the geometry of the adhesive bonded tensile specimen showing increasing number of defects and different locations of defects in the adhesive layer in the same sample. The geometry of IPPS forming test specimen is shown in Fig. 3.1(d) as an adhesive bonded blank with finite defects in the adhesive layer. Because of smaller gauge region (13 mm × 8 mm notch) of IPPS forming test specimen, the IPPS formability test was carried out to investigate the effect of shape and aspect ratio of the adhesive finite defects in adhesive bonded blanks. Fig. 3.1(e-g) shows the magnified view of three types of defect with a/b = 1, 0.5 and 1.5 which were captured by stereomicroscope.

The preparation of adhesive bonded blanks was followed as per the procedure discussed in Chapter 2 in Section 2.3. The finite defects in the adhesive layer of adhesive bonded blanks were artificially generated by using chips of polystyrene sheet. Once the adhesive was spread uniformly on the first blank, the polystyrene chip was introduced at the defect location. The second blank was bonded after that by keeping the polystyrene chip inside the adhesive bonded. After allowing the adhesive layer to the stage of rubbery, the polystyrene chip was dissolved by Xylene rectified solvent drop that was injected by a syringe having needle diameter of 0.3 mm. The diameter of circular finite defect characterized as a/b = 1 was maintained as ∅6±0.05 mm. The other two finite defects were made at a/b = 0.5 (a = 3±0.017 mm; b = 6±0.021 mm), and a/b = 1.5 (a = 9±0.015 mm; b = 6±0.015 mm).

The choice of aspect ratios and shapes in the present work is based on the minimum dimension of defect that can be generated and handled manually. The choice of different locations is based on the aim to understand the effects of defects in the gauge region and away from the gauge region. The influence of multiple defects at locations far from each other is to understand the strain localization and to overcome accordingly the effect of multiple adhesive defects. To ensure the uniformity of the finite defects in the adhesive layers in adhesive bonded blanks, about five adhesive layers in the presence of finite defect with different aspect ratios were measured by using profile projector and uniform shapes of the defects were ensured. The average thickness of adhesive layers in adhesive bonded blanks was found to be 1±0.015 mm.

Similarly, the adhesive infinite defects were generated in the adhesive layer by using strips of polystyrene sheet. The orientations of adhesive infinite defects were varied like longitudinal, 45º inclined, and transverse. Here the strips of polystyrene sheet were held on one of base materials where the infinite defect to be created in the epoxy adhesive. After dissolving the polystyrene strip, the place of strip located in the adhesive was considered as a defect. Fig. 3.2(a, b) presents the adhesive bonded tensile and IPPS forming test specimen showing different orientations of adhesive infinite defects in the same sample. The average width of infinite defects in the adhesive layers in adhesive bonded blanks was found to be 2±0.017 mm. The average thickness of adhesive layers in adhesive bonded blanks was found to be 1±0.015 mm. The tensile tests and IPPS formability tests on adhesive bonded sheets were carried as discussed in Chapter 2 in Section 2.3.

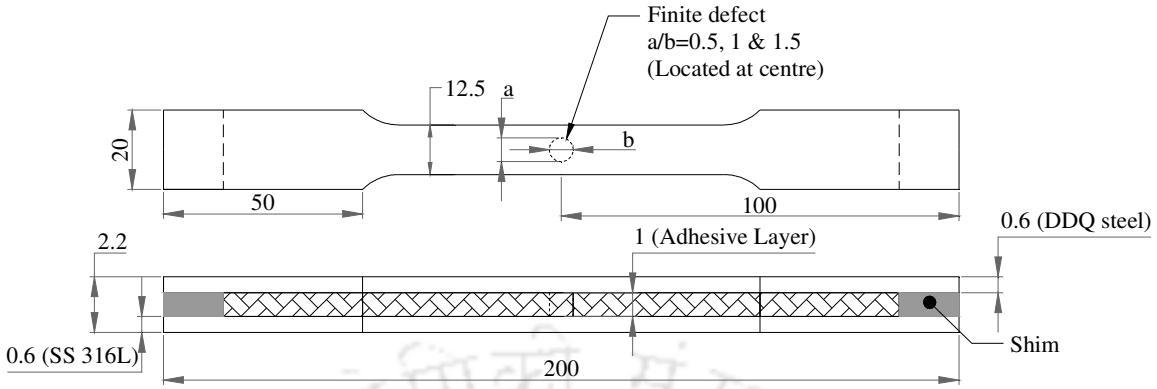

(a)

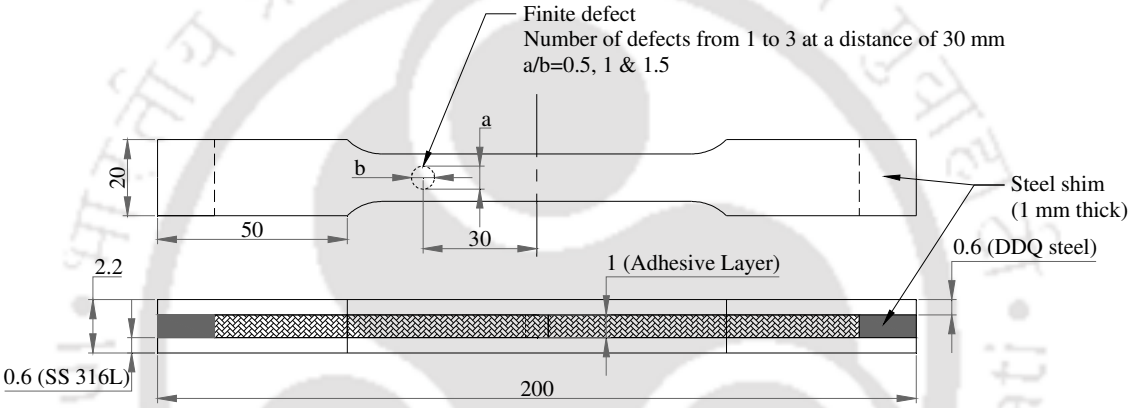

(b)

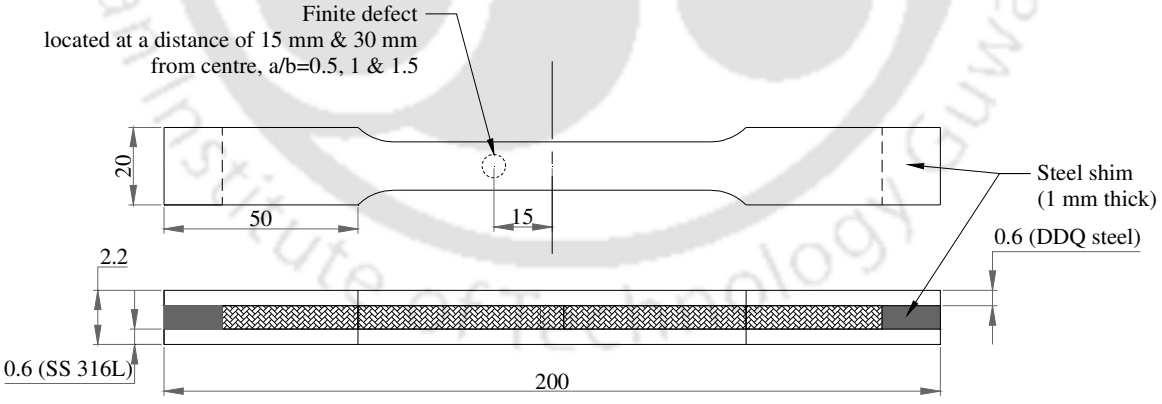

(c)

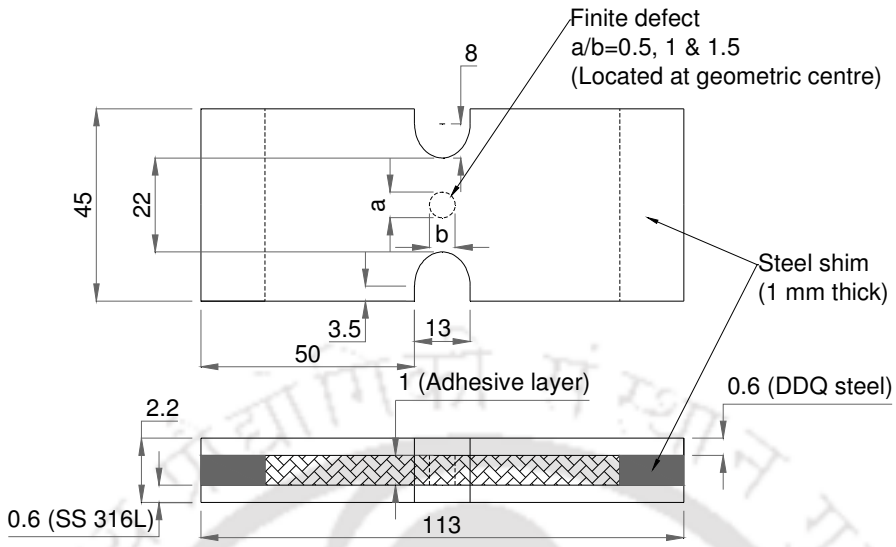

(d)

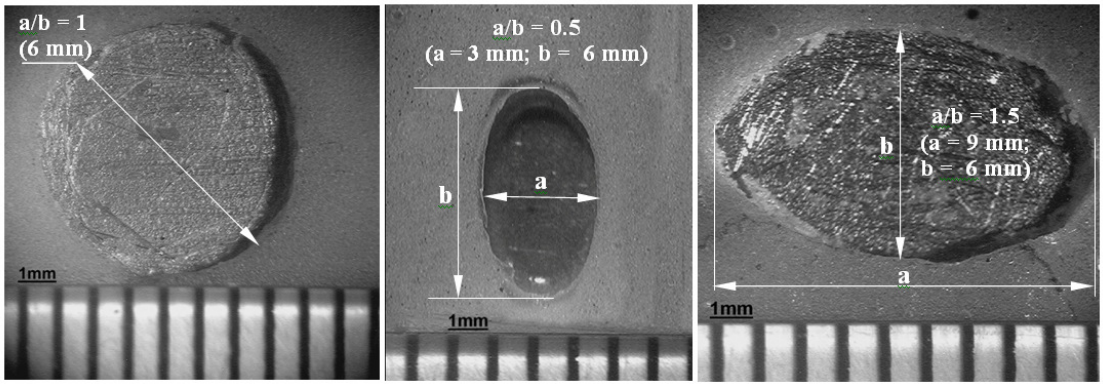

(e) (f) (g)

Fig. 3.1 Tensile sample made of adhesive bonded blanks (a) showing geometry of shape and aspect ratio of adhesive defects (Only one defect was made in each sample), (b) showing geometry of increase in number of defects from 1 to 3, (c) showing geometry for different locations of defects (Only one defect per sample), (d) geometry of IPPS adhesive bonded formability testing specimen showing different shapes and aspect ratios of adhesive finite defects; Magnified view of adhesive finite defects with (e) *a/b* = 1, (f) *a/b* = 0.5, and (g) *a/b* = 1.5 (All dimensions in mm)

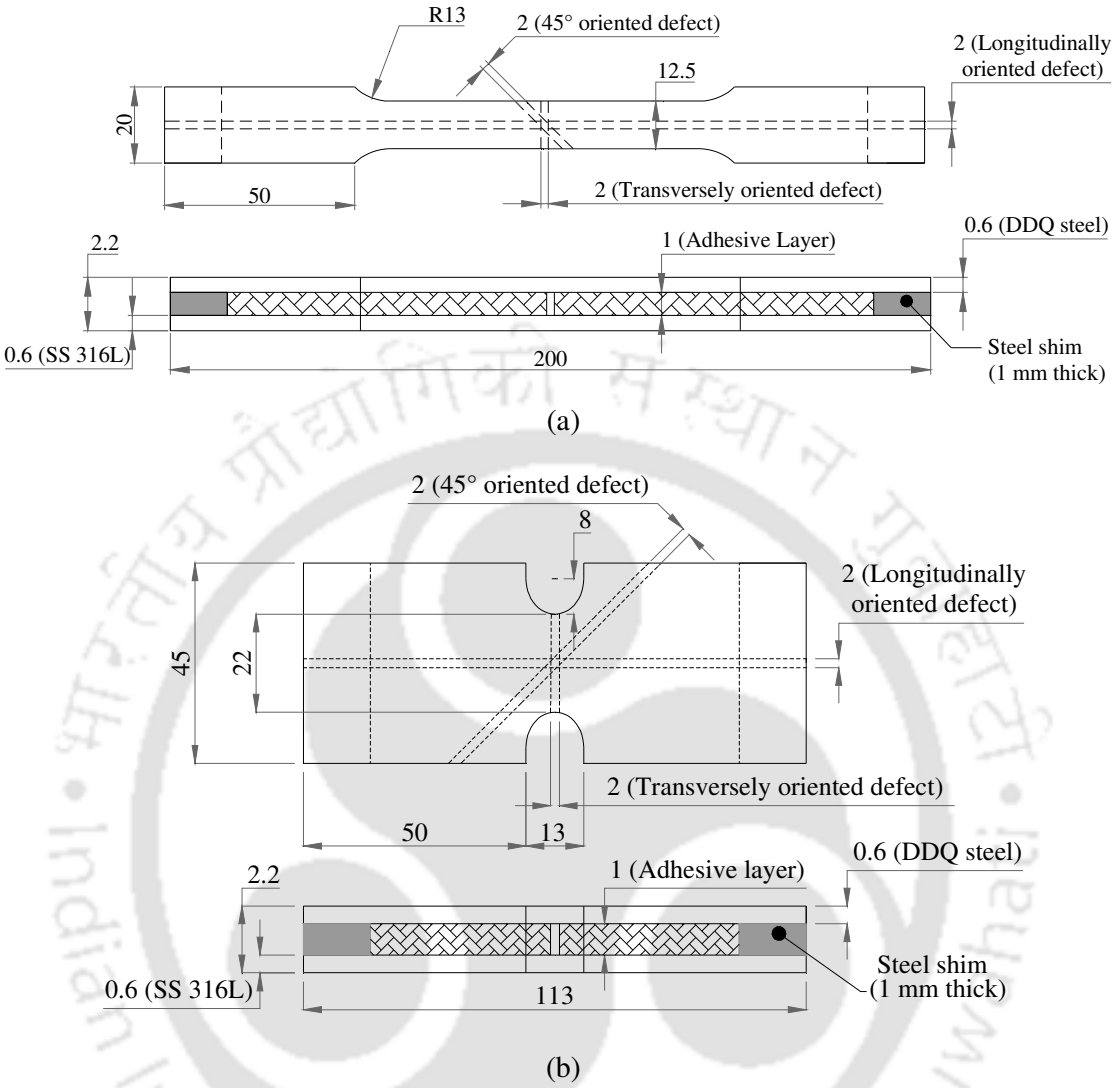

Fig. 3.2 (a) Tensile sample made of adhesive bonded steel sheets showing different orientations of adhesive infinite defects, and (b) Geometry of IPPS adhesive bonded formability testing specimen showing different orientations of adhesive infinite defects. All dimensions in mm. (Note: All the defects are shown in the same figure, and only one defect was made in each sample)

3.3 Results and discussion

3.3.1 Failure pattern of adhesive bonded blanks with finite defects in the adhesive

The failure pattern during tensile test and IPPS formability test of the adhesive bonded blanks in the presence of adhesive finite defects with different aspect ratios and shapes is proposed as follows. Fig. 3.3(a-c) presents some of the failure pattern of adhesive bonded sheets during tensile test and IPPS formability test with adhesive finite defects.

The failure of adhesive layer is observed at the location of finite defects during both tests. Early failure of adhesive layer was observed when *a/b* = 1.5 at first during testing, and the failure of finite defects is in the order, *a/b* = 1.5, 1 and 0.5, respectively. This is due to the concentration of strain at the reduced cross-section area, at the location of finite defects in the adhesive layer. First, the adhesive fails in the gauge region where defect is located. Later, the interfacial layer and bonding between adhesive layer failed due to relative motion between them and the base materials. As like the failure pattern of adhesive bonded blanks discussed in Chapter 2 during tensile testing in Section 2.4.2 and IPPS formability testing in Section 2.6.1, here also the base materials, DDQ steel and SS 316L sheets bear the tensile load and behave as a double sheet after failure of adhesive layer. Further, the failure of DDQ steel sheet was noticed at the location of failure of adhesive layer. At last, the failure of SS 316L sheet of the adhesive bonded blank was observed in the gauge region, but randomly after the failure of DDQ steel specimen.

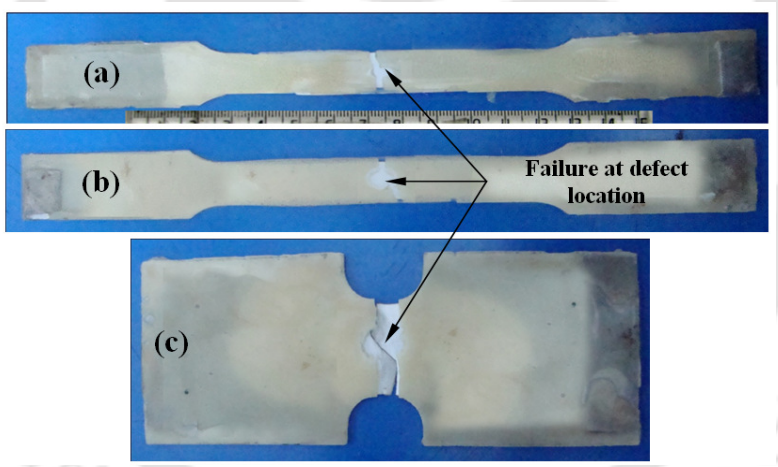

Fig. 3.3 Failure pattern of adhesive layer in adhesive bonded blanks with different aspect ratios, (a) *a/b* = 0.5 (tensile specimen), (b) *a/b* = 1 (tensile specimen), and (c) *a/b* = 1.5 (IPPS specimen)

The typical failure pattern of the adhesive bonded blanks with increase in number of finite defects in the adhesive layer during tensile test is proposed as follows. Fig. 3.4(a-c) shows some of the failure pattern of adhesive bonded specimens with increase in number of finite defects. Though there is an increase in number of finite defects, the failure of adhesive layer is noticed at only one location among the defects. Most of the failures were noticed at the centre of gauge region where one of the defects was located (Fig. 3.4(a)), for the aspect ratios of 0.5 and 1. A random failure location was witnessed in the case of aspect ratio of 1.5 (Fig. 3.4(b)). It is expected that the failure will occur within the gauge region of tensile sample as large deformation

happens here. The deformation/strain decreases from the gauge region centre towards the gripping region. Hence, failure will happen in the adhesive defect located as the geometric centre of the sample. There may not be considerable deformation in the defects located at eccentric location because of lesser strain development as compared to the geometric centre. The same has happened in the cases of defective cases with 0.5 and 1. But a random failure is witnessed in the case of 1.5 aspect ratio defect which could be due to the larger contribution of defect width (a = 9 mm) as compared to tensile sample width of 12.5 mm. Even a small variation in the defect dimension would change the failure location randomly, in this case. Here also early failure of adhesive layer was observed during testing in the order of finite defects with a/b = 1.5, 1 and 0.5, respectively, regardless of increase in number of defects. The failure pattern of base materials remain unchanged, with DDQ steel failing first and then SS 316L, after adhesive failure. During testing of adhesive bonded blanks with increase in number of defects, about 78% and 89% of adhesive failure was observed at the centre defect for a/b = 0.5 and 1, respectively. About 67% of adhesive failure was noticed at the centre defect location for a/b = 1.5, respectively.

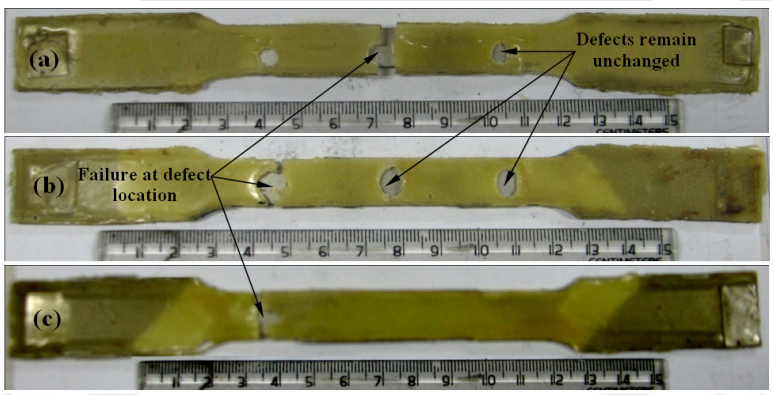

Fig. 3.4 Failure pattern of adhesive layer in the adhesive bonded blanks with different numbers and location of adhesive defects: (a) a/b = 1 (presence of three defects), (b) a/b = 1.5 (presence of three defects), and (c) a/b = 0.5 located at 30 mm from centre

The failure of adhesive layer is noticed at the adhesive defect location (Fig. 3.4(c)). Early failure of adhesive layer was observed during testing in the order of finite defects with a/b = 1.5, 1 and 0.5, respectively, regardless of different locations of adhesive defects. The base materials failed in the usual manner as presented in previous sub-sections.

3.3.2 Effect of aspect ratio and shape of adhesive finite defect on the tensile behaviour and IPPS formability of adhesive bonded blanks

3.3.2.1 Load – extension behaviour of adhesive bonded blanks

Figs. 3.5(a) and 3.5(b) show the comparison of load–extension behaviour of adhesive bonded tensile specimens and IPPS formability testing specimens, respectively. Here all three regions A, B and C are observed with respect to global behaviour of adhesive bonded blank, global behaviour of double sheet (DDQ steel and SS 316L), and behaviour of SS 316L sheet.

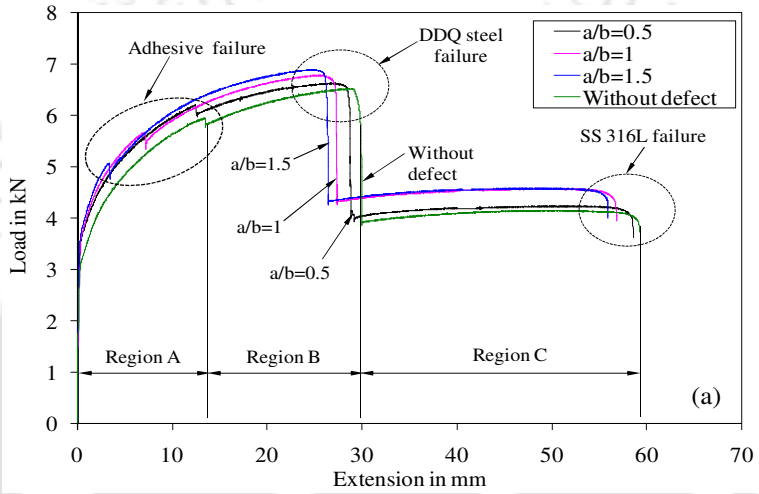

Error variation in maximum load = ±0.4 kN and total extension = ± 0.55 %

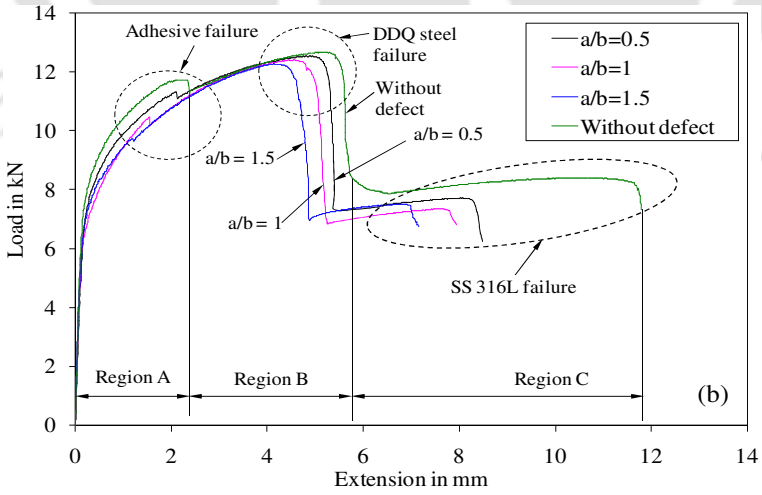

Error variation in maximum load = ±0.25 kN and total extension = ± 0.65 %

Fig. 3.5 Comparison of load – extension behaviour of adhesive bonded blanks with and without adhesive finite defect (a) tensile tested epoxy bonded blanks, and (b) IPPS formability tested epoxy bonded blanks

It is understood from the results discussed in Chapter 2 that the improved plastic deformation of the adhesive layer increases the formability of adhesive bonded blanks. But here, a decrease in extension with increase in aspect ratio (*a/b*) of adhesive defect is noticed in region A, which also reduces the extension till failure in the regions B and C.

From Fig. 3.5(a, b), with respect to the extension at failure observed in region A, B and C of the adhesive bonded blank without adhesive defect, the decrease in extension at failure is calculated for the adhesive bonded blanks with different aspect ratios of adhesive defect during tensile and IPPS forming tests in Fig. 3.6(a, b). A significant decrease in extension (of about 5-70% in tensile tests, and about 10-50% in IPPS forming tests) is observed in all regions (region A, B and C) due to the presence of adhesive finite defects.

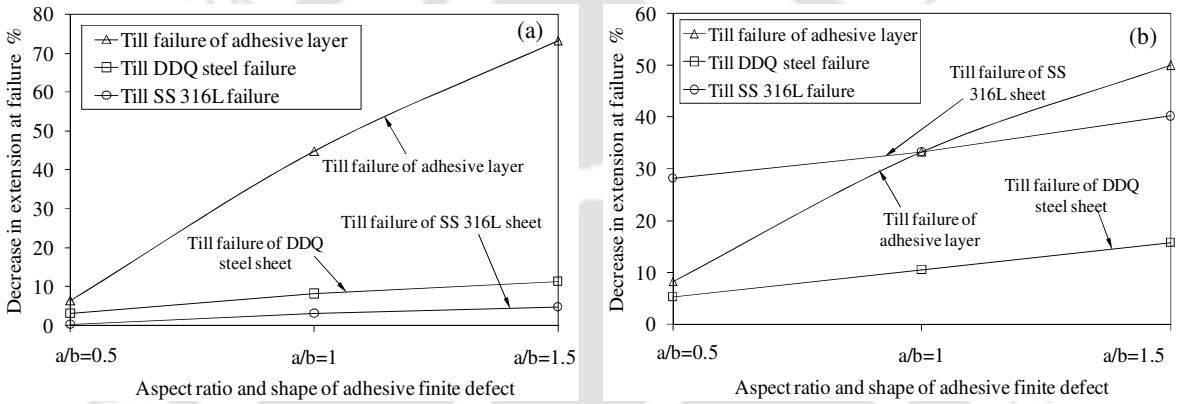

Fig. 3.6 Decrease in extension at failure % in different deforming regions A, B, and C: (a) tensile test, and (b) IPPS forming test (Note: Decrease in total extension (%) = (Extension of ABB without infinite defect till failure of DDQ steel sheet or SS 316L sheet – extension of ABB with infinite defect till failure of DDQ steel sheet or SS 316L sheet) / (Extension of ABB without infinite defect) ×100)

It is understood that the additional plastic deformation caused by the global deformation of adhesive bonded blank to DDQ steel and SS 316L is reduced by the shape and aspect ratio of the adhesive finite defects. It can also be perceived that the increase in plastic deformation of adhesive layer that improves the formability of adhesive bonded blank is reduced by shape and aspect ratio of adhesive finite defects.

3.3.3 Limit strain of adhesive bonded blanks

Figs. 3.7(a) and 3.7(b) show the comparison of limit strains of DDQ steel and SS 316L sheets from tensile tests, respectively, in adhesive bonded blanks with different aspect ratios (*a/b*) of finite defects. The adhesive bonded blank without adhesive defect is also compared.

Similarly, Figs. 3.8(a) and 3.8(b) present the comparison of limit strains, from IPPS formability test. It is observed that there is a significant decrease in forming limit strains of DDQ steel and SS 316L in adhesive bonded blanks with finite defects as compared to the limit strains of DDQ steel and SS 316L in adhesive bonded blank without defect. There is about 0.9–12.6% reduction in true major strain and around 2.9–19.5% reduction in true minor strain of DDQ steel sheet, and about 0.5–11.9% in true major strain and about 2.8–10.5% reduction in true minor strain of SS 316L sheet with respect to true major strain of adhesive bonded sheets without adhesive defect during tensile test. Similarly, there is about 1.2–5.3% reduction in major strain and about 0.2–1.1% reduction in true minor strain of DDQ steel sheet, and about 1.5–9.7% in major strain and about 0.2–1.7% reduction in true minor strain of SS 316L sheet during IPPS formability test.

It is observed that the limit strain of DDQ steel and SS 316L in adhesive bonded blank with defect aspect ratio of 0.5 shows less difference (0.9%) as compared to base materials in adhesive bonded blank without adhesive defect. When comparing the limit strain results among the aspect ratios, there is about 6.3% and 4.8% difference between a/b = 0.5 and 1 with respect to DDQ steel and SS 316L, respectively. Similarly, about 13.4% and 13.2% difference is observed between a/b = 0.5 and 1.5, and about 7.1% and 8.4% difference is determined between a/b = 1 and 1.5. From these results, it can be perceived that the aspect ratio of a defect below a certain limit, that is a/b = 0.5 in the present work, does not have considerable effect on the formability of adhesive bonded blanks. This again reveals that micro-bubbles having volume equivalent of less than or equal to a/b = 0.5 in the adhesive may not affect the formability of adhesive bonded blanks significantly.

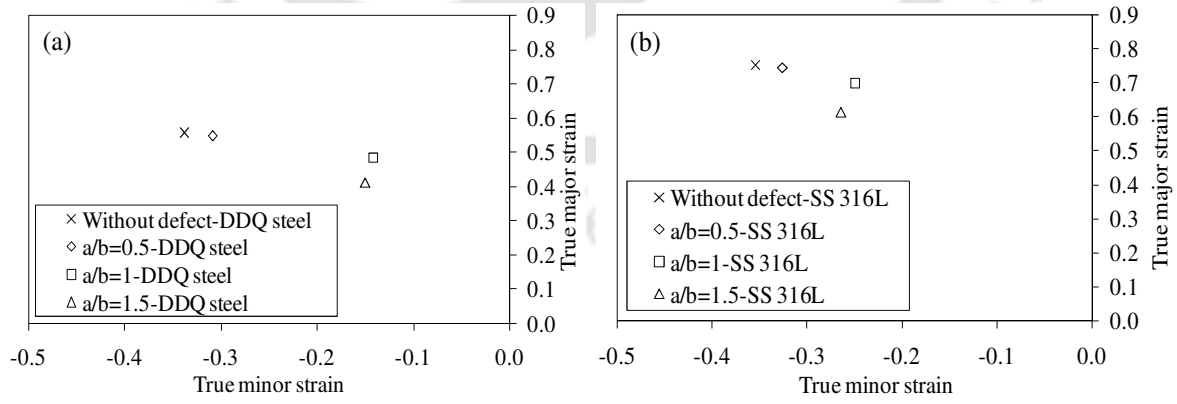

Fig. 3.7 Comparison of limit strain of base materials constituting adhesive bonded blanks with influence of different aspect ratios of adhesive finite defect in tensile test, (a) DDQ steel specimen, and (b) SS 316L specimen

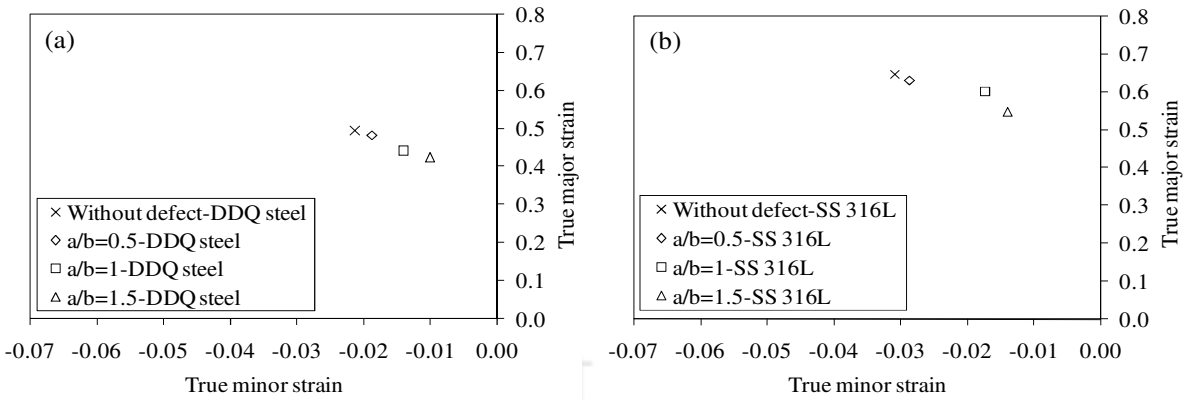

Fig. 3.8 Comparison of limit strain of base materials constituting adhesive bonded blanks with influence of different aspect ratios of adhesive finite defect in IPPS forming test, (a) DDQ steel specimen, and (b) SS 316L specimen

Table 3.1 Uncertainty measurement of limit strain

Formability test	Standard deviation			
	True major strain		True minor strain	
	DDQ steel	SS 316L	DDQ steel	SS 316L
Tensile test	0.020 to 0.048	0.003 to 0.035	0.020 to 0.047	0.001 to 0.004
IPPS forming test	0.004 to 0.046	0.012 to 0.036	0.007 to 0.022	0.005 to 0.032

Further, uncertainty analysis on determination of limit strain was carried out. Table 3.1 shows the standard deviation of true major limit strain and true minor limit strain ranges for DDQ steel and SS 316L sheets in adhesive bonded blanks with and without adhesive defect. These error variations are much smaller than the limit strain variation among different adhesive bonded samples. Hence, these results confirm an inherent reduction in the limit strain rather than just the scatter of limit strain results.

3.3.4 Comparison of strain hardening exponent (*n*) between adhesive bonded blanks with adhesive finite defects and without defect

The reduction in limit strains can be related to the strain hardening exponent (*n)* determined in the regions A, B and C of the tensile behaviour of adhesive bonded blanks with and without adhesive defect. Table 3.2 shows the *n*-value in regions A, B and C of adhesive bonded blanks without adhesive defect case from tensile and IPPS forming tests. Table 3.3 shows the comparison of *n*-value in regions A, B and C of adhesive bonded blanks with different aspect ratios (*a/b*) in tensile and IPPS forming tests. While comparing the '*n*' values of all three regions,

the adhesive bonded blanks without pregenerated adhesive defect has larger '*n*' values, as compared to the cases with defect. A decrease in '*n*' value is observed in the order of *a/b* = 0.5, 1 and 1.5 aspect ratio, in all three regions. This has basically reflected in ductility and limit strain of base materials. With decrease in '*n*' value from *a/b* = 0.5 to 1.5, the ductility and limit strains have decreased.

Table 3.2 Strain hardening exponent (*n*) in regions A, B and C of adhesive bonded blanks without pregenerated adhesive finite defect from tensile and IPPS formability tests

Test type	Region		
	A	B	C
Tensile test	0.287	0.394	0.517
IPPS formability test	0.291	0.425	0.663

Error variation in *n*-value in region A = ±0.003, region B = ±0.002, and region C = ±0.002

Table 3.3 Strain hardening exponent (*n*) in regions A, B and C of adhesive bonded blanks with different aspect ratios (*a/b*) of adhesive finite defect from tensile and IPPS formability tests

Aspect ratio (*a/b*)	Tensile test			IPPS formability test		
	Region			Region		
	A	B	C	A	B	C
0.5	0.281	0.374	0.483	0.275	0.401	0.635
1.0	0.219	0.339	0.480	0.259	0.394	0.620
1.5	0.204	0.319	0.469	0.232	0.378	0.558

Error variation in *n*-value in region A = ±0.003, region B = ±0.002, and region C = ±0.001

3.3.5 Comparison of strain gradient between adhesive bonded blanks with and without adhesive finite defects

Fig. 3.9 shows the strain gradient of DDQ steel sheet in adhesive bonded blanks without adhesive defect and with adhesive finite defect for *a/b* = 1 and 1.5 which were tested till failure of DDQ steel sheet. In the comparison of strain distribution in DDQ steel between without and with defect cases, a decrease in peak major strain (nothing but limiting major strain) and hence a lower strain gradient distribution is observed in the presence of adhesive defect cases. It is also seen that there is a decrease in peak major strain and hence the strain gradient with increase in aspect ratio from 1 to 1.5. This reveals that increase in aspect ratio or on the other hand increase in aspect ratios of adhesive finite defect results in early failure of adhesive layer reducing the formability/forming limit of base materials in adhesive bonded blanks.

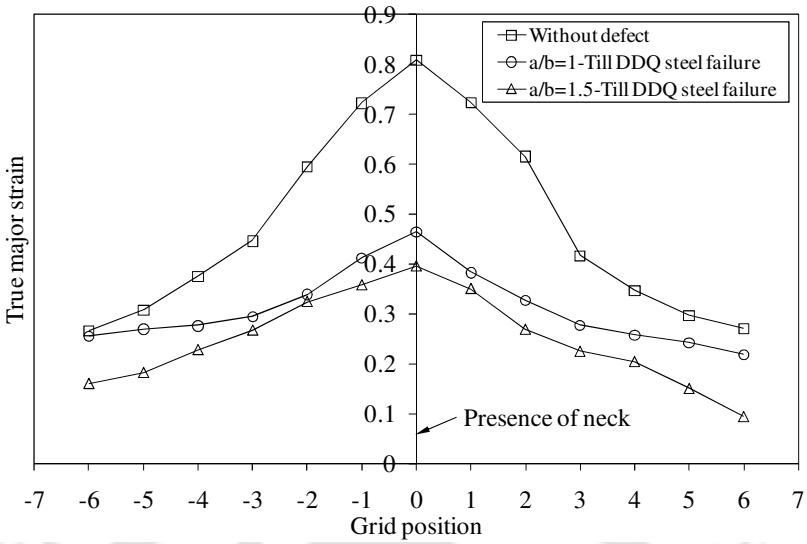

Fig. 3.9 Comparison of strain gradient of DDQ steel sheet in adhesive bonded blanks between with and without adhesive finite defect till failure of DDQ steel from tensile test with different aspect ratios

3.3.6 Effect of number of adhesive finite defects on the tensile behaviour of adhesive bonded blanks

3.3.6.1 Influence on the load-extension behaviour

The comparison of load–extension behaviour obtained from the tensile testing of adhesive bonded sheets with increase in number of adhesive defects for different aspect ratios, a/b = 0.5, 1, and 1.5 is presented in Fig. 3.10(a-c). The adhesive bonded blanks without pregenerated adhesive defects and with increase in number of adhesive defects are compared. It is seen that there is no considerable difference in load-extension behaviour with increase in number of finite defects.

From Fig. 3.10(a-c), with respect to the extension at failure observed in region A, B and C of the adhesive bonded blank without adhesive defect, the decrease in extension at failure is calculated for the adhesive bonded blanks with increase in number of adhesive defects. There is about 2% decrease in extension in all regions (region A, B and C) with increase in the number of adhesive finite defects in the adhesive layer, which is insignificant. From these results, it is understood that the additional plastic deformation caused by the global deformation of adhesive bonded blank to DDQ steel and SS 316L is not influenced by increase in number of finite defects. Also the improved plastic deformation of adhesive layer which imparts additional plastic deformation to the base materials in adhesive bonded blanks is not influenced by increase in number of adhesive finite defects which are located at equi-distance. This is due to the strain

concentrated locally at reduced cross-section of adhesive layer, where the centre finite defect is located in the gauge region. Sometimes the failure has happened at the defects located away from the gauge region also (Fig. 3.4(b)) as discussed in Section 3.3.1. Once the strain is localized at one of the defects, there is no deformation at all in the other defects presented in the adhesive layer (Fig. 3.4(a-c)). This type of adhesive bonded blanks failure is equivalent to the behaviour of the adhesive bonded blanks with single adhesive defect. Hence, there is not much difference in the ductility with increase in number of adhesive finite defects.

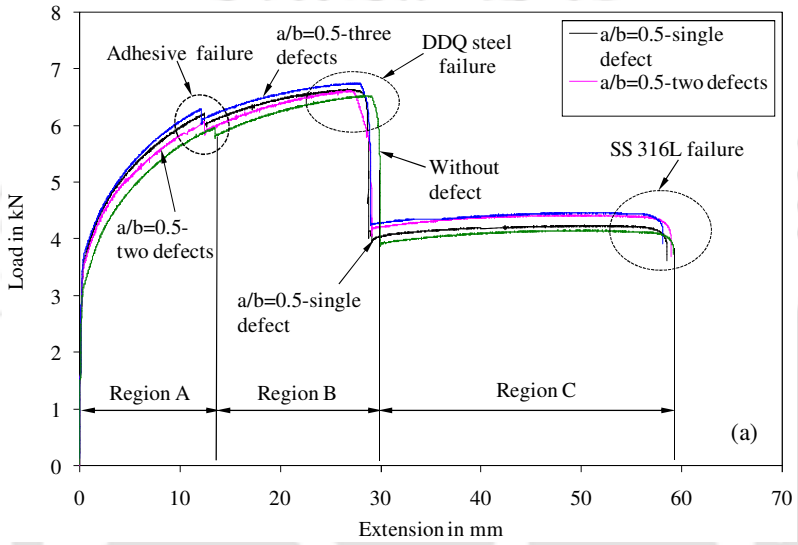

Error variation in maximum load = ±0.25 kN and total extension = ± 0.5%

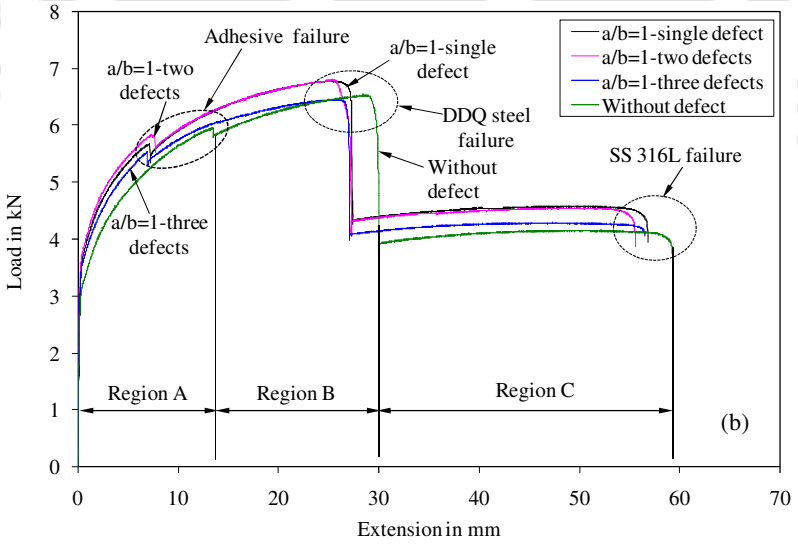

Error variation in maximum load = ±0.5 kN and total extension = ±0.4%

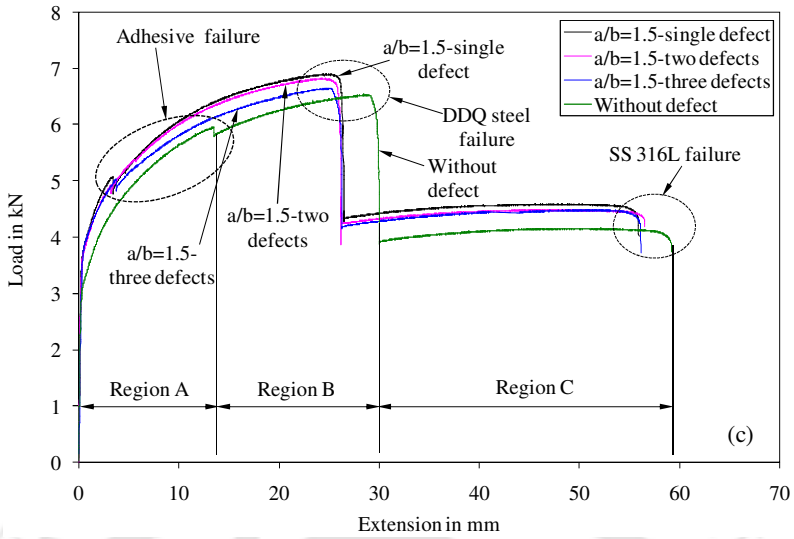

Error variation in maximum load = ±0.3 kN and total extension = ±0.55 %

Fig. 3.10 Comparison of load – extension behaviour of adhesive bonded blanks with increase in number of adhesive finite defects from tensile test (a) *a/b* = 0.5, (b) *a/b* = 1, and (c) *a/b* = 1.5

3.3.7 Influence on the limit strain of adhesive bonded blanks with increase in number of adhesive finite defects

The comparison of limit strain results with increase in number of defects for different aspect ratios (0.5, 1 and 1.5) were carried out. Fig. 3.11(a, b) shows the comparison of limit strains of DDQ steel and SS 316L sheets in adhesive bonded blanks with increase in number of defects for aspect ratio, *a/b* = 1.5 through tensile test. The adhesive bonded blank without defect is also compared. There is about 0.3–13.9% reduction in true major strain and about 3.8–15.4% reduction in true minor strain of DDQ steel, and about 0.2–12.6 % in true major strain and about 1.8–11.6% reduction in true minor strain of SS 316L in bonded sheets for different aspect ratios with respect to true major strain of adhesive bonded sheets without adhesive defect, among all the defect aspect ratios. But not much difference is noted in the reduction of major strain results obtained for increasing number of adhesive defects. The major limit strains of adhesive bonded blanks with single, double, and three defects are almost same, with negligible difference. This reveals that there is no considerable influence of increase in number of defects in the adhesive layer on the limit strain of base materials. In the case of multiple defects also, the strain is concentrated locally among one of the defects, and the limit strain results are same as like the case of single defect.

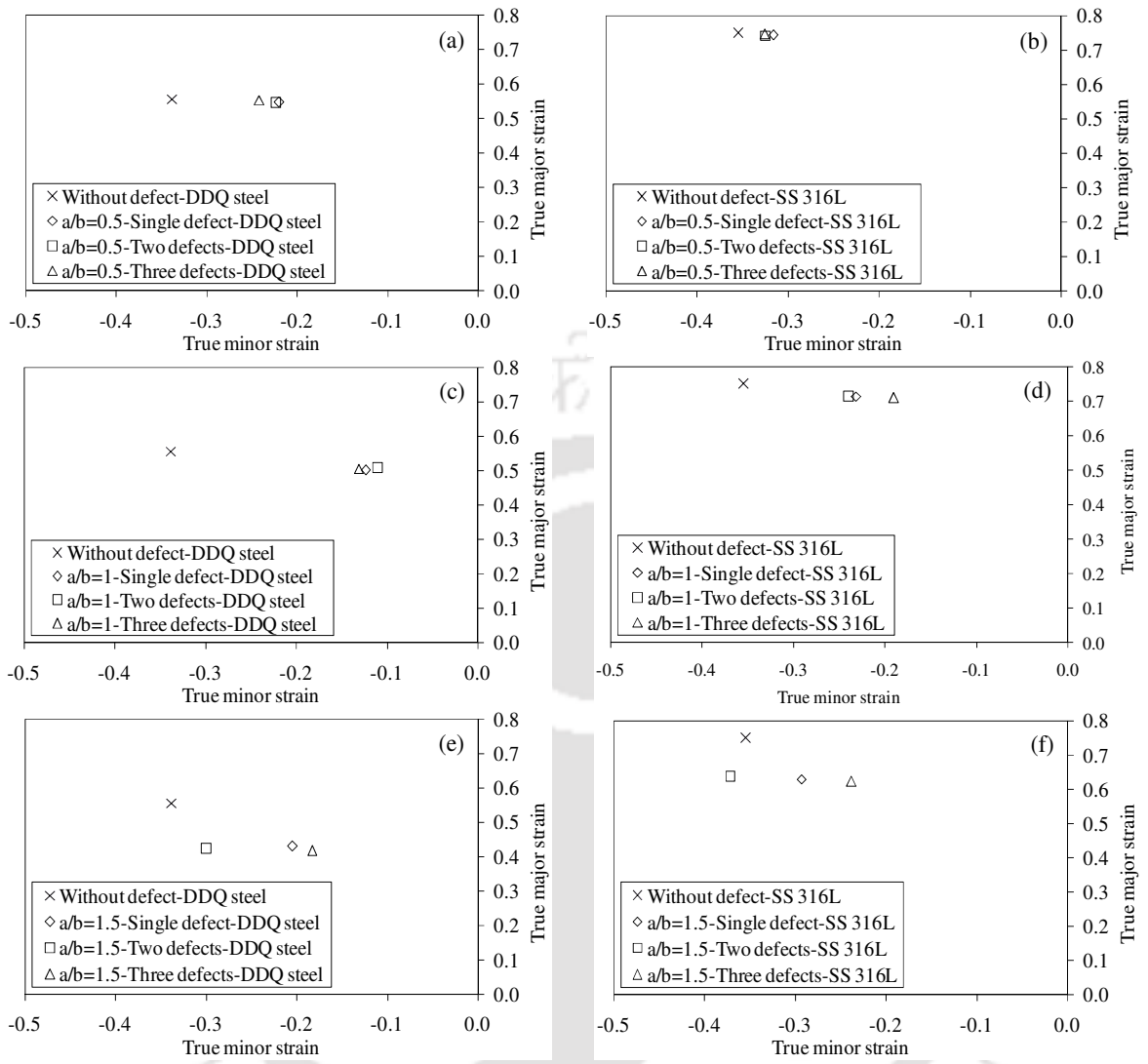

Fig. 3.11 Comparison of limit strain of base materials in adhesive bonded blanks with increase in number of adhesive finite defects at different aspect ratios: (a) *a/b* = 0.5-DDQ steel, (b) *a/b* = 0.5-SS 316L, (c) *a/b* = 1-DDQ steel, (d) *a/b* = 1-SS 316L, (e) *a/b* = 1.5-DDQ steel, and (f) *a/b* = 1.5-SS 316L

The standard deviation of true major limit strain and true minor strain ranges for DDQ steel and SS 316L sheets in adhesive bonded blanks with increase in number of adhesive defects from the tensile test was determined. The error variations are much smaller than the limit strain variation among different adhesive bonded samples with increase in number of adhesive defects at different aspect ratios (*a/b*).

3.3.8 Comparison of strain hardening exponent (*n*) with increase in number of adhesive finite defects in adhesive bonded sheets

The comparison of *n*-value in regions A, B and C of adhesive bonded blanks with increase in number of adhesive defects is shown in Table 3.4 at *a/b* = 0.5, 1 and 1.5, respectively. It is observed that there is not much difference in the '*n*' values with increase in number of adhesive defects. These results basically confirm the unchanged ductility and limit strain of base materials constituting adhesive bonded sheets.

Table 3.4 Strain hardening exponent (*n*) in regions A, B and C of adhesive bonded blanks with increase in number of adhesive finite defects at *a/b* = 0.5, 1, and 1.5

Number of defects	*a/b* = 0.5			*a/b* = 1			*a/b* = 1.5		
	Region			Region			Region		
	A	B	C	A	B	C	A	B	C
Single defect	0.281	0.374	0.483	0.219	0.339	0.480	0.204	0.319	0.469
Two defects	0.281	0.374	0.486	0.220	0.340	0.473	0.204	0.319	0.469
Three defects	0.281	0.372	0.483	0.218	0.338	0.478	0.204	0.320	0.469

Error variation in *n*-value in region A = ±0.002, region B = ±0.001, and region C = ±0.002

3.3.9 Influence of volume of adhesive finite defect on the forming behaviour of adhesive bonded blanks

Two circular adhesive defects with diameter of 6 mm (*a/b* = 1) each were combined together as a single defect and the diameter was determined as ∅8.5 mm for an equivalent volume. Similarly, three circular adhesive defects were combined as a single defect with diameter of ∅10.4 mm. The adhesive bonded blanks in the presence of combined defects were tensile tested. Fig. 3.12 shows the comparison of load – extension behaviour between adhesive finite defects with diameter of 6 mm, 8.5 mm and 10.4 mm. It is observed that there is a decrease in extension in regions A and B, but not much difference in region C for adhesive defects with ∅8.5 mm with respect to ∅6 mm defect. Only two regions of deformation are observed in Fig. 3.12 in the case of adhesive defect with ∅10.4 mm, unlike in other two cases where adhesive failure is prominent. This reveals that there is no influence of adhesive layer on the adhesive bonded blank and merely behaves as a double sheet. From these results, it is understood that increase in volume of adhesive defect decreases the formability of adhesive bonded blanks, where the strain is locally concentrated. These finite adhesive defects can also be characterised as different aspect

ratios of defects. It can be said that there is a decrease in ductility of adhesive bonded blanks with increase in aspect ratio and shape of the adhesive defects. This is also confirmed with the limit strain results of DDQ steel and SS 316L in adhesive bonded blanks as shown in Fig. 3.13(a, b) for different aspect ratios of adhesive defects. There is about 4.3% and 6.7% difference in limit strain between the defects with ∅6 mm and 8.5 mm (equivalent to two defects) with respect to DDQ steel and SS 316L, respectively. Similarly, about 5.6% and 7.1% difference in limit strain between the defects with ∅6 mm and 10.4 mm (equivalent to three defects). From these results, it can be summarized that increase in number of equi-sized finite adhesive defects (say 2 or 3 defects) located at different positions will not affect the formability of adhesive bonded blanks. The failure location will be at any one of the defect locations, without considerable deformation at other defect locations. But if these defects are combined as one defect with equivalent volumes, the different aspect ratios of such defects affect the ductility of adhesive bonded sheets as the failure occurs at the defect location.

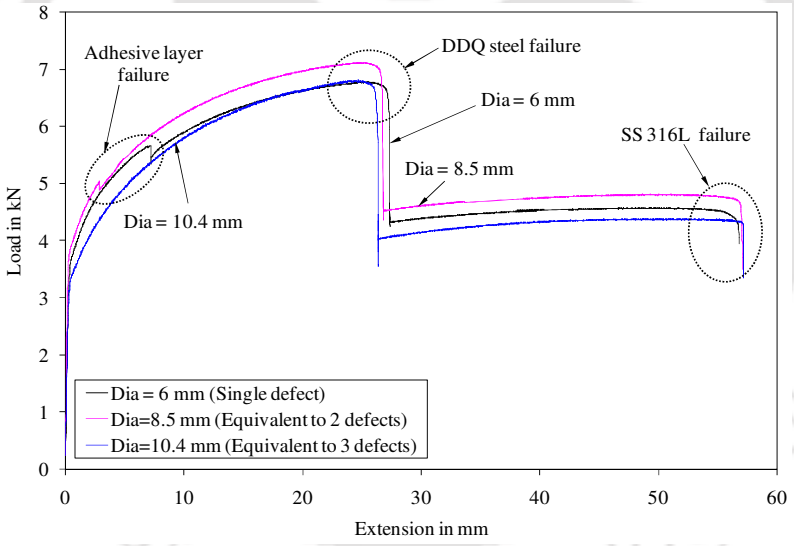

Fig. 3.12 Comparison of load-extension behaviour between increasing number of adhesive defects from 1 to 3 combined as a single defect for an equivalent volume in adhesive bonded blanks

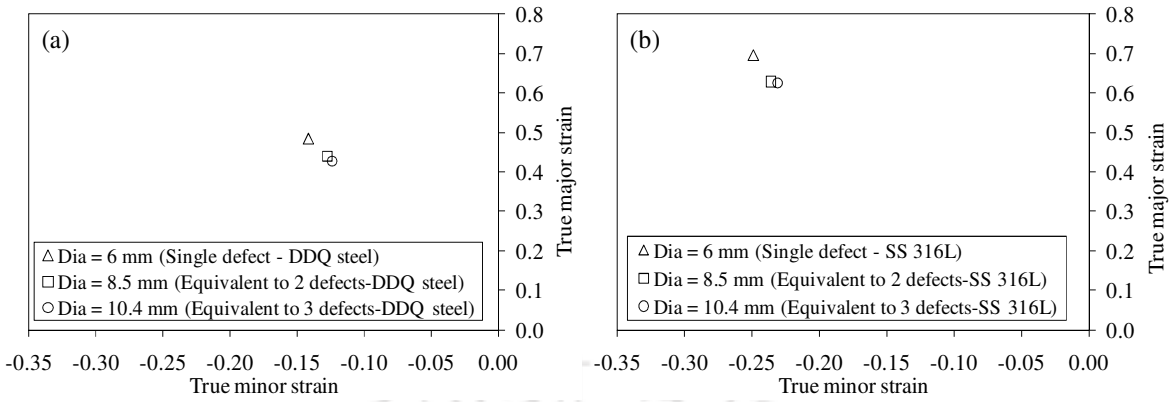

Fig. 3.13 Comparison of limit strain between increasing number of adhesive defects from 1 to 3 combined as a single defect for an equivalent volume in adhesive bonded blanks (a) DDQ steel specimen, and (b) SS 316L specimen

3.3.10 Effect of location of adhesive finite defects on the tensile behaviour of adhesive bonded blanks

3.3.10.1 Influence on the load-extension behaviour

Fig. 3.14(a-c) presents the comparison of load–extension behaviour obtained from the tensile testing of adhesive bonded sheets with different locations of adhesive defects at different aspect ratios. The adhesive bonded blanks without pre-generated adhesive defect and with different locations of adhesive defects are compared. It is observed that there is not much difference between the load-extension behaviour of adhesive bonded blanks with different locations of adhesive defects. Though the defects are located at different locations, the failure of adhesive layer, DDQ steel sheet and SS 316L sheet is observed almost at same level of extension. From Fig. 3.14(a-c), with respect to the total extension values observed in regions A, B and C of the adhesive bonded blank without adhesive defect, the decrease in total extension is determined for the adhesive bonded blanks with different locations of adhesive defects. There is not much difference in decrease in extension (only 2% difference) till failure of adhesive layer (Region A) which reflects in the deformation of DDQ steel and SS 316L sheet that were unchanged with different locations of adhesive defects.

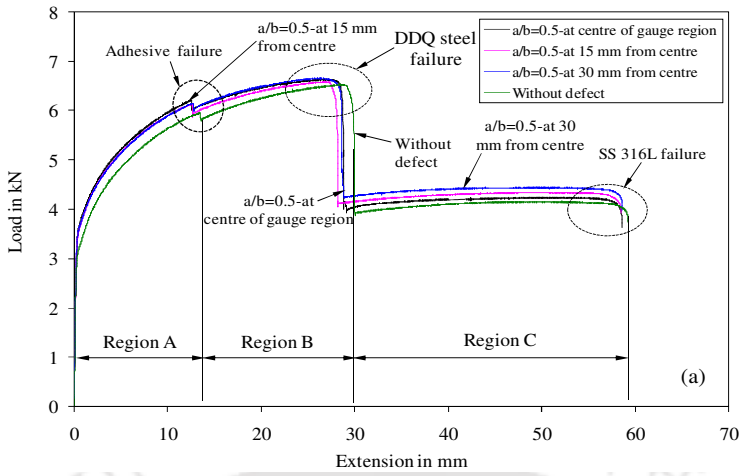

Error variation in maximum load = ±0.25 kN and total extension = ± 0.55 %

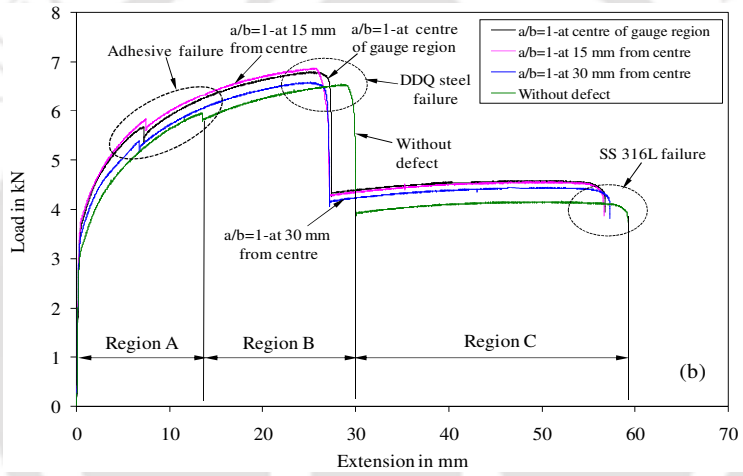

Error variation in maximum load = ±0.35 kN and total extension = ± 0.6%

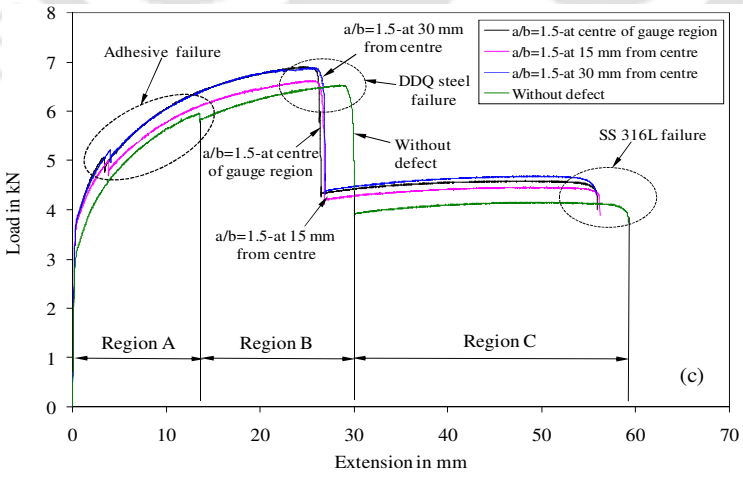

Error variation in maximum load = ±0.25 kN and total extension = ± 0.7%

Fig. 3.14 Comparison of load – extension behaviour of adhesive bonded blanks with different locations of adhesive finite defects: (a) *a/b* = 0.5, (b) *a/b* = 1, and (c) *a/b* = 1.5

From these results, it is understood that the additional plastic deformation caused by the global deformation of adhesive bonded blank to DDQ steel and SS 316L is not affected by location of adhesive defects. Also the improved plastic deformation of adhesive layer which contributes to the additional plastic deformation of the base materials in adhesive bonded blanks is not influenced by location of the adhesive defects which are equi-sized.

3.3.11 Influence on the limit strain of adhesive bonded blanks

The comparison of limit strain results with different locations of defect for different aspect ratios (0.5, 1 and 1.5) was carried out. Fig. 13 shows the comparison of limit strains of DDQ steel and SS 316L sheets in adhesive bonded blanks with different locations of adhesive defects for aspect ratio 1.5. The adhesive bonded blank without defect is also compared. There is about 0.9 –12.6% reduction in true major strain and about 13.7–15.0% reduction in true minor strain of DDQ steel, and about 0.5–11.9% in true major strain and about 8.0–18.0% reduction in true minor strain of SS 316L in bonded sheets for different aspect ratios with respect to true major strain of adhesive bonded sheets without adhesive defect during tensile test. In the comparison of reduction in true major strain results between the adhesive defects located at different locations, not much difference is noted among them. This indicates that there is no considerable influence of location of adhesive defects located in the deforming region on the limit strains of base materials. Though the adhesive defect is located at different locations in the deforming region of adhesive bonded blanks, the failure of adhesive layer occurs at the location of defect. This deformation behaviour is same as that of adhesive bonded blanks with adhesive defect located in the centre of gauge region. It leads to the conclusion that there is no effect of defect location on ductility and limit strain.

The standard deviation of true major limit strain and true minor strain ranges for DDQ steel and SS 316L sheets in adhesive bonded blanks with different locations of adhesive defects was determined. These error variations are much smaller than the limit strain variation among different adhesive bonded samples with different locations of adhesive defects for different aspect ratios (*a/b*).

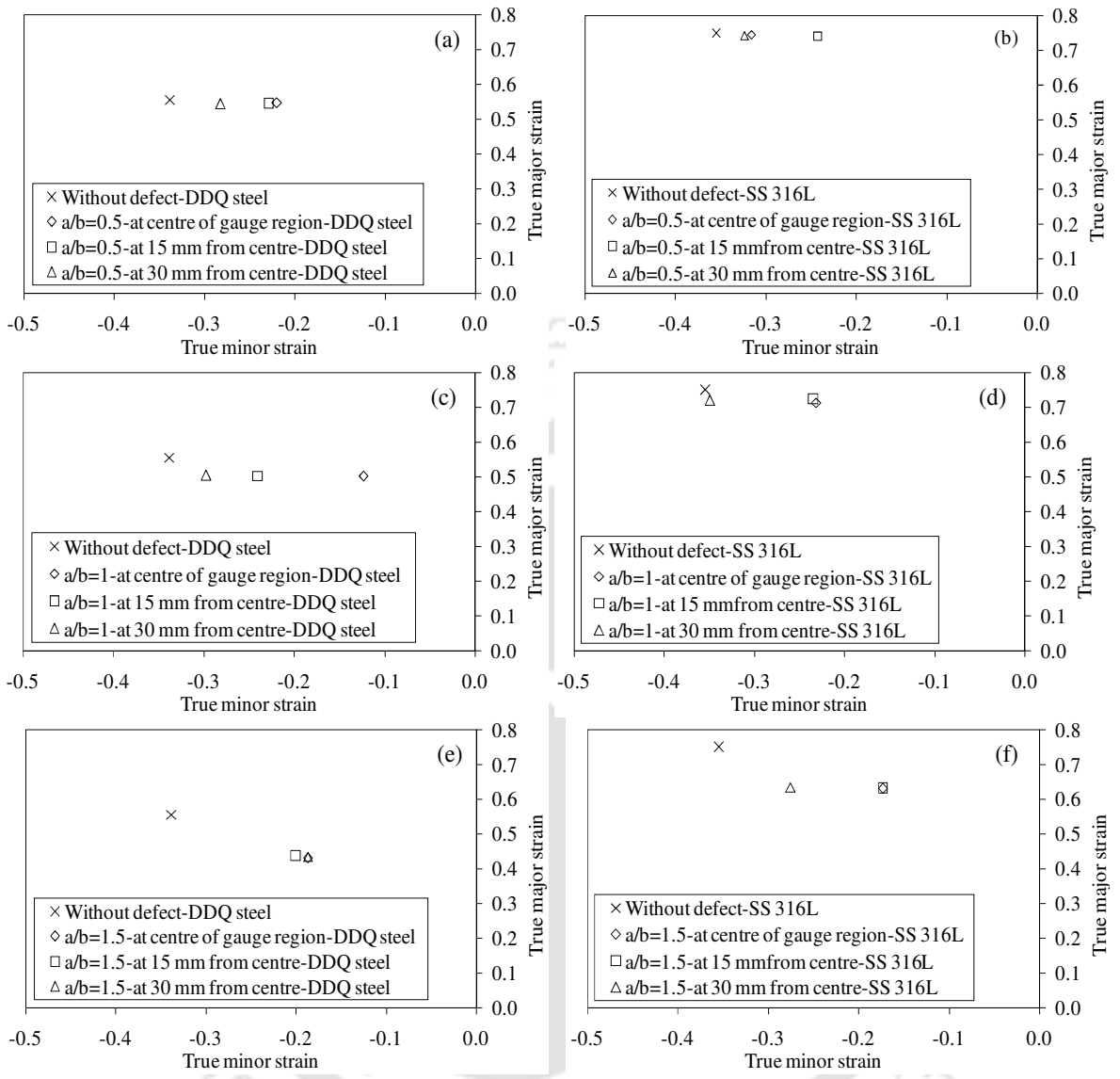

Fig. 3.15 Comparison of limit strains of base materials in adhesive bonded blanks with different locations of adhesive defects at different aspect ratios (a) *a/b* = 0.5-DDQ steel, (b) *a/b* = 0.5-SS 316L, (c) *a/b* = 1-DDQ steel, (d) *a/b* = 1-SS 316L, (e) *a/b* = 1.5-DDQ steel, and (f) *a/b* = 1.5-SS 316L

3.3.12 Comparison of strain hardening exponent (*n*) with different locations of adhesive finite defects in adhesive bonded blanks

Table 3.5 presents the comparison of *n*-value in regions A, B and C of adhesive bonded blanks with different locations of adhesive defects for *a/b* = 0.5, 1 and 1.5. There is not much difference in the '*n*' values with different locations of adhesive defects in all three regions A, B and C for

different defect aspect ratios. These results basically reflected in the unchanged ductility and limit strain of base materials of adhesive bonded blanks.

Table 3.5 Strain hardening exponent (n) in regions A, B and C of adhesive bonded blanks with different locations of adhesive defect for a/b = 0.5, 1 and 1.5

Defect location	a/b = 0.5			a/b = 1			a/b = 1.5		
	Region			Region			Region		
	A	B	C	A	B	C	A	B	C
At centre	0.281	0.374	0.483	0.219	0.339	0.480	0.204	0.319	0.469
At 15 mm from centre	0.281	0.352	0.475	0.220	0.340	0.491	0.202	0.321	0.474
At 30 mm from centre	0.281	0.361	0.484	0.218	0.343	0.494	0.199	0.319	0.475

Error variation in n-value in region A = ±0.001, region B = ±0.004, and region C = ±0.008

3.3.13 Failure pattern of adhesive bonded blanks with and without infinite adhesive defects

The failure pattern during the tensile testing and IPPS formability testing of the adhesive bonded steel sheets in the presence of infinite defects with different orientations is proposed as follows. Fig. 3.16(A, B) presents the failure pattern of tensile and IPPS adhesive bonded specimens with different infinite defect orientations such as transverse, 45° inclined, longitudinal.

(i) Failure of adhesive bonded blank with transversely oriented infinite defect

In the adhesive bonded blanks with transverse infinite defect in the adhesive layer, the separation of adhesive layer (Fig. 3.17(a)) due to the deformation of DDQ steel and SS 316L sheets was observed at the location of transverse infinite defect during tensile and IPPS tests as shown in Figs. 3.16A (a) and 3.16B(a). This is due to the concentration of strain at the reduced cross-section area that is at the location of transverse oriented infinite defect in the adhesive layer.

(ii) Failure of adhesive bonded blank with 45° oriented infinite defect

In the case of 45° defect orientation, no adhesive failure is observed during tensile testing and the adhesive layer is split into two parts at the place where defect is present without any adhesive deformation as shown in Fig. 3.16A(b). On the contrary, during IPPS tests, the failure of adhesive layer due to deformation occurred in the gauge region rather than splitting into two parts as shown in Fig. 3.16B(b). This is mainly due to the presence of notch in IPPS sample, which is absent in tensile test sample. The notch acts as the strain concentration region resulting in failure of adhesive. Moreover, in tensile test sample, the gauge length very large as compared to defect length, which is vice-versa in the case if IPPS sample. These properties together result

in deformation of all the three regions in IPPS samples, while only base materials (DDQ, SS 316L) deform in tensile tests (Fig. 3.17(a, b)).

(iii) Failure of adhesive bonded blank with longitudinally oriented infinite defect

In this case, failure of adhesive bonded blank has occurred in the gauge region as shown in Figs. 3.16A(c) and 3.16B(c), respectively. First, the adhesive fails in the gauge region. Later, the interfacial layer and bonding between adhesive layer, failed due to relative motion between them and the base materials. As discussed in Chapter 2 in Sections 2.4.2 and 2.6.1 about the failure pattern of adhesive bonded blanks during tensile testing and IPPS formability testing, here also the base materials, DDQ steel and SS 316L sheets bear the tensile load and behave as a double sheet after failure of adhesive layer. The failure of DDQ steel sheet is noticed after the failure of adhesive layer. At last, the failure of SS 316L sheet of the adhesive bonded blank is observed after the failure of DDQ steel specimen.

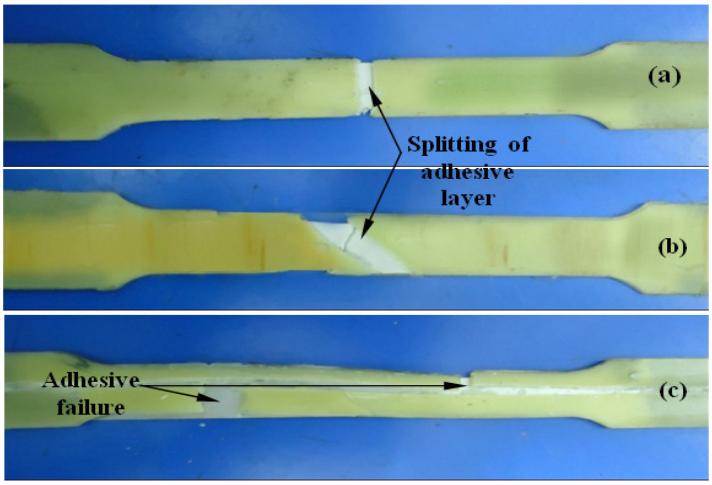

(A)

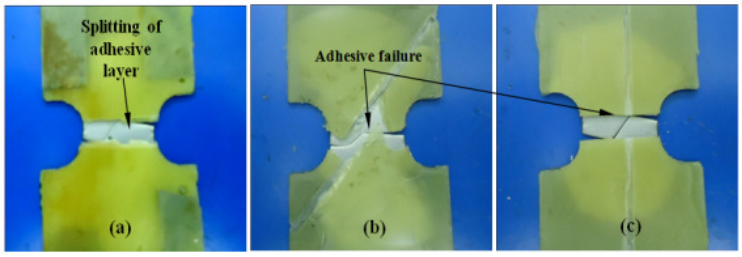

(B)

Fig. 3.16 Failure pattern of adhesive layer with different orientations of infinite defect in adhesive bonded blanks (A) tensile test, and (B) IPPS formability test. (Note: (a) transverse oriented defect, (b) 45° oriented defect, and (c) longitudinally oriented defect)

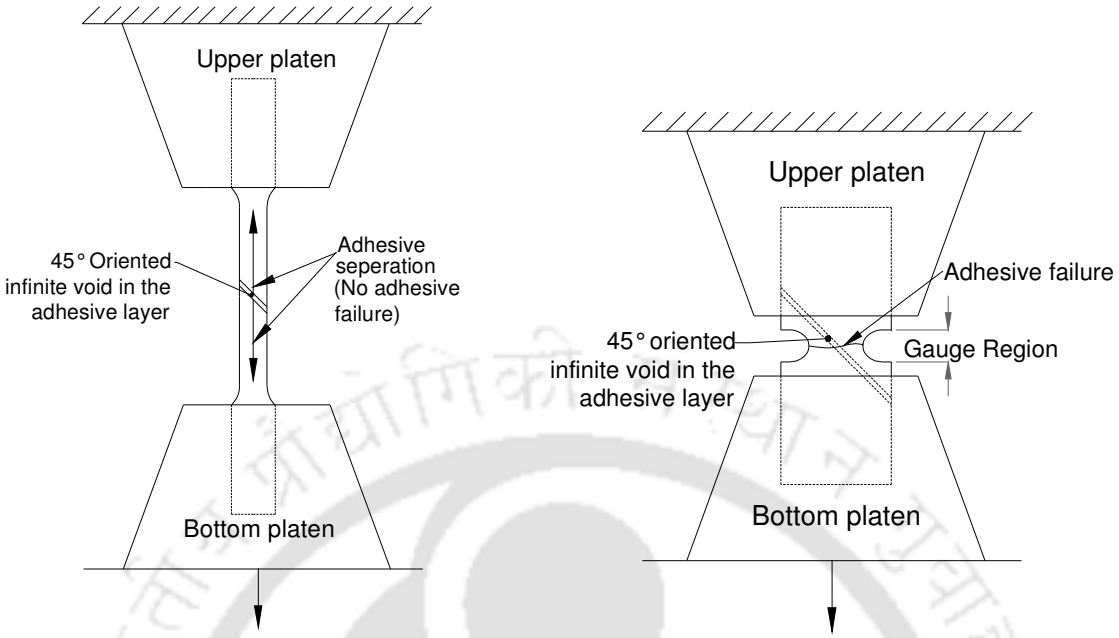

Fig. 3.17 Gripping of adhesive bonded specimens in the presence of 45° oriented infinite defect in the adhesive layer, (a) Tensile specimen, and (b) IPPS specimen

3.3.14 Effect of orientation of infinite defect in the adhesive layer on the tensile behaviour of adhesive bonded blanks

3.3.14.1 Comparison of tensile behaviour between adhesive bonded blanks with and without defects

Figs. 3.18(a) and 3.18(b) show the comparison of load–extension behaviour of adhesive bonded tensile specimens and IPPS specimens, respectively. The adhesive bonded blanks without defects and with defects in the adhesive layer with different orientations such as transverse, 45° inclined and longitudinal are compared. There is a decrease in extension with respect to region B and region C for the adhesive bonded blanks having infinite defects till failure of DDQ steel and SS 316L sheets regardless of different orientations. In the case of longitudinally oriented infinite defect, the load-extension behaviour follows the similar load-extension behaviour (regions A, B and C) of adhesive bonded blank without infinite defect in the adhesive layer. This implies that there is a global deformation of three layers (adhesive layer, DDQ steel and SS 316L sheets) which causes added plastic deformation or extension to DDQ steel and SS 316L till failure of adhesive layer, even in the presence of longitudinally oriented infinite defect in both tensile and IPPS formability tests. In the cases of tensile testing of adhesive bonded blanks with transverse

and 45° oriented infinite defect, only two regions (region 1 and 2) are observed, since there is no failure of adhesive layer (Fig. 3.18(a)). There is not much difference between the load-extension behaviour of transverse and 45° oriented infinite defect cases. This reveals that only DDQ steel and SS 316L sheets deform, even in the presence of adhesive layer. Thus, the absence of additional plastic deformation caused by the adhesive layer reduces the plastic deformation of DDQ steel and SS 316L sheets comparatively. But in the load-extension behaviour of IPPS adhesive bonded blank with 45° oriented infinite defect, three regions, such as global deformation of all three layers (region A), deformation of DDQ steel and SS 316L (region B) and deformation of SS 316L (region C) are observed (as discussed in Section 3.3.1) and there is not much difference between load-extension behaviour of adhesive bonded blanks having 45° and longitudinally oriented infinite defects.

The decrease in IPPS sample with transverse adhesive defect show least formability, as it is characterised by adhesive separation, indicating double sheet deformation. From Figs. 3.18(a) and 3.18(b), the total extension of about 29.8 mm and 59 mm is found from the load–extension behaviour of the tensile adhesive bonded blank without infinite defect till failure of DDQ steel and SS 316L sheets respectively. Similarly, about 5.7 mm and 11.7 mm is observed from the load–extension behaviour of the IPPS adhesive bonded blank without infinite defect till failure of DDQ steel and SS 316L sheets, respectively. With respect to these total extension values, the decrease in total extension is calculated between the adhesive bonded sheets in absence of infinite defect and in the presence of infinite defects with different orientations in both the tests as shown in Fig. 3.19(a, b).

It can be perceived from these results that different orientations of infinite defect in the adhesive layer decrease the total extension of adhesive bonded sheets by causing early failure of adhesive layer, thereby reducing the formability of the adhesive bonded blanks. In addition, the adhesive layer separation (in tensile tests and IPPS formability tests of transverse defect case, tensile tests of 45° oriented defect case) and adhesive layer failure (in IPPS forming of 45° oriented case, in tensile test and IPPS forming of longitudinal defect case) also decides the formability (elongation) of adhesive bonded blanks. The cases with adhesive layer separation is an indication of double sheet forming and hence showed a reduced formability, as compared to cases with adhesive layer failure; which involves deformation of all three layers (adhesive, DDQ, SS 316L). In the later case, adhesive helps in providing additional plastic deformation improving the formability (or elongation).

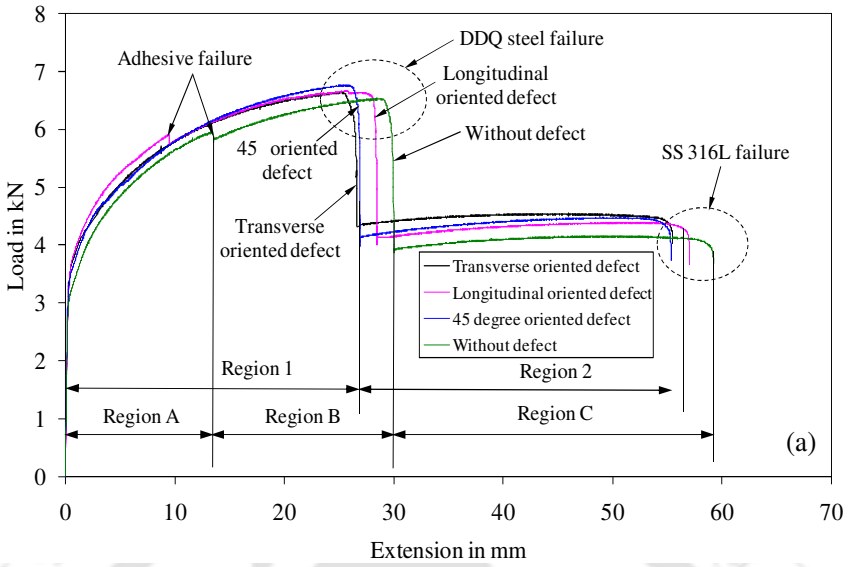

Error variation in maximum load = ±0.25 kN and total extension = ± 0.6 %

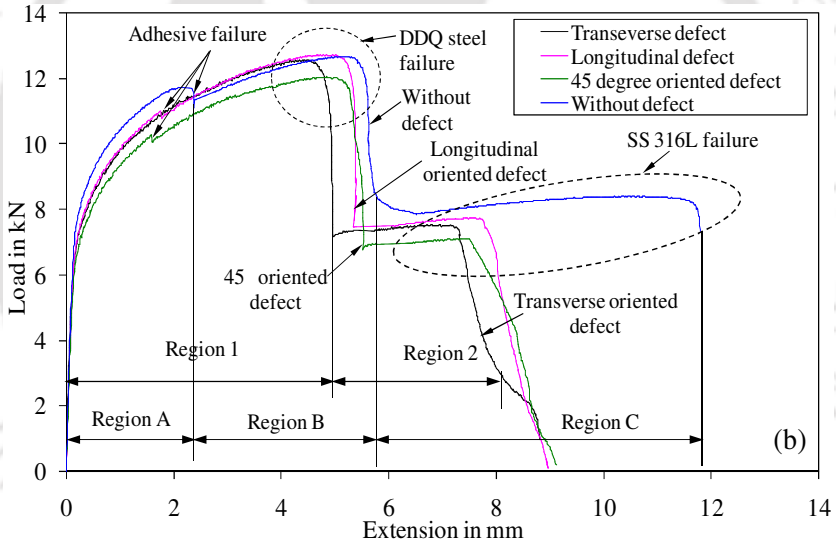

Error variation in maximum load = ±0.3 kN and total extension = ± 0.4%

Fig. 3.18 Comparison of load – extension behaviour of adhesive bonded blanks with and without transverse oriented defect (a) tensile tested epoxy bonded blanks, and (b) IPPS formability tested epoxy bonded blanks

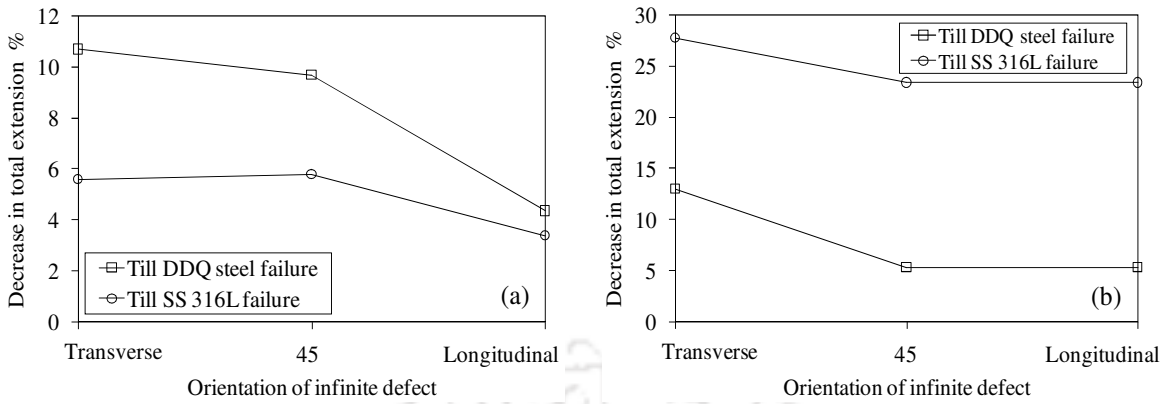

Fig. 3.19 Comparison of decrease in percentage of total extension of DDQ steel sheets and SS 316L sheets in adhesive bonded blanks in the presence of infinite defect with respect to the adhesive bonded blank without infinite defect, (a) adhesive bonded tensile specimens, and (b) adhesive bonded IPPS specimens

3.3.15 Influence of orientations of infinite defect in the adhesive layer on the limit strain of adhesive bonded steel sheets

In this section, the effect of orientations of infinite defect in the adhesive layer on the formability of adhesive bonded blanks are discussed through limit strains by measuring the length of major and minor axes of deformed circular grids at the necked region of DDQ steel and SS 316L sheets in adhesive bonded blanks. Figs. 3.20(a) and 3.20(b) show the comparison of limit strains of DDQ steel and SS 316L sheets tensile tests, respectively, in adhesive bonded blanks with different defect orientations. The adhesive bonded blank without defect is also compared. Similarly, Fig. 3.21(a, b) presents the comparison of limit strains from IPPS formability test. It is observed that there is a decreasing trend of forming limit strains of DDQ steel and SS 316L adhesive bonded blanks due to different orientations of infinite defect when compared to the limit strains of DDQ steel and SS 316L in adhesive bonded blank without defect. Though there is a considerable difference in limit strains of adhesive bonded blanks and without infinite defects, not much difference in limit strains of the base materials is observed at different orientations.

From Fig. 3.21(a, b), lower limit strain is noticed in the case of transverse infinite defect during IPPS formability test as compared to 45° and longitudinal defects. There is about 1.4–3.5% reduction in major strain of DDQ steel sheet and about 2–4.5% in major strain of SS 316L sheet with respect to major strain of adhesive bonded sheets without adhesive defect during tensile test. Similarly, there is about 8.4–10.8% reduction in major strain of DDQ steel sheet and about 11.3–14.4% in major strain of SS 316L sheet during IPPS formability test.

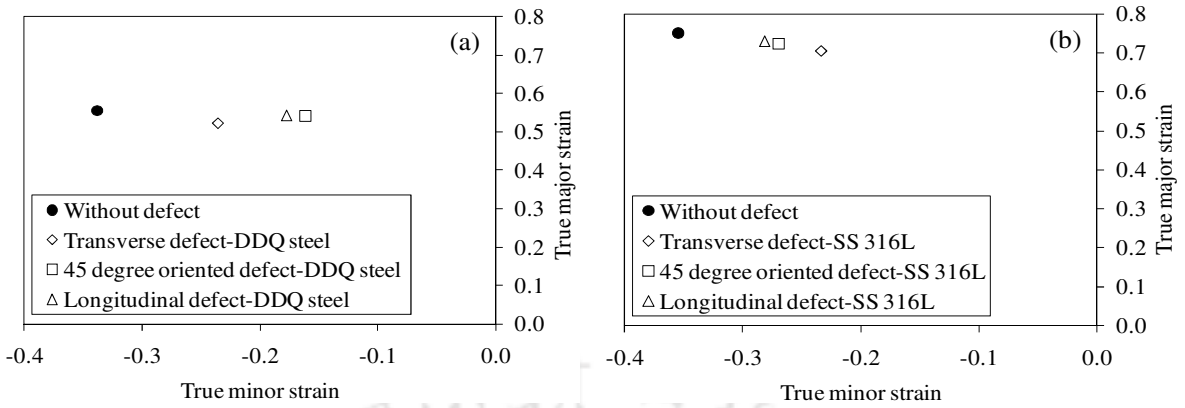

Fig. 3.20 Comparison of limit strains of adhesive bonded blanks with influence of different orientations of infinite defect from tensile test, (a) DDQ steel, and (b) SS 316L

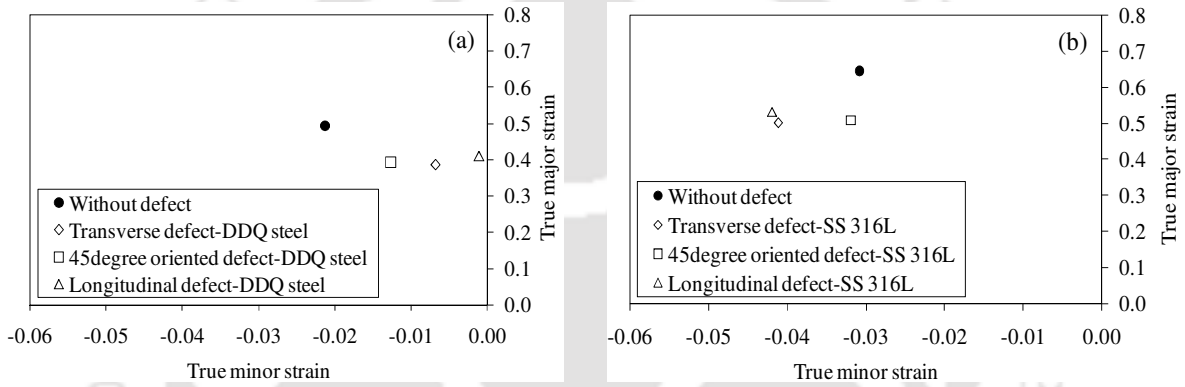

Fig. 3.21 Comparison of limit strains of adhesive bonded blanks with influence of different orientations of infinite defect from IPPS formability test, (a) DDQ steel, and (b) SS 316L

3.3.16 Comparison of strain hardening exponent (*n*) between with and without infinite defects in adhesive bonded blanks

The reduction in limit strains are related to the strain hardening exponent (*n)* determined in the regions A, B and C, and in the regions 1 and 2 of the tensile behaviour of adhesive bonded blanks. Table 3.6 shows the *n*-value in regions A, B and C of adhesive bonded steel sheets without defects. Similarly, Table 3.7 presents the *n*-value in region 1 and region 2 of adhesive bonded steel sheets characterised by adhesive separation (45° and transversely oriented adhesive infinite defect in tensile test and transversely oriented defect in IPPS test). Table 3.8 shows *n*-value in regions A, B and C of adhesive bonded steel sheets characterised by adhesive failure (longitudinally oriented adhesive infinite defect in tensile test, and 45° and longitudinally oriented defect in IPPS test). While comparing the '*n*' values of region 1 with region B, and region 2 with region C, from Tables 3.6 and 3.7, it is seen that the adhesive bonded blanks without pregenerated defect has larger '*n*' values. This has basically reflected in ductility and limit strain of base

materials. The bonded blanks without defects showed larger ductility and limit strain as compared to adhesive bonded blanks with defects characterised by adhesive separation (Table 3.7). Similarly, adhesive bonded blanks without defects (Table 3.6) has better '*n*' value as compared to adhesive bonded blanks with adhesive defects characterised by adhesive failure (Table 3.8) in all the three regions of deformation. This has potentially reduced the forming limit and ductility of adhesive bonded blanks with defects characterized by adhesive failure (Table 3.8). While comparing the '*n*' values of adhesive bonded blanks characterised by adhesive separation (Table 3.7) with adhesive failure (Table 3.8), the later shows improved strain hardening exponent resulting in better ductility and forming limit strain. But this effect is quite considerable in ductility (Fig. 3.18), but not in limit strains (Figs. 3.20 and 3.21). Same *n*-value in region 1 and region 2 of tensile adhesive bonded blanks with transverse and 45° oriented infinite defect in the adhesive layer is observed (Table 3.7), which reflects in the limit strain results with negligible difference between these two cases (Fig. 3.20(a, b)).

Table 3.6 Strain hardening exponent (*n*) in region A, B and C of adhesive bonded steel sheets without infinite defect in the adhesive layer

Test type	Region		
	A	B	C
Tensile	0.287	0.394	0.517
IPPS forming	0.291	0.425	0.663

Table 3.7 Strain hardening exponent (*n*) in region 1 and region 2 of adhesive bonded steel sheets characterised by adhesive separation (45° and transversely oriented adhesive infinite defect in tensile test and transversely oriented defect in IPPS test)

Test type	Defect orientation type	Region	
		1	2
Tensile	Transverse	0.328	0.511
	45°	0.328	0.511
IPPS	Transverse	0.391	0.516

Error variation in *n*-value in region 1 = ±0.004, and region 2 = ±0.006

Table 3.8 Strain hardening exponent (n) in regions A, B and C of adhesive bonded steel sheets characterised by adhesive failure (longitudinally oriented adhesive infinite defect in tensile test, and 45° and longitudinally oriented defect in IPPS test)

Test type	Defect orientation type	Region		
		A	B	C
Tensile	Longitudinal	0.221	0.351	0.514
IPPS forming	45°	0.261	0.382	0.574
	Longitudinal	0.273	0.388	0.583

Error variation in n-value in region A = ±0.002, region B = ±0.001, and region C = ±0.001

Table 3.9 Uncertainty measurement of limit strain

Test type	Standard deviation range			
	True major limit strain		True minor limit strain	
	DDQ steel	SS 316L	DDQ steel	SS 316L
Tensile	0.022 to 0.046	0.006 to 0.041	0.021 to 0.049	0.016 to 0.066
IPPS forming	0.001 to 0.016	0.005 to 0.056	0.003 to 0.007	0.002 to 0.026

Further, uncertainty analysis on determination of limit strain was carried out. Table 3.9 shows the standard deviation of true major limit strain and true minor strain ranges for DDQ steel and SS 316L sheets in adhesive bonded blanks with and without infinite defect in the adhesive layer from the tensile test and IPPS formability test. These error variations are much smaller than the limit strain variation among different adhesive bonded samples with different orientations of infinite defect in the adhesive layer. Hence, these results confirm an inherent reduction in the limit strain rather than just the scatter of limit strain results.

3.4 Conclusions

The present work aims at investigating the influence of artificial adhesive defects on the formability of adhesive bonded blanks, through tensile test and plane-strain formability test. The following conclusions are drawn from the results.

- The adhesive bonded sheets with different aspect ratios and shapes of finite adhesive defects show a typical failure pattern: the adhesive fails earlier with increase in aspect ratio in the order, a/b = 1.5, 1 and 0.5 at the location of defect, then DDQ steel fails, and finally SS316L

sheet fails because of larger elongation as compared to DDQ steel. The ductility of adhesive layer depends on the functional group, hardener/resin ratio, and the defect volume.

- Even though multiple adhesive defects are present, the failure of adhesive occurred at only one location of defect. About 78%, 89% and 67% of adhesive failure was observed at the centre defect for a/b = 0.5, 1 and 1.5, respectively. The remaining defect(s), other than failed one, were observed un-deformed in the adhesive layer. It is expected that the failure will occur within the gauge region of tensile sample as large deformation happens here. The deformation/strain decreases from the gauge region centre towards the gripping region. Hence, there exists strain gradient within the gauge region itself. So failure will happen in the adhesive defect located as the geometric centre of the sample. There may not be considerable deformation in the defects located at eccentric location because of lesser strain development as compared to the geometric centre.
- In the case of different locations of adhesive defects (only one defect per sample), the adhesive fails at the location of defect. The failure pattern of base materials constituting adhesive bonded blanks is independent of number of defects and different locations of defects.
- The adhesive bonded blanks with finite adhesive defects show reduced forming limit strain as compared to the adhesive bonded blank without adhesive defect. The reduction in the formability adhesive bonded blanks is in the order of a/b = 1.5, 1 and 0.5. Though there are multiple defects and single defect placed at different locations of the bonded sample, the forming limit of these cases remains same as that of adhesive bonded blanks with single defect.
- It can also be concluded that the aspect ratio of a defect below a certain limit, that is a/b = 0.5 in the present work, does not have considerable effect on the formability of adhesive bonded blanks. This again concludes that micro-voids of volume less than or equal to a/b = 0.5 in the adhesive may not affect the formability of adhesive bonded blanks significantly. Since the formability of adhesive bonded blanks is influenced by volume of an adhesive defect; not number of adhesive defects, reasonable numbers of equi-volume adhesive defects can be present in the adhesive bonded blanks.
- The advantage of deformation concentrated locally at the location of adhesive defect can be utilized to control the formability of base materials. Instead of failure occurring in the critical region of the sheet due to the presence of defects, the adhesive defects slightly larger than the existing voids/defects generated at a non-critical region, would concentrate the adhesive failure

at the non-critical region. This way one can preserve the overall formability of the base material, and delayed failure can be achieved in the critical region.

- The adhesive bonded sheets with adhesive infinite defects show a typical failure pattern: two patterns of adhesive failure characterised by
  - (i) adhesive separation – 45° and transversely oriented adhesive infinite defect in tensile test and transversely oriented defect in IPPS test,
  - (ii) adhesive failure – longitudinally oriented adhesive infinite defect in tensile test, and 45° and longitudinally oriented defect in IPPS test, then DDQ steel fails, and finally SS316L sheet fails because of larger elongation as compared to DDQ steel.
- The adhesive bonded blanks with adhesive infinite defects show reduced elongation as compared to the adhesive bonded blank without defect. This is due to the absence of additional plastic deformation caused by the adhesive layer that fails earlier in the presence of infinite defects.
- The DDQ and SS316L sheets constituting bonded blanks show reduced limit strains with adhesive infinite defect as compared to the bonded blank without adhesive defect. This is due to the reduced plasticization of adhesives with infinite defects.
- The strain hardening exponent (n) of adhesive bonded blanks shows decrease in trend with adhesive infinite defects in both types of failure patterns characterised by adhesive separation and adhesive failure as compared to adhesive bonded blank without adhesive defect. The reduction in 'n' value of bonded blanks is an indication of reduction in formability.

Chapter 4

Prediction of formability of adhesive bonded steel sheets with the influence of hardener/resin ratio of adhesive and experimental validation

4.1 Methodology

In this section, the forming behaviour evaluation of adhesive bonded sheets in the experiment and prediction is discussed. The methodology of prediction of adhesive bonded sheets stress-strain behaviour, and the limit strains of base materials constituting adhesive bonded sheets are described. The mechanical properties of base materials and epoxy adhesive are already discussed in Chapter 2 in Sections 2.1.1 and 2.4.1, respectively.

4.2 Experimental evaluation of forming of adhesive bonded blanks

The epoxy adhesive bonded tensile specimens and IPPS specimens preparation with different hardener/resin ratios and testing methods are already discussed in Chapter 2 in Section 2.3. The density of epoxy adhesive with different hardener/resin ratios were measured as per ASTM D1505-10 standard and incorporated during FE simulation. For evaluating the density of epoxy, cubic shaped adhesive samples with different hardener/resin ratios were prepared. The density was measured using density meter as per standard procedure and shown in Table 4.1. Three samples were tested in each case and good repeatability was observed, and the average density in each case was taken into account during the FE simulation.

Table 4.1 Density of epoxy adhesive with different hardener/resin ratios

H/R ratio	0.6:1	0.7:1	0.8:1	0.9:1	1:1
Density (kg/m^3)	785	785	778	770	776

4.3 Predicting the forming behaviour of adhesive bonded blanks with different hardener/resin ratios

Figs. 4.1(a) and 4.2(a) show the finite element models with boundary conditions before deformation in tensile and IPPS formability tests, respectively. The CAD models of tensile and IPPS specimens were meshed using the facility available in the code. The meshing was done

with quadrilateral shell elements of the Belytschko-Tsay formulation. The mesh sensitivity analysis was carried with different mesh sizes like 0.5 mm, 1 mm, 1.5 mm, and 2 mm in DDQ steel and SS 316L tensile tested as single sheet during FE simulation (results are described later). After mesh analysis, the average mesh size of about 2 mm was used throughout the tensile specimen, and 1 mm was used for IPPS specimen, as there is a notch region in the IPPS sample. In order to generate adhesive bonded blanks for FE simulations, three similar specimens were generated on the same plane, and positioned one above other as shown in Figs. 4.1(a) and 4.2(a) without considering any bonding conditions. The top and bottom layers are base materials (DDQ steel and SS 316L), and the centre layer is adhesive. The base materials properties as given in Tables 2.2 and 2.3 (Chapter 2 in Section 2.1.1) were incorporated during FE simulations. The Young's modulus of 210 GPa and 200 GPa were used for DDQ steel and SS 316L sheets, respectively. The Poisson's ratio of 0.3 was used for both materials, and 0.35 was used for adhesive layer throughout all finite simulations.

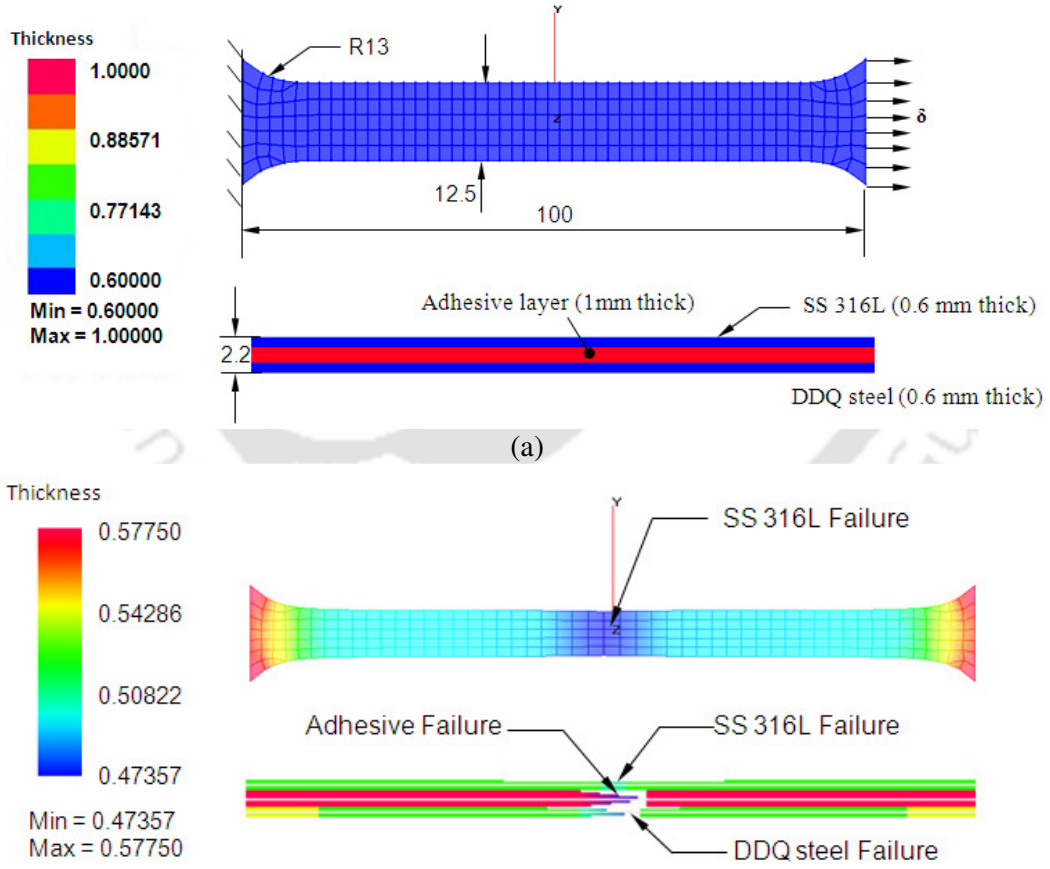

Fig. 4.1 FE model and boundary conditions of tensile adhesive bonded blanks in the simulation: (a) before deformation, and (b) after failure (All dimensions in 'mm')

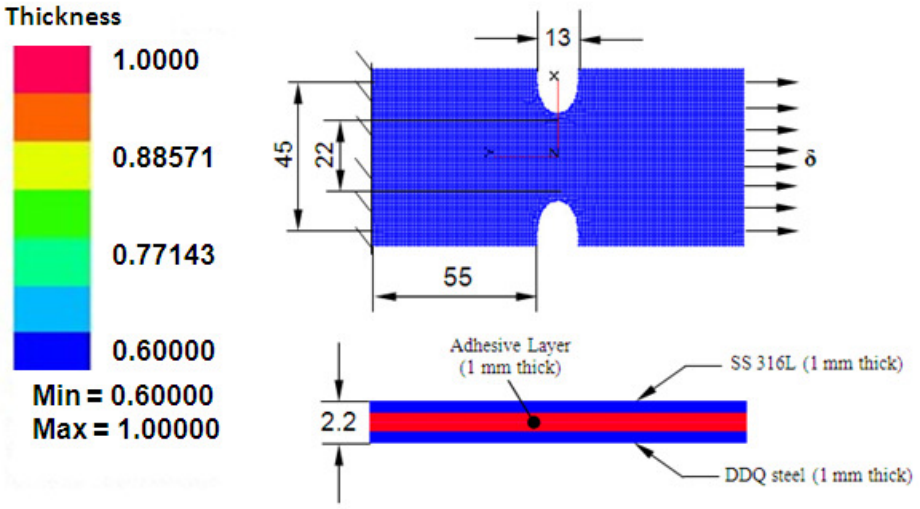

(a)

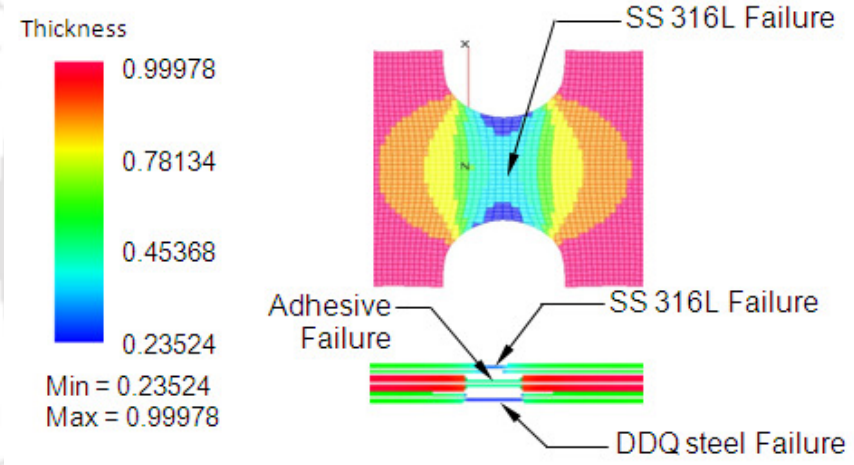

(b)

Fig. 4.2 FE model and boundary conditions of IPPS adhesive bonded blanks in the simulation: (a) before deformation, and (b) after failure

The total number of elements was about 805 in tensile test and about 15174 in IPPS formability test. Hollomon's power law ($\sigma = K\varepsilon^n$; where, K – strength coefficient, and n – strain hardening exponent) was used to describe the strain hardening behaviour of base materials. Hill's 1948 isotropic hardening yield criterion (Banabic, 2010) was used as the plasticity model for DDQ steel and SS 316L materials. Figs. 4.1(b) and 4.2(b) show the failed samples of adhesive bonded blanks in tensile and IPPS forming tests during simulations, respectively. The adhesive stress-strain behaviour was obtained from experiments (Fig. 2.4(a) in Chapter 2). The data was converted into true stress-strain behaviour by following standard procedure. The

adhesive layer positioned between base materials was considered as an isotropic material. The true stress-strain behaviour and forming limit strains were predicted in FE simulations of tensile and IPPS forming tests. The limit strains are predicted using two necking criteria namely effective strain rate ratio based necking criterion (ESRC), and thickness gradient based necking criterion (TGNC) (described later), and validated with experimental results.

4.3.1 Prediction of stress-strain behaviour of adhesive bonded sheets

Fig. 4.3(a-c) shows the schematic of failure pattern and load sharing during tensile and IPPS formability testing of adhesive bonded blanks. The deformation of adhesive bonded blanks is designated by different regions such as region A, B and C in the true stress-strain behaviour. The global deformation of adhesive layer, DDQ steel and SS 316L is designated as region A, the deformation of DDQ steel sheet and SS 316L sheet is termed as region B and the deformation of SS 316L only is termed as region C. Since the base materials and adhesive layer constituting in the adhesive bonded blank hold their individual mechanical properties during simulation, the true stress is calculated by the governing eq. (4.3), eq. (4.4) and eq. (4.5) in regions A, B and C, respectively. The above observations are made from many experimental results.

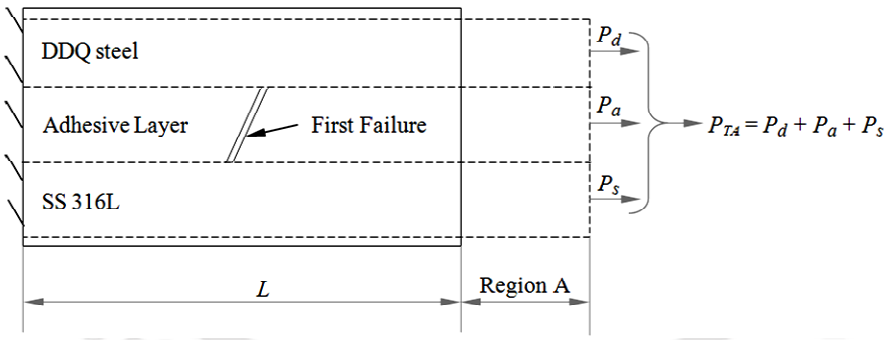

(a)

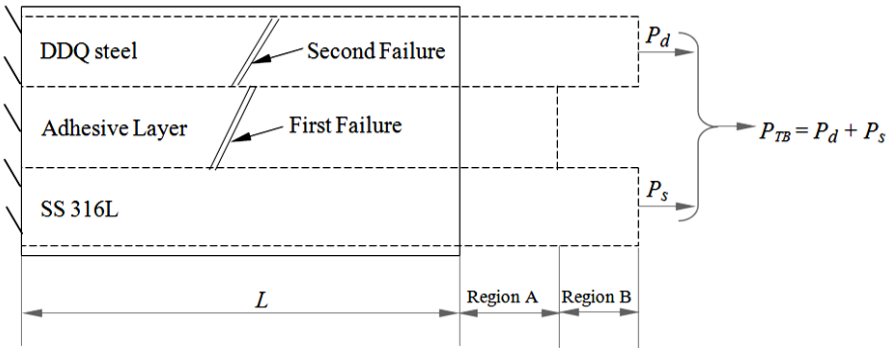

(b)

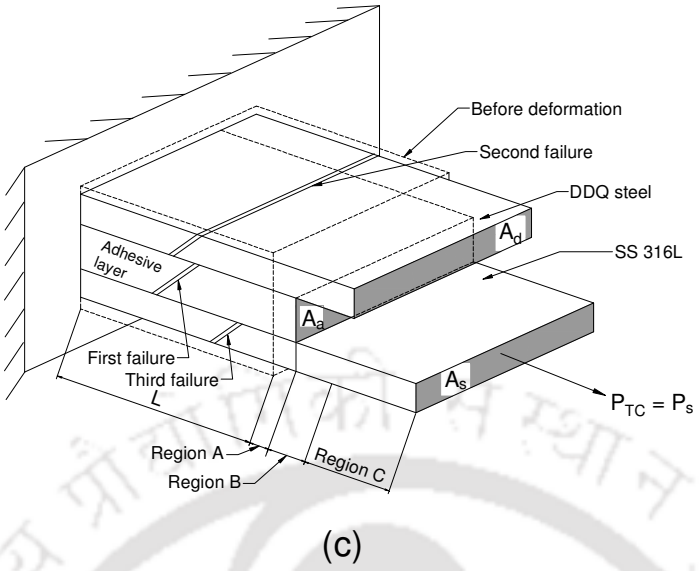

(c)

Fig. 4.3 Schematic of load sharing in adhesive bonded blank during tensile test showing different deforming regions (Regions A, B and C) (where P_{TA}, P_{TB} and P_{TC} – total load in regions A, B and C, respectively)

Let, total load, $P_T = P_d + P_a + P_s$ (4.1)

where P_d – load on DDQ steel sheet in adhesive bonded blank

P_a – load on adhesive layer in adhesive bonded blank

P_s – load on SS 316L sheet in adhesive bonded blank

$$P_T = \sigma_a A_a + \sigma_d A_d + \sigma_s A_s \quad (4.2)$$

where σ_a, σ_d and σ_s – respectively true stress of adhesive layer, DDQ steel and SS 316L sheets. A_a, A_d and A_s – respectively instantaneous area of adhesive layer, DDQ steel and SS 316L. In region A, the total load is shared by all three layers (DDQ steel, adhesive and SS 316L) which are deformed together till failure of adhesive layer as shown in Fig. 4.3(a) and the total true stress (σ_A) is calculated by eq. (4.3).

$$\text{Region A} \rightarrow \sigma_A = \frac{(\sigma_a A_a + \sigma_d A_d + \sigma_s A_s)}{A_{T1}} \quad (4.3)$$

where σ_A – overall true stress in region A, A_{T1} – total instantaneous area in region A. Similarly, in region B, the total load is shared by base materials only (DDQ steel and SS 316L) as the adhesive has failed, and they deform together till failure of DDQ steel sheet as shown in Fig. 4.3(b) and eq. (4.4) is followed for σ-ε evaluation.

$$\text{Region B} \rightarrow \quad \sigma_B = \frac{(\sigma_d A_d + \sigma_s A_s)}{A_{T2}} \quad (4.4)$$

where σ_B – overall true stress in region B, A_{T2} – total instantaneous area in region B. In region C, the load is taken by SS 316L only which fails at last as shown in Fig. 4.3(c) and total stress (σ_C) is given by eq. (4.5)

$$\text{Region C} \rightarrow \quad \sigma_C = \frac{\sigma_s A_s}{A_{T3}} \tag{4.5}$$

where A_{T2} – total instantaneous area in region C which is equal to A_s.

4.3.2 Prediction of limit strains of adhesive bonded sheets: Necking criteria

The flow localization of sheet forming occurs subsequent to uniform deformation and limits formability. The flow localization is generally characterized by a necking phenomenon and finally failure occurs when the critical limit strains are attained. Narasimhan and Wagoner, 1991 predicted forming limit diagrams of thin sheets based on two-dimensional finite thickness defects. It is seen from this analysis that the absolute location of FLC depends not only on material properties, but also on the choice of failure criterion, defect geometry, and details of simulative model mainly like mesh size, number of defect dimensions. Sujit *et al.,* 1994 developed a new failure criterion termed by thickness gradients that develop during biaxial stretching. This new criterion can be used under a wide range of forming conditions to predict limit strains. The developed criterion predicts less dependence of limit strains on the degree of biaxiality for the range of material properties investigated.

4.3.2.1 Effective strain rate based criterion (ESRC)

ESRC is defined as the ratio of effective strain rate in the neck to that in the safe region (or bulk), and is written as (Narasimhan and Wagoner, 1991)

$$\text{ESRC} = \frac{\text{Effective strain rate in the neck region}}{\text{Effective strain rate in the bulk region}} \geq 4 \Rightarrow \text{Material failure or necking} \tag{4.6}$$

The ratio 4 is a 'lower bound value' below which limit strains are not reached, and the strain rate ratio increase unstably once the criterion is reached, which is the indication for the occurrence of necking. The major strain and minor strain in the bulk element at which the criterion is satisfied indicate the limit strain in that strain path.

4.3.2.2 Thickness gradient based necking criterion (TGNC)

Generally, necking is understood as a localized thinning phenomenon and this criterion basically determines localized region within the deforming sheet where a thickness gradient develops. The necking occurs in the sheet metal when the thickness gradient falls below 0.92 and is also applied to predict the FLC (Sujit Kumar *et al.,* 1994). In the present simulations, element pairs where the thickness ratio equals or falls below 0.92 are considered as necked elements. The major strains in all the thicker elements are noted. The largest major strain and the corresponding minor strain of such elements are treated as the forming limit strain. The thickness gradient necking criterion is given by eq. (4.7),

$$\text{TGNC} = \frac{\text{Thickness in necking element}}{\text{Thickness in bulk element}} = \frac{t_n}{t_{n-1}} \text{ or } \frac{t_n}{t_{n+1}} \leq 0.92 \Rightarrow \text{Material failure or necking} \tag{4.7}$$

These ESRC and TGNC criteria have been applied for single metal sheets and also for welded sheets which are on the same plane. In this work, the applicability of ESRC and TGNC criteria for adhesive bonded sheets will be checked and discussed. It is expected that the criteria are modified because of the presence of adhesive, and the original criteria are unsuitable for adhesive bonded blanks.

4.4 Results and discussion

In this section, the failure of adhesive bonded blanks with different hardener/resin ratios is compared between experiment and prediction. The tensile behaviour of adhesive bonded sheets is compared and analysed between experiment and prediction. Further, the forming limit strains in base materials constituting adhesive bonded blanks with effect of hardener/resin ratio predicted by TGNC and ESRC are compared with experiment and discussed.

4.4.1 Failure of adhesive bonded blanks at different hardener/resin ratios: Experiment and prediction

Fig. 4.4 shows the limit strain results evaluated during simulation with different mesh sizes. The necking criterion ESRC was used in the prediction of limit strains in base materials. There is not much variation in the predicted limit strains in DDQ steel and SS 316L. About 0.2% to 0.6% variation in true major strain and about 0.1% to 0.9% variation in true minor strain are observed. These results reveal that the mesh varying from 0.5 mm to 2 mm would not affect the forming limit strains predictions.

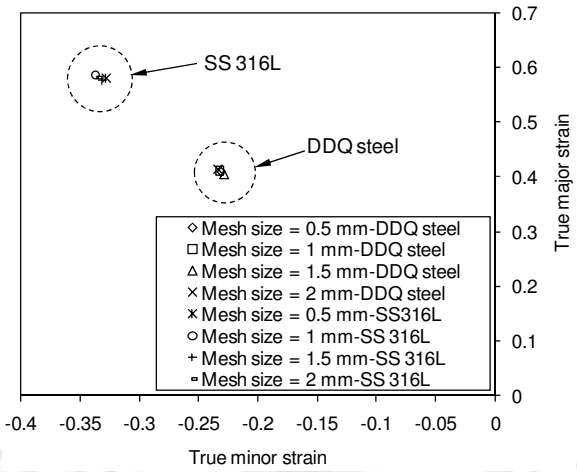

Fig. 4.4 Limit strains of DDQ steel and SS 316L tensile tested as single sheet with different mesh size during FE simulation

Fig. 4.5(a, b) shows the comparison of true stress-strain behaviour of DDQ steel and SS 316L between experimental and predicted results, respectively, from tensile test. For DDQ steel, there is about 7 MPa variation in true stress at failure and about 2.2% variation in true strain between experimental and predicted results. There is a good agreement between experimental and predicted results in the case of SS 316L.

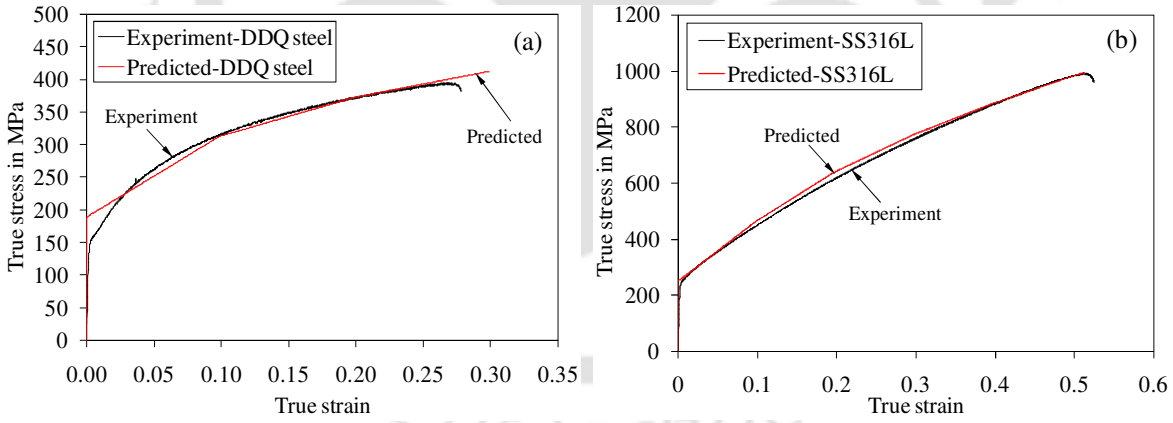

Fig. 4.5 Comparison of true stress-strain behaviour of base materials between experimental and prediction: (a) DDQ steel, and (b) SS 316L

Tables 4.2 and 4.3 compare the progression at failure of adhesive and base materials from experiments and FE simulations for varying hardener/resin ratios during tensile test and IPPS formability test, respectively. In simulation results, the failure stage of base materials are obtained from effective strain rate based necking criterion (ESRC) and thickness gradient based necking criterion (TGNC). It is understood that whenever the failure criteria are satisfied, necking occurs

in the base materials and that progression is noted as failure progression. The adhesive failure stage is determined from the load drop observed in the load-progression data from FE predictions. In the case of experiments, all the failure stages were obtained from the load drop of load-progression behaviour of tensile test. It is observed from the experimental results that the progression at failure of adhesive layer and base materials in adhesive bonded sheets increases with increase in hardener/resin ratio. In the simulation results, a similar trend of delay in failure is noticed only in the case of adhesive layer deformation, but not in the constituting base materials.

Table 4.2 Prediction of progression at failure of adhesive bonded blanks with different H/R ratios in tensile test

H/R ratio	Adhesive layer failure (mm)			DDQ steel sheet failure (mm)					SS316L sheet failure (mm)				
	Experiment	Simulation	Variation %	Experiment	Simulation				Experiment	Simulation			
					ESRC	Variation %	TGNC	Variation %		ESRC	Variation %	TGNC	Variation %
Single sheet	-	-	-	26.3	27.42	4.3	28.68	9.1	52.4	51.72	1.3	53.46	2.0
0.6:1	9.34	9.5	1.7	27.12	24.54	9.5	26.52	2.2	55.0	52.8	4.0	55.38	0.7
0.7:1	9.5	10.0	5.3	29.0	24.54	15.4	26.52	8.1	53.9	53.1	1.5	55.56	3.1
0.8:1	12.5	10.5	16.0	28.1	24.54	12.7	26.52	5.6	55.5	50.88	8.3	56.16	1.2
0.9:1	12.7	11.0	13.4	29.3	24.54	16.3	26.52	9.5	57.8	53.1	8.1	56.16	2.8
1:1	13.7	11.5	16.1	30.0	24.42	18.6	26.4	12.0	59.2	52.68	11.0	56.28	5.5

Table 4.3 Prediction of progression at failure of adhesive bonded blanks with different H/R ratios in IPPS formability test

H/R ratio	Adhesive layer failure (mm)			DDQ steel sheet failure (mm)					SS316L sheet failure (mm)				
	Experiment	Simulation	Variation %	Experiment	Simulation				Experiment	Simulation			
					ESRC	Variation %	TGNC	Variation %		ESRC	Variation %	TGNC	Variation %
Single sheet	-	-	-	4.7	5.88	25.1	5.94	26.4	8.6	15.8	83.7	15.88	84.7
0.6:1	1.1	5.02	78.1	5.1	6.46	26.7	6.56	28.6	8.6	16.76	94.9	16.58	92.8
0.8:1	1.3	5.50	76.4	5.3	6.46	21.9	6.56	23.4	9.6	16.76	74.6	16.58	72.7
1:1	2.4	6.12	60.8	5.6	6.46	15.4	6.56	17.1	11.8	16.76	42.0 .	16.58	40.5

In the case of predicted (simulation) results from Table 4.2, it is observed that with increase in hardener/resin ratio, the progression at failure of adhesive increases from 9.5 mm to 11.5 mm. Similar results are seen in the case of IPPS formability tests, that is from 5.02 mm to 6.12 mm (Table 4.3). In the case of tensile test (Table 4.2), there exists moderate agreement between the

experimental and predicted results. In the case of IPPS forming tests, the predictions are considerably different. The influence of hardener/resin ratios on base materials failure is not predicted properly during simulation results, unlike in experiments. The progression at failure of constituting base materials is almost constant during predictions. This implies that the accuracy of predictions decreases with increase in hardener/resin ratio in the case of tensile test and vice-versa in the case of IPPS forming test.

Among the two failure criteria, TGNC predicts the failure stage later than ESRC in most of the cases of tensile and IPPS forming tests. In other words, TGNC is accurate than ESRC in predicting the constituting base material failure in the case of tensile test, while both perform equally, not accurately in the case of IPPS forming test. With respect to adhesive bonded blanks, there is about 4% to 18.6% variation between experiment and ESRC prediction, and about 0.7% to 12% variation between experiment and TGNC prediction in the case of tensile test.

In the case of prediction through FE simulations, the effect of adhesive properties is not captured and hence the progression at failure of base materials remains same in all the cases. This is believed to happen mainly because of absence of adhesive bonding (or adhesion) during FE simulations. So, the change in mechanical behaviour of adhesive bonded sheets is not only because of change of adhesive properties, but also due to adhesion methods and properties. There is a poor agreement between experiment and predicted progression at failure in the case of IPPS forming test which is unexpected. This is believed to happen because of the presence of notch, changing the behaviour of whole adhesive bonded sheets during prediction. Moreover, this sample deforms near plane-strain conditions, which is the critical strain path in sheet deformation.

4.4.2 Experimental evaluation and prediction of tensile behaviour of adhesive bonded sheets

Figs. 4.6(a) and 4.6(b) show the overall comparison of tensile (true stress-strain) behaviour of adhesive bonded blanks with different hardener/resin ratios obtained from experiments and FE simulations, respectively. Figs. 4.6(c) and 4.6(d) show the individual comparison of tensile (true stress-strain) behaviour of adhesive bonded blanks with different hardener/resin ratios obtained from experiments and predictions. While evaluating the tensile (true stress-strain) behaviour of adhesive bonded blanks from the load-progression experimental data, the deformation of all three layers constituting adhesive bonded blanks (adhesive layer, DDQ steel and SS 316L) was taken into account and true stress-strain was calculated in region A through eq. (4.3). After failure of adhesive layer, the deformation of DDQ steel and SS 316L sheets was taken into account for calculating true stress-strain in region B through eq. (4.4). Similarly, after failure of DDQ steel

sheet, eq. (4.5) was used in region C to evaluate σ-ε behaviour. It is observed from experimental results that the true strain at failure increases with increase in hardener/resin ratio in all the regions A, B and C (Fig. 4.6(a)). It is due to improved plasticity of adhesive layer which hold rich in hardener formulation in the adhesive system as discussed in Chapter 2 in Section 2.6.1.

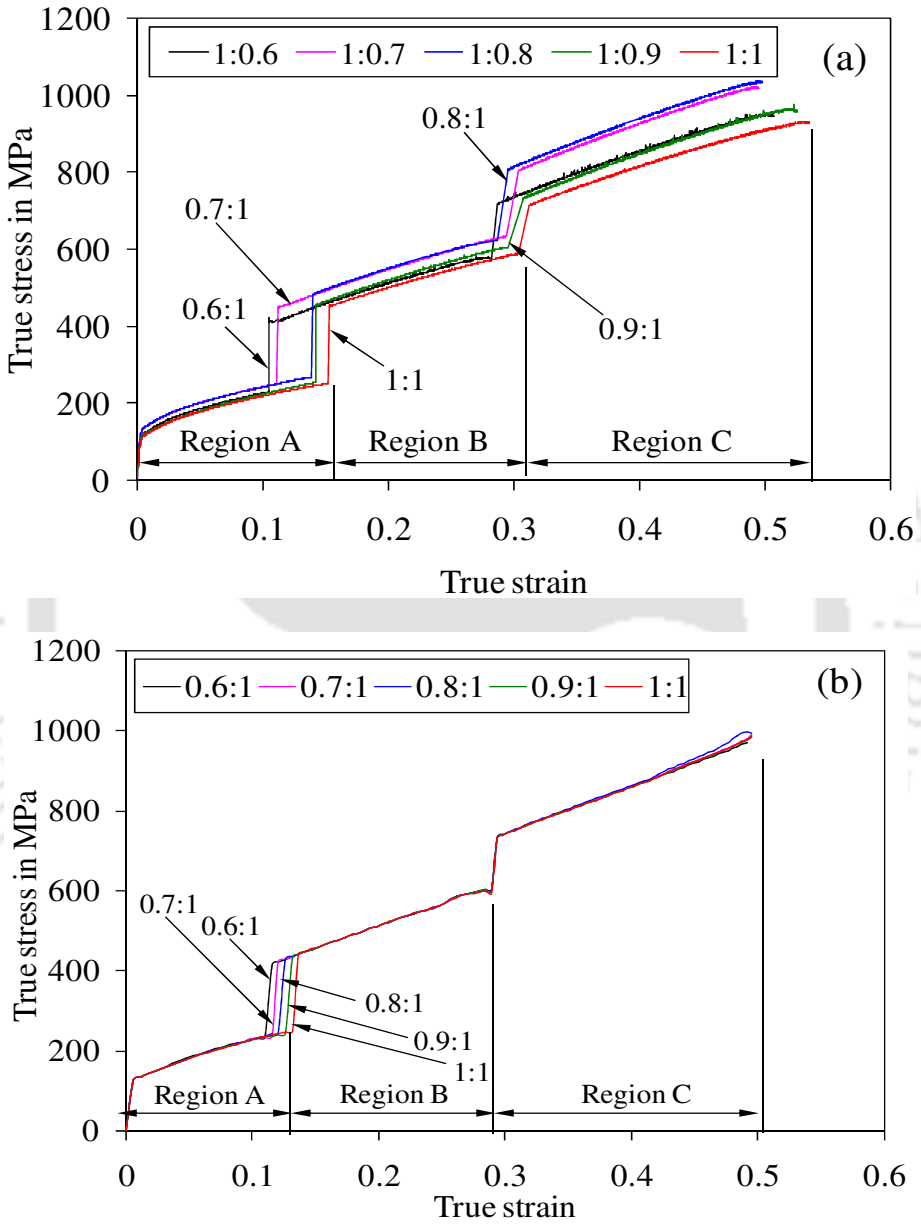

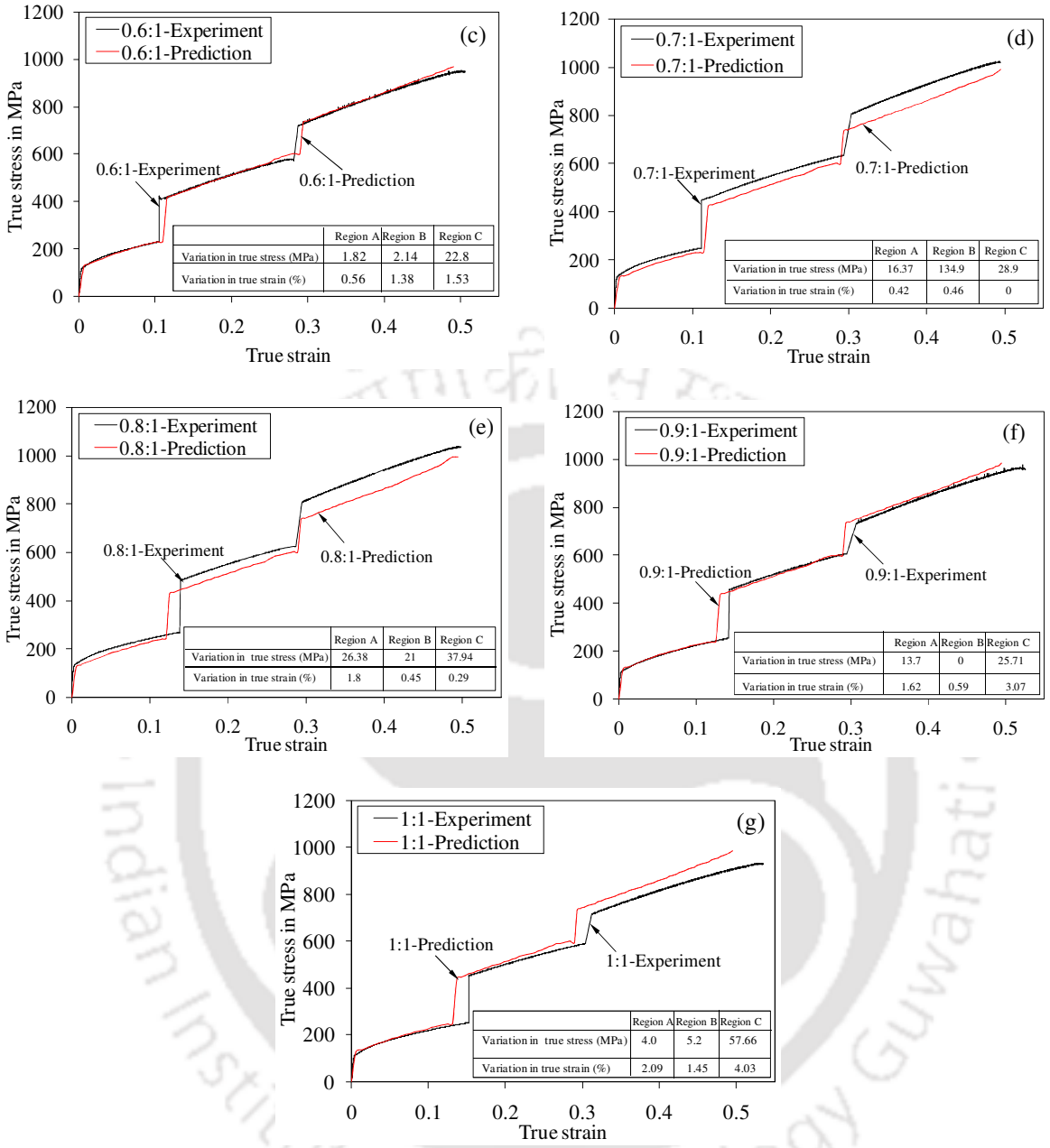

Fig. 4.6 Comparison of tensile (true stress-strain) behaviour of adhesive bonded blanks with different hardener/resin ratios: (a) Experiments (Variation in maximum tensile strength = ±8 MPa, and in elongation at failure = ±1 %), (b) Simulations, (c) H/R = 0.6:1, (d) H/R = 0.7:1, (e) H/R = 0.8:1, (f) H/R = 0.9:1, and (g) H/R = 1:1 (where Region A → tensile behaviour of adhesive layer, DDQ steel sheet and SS316L sheet, Region B → tensile behaviour of DDQ steel sheet and SS316L sheet of adhesive bonded blank, Region C → tensile behaviour of SS 316L sheet of adhesive bonded blank)

While comparing experimental and predicted results (Figs. 4.6(c-g)), the global tensile behaviour of adhesive bonded blanks follows the same trend till adhesive failure that is with increase in hardener/resin ratio, the true strain at failure of adhesive (region A) increases. This is true in the case of experiment and simulation results. But it does not occur in regions B and C.

In the prediction of true stress-strain behaviour of (Fig. 4.6(b)), the adhesive layer that is governed by its mechanical properties shows improvement in ductility in region A. But there is no influence of adhesive layer on ductility of base materials constituting adhesive bonded blanks as compared to the tensile (true stress-strain) behaviour obtained from experiments (Fig. 4.6(a)). From these results, it is believed that the ductility of adhesive bonded blanks is not only influenced by the plasticity of adhesive, but also its interfacial bonding (adhesive bonding) between base materials. There is about 0.42% to 2.09%, 0.45% to 1.45% and 0% to 4.03% variation in true strain in regions A, B and C, respectively. Almost there is a good agreement in true stress between experimental and predicted results in all three regions except a few. On the whole, though the improvement in ductility of base materials constituting adhesive bonded blanks is not predicted accurately, the overall tensile behaviour prediction is encouraging.

Fig. 4.7(a, b) shows the comparison of % elongation (true strain) of regions A, B and C with different hardener/resin ratios between experiment and predicted results respectively from tensile and IPPS forming tests. Here the elongation % is obtained using the failure criteria (TGNC and ESRC). The elongation increases with increase in hardener/resin ratio till failure of adhesive layer (Region A). This is true in the case of experiments and simulations. But in regions B and C, though the difference between experiment and predicted elongation values is less (< 2%), the trend of increased elongation with increase in hardener/resin ratio is not observed (Fig. 4.7(a)). The true stress-strain behaviour of adhesive bonded sheets during IPPS forming test was evaluated for all the cases. The elongation at failure for different hardener/resin ratios is depicted in Fig. 4.7(b). There is an increasing trend of elongation % with increase in hardener/resin ratio, from experiments and prediction in region A. But it is not reflected during predictions in regions B and C as compared to the experiments. Also there is a considerable disagreement between experimental and predicted elongation data.

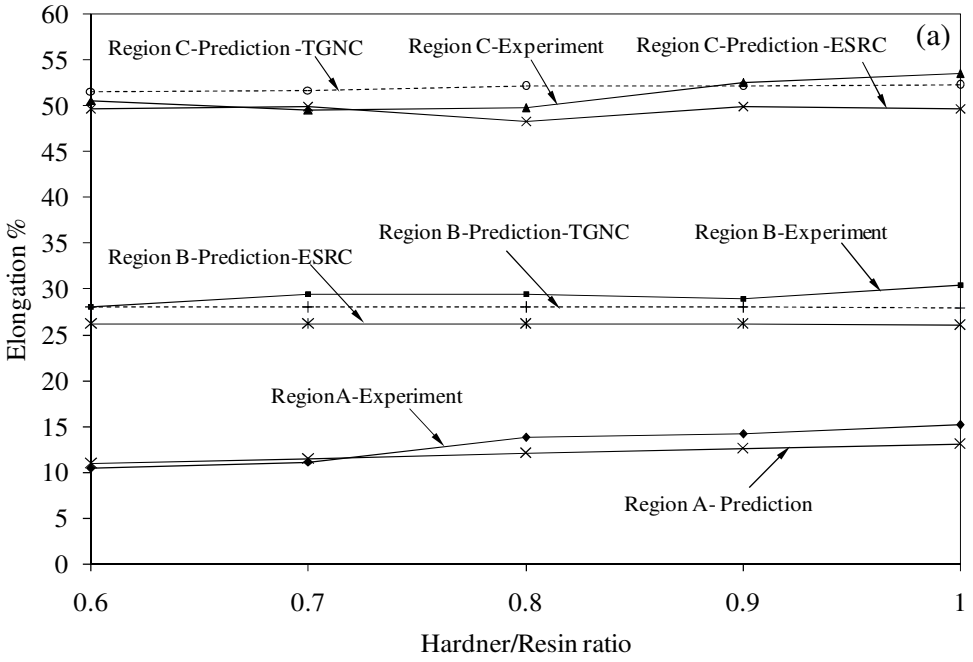

Variation in Region A between experiment and prediction :
In region A - 0.4% to 2.1%
In region B - 1.8% to 4.3% (ESRC) and 0.02 to 2.5% (TGNC)
In region C - 0.43% to 3.88% (ESRC) and 0.33-2.37% (TGNC)

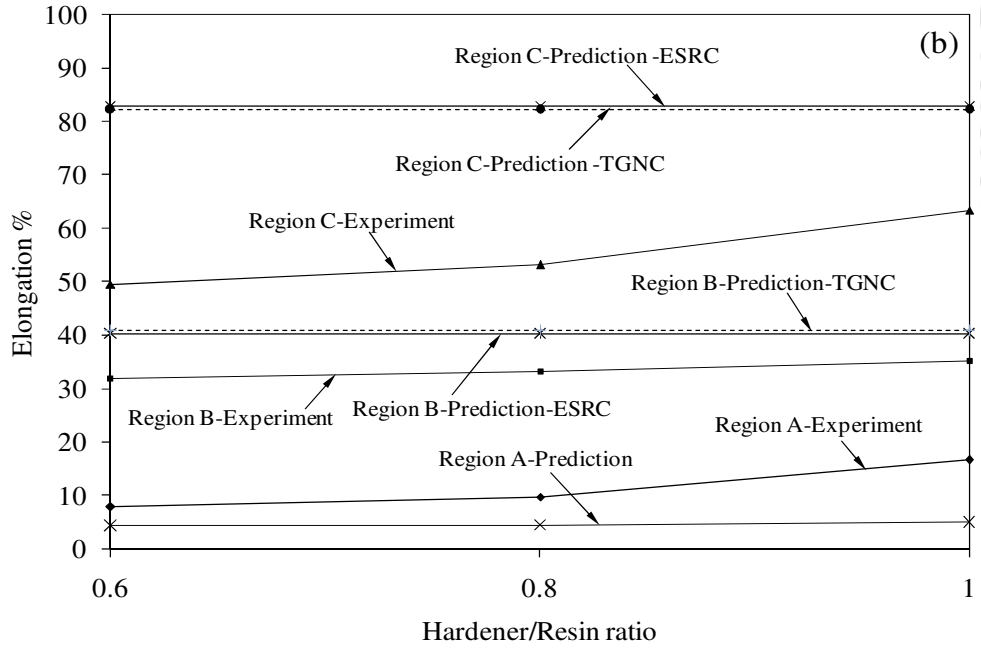

Variation in elongation between experiment and prediction:
In region A - 3.5% to 11.8%
In region B - 5.06% to 8.33% (ESRC) and 5.57 to 8.84% (TGNC)
In region C - 19.4% to 33.27% (ESRC) and 18.79-32.6% (TGNC)

Fig. 4.7 Comparison of percentage elongation (true strain) of adhesive bonded blanks with different hardener/resin ratios between experiment and predicted results: (a) Tensile test, and (b) IPPS formability test

4.4.3 Forming limit strain prediction of adhesive bonded blanks with effect of hardener/resin ratio

Fig. 4.8(a, b) demonstrates the variation of effective strain rate ratio with true major strain in bulk in base materials in adhesive bonded blanks with different hardener/resin ratios during tensile and IPPS forming tests simulation. It is understood that the effective strain rate ratio increases unstably once the criterion is reached, which is the indication for the occurrence of necking. The corresponding major strain and minor strain in the bulk element indicate the limit strain in that strain path. It should be noted that the ratios shown in the figures are arbitrary numbers that are less than or equal to ESRC above which a sudden increase in ratio is seen.

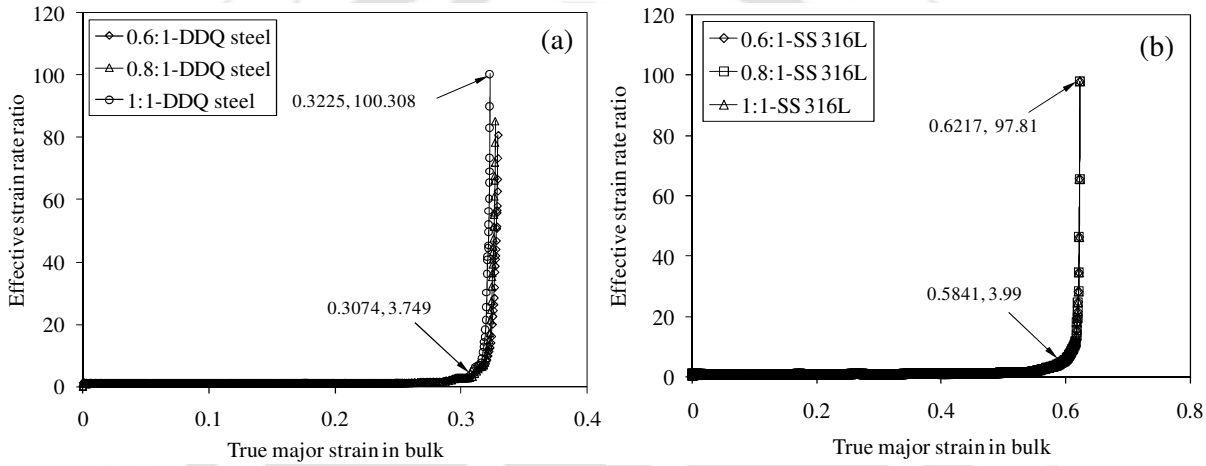

Fig. 4.8 Variation of effective strain rate ratio with true major strain in bulk in base materials in adhesive bonded blanks with different H/R ratios: (a) DDQ steel (tensile test), and (b) SS 316L (IPPS forming test)

It is observed that the ESRC defined for base materials that are unbonded is suitable for adhesive bonded sheets also. The true major strain in bulk saturates when the criterion is satisfied. Hence the criterion is not modified, and original criterion of ESRC ≥ 4 for failure to occur is used for prediction.

Fig. 4.9(a, b) shows the comparison of limit strains of DDQ steel and SS 316L base materials evaluated through experiment and prediction during tensile and IPPS forming tests, respectively. The limit strains of base materials are predicted by the necking criteria, ESRC and TGNC, and compared with experimental results. The difference in strain results between experiment and prediction is shown in percentage directly. In tensile test (Fig. 4.9(a)), there is not much difference in major strain (<1.3%) between experiment and prediction by TGNC. About 4.2% and 6.3% difference in major strain is observed with DDQ steel and SS 316L, respectively, when the

base materials are predicted by ESRC. A large difference (13.2% to 17.9%) in minor strain is observed between experiment and prediction by both TGNC and ESRC. While comparing limit strains obtained from IPPS forming test (Fig. 4.9(b)), a significant difference in both major and minor strain is noted between experimental and predicted (TGNC and ESRC) results. In the case of SS 316L, there is a slight variation in strain path from plane strain condition, as indicated by limit strain predicted through TGNC and ESRC. In general, the limits strains predicted by TGNC show less difference between experimental results than predicted by ESRC.

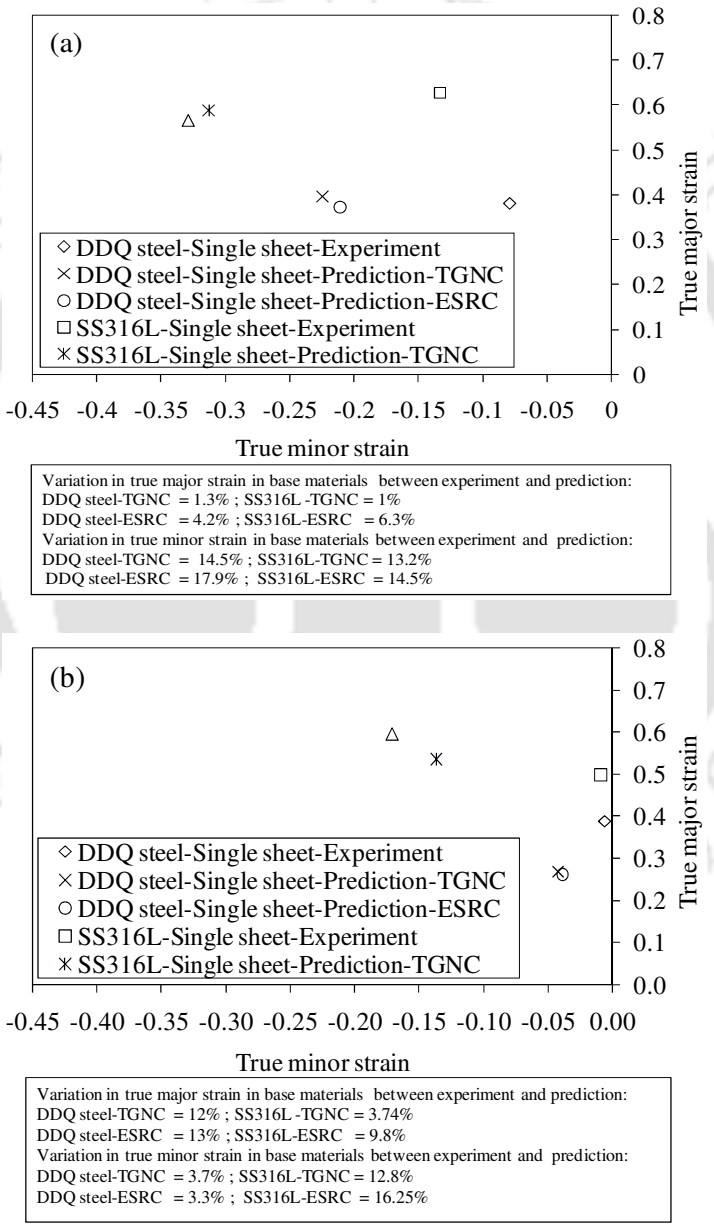

Fig. 4.9 Comparison of experiment and prediction of base materials limit strain: (a) tensile test, and (b) IPPS forming test

Fig. 4.10(a-f) shows the comparison of limits strains in DDQ steel and SS 316L constituting adhesive bonded blanks with different hardener/resin ratios predicted by TGNC and ESRC in tensile test. Similarly, Fig. 4.11(a-f) shows the comparison of limit strains of base materials in IPPS forming test. The predicted results are compared with experimental results, and the variation in limit strains is also shown. It is observed that a considerable difference exists between experimental and predicted (by TGNC and ESRC) limit strain results.

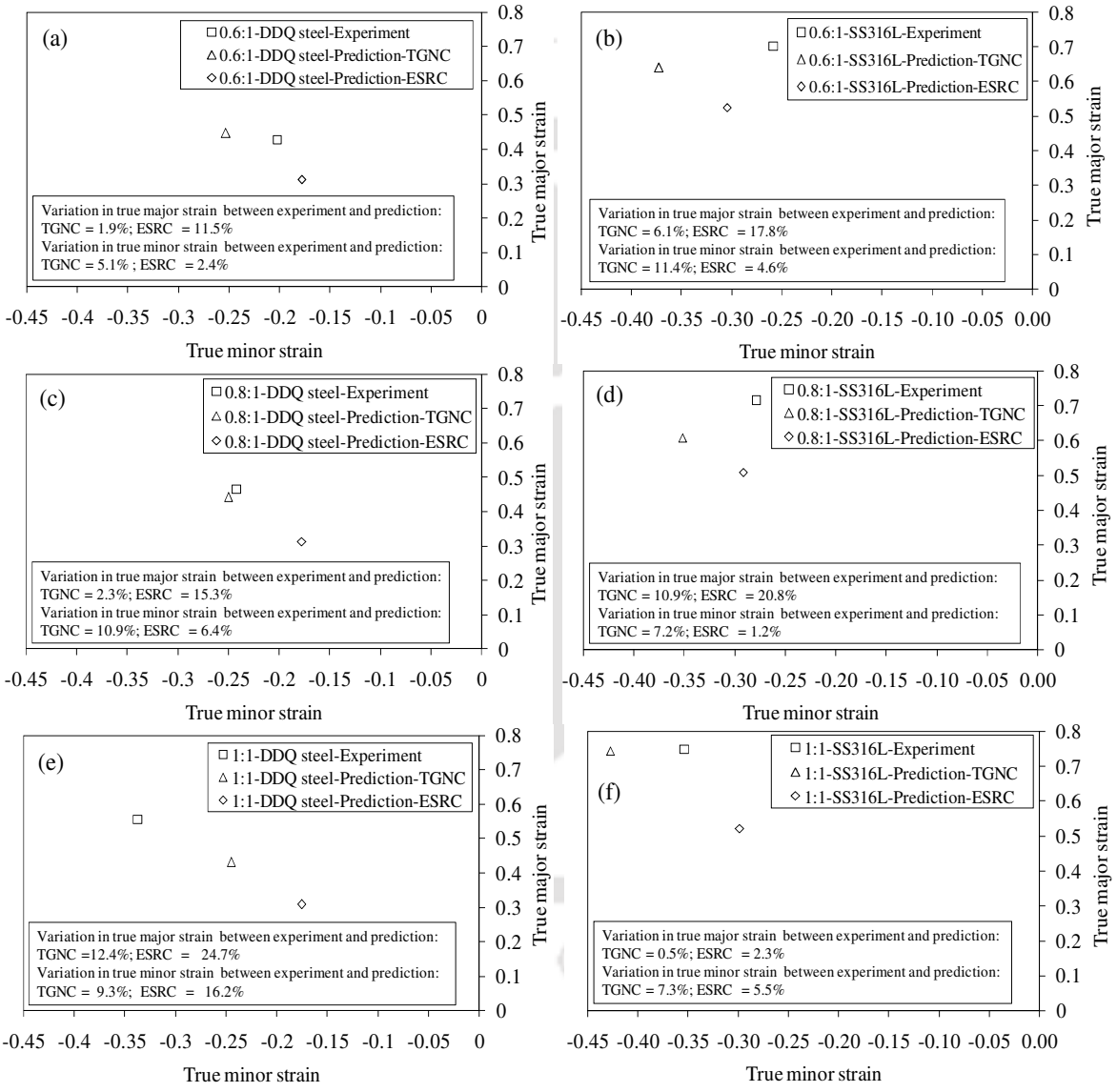

Fig. 4.10 Comparison of limit strains base materials in adhesive bonded blanks with different H/R ratios between experiments and predictions in tensile test: (a) H/R = 0.6:1-DDQ steel, (b) H/R = 0.6:1-SS 316L, (c) H/R = 0.8:1-DDQ steel, (d) H/R = 0.8:1-SS 316L, (e) H/R = 1:1-DDQ steel, and (f) H/R = 1:1-SS 316L

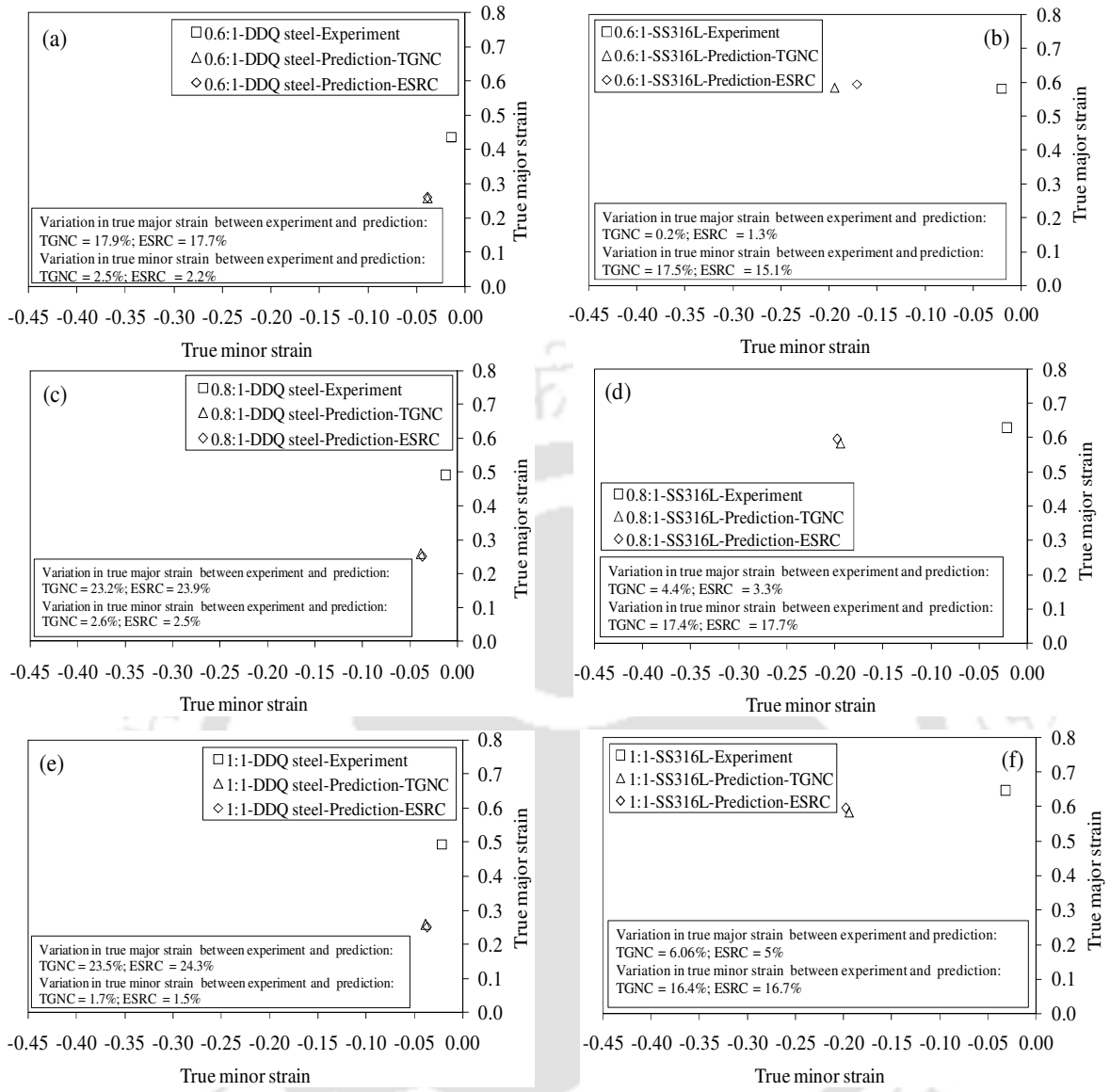

Fig. 4.11 Comparison of limit strains base materials in adhesive bonded blanks with different H/R ratios between experiments and predictions in IPPS forming test: (a) H/R = 0.6:1-DDQ steel, (b) H/R = 0.6:1-SS 316L, (c) H/R = 0.8:1-DDQ steel, (d) H/R = 0.8:1-SS 316L, (e) H/R = 1:1-DDQ steel, and (f) H/R = 1:1-SS 316L

In tensile test, the true major strain varies from 0.5% to 6% and the true minor strain varies from 7.3% to 11.5%, during TGNC predictions. While through ESRC predictions, the true major strain varies from 2.3% to 17.8% and the true minor strain varies from 4.6% to 6.4%. It is noted that the major strain predicted by TGNC show better agreement to the experimental results in most of the cases. In IPPS forming test, there is about 4.5% to 23.5% difference in true major strain and about 1.7% to 17.5% difference in true minor strain, during TGNC predictions. In the case of prediction by ESRC, there is about 3.3% to 24.3% difference in true major strain and about 2.2% to 17.7% difference in true minor strain. Though there is a large difference between

experimental and predicted (by TGNC and ESRC) limit strain results, the predicted limit strain results are closer to each other. In specific, during IPPS forming test, there exists a significant difference in the progression till failure of SS 316L between experimental and prediction results (Table 4.3). This large difference in progression is not reflected on the true major limit strains, but on the true minor strains of base materials predicted by TGNC and ESRC.

On the whole, though both the necking criteria, TGNC and ESRC are meant for base material (unbonded) formability prediction, the TGNC shows its superiority with less difference between experimental limit strain results in the present study. Since there is no interfacial bonding between adhesive and base materials, the base materials constituting adhesive bonded blanks behave as if like a single sheet. Further, the applicability of TGNC and ESRC will be checked for adhesive bonded blanks by considering interfacial bonding between adhesive and base materials.

4.5 Conclusions

From this chapter, the following conclusions are drawn.

- The ductility of adhesive bonded blanks increases with increase in hardener/resin ratio till adhesive failure and this improvement in plasticity of adhesive layer increases the ductility of the base materials.
- There is a good agreement between experimental and predicted overall true stress-strain behaviour of adhesive bonded sheets. Though this is the case, the influence of changing adhesive properties on the tensile behaviour and IPPS formability accurately is not predicted.
- During forming limit strain prediction of adhesive bonded blank under the influence of hardener/resin ratio of the adhesive system, both ESRC and TGNC are applicable only to a moderate extent. On the whole, the predicted limit strain results based on TGNC shows better accuracy as compared to ESRC.
- Finally, in this work, a simulation methodology has been analysed thoroughly to predict the formability of adhesive bonded sheets. The inaccuracies in formability predictions are believed due to the absence of interface interaction between adhesive and base materials during simulation. Further investigation is required in this direction to improve the prediction accuracy.

Chapter 5

Evaluation of adhesive mechanical properties by rule of mixtures and its application in necking prediction

5.1 Methodology

In this section, the method of evaluating the stress-strain behaviour of adhesive with different hardener/resin ratios by two different approaches such as direct evaluation from tensile testing of adhesive samples, and rule of mixtures method. The mechanical properties of base materials and epoxy adhesive are already discussed in Chapter 2 in Sections 2.1.1 and 2.4.1, respectively.

5.2 Approach 1: Experimental evaluation of adhesive properties

In approach-1, the mechanical properties of epoxy adhesive samples with different hardener/resin ratios were evaluated as per procedure discussed in Chapter 2 in Section 2.2. The engineering stress-strain data of tensile tested adhesive samples was converted into true stress-strain data of epoxy adhesive with different hardener/resin ratios was incorporated during prediction.

5.3 Approach 2: Rule of Mixtures

In approach-2, the tensile behaviour of epoxy adhesive was evaluated from the tensile behaviour of adhesive bonded blanks with different hardener/resin ratios based on rule of mixtures concept. Abdullah *et al.,* 2001 used the rule of mixtures method to determine the weld metal properties from the tensile specimens in which the weld lies parallel to the axis of tension. It was found that the rule of mixtures is a useful method of weld metal property determination. Though the work of Abdullah et al. is not exactly relevant to the present work, the concept of rule of mixtures used for welded sheets is applied for adhesive bonded sheets in the present work. The tensile behaviour of adhesive bonded blanks evaluated as per procedure discussed in Chapter 2 in Section 2.3 was utilized in the evaluation of adhesive properties. It is believed that the tensile (σ-ε) behaviour of adhesive derived by approach-2 is the constitutive tensile behaviour of adhesive and its interfacial bond strength between base materials, which may improve the accuracy of formability of adhesive bonded blanks during prediction. The σ-ε data

of adhesive bonded sheets till adhesive failure was taken into account to evaluate the σ-ε behaviour of adhesive layer by applying rule of mixtures concept (Fig. 5.1).

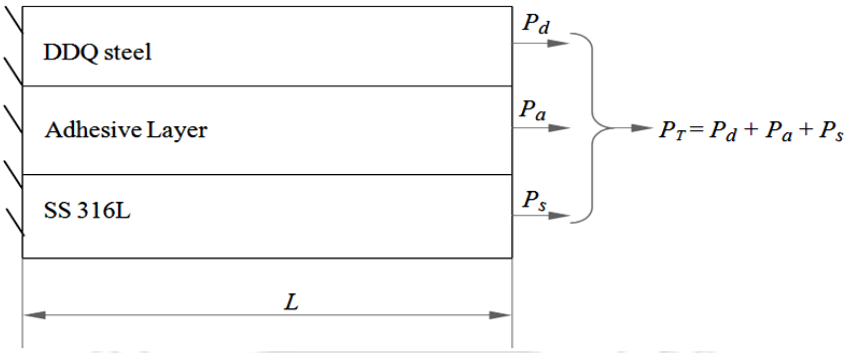

Fig. 5.1 Schematic of load sharing by adhesive bonded sheets during tensile test

Let, total load, $P_T = P_d + P_a + P_s$ (5.1)

where P_T – total load during tensile test of adhesive bonded blank from experiment.

P_d – load on DDQ steel sheet in adhesive bonded blanks

P_a – load on adhesive layer in adhesive bonded blanks

P_s – load on SS 316L sheet in adhesive bonded blanks

The total load is written in terms of true stress as eq. (5.2)

$$P_T = \sigma_a A_a + \sigma_d A_d + \sigma_s A_s \tag{5.2}$$

Based on the Hollomon's strain hardening law, eq. (5.2) is modified as eq.(5.3)

$$\sigma_a = \frac{P_T - (K_d \varepsilon_d^{n_d}) A_d - (K_s \varepsilon_s^{n_s}) A_s}{A_a} \tag{5.3}$$

Since adhesive and base materials are bonded along the longitudinal direction and assuming iso-strain condition ($\varepsilon_a = \varepsilon_d = \varepsilon_s$) till failure of adhesive, the true stress-strain relation of adhesive layer is given by eq. (5.4)

$$\sigma_a = \frac{P_T - (K_d \varepsilon_a^{n_d}) A_d - (K_s \varepsilon_a^{n_s}) A_s}{A_a} \tag{5.4}$$

where

K_d and K_s – strength coefficients of DDQ steel and SS 316L, respectively.

n_d and n_s – strain hardening exponent of DDQ steel and SS 316L, respectively.

σ_a, σ_d and σ_s –true stress of adhesive layer, DDQ steel and SS 316L sheets, respectively.

A_a, A_d and A_s – instantaneous cross-section area of adhesive layer, DDQ steel and SS 316L, respectively. (Here $A_a = A_T - A_d - A_s$)

A_T – total instantaneous cross-section area of adhesive bonded sheets

The true stress-strain data of epoxy adhesive obtained by Approach-1 and Approach-2 were incorporated during simulation of adhesive bonded sheets to predict the forming limit strains in tensile test and IPPS formability test.

5.4 Prediction of limit strains of adhesive bonded sheets

The tensile and IPPS adhesive bonded blanks were modelled as described Chapter 4 in Section 4.3. Here also two necking criteria namely ESRC and TGNC were used to predict the forming limit strain of base materials constituting adhesive bonded sheets as discussed in Chapter 4 in Section 4.3.2.

5.5 Results and discussion

In this section, the limit strains of base materials constituting adhesive bonded sheets predicted by approach-1 and approach-2 are compared.

5.5.1 Comparison of limit strains of base materials constituting adhesive bonded sheets through approach 1 and approach 2

Fig. 5.2(a, b) shows the comparison of true stress-strain behaviour of cured epoxy adhesive obtained by approach-1 and approach-2 with different hardener/resin ratios. It is observed that the true strain increases with increase in hardener/resin ratio during testing of adhesive samples. The same trend is seen in the tensile behaviour of adhesive layer derived from the adhesive bonded blanks through approach-2. There is about 2 MPa variation in true stress and about 0.5% variation in true strain at failure between approach-1 and approach-2.

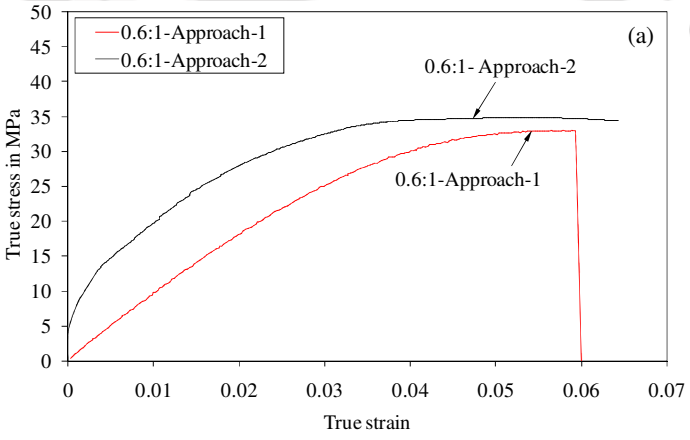

Error variation in true stress at failure during experiment =	1.5 MPa
Error variation in true strain at failure during experiment =	0.5%
Variation in true stress at failure between Approach-1 and Approach-2 =	1.96 MPa
Variation in true strain at failure between Approach-1 and Approach-2 =	0.5%

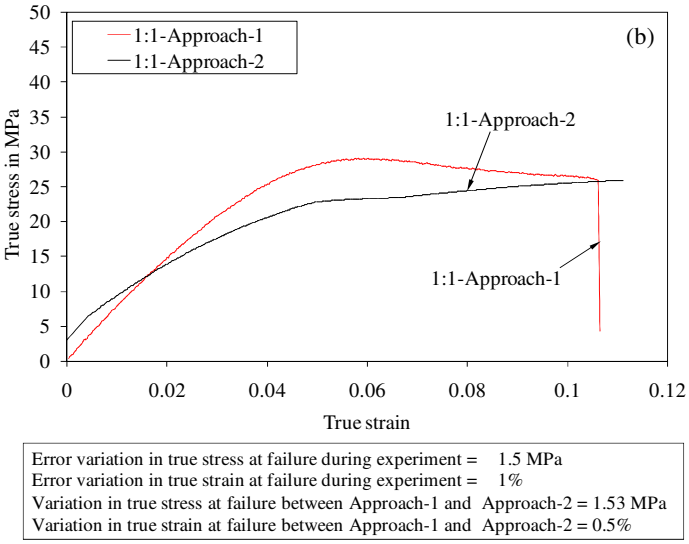

Fig. 5.2 Comparison of true stress-strain behaviour of epoxy adhesive obtained by approach-1 and approach-2 with different hardener/resin ratios: (a) H/R = 0.6:1, and (b) H/R = 1:1

Fig. 5.3(a-d) shows the comparison of limits strains in base materials constituting adhesive bonded blanks with different hardener/resin ratios between experiments and predictions during tensile test. Similarly, the limit strains during IPPS formability test are shown in Fig. 5.4(a-d). During simulations of tensile and IPPS forming tests, the limit strains evaluated by the necking criteria TGNC and ESRC through approach-1 and approach-2 are compared. It is observed that the limit strains evaluated through approach-1 and approach-2 during predictions exhibit almost same results. These results reveal that either approach-1 or approach-2 could be followed to evaluate adhesive mechanical properties so that limit strains of base materials can be predicted. It is noted that the limit strains evaluated by TGNC predictions in both the approaches show less difference with respect to experimental limit strains. It is also noted that the limit strains predicted by TGNC through both the approaches are close to each other in most of the cases. Similarly, in the case of ESRC predictions, the limit strains from approach-1 and approach-2 are very close to each other. Particularly, in the case of SS316L during IPPS forming test, the limit strains from both necking criteria are almost same and there is a slight change in the strain paths.

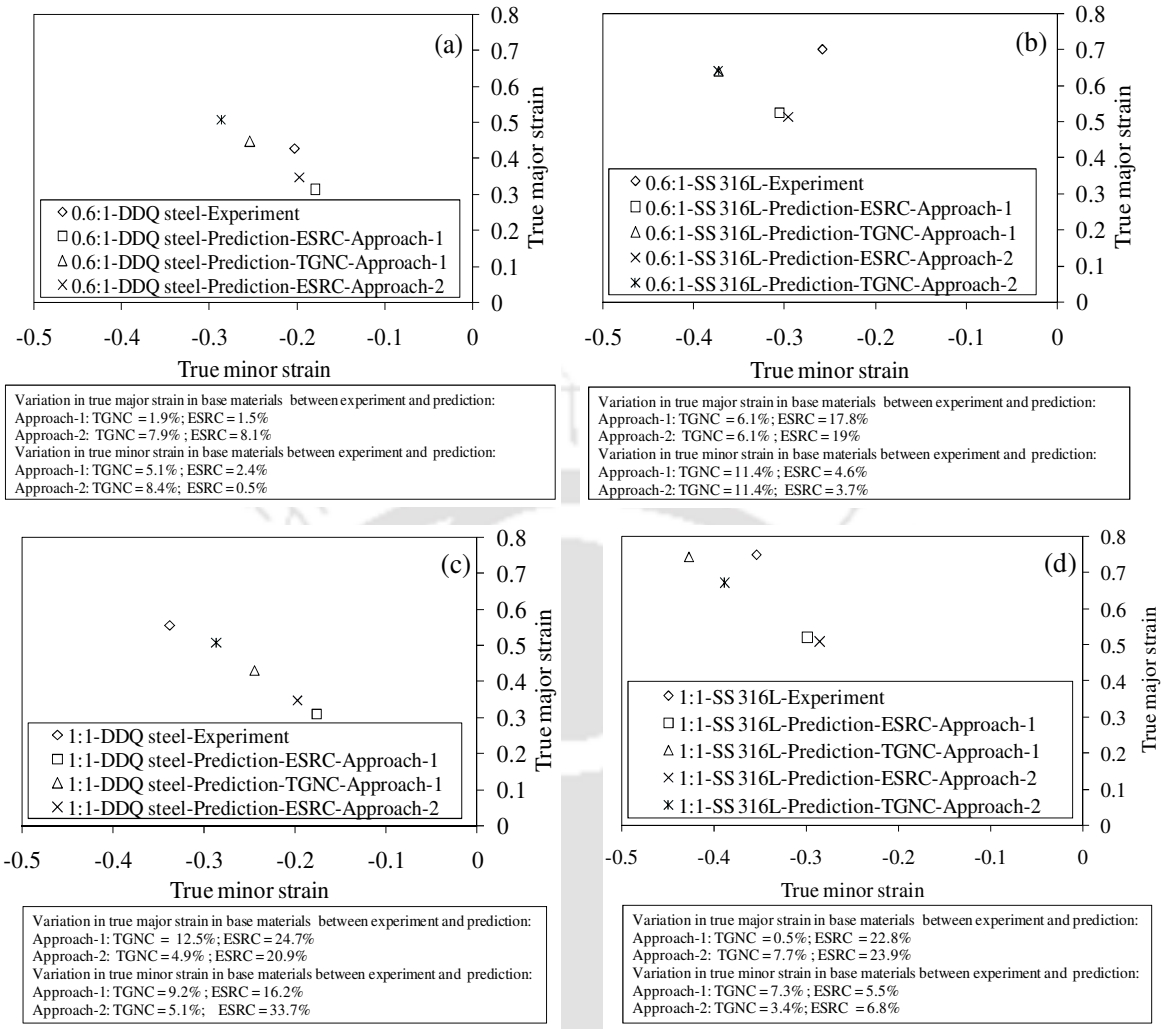

Fig. 5.3 Comparison of limit strain results of adhesive bonded sheets with different H/R ratios between experiments and predictions during tensile test: (a) H/R = 0.6:1-DDQ steel, (b) H/R = 0.6:1- SS 316L, (c) H/R = 1:1-DDQ steel, and (d) H/R = 1:1-SS 316L

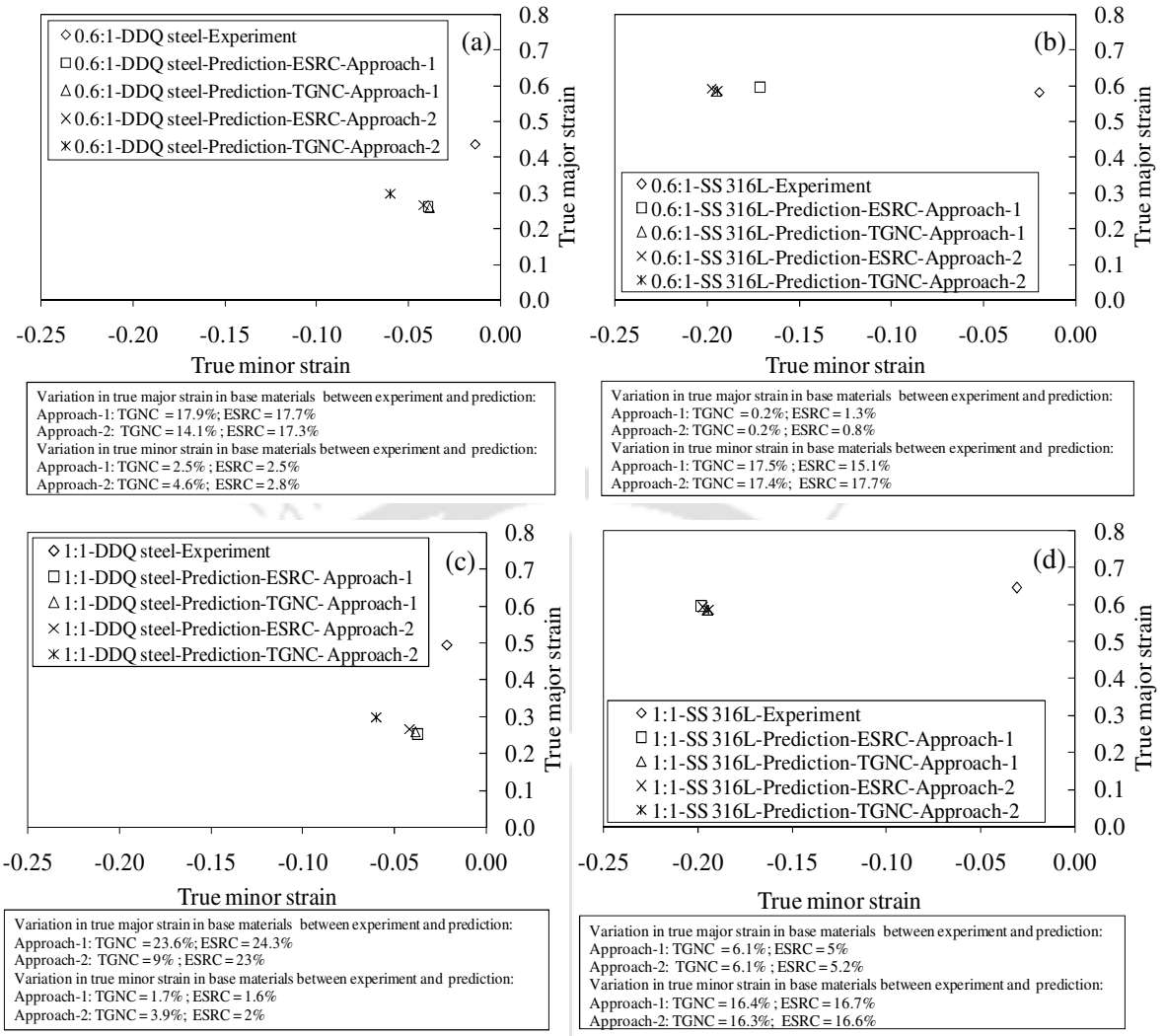

Fig. 5.4 Comparison of limit strain results of adhesive bonded blanks with different H/R ratios between experiments and predictions during IPPS formability test: (a) H/R = 0.6:1-DDQ steel, (b) H/R = 0.6:1-SS 316L, (c) H/R = 1:1-DDQ steel, and (d) H/R = 1:1-SS 316L

5.6 Conclusions

From this work, the following conclusions are drawn.

- It is suggested that the σ-ε behaviour of adhesive obtained either from rule of mixtures approach or from experiments could be followed in the forming limit strain predictions of adhesive bonded sheets. Limit strains predicted through these approaches are almost same.
- The limit strains evaluated by TGNC show less difference with respect to experimental limit strains, while following both the approaches. This suggests that prediction of forming limit strains of adhesive bonded blanks by the necking criterion, TGNC, is more

suitable than the necking criterion, ESRC. It is believed that the considerable difference is due to the absence of interface bonding between adhesive layer and base materials during simulation.

- The stress-strain behaviour evaluated from the rule of mixtures approach includes interfacial bonding, while it is not from experiment (Approach 1). Hence, if interfacial bonding is modelled during simulations, then the rule of mixtures approach would provide accurate formability results as compared to the experimentation approach, i.e., adhesive mechanical properties evaluated through experiments.

Chapter 6

Experimental evaluation and prediction of formability of carbon black filled adhesive bonded steel sheets

6.1 Methodology

The mechanical properties of base materials and epoxy adhesive are already discussed in Chapter 2 in Section 2.1.1 and Section 2.4.1, respectively. The epoxy adhesive properties were varied by filling the carbon black (CB) nano powder with different wt.%. Since adhesive layer which joins metallic sheets is a non-conductive polymer material, carbon black nano powder is filled in adhesive layer with the aim of changing the adhesive layer as an electrically conductive polymer material, and the influence of different wt.% of CB nano powder on formability of adhesive bonded blanks is investigated.

The commercially available CB nano powder grade-N774 (supplied by Swastika Constant Care, Kolkata, India) was used to fill in the epoxy adhesive. The CB nano powder was characterized by transmission electron microscope (TEM).

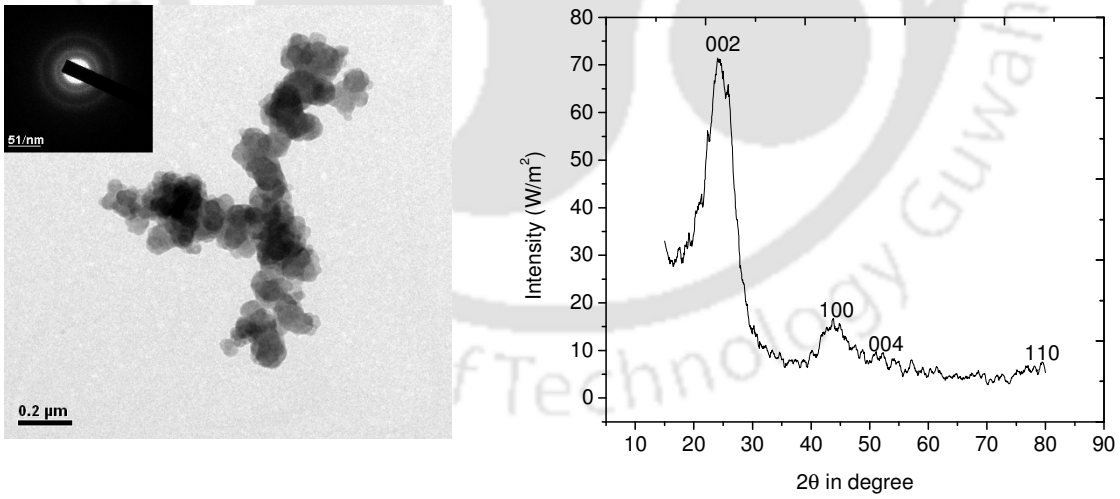

(a) (b)

Fig. 6.1 (a) TEM photograph of CB nano sized powder and (b) diffraction pattern of carbon black nano sized powder

The CB powder was ultrasonically agitated in the acetone solution for 1 hr before dispersion on the copper grid. This was performed to reduce the agglomeration in the powders. The average particle size from the TEM analysis is found to be about 50 nm with a standard deviation of 11.358, and the particles are found to be spherical in shape (Fig. 6.1(a)). The diffraction pattern of carbon black nano powder used in this work is shown in Fig. 6.1(b). The diffraction pattern of carbon black N774 was compared and confirmed with the available data (Ungar *et al.,* 2002).

6.2 Testing of carbon black filled epoxy adhesive

The adhesive samples with different CB wt.% were prepared by using appropriate moulds and tested as per ASTM D638-10 standard. The CB nano powder was filled in resin (Part A) and stirred manually for 15 min. Further, the resin and CB mixture was filled in the extruder, which was adapted for the present work. Then the mixture was extruded through perforated die with holes having diameter of 1 mm each. The batch mixing was repeated for 5 times. After obtaining homogenous mixture of resin and CB, the hardener (Part B) was added to the mixture and stirred manually for 20 min, and then the adhesive mixture was cast between two base materials with the help of a mould. This mixing method is suggested to be effective with good repeatability of results. In the case of CB wt.% variation, the hardener/resin ratio was maintained as 1:1, which exhibits larger elongation when the adhesive is deformed (Chapter 2 in Section 2.3). The density of epoxy adhesive with different CB wt.% were measured as per method discussed in Chapter 4 in Section 4.2. Table 6.1 shows the measured density of epoxy adhesive with different CB wt.% and the average density in each case was taken into account during the FE simulation.

Table 6.1 Density of epoxy adhesive with different CB wt.%

CB wt.%	1%	2%	3%	4%	5%	6%
Density (kg/m^3)	11.9	12.5	12.5	11.8	12.2	11.3

6.3 Forming of carbon black filled adhesive bonded blanks: Experiment

The adhesive bonded tensile specimens were prepared by using epoxy adhesive system with different CB wt.% like 1 wt.%, 2 wt.%, 3 wt.%, 4 wt.%, 5 wt.%, and 6 wt.%. The CB nano powder was mixed with epoxy adhesive as discussed in Section 6.2. In this work, the influence of different CB wt.% on the forming behaviour of adhesive bonded blanks were also analysed through in-plane plane-strain formability test. The tensile and IPPS specimens made of CB filled and adhesive bonded blanks were prepared as per methodology discussed in Chapter 2 in Section 2.3. The average thickness of adhesives in adhesive bonded blanks was found to be

1±0.013 mm. The testing of CB filled adhesive bonded blanks, and evaluation of results during tensile and IPPS formability tests are followed as discussed in Chapter 2 in Section 2.3.

6.4 Forming behaviour of carbon black filled adhesive bonded blanks: Prediction

The adhesive bonded blanks were modelled as per methodology discussed in Chapter 4 in Section 4.3. The stress-strain behaviour of adhesive bonded sheets was predicted as per methodology discussed in Chapter 4 in Section 4.3.1. The limit strains of base materials constituting CB filled adhesive bonded blanks with different wt.% were predicted using two necking criteria namely ESRC and TGNC as discussed in Chapter 4 in Section 4.3.2.

6.5 Results and discussion

6.5.1 Tensile behaviour of epoxy adhesive filled with different wt.% of carbon black

Fig. 6.2 shows the engineering stress-strain behaviour of adhesive samples with different CB wt.%. The epoxy adhesive system showing larger elongation with hardener/resin ratio of 1:1 was chosen for investigating the influence of CB with different wt.%. While comparing the stress-strain behaviour at different wt.% of CB filled in adhesive samples, the elongation increases with increase in CB wt.% up to 2 wt.%, but decreases with excessive addition of CB.

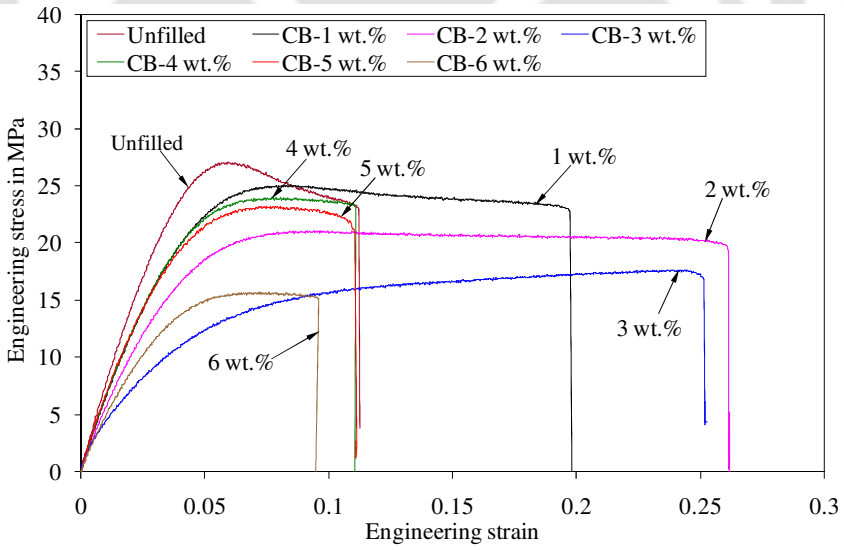

Fig. 6.2 Engineering stress-strain behaviour of adhesive samples with different CB wt.%

About 15% increase in elongation is observed in the adhesive sample with 2 wt.% of CB as compared to unfilled adhesive sample. Appropriate volume fraction of CB can remedy the defects from epoxy self-curing, it can also transfer stress, and thereby prevent the expanding of a

fine network of cracks inside the epoxy resin, thus to play a role of reinforcement and toughness. With the excessive addition of CB, the viscosity of epoxy resin increases, the dispersion of CB gets worse, the nano-sized CB is also easy to reunite, and gas bubble and excessive stress concentration points are easy to form, resulting in the mechanical properties to get declined eventually (Ma *et al.,* 2010). From the present study, it is understood that the appropriate rich mixture of CB with 2 wt.% improves deformability by accomplishing fine network between adhesive and CB particles, and thereby improves the plasticity of adhesive. But excessive addition of CB in the adhesive makes absence of adhesive and replaces with CB generating weak spots like voids in its polymeric structure from where cracks may be originated which leads decrease in the ductility of adhesive. Elsewhere, there is an evident that the tensile strength, elongation at break, flexural strength and impact strength of epoxy/CB composites increased up to 32.3%, 39.6%, 88.7% and 10.3%, respectively, with increase in mass fraction of CB up to 2% as compared to unfilled adhesive, and then decrease with excessive addition of CB (Ma *et al.,* 2010).

6.5.2 Failure of adhesive bonded sheets at different CB wt.%: Experiment and prediction

The failure pattern of tensile and IPPS CB filled adhesive bonded blanks during FE simulation is observed as discussed in Chapter 4 in Section 4.3. During experiment and FE simulation of CB filled adhesive bonded blanks, the adhesive layer fails at first, and then DDQ steel fails at second. Finally, SS 316L sheet fails at last which ductility is higher comparatively in tensile and IPPS formability tests. The progression data at failure of adhesive and base materials constituting adhesive bonded blanks at different CB wt.% during tensile test and IPPS forming test are tabulated in Tables 6.2 and 6.3, respectively.

Table 6.2 Prediction of progression at failure of adhesive bonded blanks with different CB wt.% in tensile test

CB wt.%	Adhesive layer failure (mm)		DDQ steel sheet failure (mm)			SS316L sheet failure (mm)		
	Experiment	Simulation	Experiment	Simulation		Experiment	Simulation	
				ESRC	TGNC		ESRC	TGNC
Unfilled	13.66	11.5	29.36	24.42	26.4	58.85	52.68	56.28
1%	16.14	13.0	30.59	24.54	26.52	60.94	53.10	56.16
2%	18.72	17.0	33.27	24.54	26.52	63.17	53.10	56.16
3%	17.70	16.0	32.61	24.54	26.52	62.09	53.10	56.16
4%	14.99	13.0	30.59	24.54	26.52	58.85	53.28	56.16
5%	14.84	12.0	29.36	24.54	26.52	58.85	53.10	56.16
6%	14.04	11.5	29.36	24.54	26.52	58.85	53.10	56.16

Table 6.3 Prediction of progression at failure of adhesive bonded blanks with different CB wt.% in IPPS formability test

CB wt.%	Adhesive layer failure (mm)		DDQ steel sheet failure (mm)			SS316L sheet failure (mm)		
	Experiment	Simulation	Experiment	Simulation		Experiment	Simulation	
				ESRC	TGNC		ESRC	TGNC
Unfilled	1.79	6.12	5.27	6.46	6.56	7.86	16.76	16.58
2%	3.56	7.46	5.62	6.46	6.56	8.53	16.76	16.58
6%	1.61	5.4	4.76	6.46	6.56	7.52	16.76	16.58

It is observed from the experimental results that the progression at failure of adhesive layer and base materials in adhesive bonded blanks increases with increase in CB up to 2 wt.%, and then decreases with excessive addition of CB. In the case of simulations, almost same trend is observed in the case of adhesive layer failure, but not in the case of base materials. The trend in the progression at adhesive failure constituting adhesive bonded blanks increasing up to 2 wt.% and then decreasing during experiment is well captured by simulations, but not during base materials failure. The base materials failure predictions are almost constant without showing the effect of CB wt.% variation (Tables 6.2 and 6.3). The TGNC predictions are accurate than ESRC predictions in the case of tensile test, while both predict equally in the case of IPPS forming test. There is about 10.5% to 16.4% variation in base materials between experiment and ESRC, and about 4.4% to 10.1% variation in base materials between experiment and TGNC prediction in tensile test. There is a considerable variation in the case of IPPS forming test.

The change in progression at failure (or elongation) of adhesive and base materials is because of change in adhesive properties by the addition of CB that is changing from brittle to plasticizing behaviour in the experiments. In the case of prediction through FE simulations, the effect of adhesive properties like gluing distance or conditions and failure description of adhesive like adhesive and cohesive failure were not considered and hence the progression at failure of base materials remains same in all the cases, though there is a considerable improvement in the plasticity of adhesive layer. The discrepancy between experiment and simulation results is believed to occur because of absence of adhesive bonding (or adhesion) during FE simulations. So, the change in mechanical behaviour of adhesive bonded sheets is not only because of change of mechanical properties of adhesive, but also due to adhesion properties.

A poor agreement between experiment and predicted progression at failure in the case of IPPS forming test is observed, which is unexpected. This is believed to happen because of the presence of notch, changing the behaviour of whole adhesive bonded sheets during prediction. Moreover, this sample deforms near plane-strain conditions, which is the critical strain path during sheet deformation.

6.5.3 Experimental evaluation and prediction of tensile behaviour of adhesive bonded sheets

The comparison of true stress-strain behaviour of adhesive bonded blanks with different wt.% of CB obtained from experiments and simulations during tensile test is shown in Fig. 6.3(a, b). It is observed from experiments that the true strain increases with increase in wt.% of CB up to 2 wt.%, and then decreases for further increase in wt.% of CB in all the regions A, B, and C as compared to unfilled adhesive bonded blank (Fig. 6.3(a)). From the result, it is understood that carbon black rich formulation up to 2 wt.% improves the ductility of adhesive layer, and thereby improving the ductility of base materials. The 2 wt.% of CB held more micro cracks than that of the other wt.% of CB, and the formed micro cracks could consume more energy of rupture which delays the failure of adhesive layer (Ma *et al.,* 2010). Though 2 wt.% of CB shows maximum ductility than other wt.% levels of CB, the other levels such as 1 and 3 wt.% also show improved ductility of adhesive layer as compared to unfilled adhesive layer. The improvement in the plasticity of adhesive layer filled by CB improves the ductility of constituting base materials in adhesive bonded blanks. While comparing experimental and predicted results (Fig. 6.3(b)), the global behaviour of adhesive bonded blanks till adhesive failure follows the same trend that is increase in wt. % of CB increases the true strain at failure. But it does not occur in regions B and C in the predicted result due to the absence of interfacial interaction between adhesive layer and base materials. A significant difference in true strain at failure of base materials between experiment and predicted result is observed from Figs. 6.3(c-h) though the overall stress-strain prediction is satisfactory. The considerable difference in true strain of base materials is observed in the case of CB filled adhesive bonded blank with 2 wt.%. There is about 1.5% to 3.1%, 1.2% to 4.6%, and 2.04% to 5.45% variation in true strain in regions A, B and C, respectively. A considerable disagreement with true stress-strain between experimental and predicted results in all three regions is observed in the case of CB filled adhesive bonded blanks. These results confirm that just by improving the plasticity of adhesive layer will not influence the formability of base materials constituting adhesive bonded blanks, but also the interfacial bonding between the base materials and adhesive layer, which will contribute to the improvement. Though the improvement in ductility for changing CB wt.% is not predicted accurately, the overall predictions are moderate.

The same has been plotted in Fig. 6.4(a, b) showing the comparison of percentage of elongation of adhesive bonded blanks in region A, B, and C with different wt. % of CB between experiment and predicted results in tensile and IPPS formability tests. The elongation increases with increase in wt. % of CB till up to 2 wt. %, and then it decreases for excessive addition of

CB in all regions A, B and C in the case of experimental result. While in simulation results, a similar trend is observed only in region A, but not in the regions B and C.

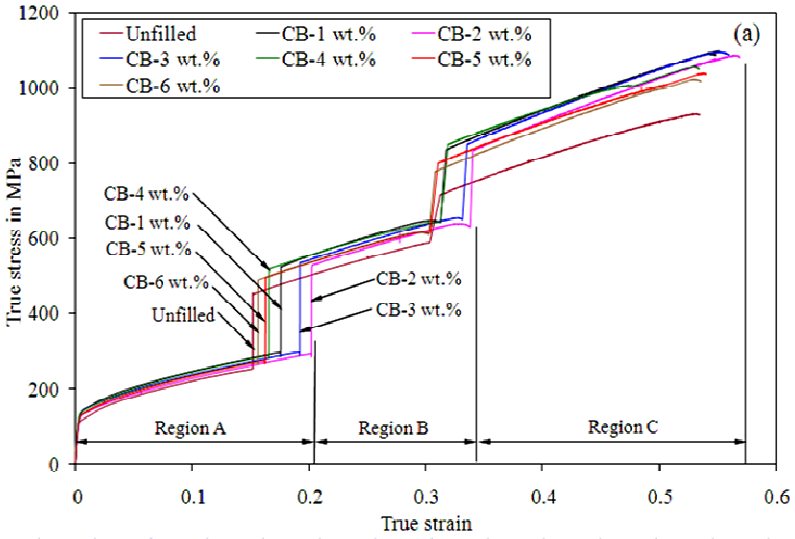

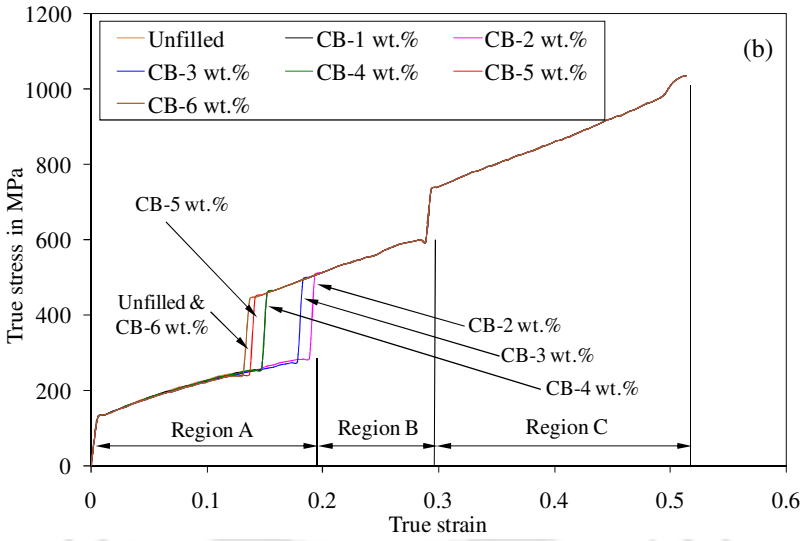

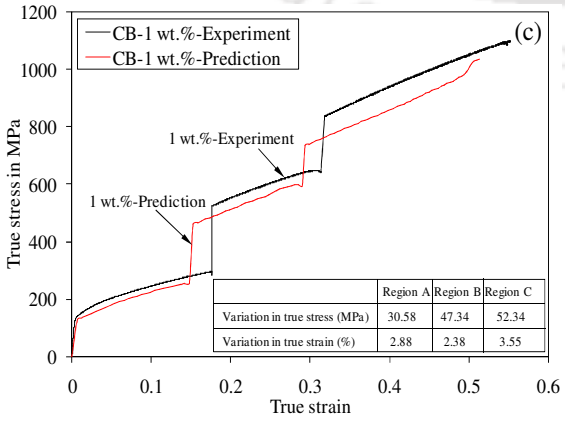

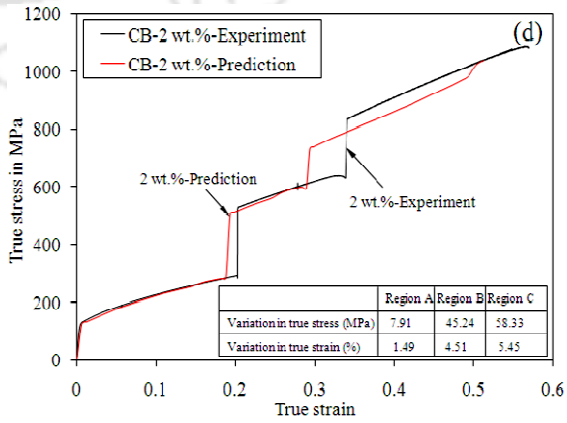

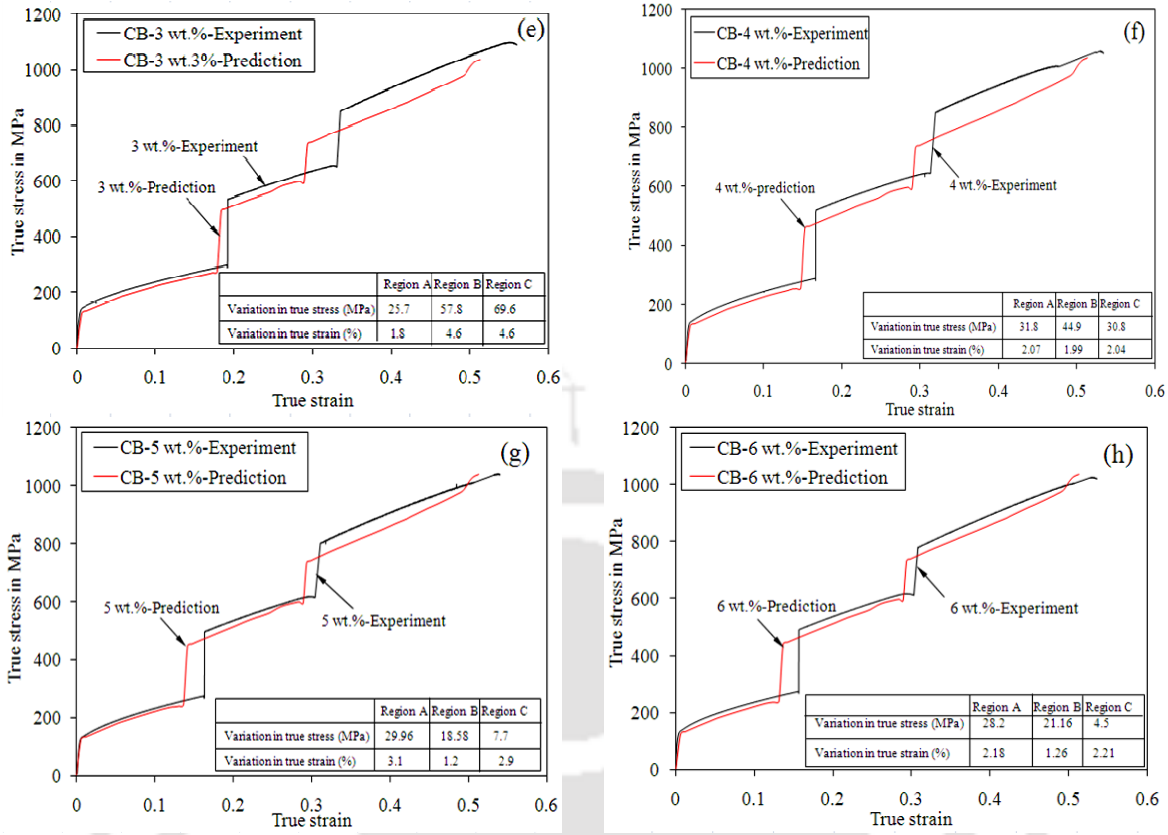

Fig. 6.3 Comparison of true stress-strain behaviour of adhesive bonded blanks with different CB wt.% from tensile test: (a) Experimental result (Variation in tensile strength = ±10 MPa, and in elongation at failure = ±1.5%), (b) Predicted result, (c) CB – 1 wt.%, (d) CB – 2 wt.%, (e) CB – 3 wt.%, (f) CB – 4 wt.%, (g) CB – 5 wt.%, and (h) CB – 6 wt.%

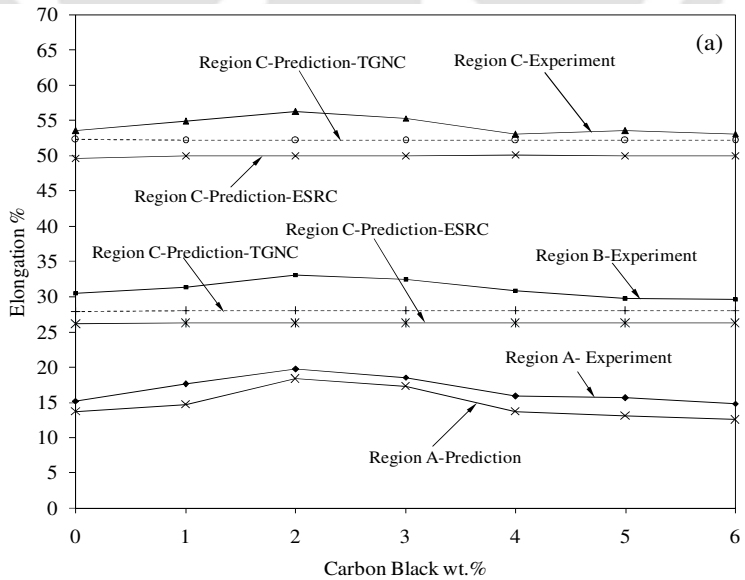

Variation in elonagtion between experiment and prediction:
In region A - 1.2% to 2.9%
In region B - 3.4% to 6.9% (ESRC) and 1.58% to 5.08% (TGNC)
In region C - 2.9% to 4.97% (ESRC) and 0.83% to 4.03% (TGNC)

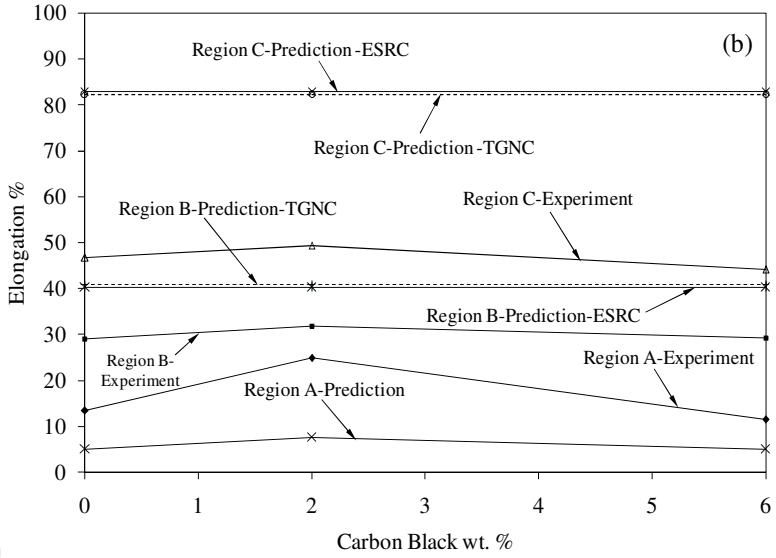

Variation in elongation between experiment and prediction:
In region A - 6.4%-17.23%
In region B - 8.46% to 11.23% (ESRC) and 8.97% to 11.74% (TGNC)
In region C - 33.59% to 38.75% (ESRC) and 32.98% to 38.14% (TGNC)

Fig. 6.4 Elongation results (true strain) with different wt.% of carbon black in adhesive bonded sheets between experiment and predicted results: (a) tensile test, and (b) IPPS formability test

6.5.4 Forming limit strain of adhesive bonded blanks with effect of wt.% of CB –Prediction

The experimental limit strains in DDQ steel and SS 316L constituting adhesive bonded blanks with different CB wt.% from tensile test are shown in Fig. 6.5(a, b). Similarly, Fig. 6.6(a, b) shows the limit strains from IPPS formability test. It is observed that the limit strain increases with increase in CB wt.% up to 2 wt.%, and then decreases with excessive addition of CB in both the base materials.

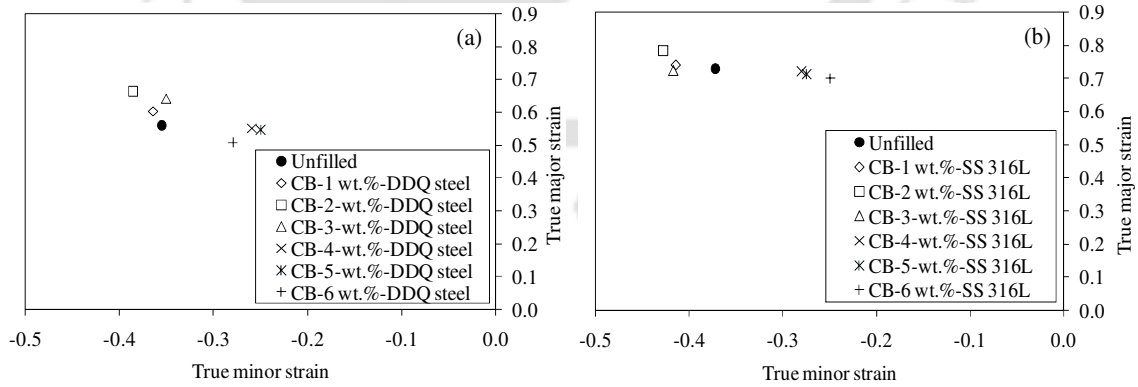

Fig. 6.5 Comparison of experimental limit strain results of adhesive bonded sheets with different CB wt.% from tensile test: (a) DDQ steel, and (b) SS 316L

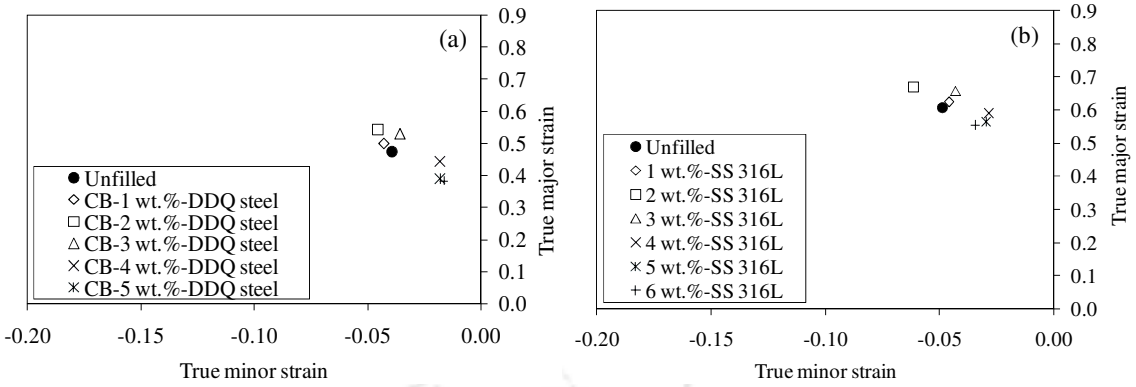

Fig. 6.6 Comparison of experimental limit strain results of adhesive bonded sheets with different CB wt.% from IPPS formability test: (a) DDQ steel, and (b) SS 316L

In the tensile test of adhesive bonded blanks, the standard deviation of true major limit strain ranges from 0.008 to 0.086 and the standard deviation of true minor strain ranges from 0.003 to 0.006 for DDQ steel sheets. Similarly, the standard deviation of true major limit strain ranges from 0.005 to 0.012 and the standard deviation of true minor strain ranges from 0.003 to 0.015 for SS 316L sheets. Similarly, in the IPPS formability test, the standard deviation of true major limit strain ranges from 0.063 to 0.091 and the standard deviation of true minor strain ranges from 0.002 to 0.003 for DDQ steel sheets. The standard deviation of true major limit strain ranges from 0.003 to 0.340 and the standard deviation of true minor strain ranges from 0.002 to 0.004 for SS 316L sheets. These error variations are much smaller than the limit strain improvement among different adhesive-bonded samples with different CB wt. %. Hence, these results confirm an inherent improvement in the limit strain, rather than falling within the standard deviation range found in the case of unfilled adhesive bonded blanks.

Fig. 6.7(a-f) presents the limit strains in the adhesive boned blanks through experiment and predicted by the necking criteria, TGNC and ESRC, during tensile test. Similarly, Fig. 6.8(a-d) shows the limit strain results during IPPS forming test. In tensile test, about 9.1% to 21.7% variation in true major strain and about 10.3% to 13.4% in true minor strain during TGNC predictions are noted. In the case of ESRC prediction, there is about 18.2% to 35.2% difference in true major strain and about 4.9% to 20.9% difference in the true minor strain. Similarly, in IPPS forming test, about 8.3% to 12.4% in true major strain and about 2.2% to 13.4% difference in minor strain are noticed during prediction by TGNC, and about 7.3% to 13.4% variation in true major strain and 2.1% to 13.7% variation in true minor strain are observed in the prediction of limit strains by ESRC.

Particularly, the large difference in progression at failure of SS 316L during IPPS forming test between experimental and prediction results (Table 6.3) is not reflected on the true major limit strains. But a reasonable change in strain path is noted. Though both the necking criteria, TGNC and ESRC are meant for base material (unbonded) formability prediction, the TGNC shows less difference between experimental limit strain results in the case of adhesive bonded blanks. It is believed that the absence of interfacial bonding between adhesive and base materials causes the base materials constituting adhesive bonded blanks to behave as if like a single sheet.

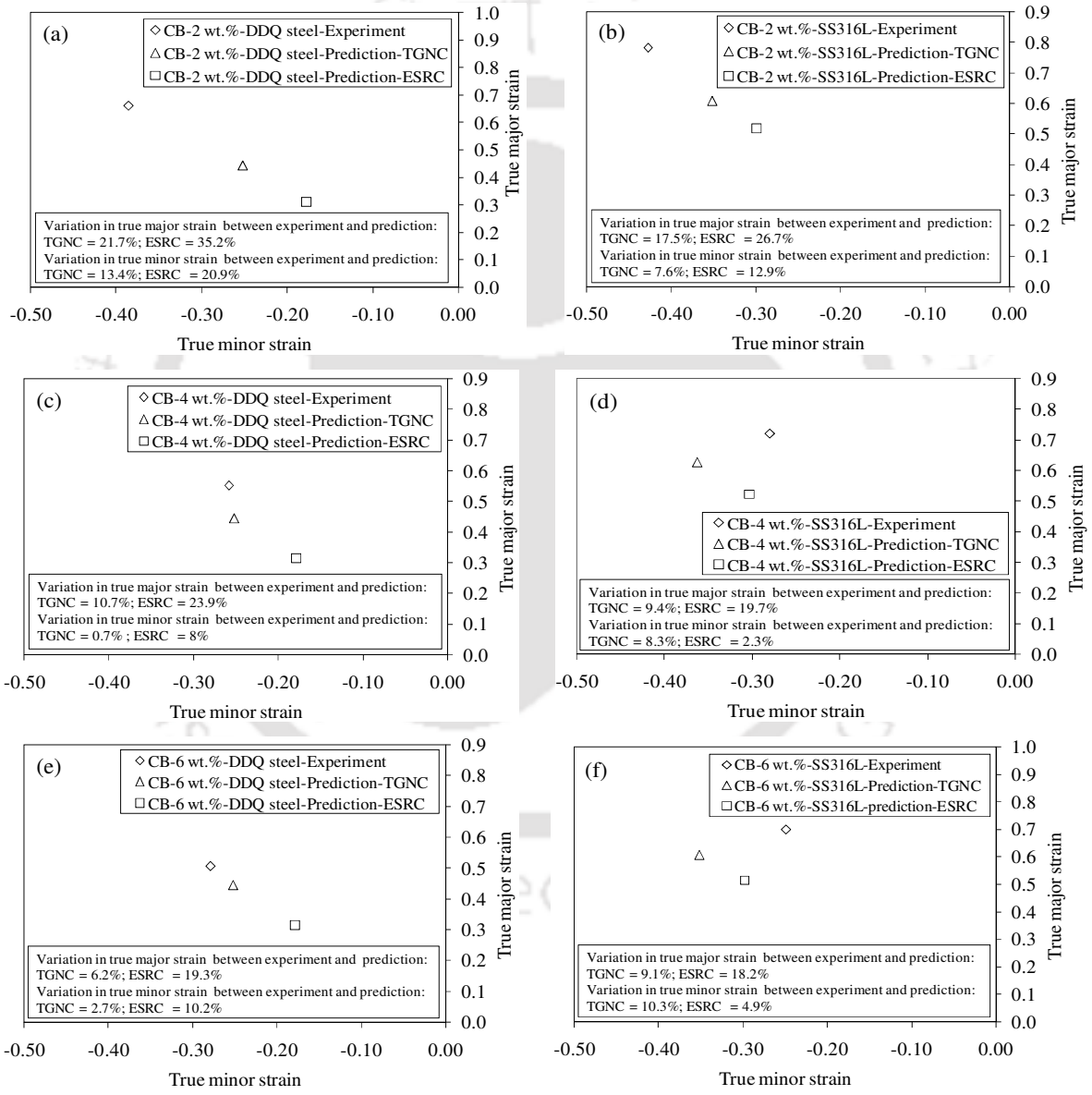

Fig. 6.7 Comparison of limit strain results of adhesive bonded sheets with different CB wt.% between experiments and predictions in tensile test: (a) CB wt.% = 2–DDQ steel, (b) CB wt.% = 2–SS 316L, (c) CB wt.% = 4–DDQ steel, (d) CB wt.% = 4–SS 316L, (e) CB wt.% = 6–DDQ steel, and (f) CB wt.% = 6–SS 316L

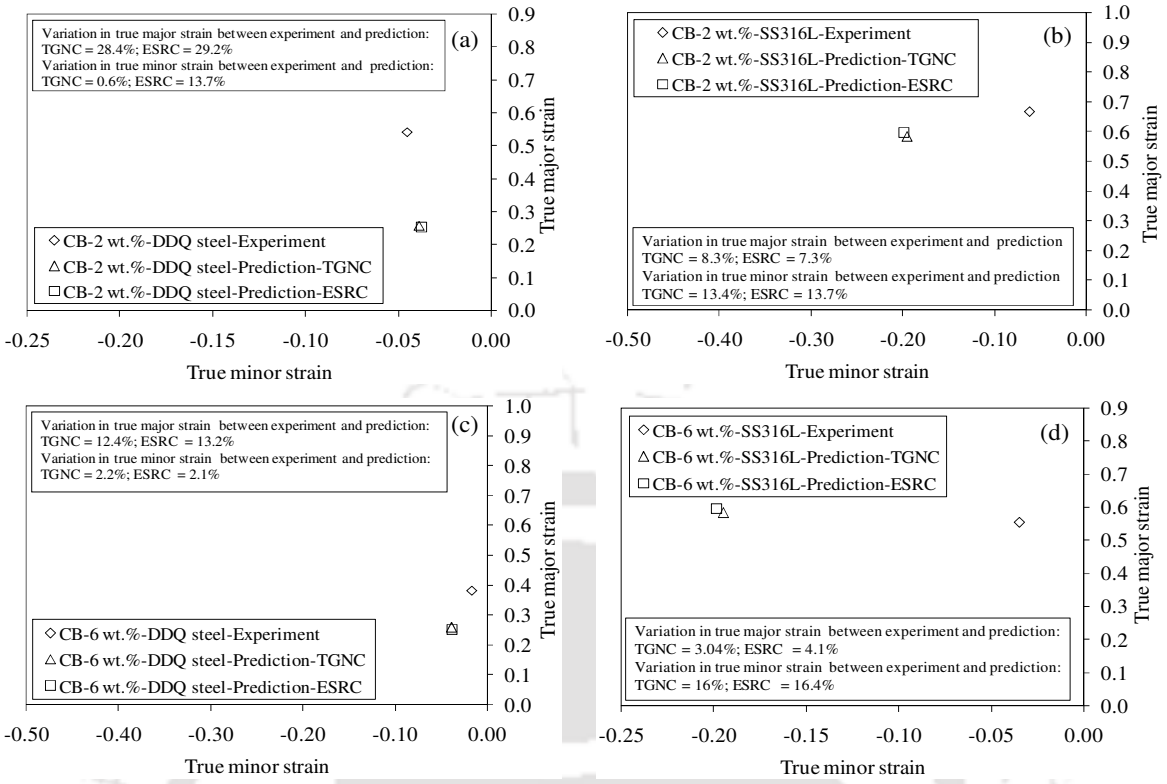

Fig. 6.8 Comparison of limit strain results of adhesive bonded sheets with different CB wt.% between experiments and predictions in IPPS formability test: (a) CB wt.% = 2–DDQ steel, (b) CB wt.% = 2–SS 316L, (c) CB wt.% = 4–DDQ steel, (d) CB wt.% = 4–SS 316L, (e) CB wt.% = 6–DDQ steel, and (f) CB wt.% = 6–SS 316L

In addition, the influence of different thickness values like 1 mm, 1.5 mm, 2 mm, and 2.5 mm of adhesive layer on the limit strains of base materials constituting adhesive bonded blanks was predicted at 2 wt.% of CB in the adhesive as shown in Fig 6.9.

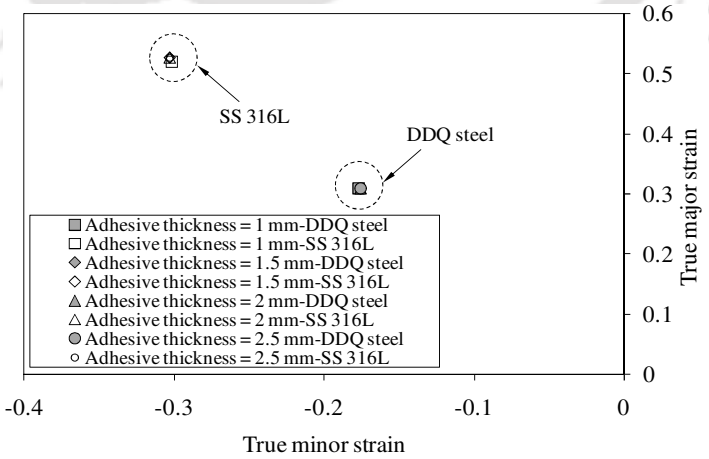

Fig. 6.9 Comparison of limit strain results of DDQ steel and SS 316L sheets constituting adhesive bonded sheets with different thickness values of adhesive layer at 2 wt.% of CB in the adhesive

The limit strains were predicted using ESRC necking criterion. There is no difference in the limit strain results of both the base materials. It is understood that there is no influence on limit strain results of base materials constituting adhesive bonded blanks with different thickness values of adhesive in the absence of interface bonding between base materials and adhesive layer.

6.6 Conclusions

The following conclusions are drawn from this work.

- The ductility of adhesive bonded blanks increases with increase in wt.% of CB in adhesive layer of adhesive bonded blanks up to 2 wt.% and then decreases with increase in wt.% of carbon black.
- This means that the ductility of adhesive and overall formability of adhesive bonded blanks can be improved by filling the CB nano powder in the adhesive up to an appropriate level (2 wt.% in this work) for constant hardener/resin ratio, without compromising the bondability of adhesive. This is not limited to improvement in formability, but also with aim of utilizing adhesive layer as a conductive polymer layer in adhesive bonded blanks.
- There is a good agreement between experimental and predicted overall true stress-strain behaviour of adhesive bonded sheets. Though this is the case, the influence of changing adhesive properties by filling CB nano powder on the tensile behaviour is not predicted accurately. This is believed to happen because of absence of interfacial interaction between base materials and adhesive layer during modelling of adhesive bonded blanks.
- During forming limit strain prediction of adhesive bonded blanks under the influence of wt.% of CB in the adhesive system, both ESRC and TGNC are applicable only to a reasonable extent. On the whole, the predicted limit strain results based on TGNC shows better accuracy as compared to ESRC. The inaccuracies in formability predictions believed due to the absence of interface interaction between adhesive and base materials during simulation.
- It is also observed that there would not be any influence of thickness of adhesive on the limit strain results of base materials constituting adhesive bonded blanks in the absence of interface bonding between base materials and adhesive layer.

Chapter 7

Improving the formability of adhesive bonded sheets through wire reinforcement

7.1 Methodology

In this section, the materials used in the fabrication of wire reinforced adhesive bonded sheets, evaluation of forming behaviour of adhesive bonded sheets through experiments and predictions are discussed.

7.1.1 Materials and mechanical properties

The mechanical properties of base materials and epoxy adhesive are already discussed in Chapter 2 in Sections 2.1.1 and 2.4.1, respectively. The commercially available Copper (Cu) and Aluminium (Al) wires with Ø0.3 mm were used in the reinforcement of adhesive. The Cu and Al wires were tested as per ASTM A931–08 (2013) standard. Fig. 7.1 shows the stress-strain behaviour of Cu and Al wires. It is noted that the ductility of Cu wire is larger than Al wire.

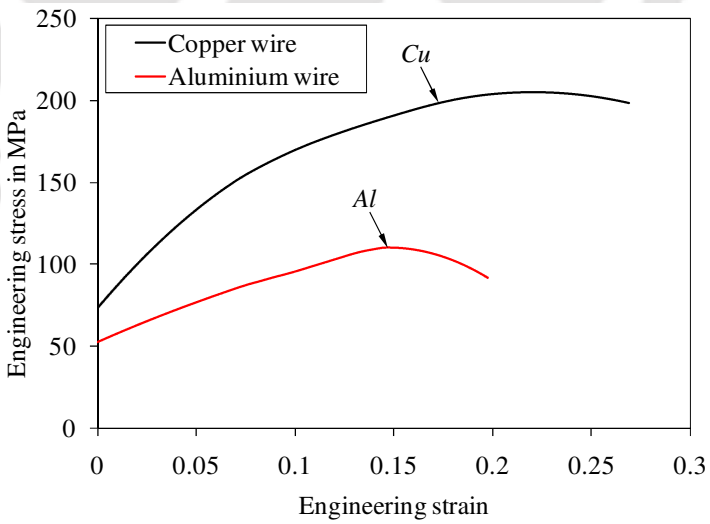

Fig. 7.1 Engineering stress-strain behaviour of Cu and Al wires (data variation in ultimate tensile strength = ±2 MPa, and in elongation at failure = ±2%)

7.2 Experimental evaluation of formability of wire reinforced adhesive bonded sheets

Fig. 7.2(a-c) shows the schematic of wire reinforced adhesive bonded sheets with different number of reinforcements and orientations. The adhesive mixture with hardener/resin ratio of 1:1 was cast on one of the base materials kept in the mould. In case of tensile specimen, the Cu and Al wires with different number of wires like 1, 2, 3, 4 and 5 with 2 mm gap each other were longitudinally reinforced in the adhesive layer (Fig. 7.2(a, b)). In the case of transverse orientation, Cu wires were reinforced with different numbers of wires like 1, 3 and 5 with the gap of 2 mm each other in the adhesive (Fig. 7.2(c)). The second base material was then bonded on the adhesive layer. The curing process and examining the specimens were done as per methodology discussed in Chapter 2 in Section 2.3. The average thickness of adhesive bonded sheets was found to be 2.2±0.05 mm.

Similarly, the IPPS specimens (Fig. 7.2(b)) were fabricated with different numbers of wire reinforcements in adhesive. The number of Cu and Al wires was varied like 2, 4, 6, 8, and 10 during fabrication of IPPS wire reinforced adhesive bonded sheets. The average thickness of adhesive bonded sheets was found to be 2.2±0.03 mm. The testing of wire reinforced adhesive bonded sheets, and evaluation of results during tensile and IPPS formability tests are followed as discussed in Chapter 2 in Section 2.3.

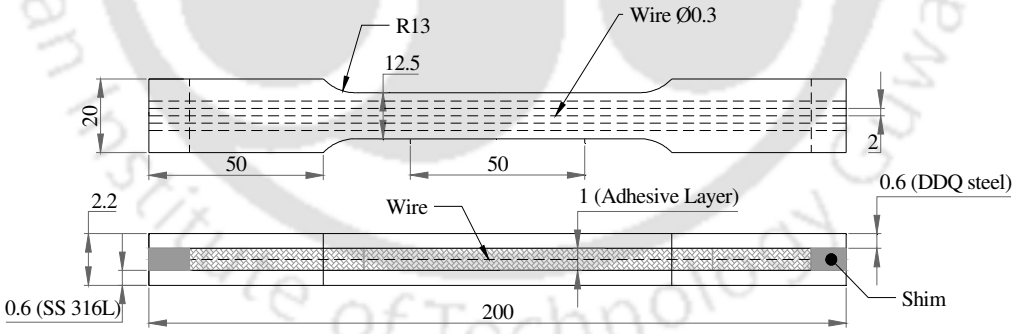

(a)

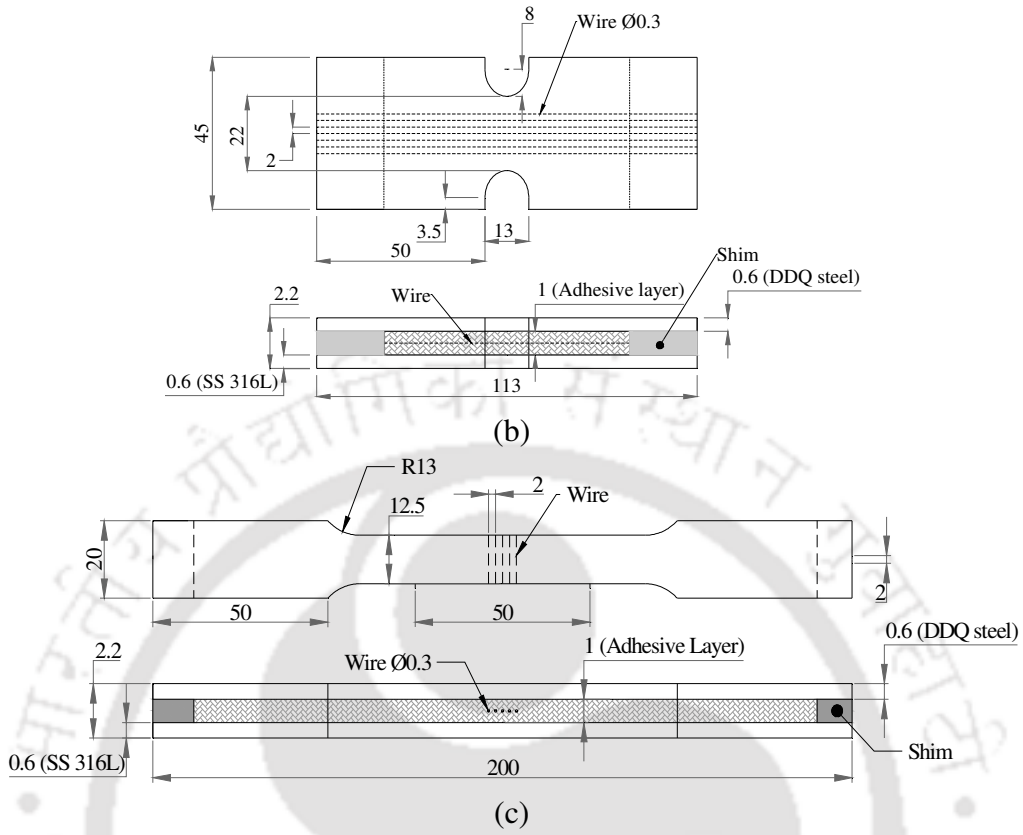

Fig. 7.2 Wire reinforced adhesive bonded sheets with different orientations: (a) Longitudinal reinforcement – Tensile specimen, (b) Longitudinal reinforcement – IPPS specimen, and (c) Transverse reinforcement – Tensile specimen (All dimensions in 'mm')

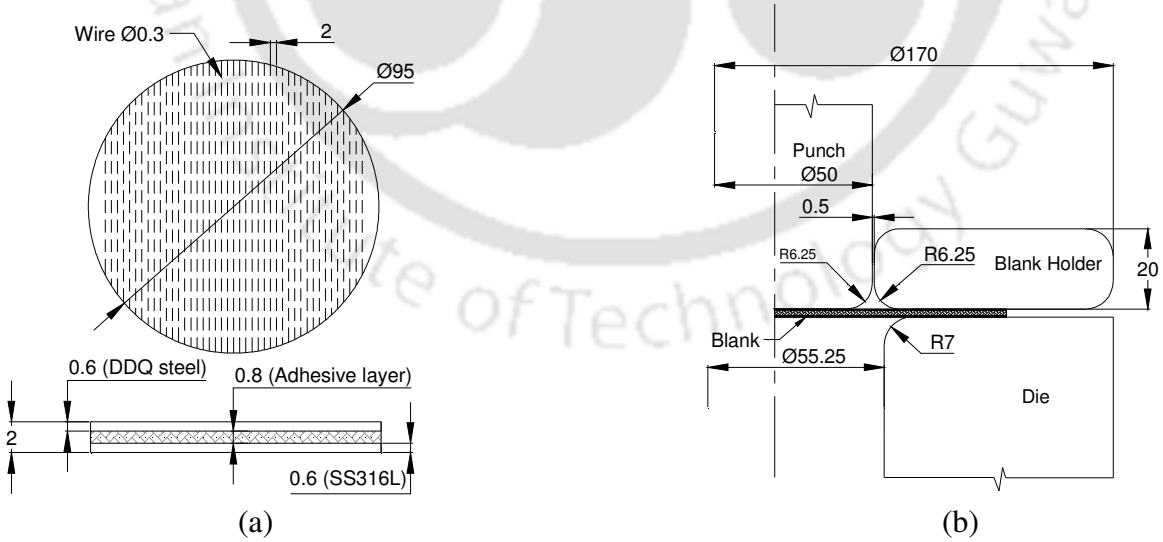

Fig. 7.3 (a) Wire reinforced adhesive bonded circular sheets, and (b) Schematic of deep drawing tools used in experiment (All dimensions are in 'mm')

Further, the wire reinforced adhesive bonded circular sheets with Ø95 mm were fabricated for deep drawing test. Uniform thickness of bonded sheets was maintained using appropriate moulds. The adhesive layer was reinforced with Cu wires at different numbers of wires like 4, 8, 16, 24, 32 and 40 (Fig 7.3(a)) at 2 mm gap each other. The adhesive mixing and curing process was followed as discussed in Chapter 2 in Section 2.3. The average thickness of circular bonded sheets was found to be 2±0.15 mm.

Fig. 7.3(b) shows the schematic of the cylindrical deep drawing tools used in the present work. In order to determine the optimum diameter of blank for constant punch diameter of 50 mm, the drawing clearance C_d parameter was defined by an empirical formula, depending on thickness of the material, as shown in eq. (7.1) (Potocnik *et Al.,* 2011).

$$C_d = t + k\sqrt{10t} \tag{7.1}$$

where C_d – drawing clearance in mm, t – thickness of blank = 2 mm , k – constant (0.07 for steel sheet)

The drawing clearance was found to be about 2.5 mm. With reference to the drawing clearance and punch diameter, the die diameter was found to be 55 mm. With respect to these tools dimensions, the diameter of blank was optimized through finite element simulation using a commercially available elasto-plastic explicit dynamic FE code. The simulation was carried out with different diameter of sheets. The die entry radius was taken as 7 mm from the empirical relation between blank thickness and die entry radius which is basically available data. Different punch nose radii of 3, 4, 5, and 6 were considered during simulation. The effective punch nose radius of 6 mm for which no severe thinning and wrinkling was observed. The same radius was considered as blank holder entry radius. After fabrication of all tools, the dimensions were measured using coordinate measuring machine (CMM) and the measured dimensions are shown in Fig 7.3(b). With these tools dimensions, the sheets with different diameter like 70, 75, 80, 85, 90 and 95 were simulated. The optimum diameter of blank was found to be 95 mm for which no failure and wrinkling was observed. The optimized blank with Ø95 mm was used in the fabrication of adhesive bonded sheets. The blank holding force was applied manually by tightening the fasteners used in the tools.

All the deep drawing testing of adhesive bonded sheets were carried out in the universal testing machine (UTM) with a maximum load capacity of 200 kN, and punch speed was maintained at

1 mm/min. The interfaces between punch, blank, die, and blank holder were well lubricated to reduce the friction during the tests. During deep drawing of adhesive bonded sheets, the maximum successful cup was drawn without any crack in the base materials observed. The load-stroke behaviour of adhesive bonded sheets was recorded as a machine data. Three sheets were tested in each case for ensuring the repeatability. The fourth blank was tested when good repeatability was not observed.

7.3 Prediction of forming behaviour of wire reinforced adhesive bonded sheets

The finite element based numerical prediction study is carried out to understand the forming behaviour of adhesive bonded sheets, when the low ductile adhesive is reinforced with high ductile metal wires. The main aim of this prediction is only to understand the final forming behaviour of the whole wire reinforced adhesive bonded sheets, and not to compare and validate the results from experiments in this work. This method of prediction is expected to check the formability of reinforced adhesive bonded sheets quickly.

Fig. 7.4 shows the FE model of the adhesive bonded sheets during tensile test. The adhesive bonded sheets were modelled as per methodology discussed in Chapter 4 in Section 4.3. The stress-strain behaviour of adhesive bonded sheets was predicted as per methodology discussed in Chapter 4 in Section 4.3.1. The middle layer was modeled in four ways – (i) the middle layer is only epoxy adhesive (Fig. 7.5(a)), (ii) the width of the middle layer is more dominated by the adhesive properties and less dominated by the Cu wire properties (Fig. 7.5(b)), (iii) the width of the middle layer is more dominated by the Cu wire and less dominated by the adhesive properties (Fig. 7.5(c)), and (iv) the middle layer holds only Cu material properties (Fig. 7.5(d)). During simulations, wires were not modelled individually; instead many wires were equivalently modeled as continuous sheet with a finite width having mechanical properties of Cu wire. The width of the strip decides the contribution of wire and adhesive in the middle layer. The true stress – strain behaviour of all these cases were compared while the base materials were DDQ steel and SS 316L in all the cases remaining same. The bonding between middle layer and base materials was not modelled in all the cases. The main motive of FE simulation prediction is to understand and demonstrate the contribution of wire reinforcement equivalence on the overall formability of adhesive bonded sheets, wire being more ductile as compared to adhesive.

The properties of base materials as given in Tables 2.2 and 2.3 (Chapter 2) were incorporated during FE simulation. The adhesive properties with hardener/resin ratio of 1:1 as discussed in Chapter 2 in Section 2.4.1, and the Cu wire properties as engineering stress-strain data were converted into true stress-strain data and incorporated in the table form during numerical simulation of wire reinforced adhesive bonded sheets. The thickness of middle layer (adhesive + Cu wire) was 1 mm. The density of 7.76×10^{-7} kg/mm^3 for epoxy adhesive at hardener/resin ratio of 1:1, and the Cu wire density of 8.933×10^{-6} g/mm^3 were also incorporated. There was no bonding between adhesive layer and adherends defined, and all three layers (DDQ + middle layer + SS 316L) were simply in surface contact during FE simulation.

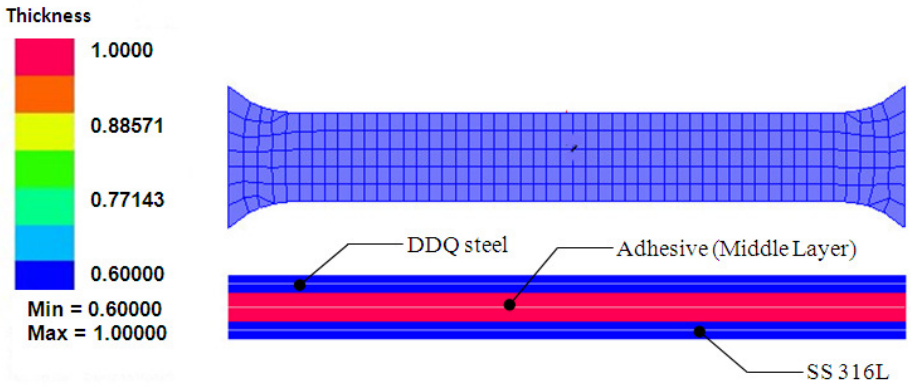

Fig. 7.4 Finite element (FE) model of adhesive bonded sheets during tensile test

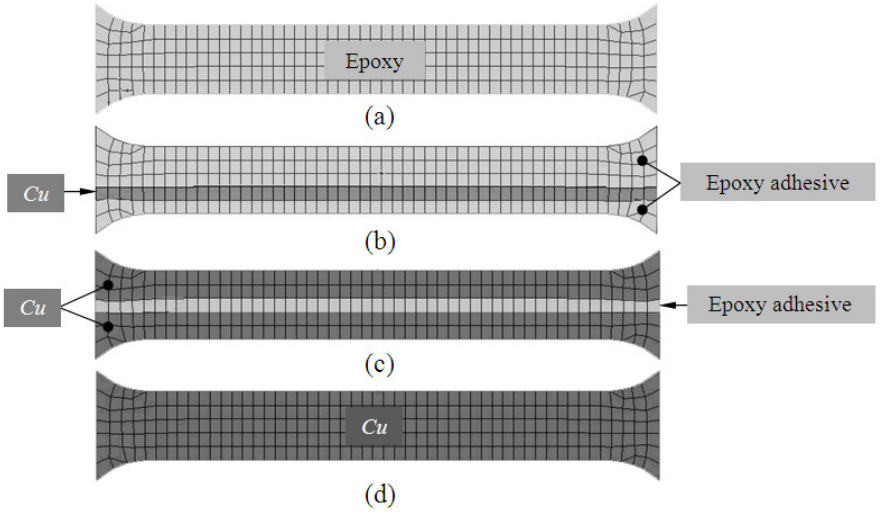

Fig. 7.5 FE model of middle layer with different cases: (a) only epoxy layer, (b) more epoxy and less Copper width, (c) less epoxy and more Copper width, and (d) Only Copper sheet

7.4 Results and discussion

7.4.1 Failure pattern of wire reinforced adhesive bonded sheets

Fig. 7.6(a-c) shows the failure pattern of wire reinforced adhesive bonded sheets during tensile test. It is proposed that the total load is shared by all three layers (DDQ steel + wire reinforced adhesive + SS 316L) during deformation of adhesive bonded sheets, and the wire reinforced adhesive layer fails at first (Fig. 7.6(a)). Then the load is shared by DDQ steel and SS 316L sheets, and DDQ steel sheet fails after the failure of adhesive layer (Fig. 7.6(b)). The SS 316L which holds more ductility than other two layers fails at last (Fig. 7.6(c)). The same failure pattern was observed during IPPS formability tests of all wire reinforced adhesive bonded sheets.

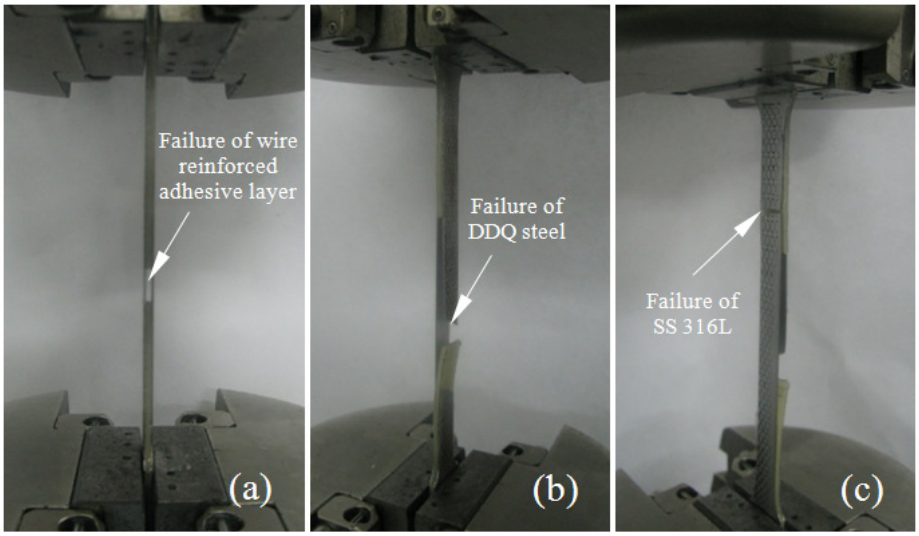

Fig. 7.6 Failure pattern of wire reinforced adhesive bonded sheets during tensile test: (a) failure of adhesive layer, (b) failure of DDQ steel, and (c) failure of SS 316L

Fig. 7.7(a-e) shows the failure pattern of wire reinforced adhesive layer constituting adhesive bonded sheets during tensile and IPPS formability tests. In tensile test, it is observed that the adhesive layer with lower number of ductile wires deforms and fails altogether at one location (Fig. 7.7(a, b)). In the case of samples with higher number of ductile wires, failures at multiple locations in adhesive layer are noticed (Fig. 7.7(c)). This reveals that the adhesive layer loses its inherent ductility with increase in number of wires. It was also observed that the extension of adhesive layer increased with increase in number of reinforcements up to a certain limit and decreased with excessive number of reinforcements. In the case of IPPS formability tests, no considerable difference is observed in the failure pattern of adhesive layer reinforced with number

of wires. This is due to critical gauge region (notch) of the sheets. In all the cases, the adhesive layer with wires deform and fail simultaneously which confirm that there is no delamination between wires and adhesive in the bonded sheets during deformation (Fig 7.7(a–e)). On the whole, it is understood that more dominance of adhesive and appropriate number of ductile wires reinforcement improves the ductility of adhesive layer constituting adhesive bonded sheets. On the other hand, beyond a limit, wires in the adhesive layer acts as defects that creates multiple failures and reduces its performance.

Fig. 7.8(a-c) shows the failure pattern of transverse Cu wire reinforced adhesive layer constituting adhesive bonded sheets. It is observed that the failure of adhesive layer occurs at the location of the wire reinforced irrespective of the number of reinforcement. It is understood that the transverse reinforcement of ductile wire in the adhesive layer acts as a defect, where strain is locally concentrated and causes adhesive failure at the wire location.

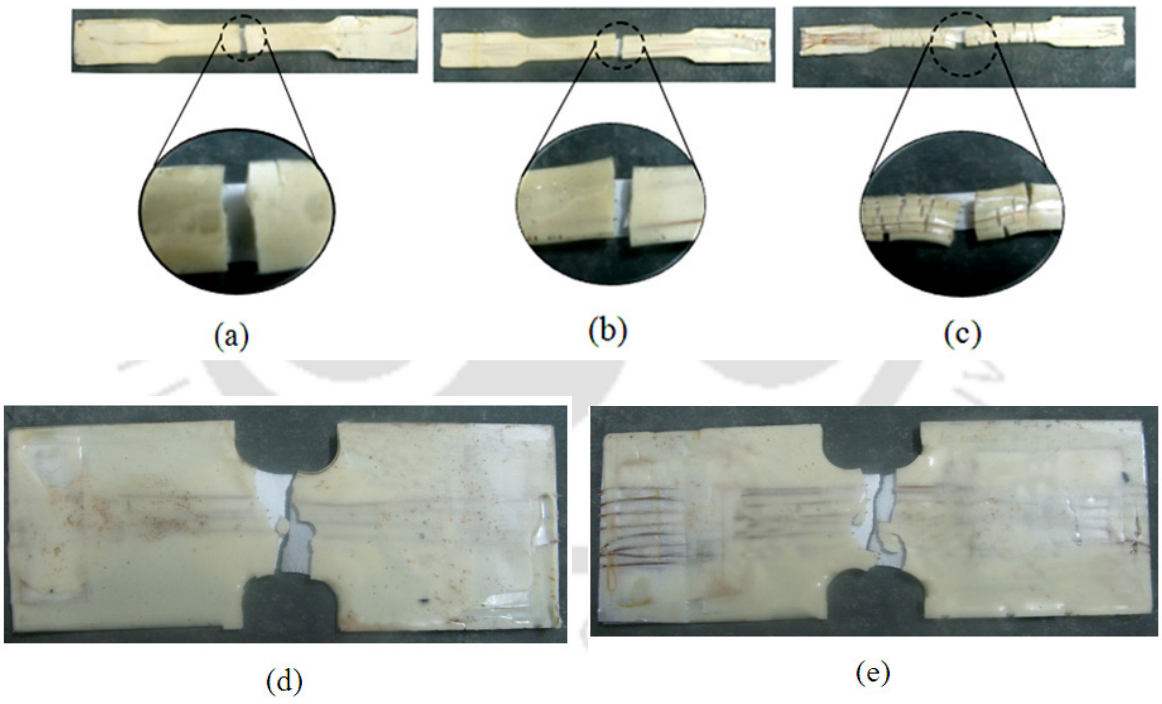

Fig. 7.7 Failure pattern of longitudinally wire reinforced adhesive layer constituting adhesive bonded sheets: (a) 1-wire-tensile test (b) 3-wires-tensile test (c) 5-wires-tensile test, (d) 4-wires-IPPS formability test, and (e) 8-wires-IPPS formability test

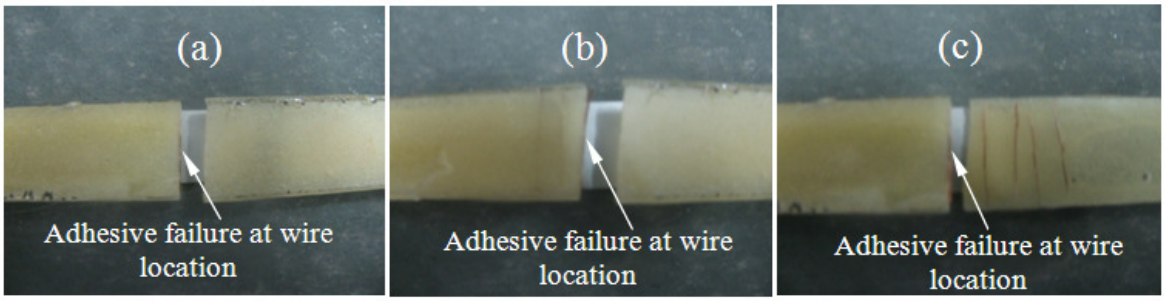

Fig. 7.8 Failure pattern of transversely wire reinforced adhesive layer constituting adhesive bonded sheets (a) 1-wire (b) 3-wires, and (c) 5-wires

7.4.2 Influence of longitudinal wire reinforcement on the stress-strain behaviour of adhesive bonded sheets

The comparison of engineering stress-strain behaviour of longitudinally wire reinforced adhesive bonded sheets with different numbers of Cu and Al wires from tensile test is shown in Fig. 7.9(a, b). A similar comparison from IPPS formability test is shown in Fig. 7.10(a, b). It is observed that the stress and strain in adhesive bonded sheets varies with different numbers of wire reinforcement in the adhesive layer.

From these results, the elongation % is evaluated in regions A, B and C. Fig. 7.11 shows the comparison of elongation % in wire reinforced adhesive bonded sheets with different numbers of Cu and Al wires in tensile test. Similarly, Fig. 7.12 shows the comparison in the case of IPPS formability test. It is observed that the elongation of the adhesive bonded sheets increases about 14.5% in region A, 5.5% in region B and 6% in region C compared to unreinforced adhesive bonded sheets, with increase in number of wires up to 2, and then decreases with excessive reinforcement of both the Cu and Al wires during tensile test (Fig. 7.11). In IPPS formability test, the elongation in adhesive bonded sheets increases, about 24.8% in region A, 9.7% in region B and 3.4% in region C as compared to unreinforced adhesive bonded sheets, with increase in number of Cu wires up to 4, and then decreases with excessive reinforcement of the Cu wires (Fig. 7.12). But in the case of Al wire reinforced adhesive bonded IPPS blank, a contradicted trend is observed (Fig. 7.10(b) and 7.12). Even there is a considerable improvement in ductility of Al wire reinforced adhesive bonded sheets in region A up to 4 wires (about 7.3%), the ductility change in regions B and C is very much less (about 3% in region B and 24% in region C) than unreinforced adhesive bonded sheets.

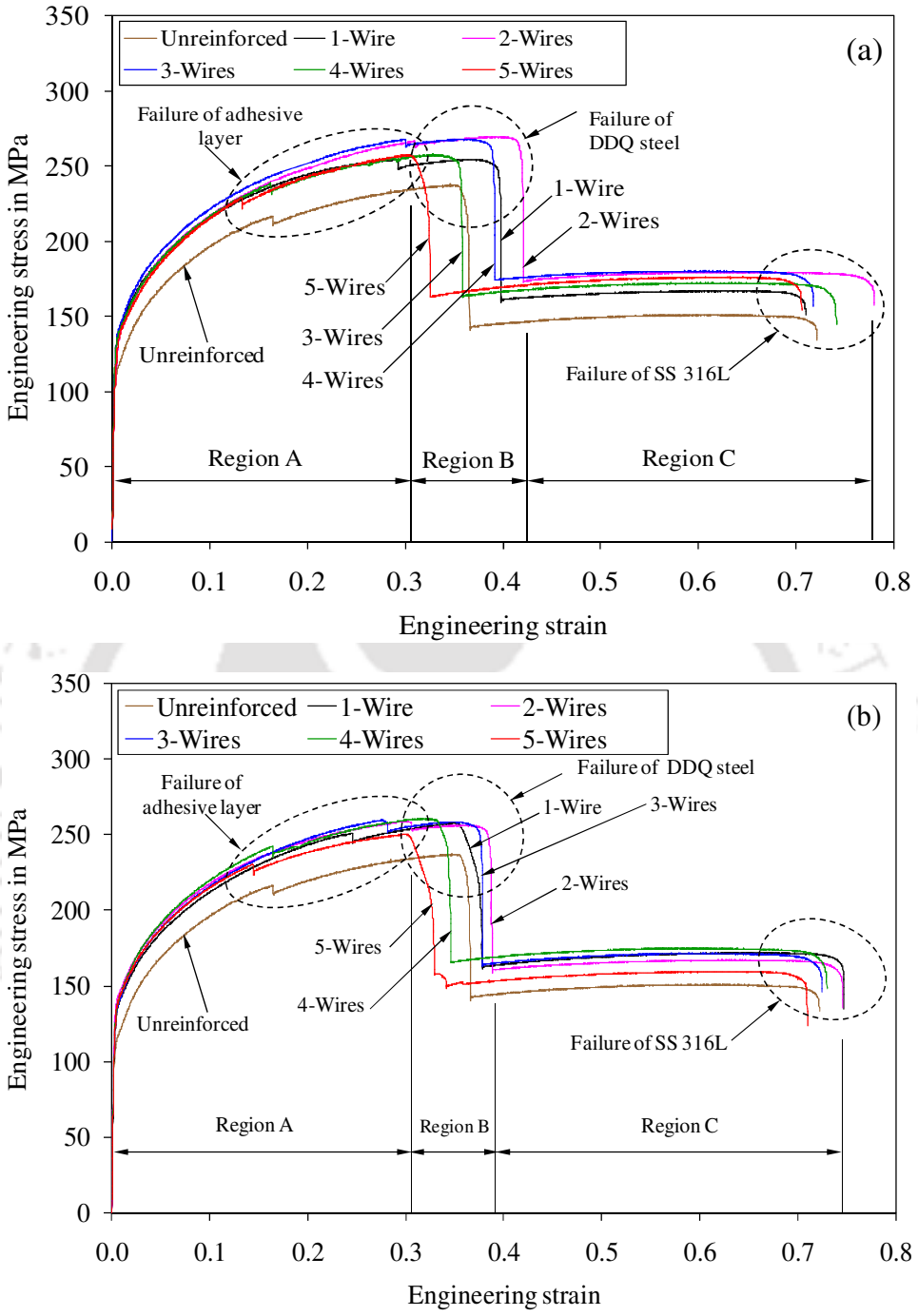

Fig. 7.9 Engineering stress-strain behaviour of wire reinforced adhesive bonded sheets with different numbers of wire from tensile test: (a) Cu wire, and (b) Al wire (Data variation in ultimate tensile strength = ±10 MPa, and elongation at failure = ±2%)

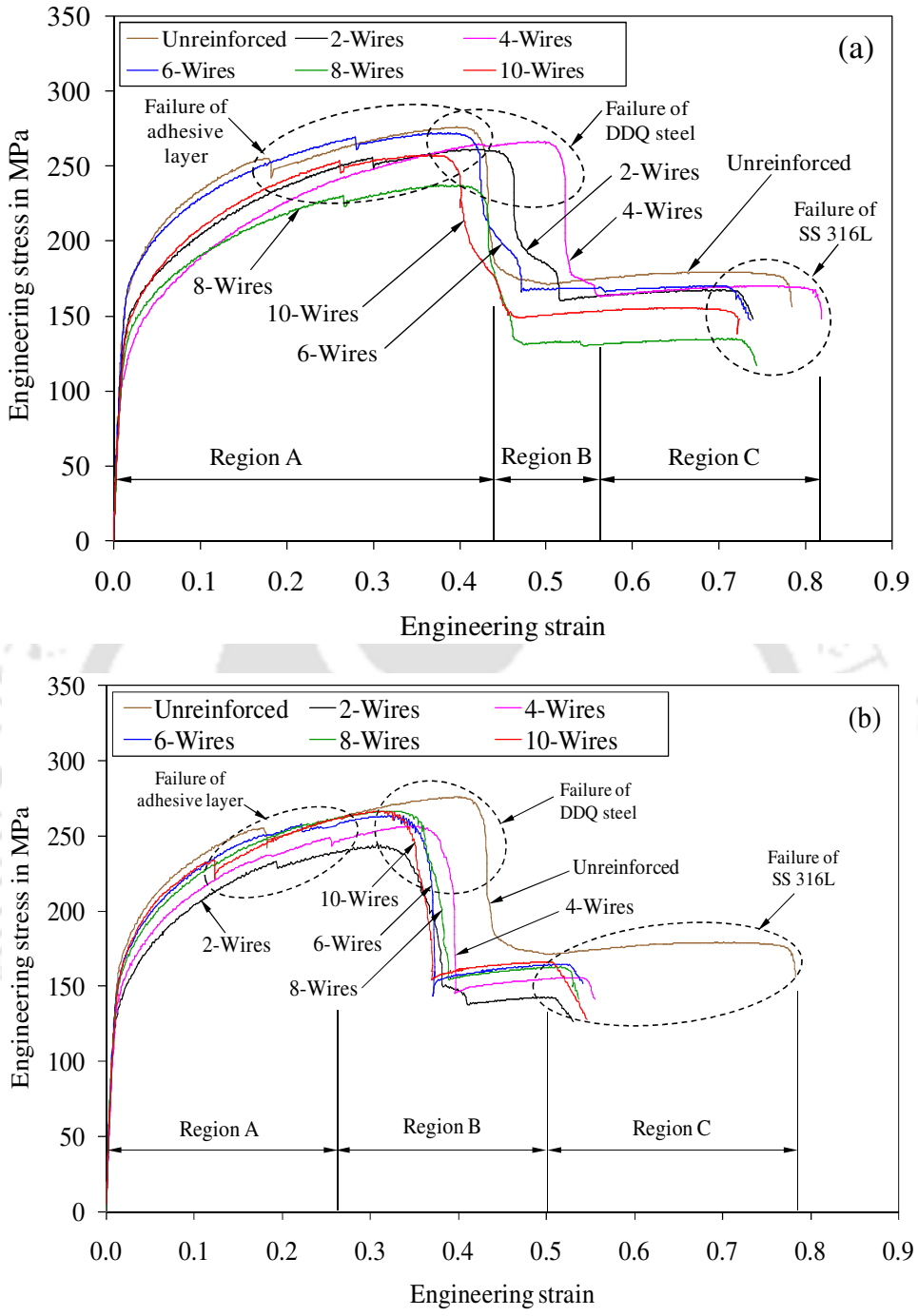

Fig. 7.10 Engineering stress-strain behaviour of wire reinforced adhesive bonded sheets with different numbers of wire from IPPS formability test: (a) Cu wire and (b) Al wire (Data variation in ultimate strength = ±15 MPa and elongation at failure = ±1.5%)

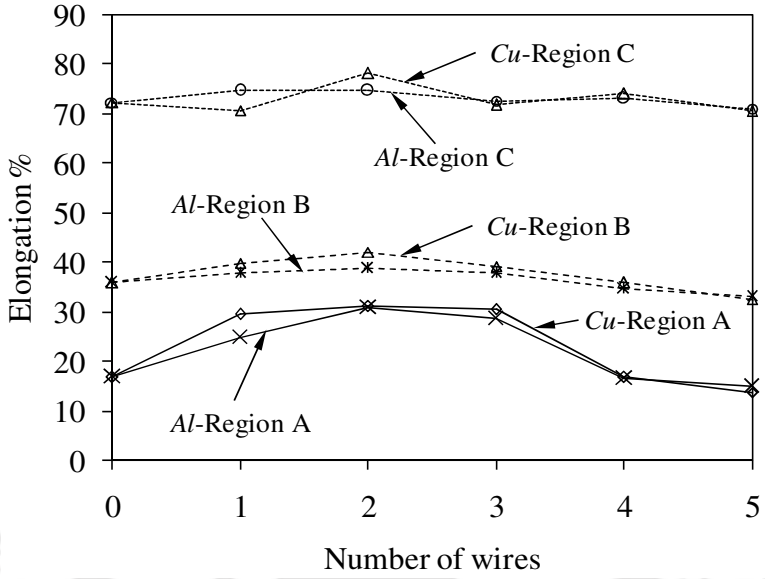

Fig. 7.11 Elongation trend of Cu and Al wire reinforced adhesive bonded sheets in regions A, B and C with different numbers of wire during tensile test (Data variation in elongation = ±2%)

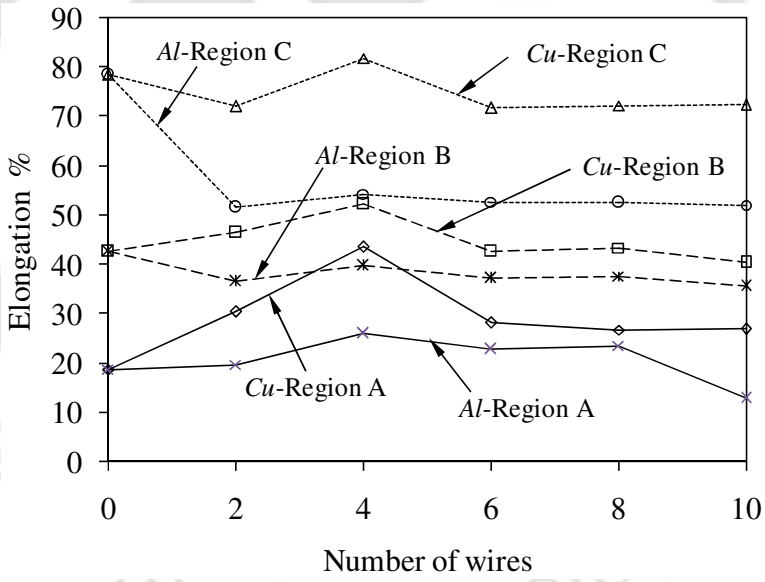

Fig. 7. 12 Elongation trend of Cu and Al wire reinforced adhesive bonded sheets in regions A, B and C with different numbers of wire during IPPS formability test (Data variation in elongation at failure = ±1.5%)

However, it is noted that the increase in elongation of wire reinforced adhesive layer, i.e., in region A, increases the elongation of base materials constituting adhesive bonded sheets in regions B and C, to a considerable level. It is understood that the reinforcement of wires in the adhesive layer or replacement of adhesive layer by high ductile wire up to a certain limit improves the ductility of adhesive layer, and thereby improves the overall ductility of adhesive bonded sheets and

base materials constituting adhesive bonded sheets. It is noted that the elongation of Cu wire reinforced adhesive bonded sheets is larger than Al wire reinforced adhesive bonded sheets with respect to effective number of reinforcements (2 wires in the tensile test, and 4 wires in the IPPS formability test). This is due to the larger elongation of Cu wire as compared to Al wire (Fig 7.1).

7.4.3 Effect of longitudinal wire reinforcement on the limit strains of adhesive bonded sheets

Fig. 7.13(a-d) shows the comparison of limit strains of base materials (DDQ steel and SS 316L sheets), constituting wire reinforced adhesive bonded sheets from tensile test. Similarly, the limit strains evaluated from IPPS formability test are shown in Fig. 7.14(a-d).

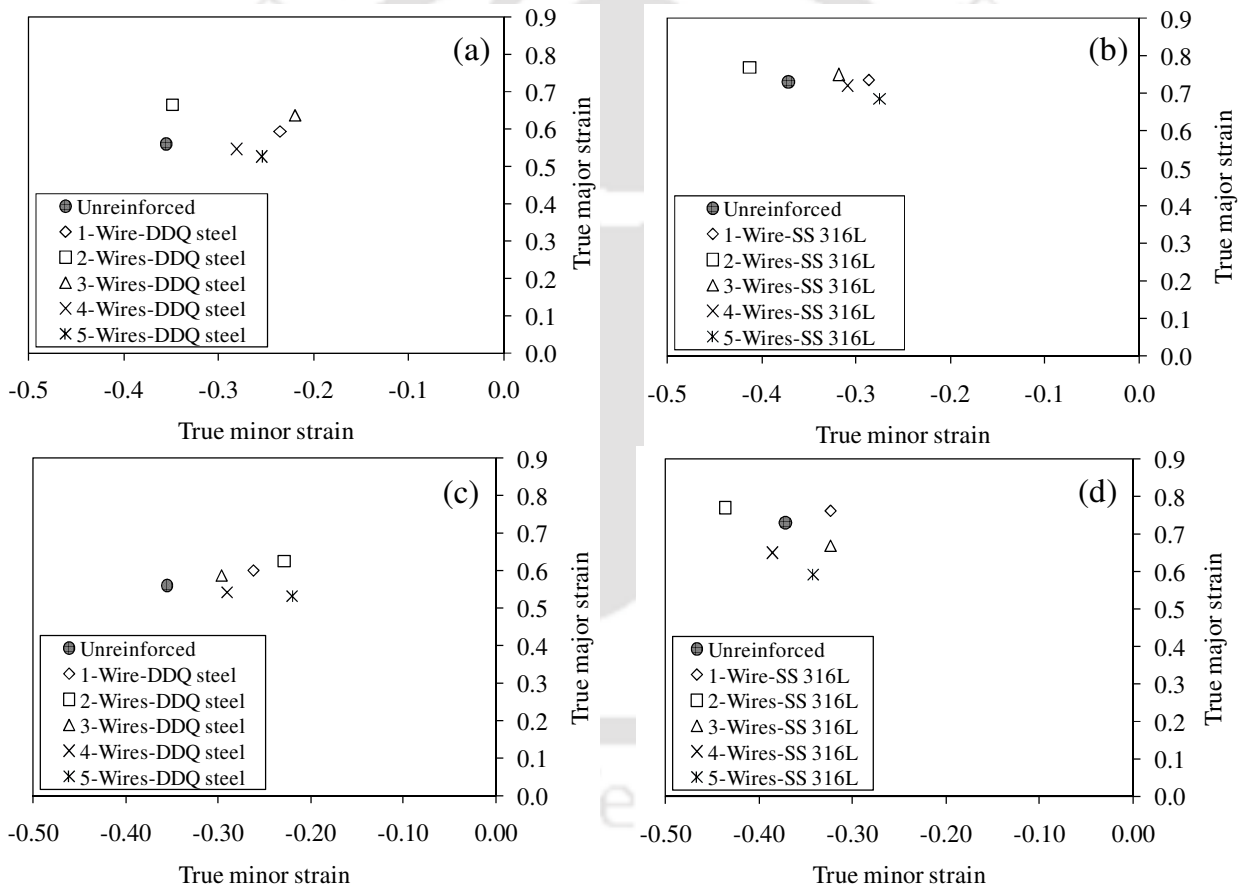

Fig. 7.13 Limit strains in base materials constituting wire reinforced adhesive bonded blanks (ABB) with different numbers of wire in tensile test: (a) DDQ steel-Cu wired ABB, (b) SS 316L-Cu wire ABB, (c) DDQ steel-Al wired ABB, and (d) SS 316L-Al wired ABB

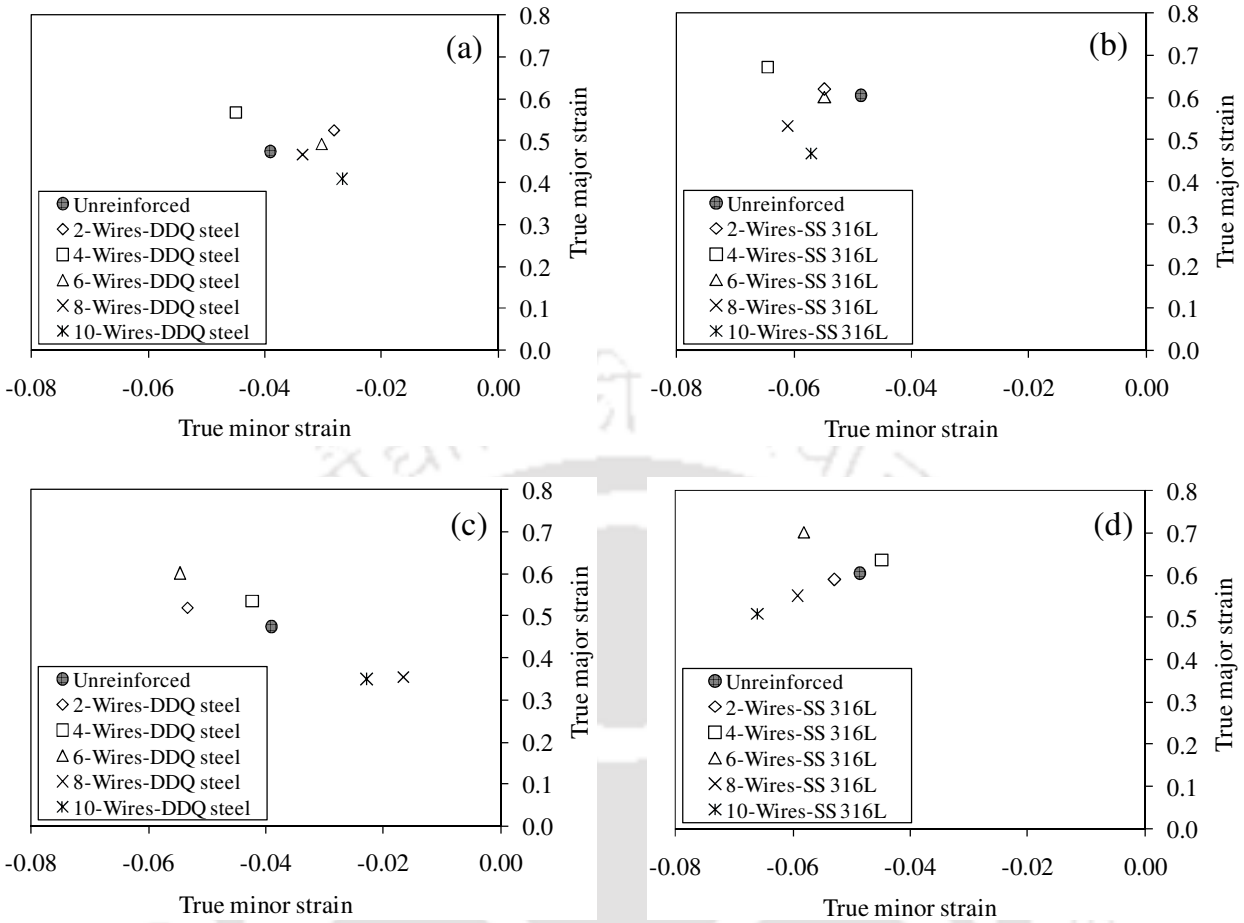

Fig. 7.14 Limit strains in base materials constituting wire reinforced adhesive bonded blanks (ABB) with different numbers of wire in IPPS formability test: (a) DDQ steel-Cu wired ABB, (b) SS 316L-Cu wired ABB, (c) DDQ steel-Al wired ABB and (d) SS 316L-Al wired ABB

It is observed that the limit strain increases with increase in number of reinforcements up to 2 wires in tensile test, and 4 wires in the case of Cu wire reinforcement and 6 wires in the case of Al wire reinforcement during IPPS formability test, and then decreases with excessive reinforcement of wires in the adhesive layer. The increase in limit strain is significant in DDQ steel and moderate in the case of SS 316L sheet. This increase in limit strain observed from base materials of adhesive bonded sheets is common in both types of wires used for reinforcement. Though the stress-strain behaviour of Al wire reinforced adhesive bonded sheets is not much clear, the limit strain result in base materials (Fig. 7.14(c, d)) shows increase with number of reinforcement up to 6 wires and then decreases with excessive reinforcement. In the comparison between 2 wire reinforced and unreinforced adhesive bonded sheets from tensile test, there is about 10.5% and 3.8% increase in major strain in DDQ steel and SS 316L constituting Cu wire reinforced adhesive bonded sheets,

respectively. There is about 6.5% and 4% increase in major limit strain in DDQ steel and SS 316L in Al wire reinforced adhesive bonded sheets, respectively. In the comparison between 4 wire reinforced and unreinforced adhesive bonded sheets from IPPS formability test, there is about 9.3% and 6.8% increase in major strain in DDQ steel and SS 316L constituting Cu wire reinforced adhesive bonded sheets, respectively. There is about 6% and 3.2% increase in major limit strain in DDQ steel and SS 316L constituting 6 Al wires reinforced adhesive bonded sheets, respectively.

Table 7.1 Uncertainty measurement of limit strain

Test type	Standard deviation range			
	True major limit strain		True minor limit strain	
	DDQ steel	SS 316L	DDQ steel	SS 316L
Tensile	0.005 to 0.027	0.002 to 0.028	0.001 to 0.053	0.003 to 0.065
IPPS forming	0.003 to 0.015	0.003 to 0.020	0.001 to 0.04	0.001 to 0.018

Table 7.1 shows the standard deviation of true major limit strain and true minor strain ranges for DDQ steel and SS 316L sheets in both the types of wire reinforced and unreinforced adhesive bonded sheets from the tensile test and IPPS formability test. These error variations are much smaller than the limit strain improvement among different adhesive bonded samples with different numbers of wire reinforcements. Hence, these results confirm an inherent improvement in the limit strain up to the optimum level rather than falling within the standard deviation range.

Usually, increase in forming limit strain implies the improvement in the formability of sheets that could be directly related to strain hardening exponent (n). The strain hardening exponent (n) is evaluated in regions A, B and C of stress-strain behaviour of adhesive bonded sheets as per standard procedure. Tables 7.2 and 7.3 show the strain hardening exponent (n) evaluated in regions A, B and C during tensile tests and IPPS formability tests, respectively. It is clearly noted that the n-value increases with increase in number of wires up to 2 and 4 in tensile and IPPS formability tests, respectively, and then decreases with excessive number of reinforcements.

Table 7.2 Strain hardening exponent (n) in regions A, B and C of wire reinforced adhesive bonded sheets from tensile test

Type of wire reinforcement in adhesive bonded sheets (ABB)	Number of wires	Region A	Region B	Region C
Unreinforced	0	0.271	0.389	0.501
Cu wired ABB	1	0.285	0.409	0.521
	2	0.296	0.412	0.521
	3	0.286	0.378	0.505
	4	0.266	0.372	0.506
	5	0.241	0.347	0.498
Al wired ABB	1	0.276	0.385	0.500
	2	0.302	0.388	0.505
	3	0.285	0.383	0.502
	4	0.259	0.363	0.501
	5	0.245	0.361	0.501

Variation in *n*-value in region A = ±0.003, region B = ±0.002, and region C = ±0.001

Table 7.3 Strain hardening exponent (n) in regions A, B and C of wire reinforced adhesive bonded sheets from IPPS formability test

Type of wire reinforcement in adhesive bonded sheets (ABB)	Number of wires	Region A	Region B	Region C
Unreinforced	0	0.276	0.422	0.633
Cu wired ABB	2	0.295	0.466	0.624
	4	0.370	0.494	0.668
	6	0.278	0.398	0.613
	8	0.274	0.396	0.619
	10	0.271	0.375	0.614

Variation in *n*-value in region A = ±0.0015, region B = ±0.002, and region C = ±0.0015

This confirms that increasing high ductile wire reinforcement in the low ductile adhesive up to a certain level (2 wires in tensile test and 4 wires in IPPS formability test) improves the plastic deformation of global behaviour (region A) of wire reinforced adhesive bonded sheets. This improved plastic deformation in region A is preserved in the regions B and C and thus shows improvement in the ductility of base materials constituting adhesive bonded sheets. This is why, the

limit strain increases with increase in number of reinforcements up to 2 wires in tensile test and up to 4 wires in IPPS formability test.

7.5 Numerical evaluation of forming behaviour of high ductile wire reinforced in the epoxy adhesive bonded sheets

Fig. 7.15 shows the true stress-strain behaviour of Cu (high ductile) strip reinforced in the epoxy (less ductile) adhesive bonded sheets. It is clearly seen that appropriate replacement of epoxy with Cu (high ductile material) improves the ductility of low ductile adhesive (Region A) as compared to the unreinforced adhesive constituting adhesive bonded sheets, thereby improves the ductility of adhesive bonded sheets. It is observed that more replacement of epoxy with Cu material (curve 3) shows the ductility equivalent to that of Cu material with negligible influence of epoxy adhesive (curve 4).

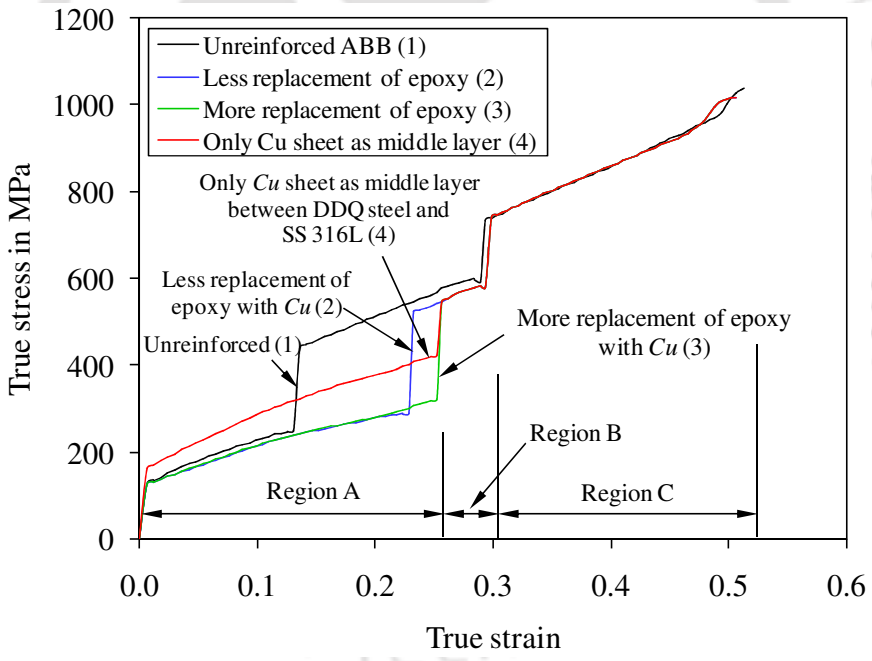

Fig. 7.15 Comparison of true stress-strain behaviour of unreinforced and *Cu* reinforced adhesive bonded sheets from numerical prediction

Though testing of only Cu sheet introduced between DDQ steel and SS 316L (curve 4) is not a case in the present study, this has been considered as a reference to understand the true stress-strain behaviour of the case with larger contribution from Cu material in place of epoxy, constituting the adhesive bonded sheets. It is also observed that there is not much difference in the ductility of the

base materials in regions B and C between curve 3 and 4, even there is a significant improvement in the replacement of epoxy with Cu material. This is mainly due to the absence of bonding between adhesive layer and base materials during simulation, and the absence of adhesive contribution while increasing the contribution of wire.

From the simulation work, it is summarized that this conceptual study was carried out by considering the formability of adhesive bonded sheets till failure of adhesive constituent which decides the overall formability, though all three layers were deformed till failure. This virtual experiment could be useful in sorting out the quick decisions about selection of materials and amount of material to be used for reinforcements during prediction of overall formability of adhesive bonded sheets, rather than carrying out real time trials in the industrial applications. Since the strip of high ductile material improves the ductility of low ductile adhesive, there would be no influence of gap between wires uniformly maintained during reinforcement in the adhesive constituting the bonded sheets. It is perceived that the improvement in the ductility of adhesive depends on the ductility of wire and appropriate amount of replacement of adhesive by high ductile wire. The appropriate amount of adhesive could be replaced by any of the methods like varying the number of reinforcements and varying the size of the reinforcements. But the reinforcements should not act as crack initiators during deformation of adhesive in the bonded sheets. Instead of modeling various number of wires in the adhesive reinforcement as like experiments, the modeling of an equivalent strip with wire material properties could predict the same trend of experimental results which is easier and quicker method. This modeling method of reinforced adhesive bonded sheets could be adapted for any type of reinforcements like fibres, fabrics and mats to study about their forming behaviour. It is also demonstrated through simulations about influence of wires on the overall ductility of base materials in adhesive bonded sheets like in the case of experiments. The results are found to be consistent in both the cases.

7.6 Effect of transverse wire reinforcement on the forming limit strain of adhesive bonded sheets

Fig. 7.16(a, b) shows the comparison of limit strains of base materials constituting transverse Cu wire reinforced adhesive bonded sheets with different numbers of wire. There is not much difference in the limit strains in the base materials with increase in number of wires reinforced in the adhesive layer. Also there is not much difference in the limit strains in base materials between

unreinforced and wire reinforced adhesive layer constituting adhesive bonded sheets. This is mainly due to the failure of adhesive layer at the location of wires during forming resulting in the negligible contribution of wires on the overall formability. A similar behaviour is expected in the case of IPPS forming test and hence it is not performed. Since there is not much difference in the failure pattern of Cu wire reinforced adhesive (Fig. 7.8), and limit strain results of base materials constituting adhesive bonded sheets with respect to the number of reinforcements of Cu wire, which exhibits better forming limit strain results during longitudinal reinforcement in the adhesive bonded sheets as compared to the cases of Al wire reinforcement (Figs. 7.13 and 7.14), the testing of transverse wire reinforced adhesive bonded sheets has been restricted with Cu wire reinforcement.

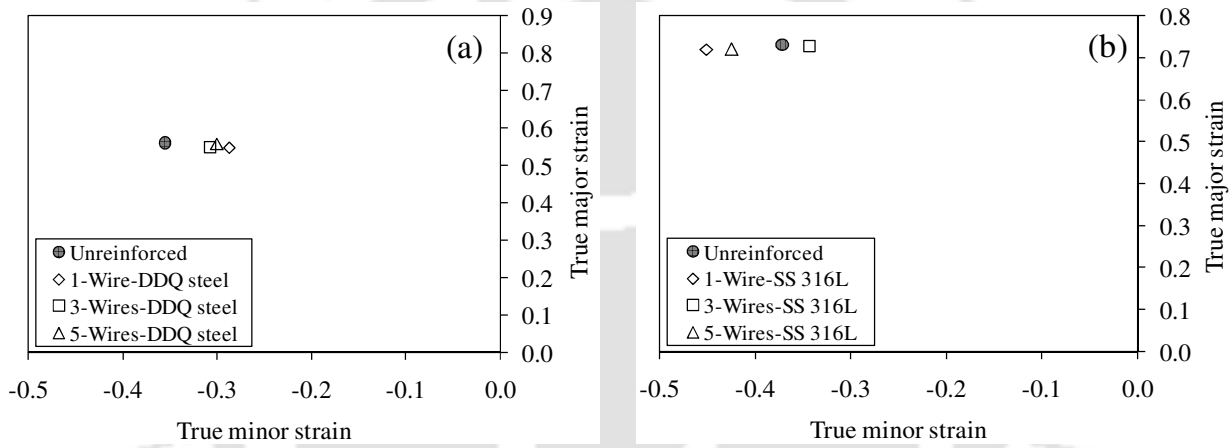

Fig. 7.16 Limit strains in base materials constituting transverse wire reinforced adhesive bonded sheets with different numbers of wires from tensile test: (a) DDQ steel, and (b) SS 316L

7.7 Influence of wire reinforcement on deep drawability of adhesive bonded sheets

In this section, the influence of wire reinforcement on deep drawability of adhesive bonded sheets is investigated with the deformation pattern of cup, load-stroke behaviour, cup height evaluated at the maximum load in load-stroke behaviour and the wrinkling behaviour with different numbers of reinforcement.

7.7.1 Deformation pattern

During deep drawing of wire reinforced adhesive bonded sheets, the blank holding force was applied manually by tightening the fasteners used in the tools. The contact surfaces between sheets and tools were well lubricated using grease. Fig. 7.17(a-e) shows the deformation pattern of unreinforced and Cu wire reinforced adhesive bonded sheets in the cup drawing process. At the end of cup drawing of wire reinforced adhesive bonded sheets, the cups were sectioned using the linear precision saw (Buehler-ISOMET 4000). The sectioned cups with numbers of reinforcement are shown in Fig. 7.17(a-e). It is observed that the adhesive layer has failed at the wall of the cup at the end of maximum drawing (since small crack length in the adhesive layer) or successful cup in the case of unreinforced adhesive bonded sheets (Fig. 7.17(a)). Thinning of adhesive layer at the bottom corner of the cup is also observed. The same adhesive failure and thinning are observed in the case of 4 wires reinforced adhesive bonded sheets also (Fig. 7.17 (b)). In the case of 8 wires reinforced adhesive bonded sheets (Fig. 7.17(c)), reduced thinning at the bottom corner of the cup is observed, but the adhesive layer has been failed in the wall of cup at the end of maximum drawing (with respect to small crack) or successful cup. There is no adhesive failure and reduced thinning at the bottom corner of the cup in the case of 16 wires reinforced adhesive bonded sheets (Fig. 7.17(d)). A severe thinning and adhesive failure in the wall of cup are observed in the case of 40 wires reinforced adhesive bonded sheets. More replacement of adhesive layer by wire causes severe thinning at the bottom corner of the cup. The reduced thinning and no adhesive failure are the indication of improvement in the plasticity of adhesive with wire reinforcement. It is perceived that reinforcement of high ductile wires in the adhesive layers up to a certain level improves plasticity of low ductile adhesive constituting adhesive bonded sheets, thereby reduces thinning and adhesive failure. The excessive replacement of adhesive by ductile wires reduces the ductility of adhesive layer constituting adhesive bonded sheets, thereby increases severe thinning and adhesive failure.

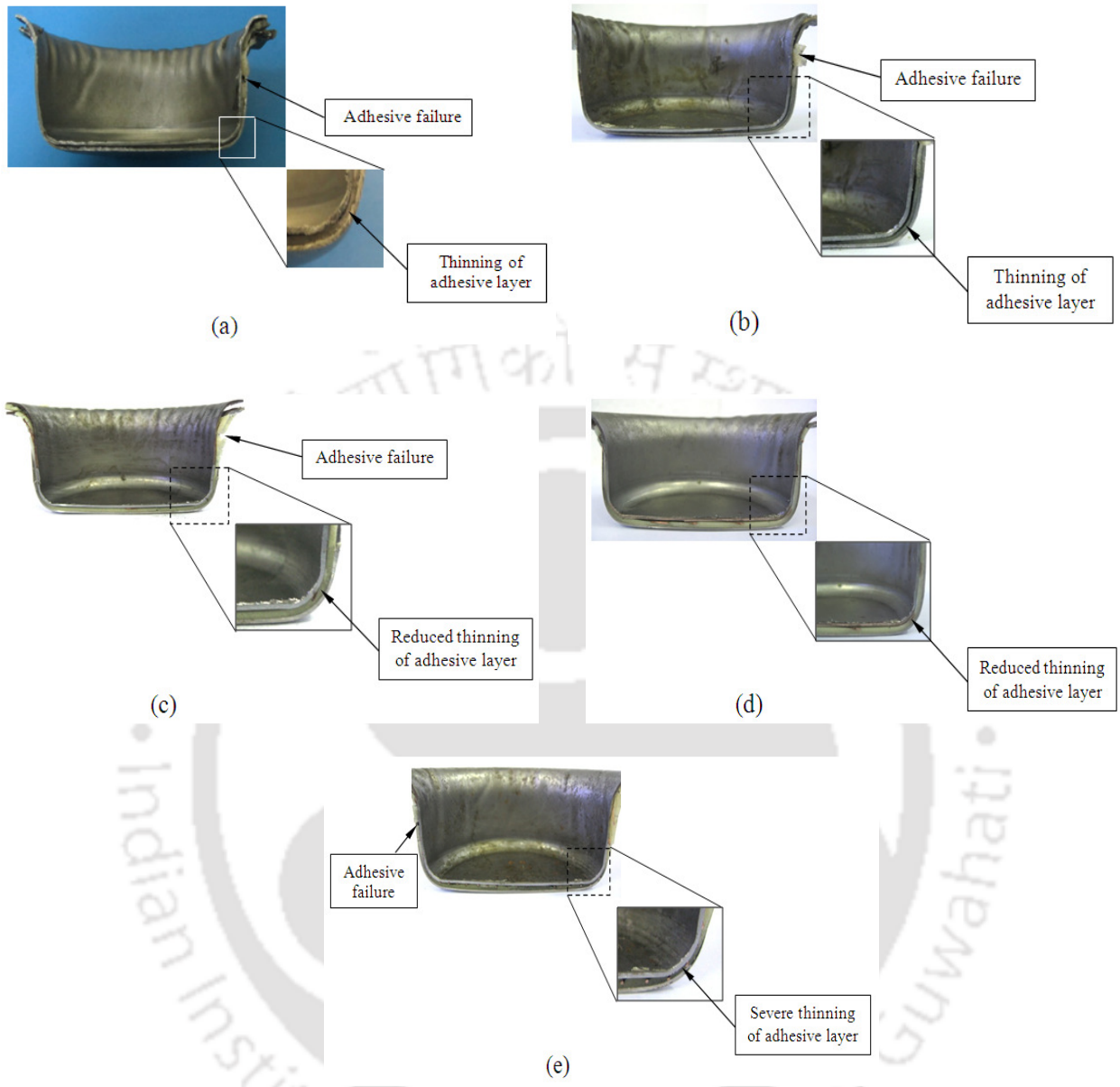

Fig. 7.17 Deformation pattern of Cu wire reinforced adhesive layer constituting adhesive bonded sheets: (a) Unreinforced, (b) 4 wires (c) 8 wires, (d) 16 wires, and (e) 40 wires

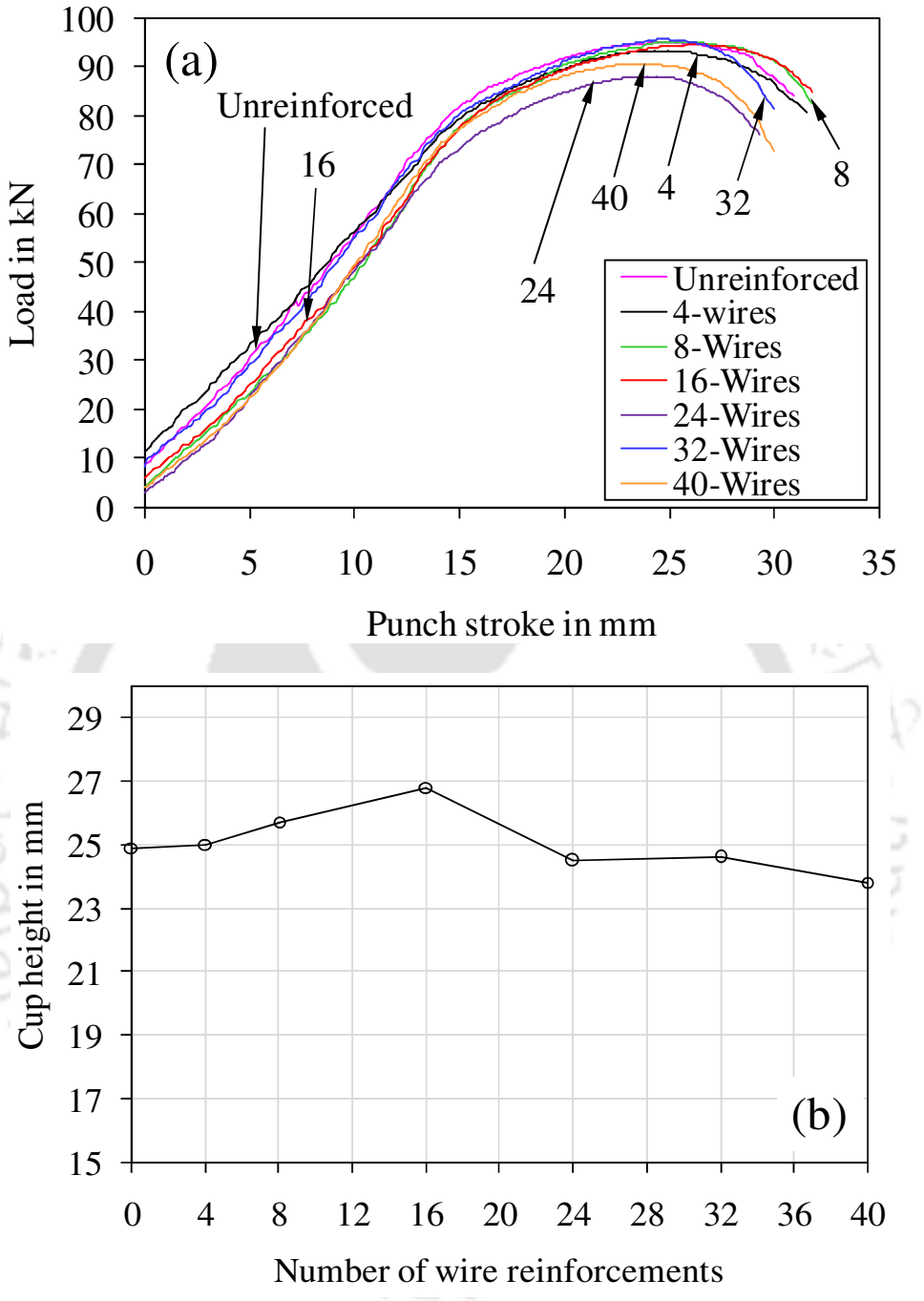

Fig. 7.18 (a) Deep drawing behaviour of Cu wire reinforced adhesive bonded sheets with different number of wires (data variation in maximum load = ±5 kN), and (b) Comparison of cup height at maximum load (data variation in cup height = ±0.25 mm)

The influence of high ductile Cu wire reinforcement in the low ductile adhesive layer constituting adhesive bonded sheets is analysed in the practical forming applications by conducting out-of- plane test like deep drawing test. The comparison of deep drawing behaviour and cup height

measured at maximum load with different numbers of reinforcements in the adhesive layer constituting adhesive bonded sheets are shown in Figs. 7.18(a) and 7.18(b), respectively.

A considerable difference in the punch-stroke at maximum load is observed in the deep drawing behaviour with increase in number of wire reinforcement (Fig. 7.18(a)). This can be seen clearly in Fig. 7.18(b) that the overall cup height of adhesive bonded sheets at maximum load increases up to 16 wires and then decreases with excessive reinforcement of high ductile wires in the low ductile adhesive layer. This confirms that reinforcing high ductile wires in the low ductile adhesive layer improves the plasticity of low ductile adhesive, and thereby improves the overall formability of bonded sheets.

7.7.2 Wrinkling behaviour during deep drawing of wire reinforced adhesive bonded sheets

Fig. 7.19(a-g) shows the wrinkling behaviour of adhesive bonded sheets reinforced with 0, 4, 8, 16, 24, 32, and 40 Cu wires. There is a moderate wrinkling in the flange region of cups made from unreinforced and 4 wire reinforced adhesive bonded sheets (Fig. 7.19 (a-b)). A reduced wrinkling in the flange region is observed in the cases of 8 and 16 wire reinforced adhesive bonded sheets (Fig. 7.19(c-d)) as compared to unreinforced and 4 wire reinforced adhesive bonded sheets. A severe wrinkling in the flange region of 24 to 40 wires reinforced adhesive bonded sheets is observed.

Fig. 7.19 Wrinkling behaviour of adhesive bonded sheets with different numbers of Cu wire reinforcements

It is perceived that failure of adhesive, and its thinning at the bottom corner of cup (Fig. 7.17(a, b, d and e)) causes instability and imperfection in the geometry of adhesive bonded during deformation. These instability and imperfection in the geometry caused by adhesive layer constituting adhesive bonded sheets lead to severe wrinkling.

7.8 Conclusions

The following conclusions are derived from the present investigation.

- The elongation of the adhesive bonded sheets increases about 14.5% (region A) with increase in number of Cu and Al wires up to 2 during tensile test. In IPPS formability test, the elongation of the adhesive bonded sheets increases about 24.8% (region A) with increase in number of Cu wires up to 4, and about 7.3% (region A) in the case of Al wires up to 6 as compared to unreinforced adhesive bonded sheets.
- In tensile test, with the increase in number of wires up to 2, the maximum increase in true major strain of adhesive bonded sheets is about 10.5% and 3.8% in DDQ steel and SS 316L, respectively, as compared to unreinforced adhesive bonded sheets. In IPPS formability test, with the increase in number of wires up to 4, the maximum increase in true major strain of adhesive bonded sheets is about 9.3% and 6.8% in DDQ steel and SS 316L, respectively, as compared to unreinforced adhesive bonded sheets.
- Reinforcement of high ductile wires to an appropriate level (2 wires in tensile test, 4 wires in IPPS formability test, and 16 wires in the deep drawing test) in the low ductile adhesive constituting adhesive bonded sheets improves ductility of adhesive, and thereby improves the overall formability of adhesive bonded sheets.
- The present study conceptualizes the forming behaviour of high ductile material reinforced with low ductile adhesive layer constituting the bonded sheets through finite element prediction with very good correlation with the experimental results. The present study also proposes the effective method of modelling the reinforced adhesive constituting the bonded sheets. The improvement in the ductility of base materials by the adhesive layer could not be captured during FE simulation due to absence of interface bonding between base materials and adhesive layer.
- There is not much difference in the forming limit strains in transverse reinforced adhesive bonded sheets irrespective to the number of wires. The failure of adhesive layer constituting adhesive bonded sheets occurs at the location of wires. It is understood that transverse oriented wire in the adhesive layer acts as a crack initiator. It is perceived that the orientation of wire reinforcement affects the formability of adhesive bonded sheets. Since there is not much difference in the limit strains, it is suggested that replacement of adhesive layer

(Ø0.3 mm in this work) with metal wires (transverse oriented) could be utilized as conductive adhesive bonded sheets (since adhesive is non-conductive polymer) without affecting the formability.

- The longitudinally reinforced adhesive bonded sheets also could be utilized as conductive adhesive bonded sheets irrespective of the number of wires.
- More replacement of adhesive layer with wires causes adhesive failure, severe thinning at the corners of the cup, and wrinkling in the deep drawing of adhesive bonded sheets.

Chapter 8

Experimental evaluation and prediction of deep drawability of adhesive bonded blanks

8.1 Methodology

The deep drawability of adhesive bonded blanks are investigated with different hardener/resin ratios of epoxy adhesive, and different CB wt.% filled in the epoxy adhesive. The mechanical properties of base materials and epoxy adhesive are already discussed in Chapter 2 in Sections 2.1.1 and 2.4.1, respectively. The mechanical properties of CB filled adhesives are already discussed in Chapter 6 in Section 6.5.1. The experimental evaluation of adhesive properties, deep drawability of adhesive bonded blanks by experiments, finite element predictions, estimation of maximum drawing load, and load-stroke behaviour prediction are discussed in this section.

8.2 Experimental evaluation of adhesive mechanical properties

The epoxy adhesive properties with different hardener/resin ratios like 0.6:1, 0.7:1, 0.8:1, 0.9:1 and 1:1, and filled with different CB wt.% like 1%, 2%, 3%, 4%, 5% and 6% were evaluated by approach-1 and approach-2 as discussed in Chapter 5 in Sections 5.2 and 5.3. The stress-strain behaviour of adhesive by approach-1 was evaluated as discussed in Chapter 5 in Section 4.3.1. Similarly, the stress-strain behaviour of adhesive by approach-2 was evaluated as discussed in Chapter 5 in Section 5.3. During FE simulation of adhesive bonded blanks in the cup drawing process, the adhesive properties were incorporated by two approaches to predict the deep drawability.

8.3 Evaluation of deep drawability of adhesive bonded blanks – Experiment

The adhesive bonded circular blanks were prepared with different hardener/resin ratios (as discussed Chapter 2 in Section 2.3) and different CB wt.% (as discussed in Chapter 6 in Section 6.3) by using circular moulds to maintain uniform thickness and diameter of constituting adhesive layer as discussed in Chapter 7 in Section 7.2. The average thickness of adhesive bonded blanks was found to be 2±0.1 mm, and the average thickness of constituting adhesive

layer was found to be 0.8±0.1 mm. The blank holding force was applied manually by tightening the fasteners used in the tools. The deep drawing process of adhesive bonded circular specimens was carried out and results were monitored as discussed in Chapter 7 in Section 7.2.

8.4 Numerical prediction of deep drawability of adhesive bonded blanks

Fig. 8.1(a) shows the FE model of the cylindrical deep drawing tools. The dimensions of tools in the FE model are same as that of used in experiments as given in Fig. 7.3(b) in Chapter 7. In order to model adhesive bonded blanks, three similar circular blanks with ∅95 mm were generated and positioned one above other (Fig. 8.1(b)). The properties of base materials as given in Tables 2.2 and 2.3 in Chapter 2, and the adhesive properties with different hardener/resin ratios and different CB wt.% determined by approach-1 and approach-2 were incorporated during deep drawability prediction of adhesive bonded blanks. Apart from these two approaches, no interface bonding between adhesive layer and base materials was modelled during prediction. The thickness of adhesive layer was 0.8 mm. This value was obtained from experiments.

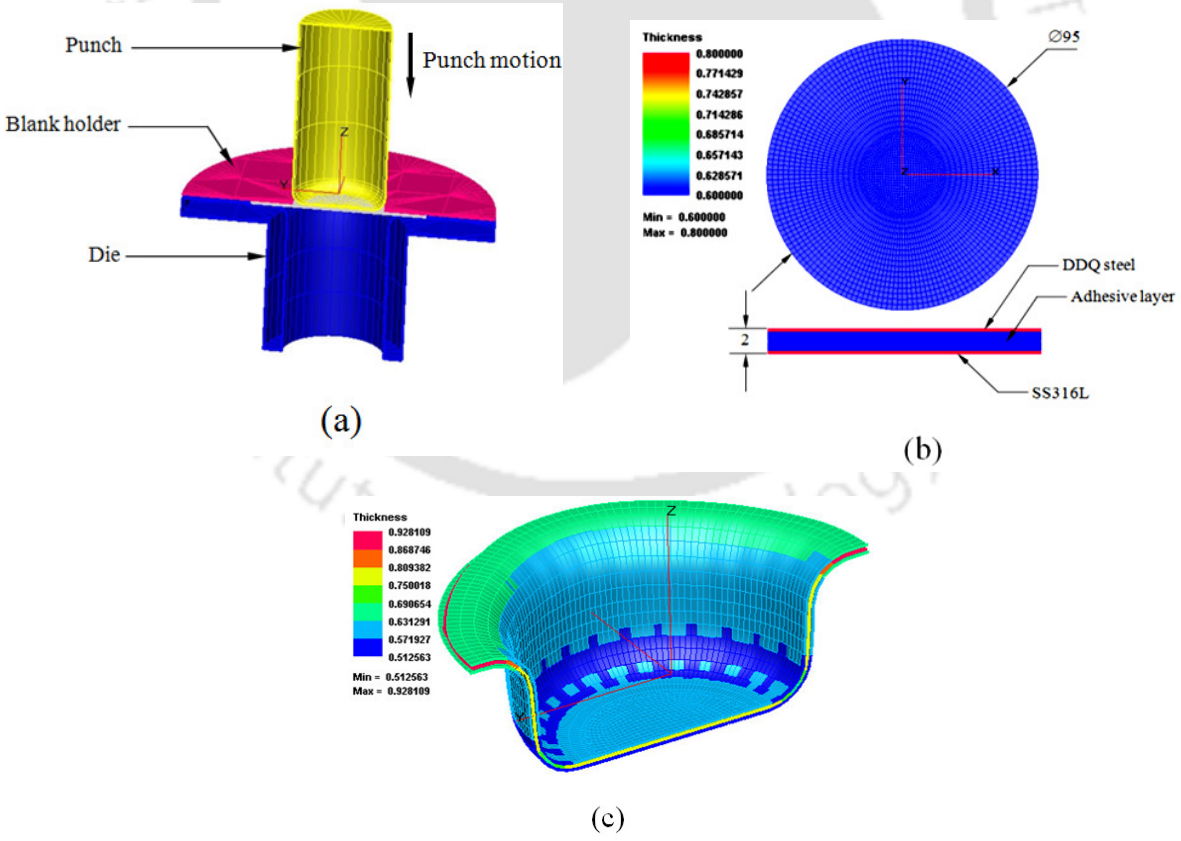

Fig. 8. 1 FE model: (a) deep drawing tools, (b) adhesive bonded blanks, and (c) deformed cup

The average mesh size of 2 mm was used after mesh sensitivity analysis of during FE simulation (described later). The density of adhesive with different hardener/resin ratios (as discussed in Chapter 4 in Section 4.2), and different CB wt.% (as discussed in Chapter 6 in Section 6.2) were incorporated during FE simulation. The friction coefficient was imposed as 0.1 between contact surfaces between blank and tools, and the contact between the surfaces of three layers constituting adhesive bonded blanks was defined.

The contact type between blank and tools surfaces was chosen as accurate which permanently prohibits the nodes of the blank sheet from penetrating the volume of the element of the tool during calculation. The total number of elements calculated in the modelled adhesive bonded blanks was about 11040. The strain hardening behaviour description, and yield criterion chosen for base material, incorporation of adhesive properties were described as discussed in Chapter 4 in section 4.3. The displacement was given on the punch during cup drawing process. The load-stroke behaviour, deformation pattern of adhesive layer and base materials constituting adhesive bonded blanks, wrinkling of adhesive bonded blanks were predicted and validated with the experimental results. Fig. 8.1(c) shows the FE model of deformed cup made of adhesive bonded blanks.

8.5 Estimation of maximum drawing load in cup drawing using simple analytical models

The main aim of this section is to theoretically develop a simple and accurate equation for quickly evaluating maximum drawing load (P_d) during deep drawing of adhesive bonded blanks for industrial applications. Already simple analytical models have been discussed and developed for estimating maximum drawing load (Korhonen, 1982; Leu, 1997; Leu and Wu, 2004). In these simple models, only the deep drawing of conventional monolayer sheet metals has been considered, and it has not been addressed about their applicability for estimating maximum drawing load during deep drawing of adhesive bonded blanks or multilayered sheet metals. Moreover, these analytical models include strain hardening exponent and normal anisotropy of monolayer sheet metals, friction coefficient and geometry of tools during evaluation of limiting drawing ratio (*LDR*). It is important to check the applicability of these models in the deep drawing of adhesive bonded blanks which constitute two dissimilar base metals, and a non-metal layer_(adhesive) between two sheets which does not exhibit strain hardening effect and anisotropy properties, and to develop a new simple model if these models are not applicable.

The cup drawing operation considered in the present study is shown in Fig. 8.2. A circular blank with original radius R_0 and total thickness t of adhesive bonded blanks is deep drawn by the flat-bottomed punch with small profile radius and the die opening of radius r_1.

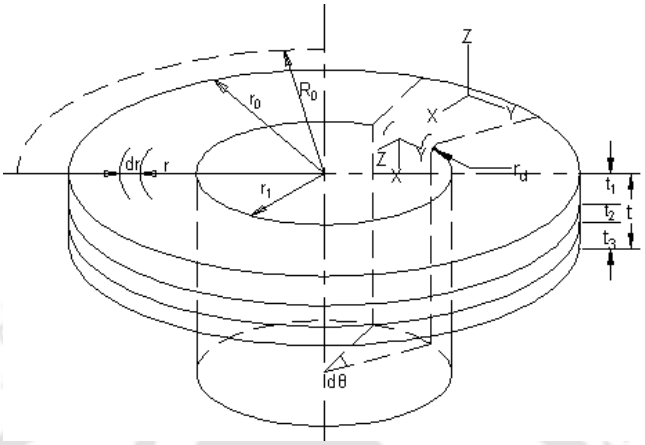

Fig. 8. 2 Schematic representation of cup drawing of adhesive bonded blanks

Normal anisotropy of the sheet is represented by a single parameter R calculated by the plastic strain ratio. The radially symmetric R-value is given by an average value of

$$R = \frac{R_0 + 2R_{45} + R_{90}}{4} \tag{8.1}$$

where R_0, R_{45}, R_{90} denote the value of R at 0°, 45°, and 90° to the rolling direction of the sheet, respectively.

The strain-hardening characteristic of the sheet is assumed to follow the Hollomon's power law

$$\sigma_e = K\varepsilon_e^n \tag{8.2}$$

where σ_e and ε_e refer to the effective stress and the effective strain, n is the strain hardening exponent and K is the strength coefficient of material.

The LDR (limiting drawing ratio at the state of critical drawing limit) was determined from the condition that the critical drawing load P_c causes tensile instability in the cup wall. For which the critical effective strain ε_e^c and the critical drawing load P_c (Leu, 1997; Leu and Wu, 2004) are given by,

$$\varepsilon_e^c = \frac{1+R}{\sqrt{1+2R}}n \tag{8.3}$$

$$P_c = 2\pi r_1 t\left(\frac{1+R}{\sqrt{1+2R}}\right)^{1+n}(n^n e^{-n} K) \tag{8.4}$$

where $(n^n e^{-n} K)$ denotes the tensile strength of material σ_u and t – blank thickness

In the present study, t = total thickness of adhesive bonded blanks = $t_1+t_2+t_3$, t_1 = thickness of DDQ steel, t_2 = thickness of adhesive layer and t_3 = thickness of SS 316L

The effective stress σ_e is assumed to be the critical effective stress, $\sigma_e^c = K\varepsilon_e^{cn}$, as

$$\sigma_e^c = K\left(\frac{1+R}{\sqrt{1+2R}}n\right)^n \tag{8.5}$$

In order to obtain the LDR, the radial force at the position r_1 in the cup wall, $P_{r1} = 2\pi r_1 t(1+F)\sigma_{r1}$ referred to Leu, 1997, Leu and Wu, 2004 can be written as

where radial stress, $\sigma_{r1} = \left(2\mu\sigma_e + \sqrt{\frac{2(1+R)}{1+2R}}\frac{\sigma_e}{1+n}\ln\frac{r_0}{r_1}\right) + \frac{t}{2r_d}\frac{1+R}{\sqrt{1+2R}}\sigma_e e^{-\mu\pi/2}$ (8.6)

then P_{r1} is written as

$$P_{r1} = 2\pi r_1 t(1+F)\left[\left(2\mu\sigma_e + \sqrt{\frac{2(1+R)}{1+2R}}\frac{\sigma_e}{1+n}\ln\frac{r_0}{r_1}\right) + \frac{t}{2r_d}\frac{1+R}{\sqrt{1+2R}}\sigma_e e^{-\mu\pi/2}\right] \tag{8.7}$$

where the factor F was used to represent the influence of unconsidered process parameters, such as shrinkage of die opening, variation of thickness etc. (Leu, 1997; Leu and Wu, 2004).

Due to continuity of stress, the P_c equals the radial drawing load force P_{r1} on the deep drawing limit, then the following relationship is obtained

$$\ln\frac{r_0}{r_1} = (1+n)\left[\left(fe^{-n} - \frac{t}{2r_d}e^{-\mu\pi/2}\right)\sqrt{\frac{1+R}{2}} - 2\mu\sqrt{\frac{1+2R}{2(1+R)}}\right] \tag{8.8}$$

where $f= 1/(1+F)$ refers to the factor of drawing efficiency (Leu, 1997; Leu and Wu, 2004) Based on the plane strain condition of the flange, the following term eq. (8.9) used for deriving LDR equation proposed by Leu, 1997 can be written as

$$\ln\frac{R_1}{r_1} = \sqrt{\frac{1+R}{2}}n \tag{8.9}$$

where R_1 refers to the original radius of r_1 before drawing. According to the condition of volume constancy of plastic deformation in the flange (eq. (8.10)), an equation for predicting the LDR was derived, eq. (8.12), by substituting Eqs. (8.8) and (8.9) into the relation of volume constancy given as eq. (8.11)

$$R_0^2 - r_0^2 = R_1^2 - r_1^2 \tag{8.10}$$

$$\frac{R_0}{r_1} = \sqrt{(R_1/r_1)^2 + (r_0/r_1)^2 - (r_1/r_1)^2} \tag{8.11}$$

$$\left[\frac{R_0}{r_1}\right]_c = LDR = \sqrt{e^{(1+n)[2fe^{-n} - e^{\mu\pi/2}t/r_d)\sqrt{(1+R)/2 - 4\mu\sqrt{(1+2R)/[2(1+R)]}}} + e^{2n\sqrt{(1+R)/2}} - 1} \tag{8.12}$$

where the subscript '*c*' refers to the critical condition of drawing limit.

Usually, an empirical linear equation

$$\frac{P_{\max}}{P_c} = \frac{DR - 1}{LDR - 1} \tag{8.13}$$

has been used to estimate the P_d from the DR. This empirical equation is formulated by the technique of linear curve fitting, and discussed by Korhonen, 1982 about the industrial usage of this empirical equation.

For a certain DR, a P_d will be produced during the drawing process. The critical condition of the drawing process, at the LDR, induces the P_c. Assuming the σ_e being constant, then the load ratio P_d/P_c was described (Leu and Wu, 2004) by the equation (8.7) as

$$\frac{P_{\max}}{P_c} = \frac{\ln(r_0/r_1)}{\ln(r_0/r_1)} \tag{8.14}$$

For practical purposes, it is assumed that the P_d may occur in the middle part of the punch stroke for a certain DR. Assuming constant thickness and the condition of volume constancy of plastic deformation in the flange, the above equation was rewritten by Leu, 1997 as

$$\frac{P_{\max}}{P_c} = \frac{\ln(DR^2 + 1) - 0.7}{\ln(LDR^2 + 1) - 0.7} \tag{8.15}$$

Further, eq. (8.12) was rewritten by Leu and Wu, 2004 as

$$\frac{P_{\max}}{P_c} = \frac{\sqrt{1 + DR^2} - \sqrt{2}}{\sqrt{1 + LDR^2} - \sqrt{2}} \tag{8.16}$$

These simple eqs. (8.13), (8.15) and (8.16) for estimating maximum drawing load were formulated by considering deep drawing process of monolayer sheet metals. In the present study, the applicability of these equations was checked for estimating the maximum drawing load during cup drawing of adhesive bonded blanks which constitute three different layers, such as DDQ steel, adhesive, and SS 316L. In order to obtain accurate estimation of maximum drawing load, the influence of blank holding force, friction around the die corner and the

bending effect were considered, and the combined mechanical effects were taken into account as a factor of drawing efficiency *f* during the evaluation of LDR.

In order to determine LDR (eq. (8.12)) which is function of normal anisotropy, strain hardening exponent, these data were evaluated through experiment, and the determined LDR was utilized in eqs. (8.13), (8.15) and (8.16) for estimating maximum drawing load. The plastic strain ratios of adhesive bonded blanks with different hardener/resin ratios and different CB wt.% were evaluated as per ASTM E517 standard. The rectangular strips made of adhesive bonded blanks were deformed till 10% strain (with reference to the failure of adhesive layer with minimum level of hardener/resin ratio of 0.6:1). The longitudinal, transverse and thickness strains were evaluated for evaluating plastic strain ratios in different rolling directions. The normal anisotropy of adhesive bonded blanks was determined by eq. (8.1) and tabulated in Table 8.1. The average normal anisotropy of DDQ steel and SS 316L sheets constituting adhesive bonded blanks were taken into account in the estimation of maximum drawing load (eqs. (8.13), (8.15), and (8.16)).

Table 8.1 Normal anisotropy of adhesive bonded blanks

Types of adhesive bonded blanks	Different levels	Average anisotropy *(R)* value of DDQ steel (R_{DDQ}) in adhesive bonded blanks	Average anisotropy *(R)* value of SS 316L (R_{SS}) in adhesive bonded blanks	Average anisotropy of adhesive bonded blanks $R = ((R_{DDQ}+R_{SS})/2)$
H/R ratio	0.6:1	1.706	1.617	1.662
	0.8:1	1.715	1.875	1.795
	1:1	1.799	1.853	1.826
CB wt.%	2 wt.%	1.861	1.851	1.856
	4 wt.%	1.845	1.861	1.853
	6 wt.%	1.821	1.720	1.771

The strain hardening exponent (n) and strength coefficient (K) evaluated in three deformation regions A, B, and C of adhesive bonded blanks tensile behaviour, and the average of n and K values (Table 8.2) were taken into account in the estimation of maximum drawing load. A constant coefficient of friction (μ) was considered during the estimation.

Table 8.2 Strain hardening exponent (n) and strength coefficient (K) of adhesive bonded blanks

Types of adhesive bonded blanks	Different levels	Average n-value	Average K-value in MPa
H/R ratio	0.6:1	0.366	439
	0.8:1	0.369	455
	1:1	0.399	448
CB wt.%	2 wt.%	0.414	474
	4 wt.%	0.394	458
	6 wt.%	0.384	450

8.6 Prediction of drawing load (P_d) – punch stroke (x) behaviour during deep drawing

In this work, a simple and accurate system of equations is also proposed by considering maximum load and punch-stroke for predicting the deep drawing behaviour of a blank. By this system of equations, the maximum drawing load obtained by anyone of the methods, such as experiment or numerical simulations can be utilised for predicting the drawing load during deep drawing of the sheet. The deep drawing behaviour is divided into two regions with the maximum load at the middle of the punch-stroke. The drawings load before and after maximum drawing load are predicted by eqs. (8.17) and (8.18) by relating maximum drawing load and punch-stroke (Fig. 8.3). This system of equations (8.17) and (8.18) is based on the exponential functions relating punch stroke and maximum drawing load. Different equations based like Boltzmann functions, double Boltzmann functions, Sigmoidal Richards function, Sigmoidal Weibull function and Gompertz Growth model to predict region A, and Asymptotic regression model, Box Lucas model and different exponential functions to predict region B which available in the basic literature were used. Finally, equations (8.17) and (8.18) are found to be more suitable for predicting the load-progression behaviour in the sheet metal deep drawing processes.

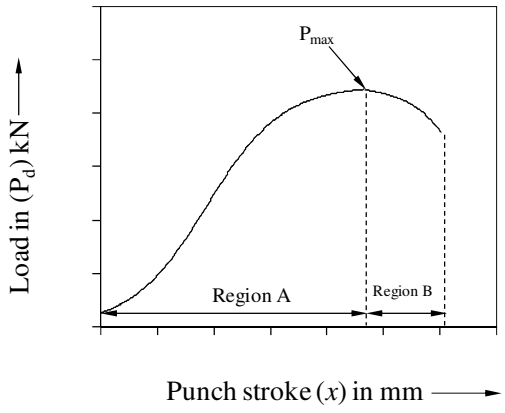

Fig. 8.3 General deep drawing behaviour of a sheet taken into consideration

$$\text{In region A} \rightarrow P_{d1} = \frac{P_{\max}}{1 + e^{-k_1(x - x_a)}} \tag{8.17}$$

$$\text{In region B} \rightarrow P_{d2} = P_{\max}\left(1 - e^{k_2(x - x_b)}\right) \tag{8.18}$$

where P_{max} = Maximum drawing load in kN (from experiments or numerical prediction or analytical models)

k_1 = 0.25 to 0.28

x = Punch stroke in mm

x_a = Punch stroke at $P_{max}/2$ in mm

k_2 = 0.2 to 0.4

x_b = Punch stroke at P_{max} + (10 to 20) in mm

8.7 Results and discussion

8.7.1 Tensile behaviour of epoxy adhesive

The comparison of true stress-strain behaviour of epoxy adhesive samples with different hardener/resin ratios obtained by approach-1 and approach-2 is already discussed in Chapter 5 in section 5.5.1 (Fig. 5.2(a, b)). Fig. 8.4 shows the comparison of true stress-strain behaviour of epoxy adhesive with different CB wt.% evaluated by approach-1 and approach-2.

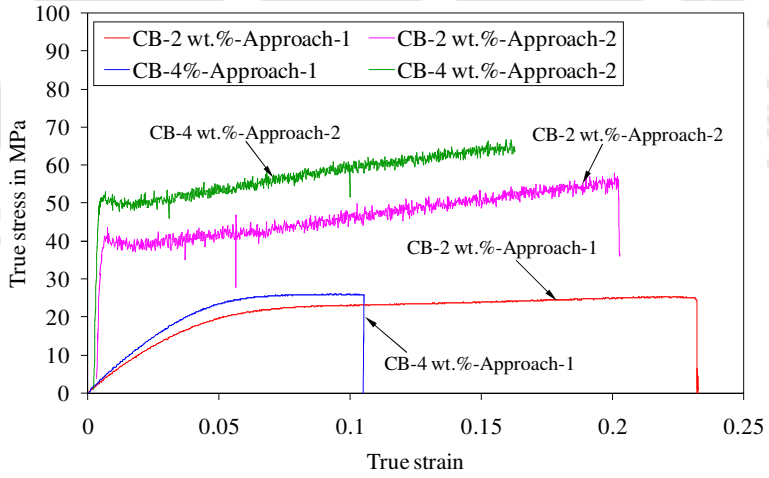

Variation in true stress at failure between approach-1 and approach-2:
CB-2 wt.% = 38.1 MPa; CB-4 wt.% = 31.9 MPa
Variation in true strain at failure between approach-1 and approach-2:
CB-2 wt.% = 5.8%; CB-4 wt.% = 2.9%

Fig. 8.4 Comparison of true stress-strain behavior of epoxy adhesive obtained by approach-1 and approach-2 with different wt.% of CB

In case of CB nano powder filled adhesive samples, the tensile behaviour obtained through approach-2 shows the same trend as approach-1, but a considerable difference in true stress at failure is observed (Fig. 8.4). There is about 10 MPa to 40 MPa variations in true stress and about 2% to 6% variations in true strain between approach-1 and approach-2.

8.7.2 Deformation pattern of adhesive layer constituting adhesive bonded blanks

The mesh sensitivity analysis was carried out during FE simulation of deep drawing process. Fig. 8.5 shows the cup height of SS 316L blank evaluated at the maximum load from the load-stroke behaviour with different average mesh size like 1 mm, 1.5 mm, 2 mm, and 2.5 mm during FE simulation of deep drawing test.

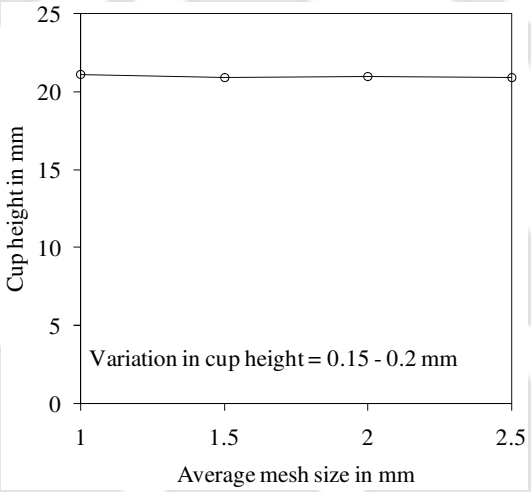

Fig. 8.5 Mesh sensitive analysis: (a) Limit strains – tensile test of DDQ steel with thickness of 0.6 mm, and (b) Cup height – deep drawing test of SS 316L with thickness of 2.1 mm

There is not much difference in the cup height (about 0.15 to 0.2 mm). These results reveal that the average mesh size from 0.5 mm to 2.5 mm do not influence the predicted results. From this evident result, the average mesh size of 2 mm in deep drawing process was chosen during prediction.

8.7.2.1 Delamination and thinning

The deformation pattern of adhesive layer constituting adhesive bonded blanks during experiment and FE simulation is shown in Fig. 8.6(a-h). There is a good agreement in the deformation pattern of adhesive bonded blanks between experiment and predicted results. Fig. 8.6(a, d) shows the failure pattern of adhesive layer in adhesive bonded blanks with different hardener/resin ratios. It is observed that the adhesive fails at the bottom corner of the cup before

drawing of successful cup of the adhesive bonded blanks with hardener/resin ratio of 0.6:1 (Fig. 8.6(a, b)). It is also observed from prediction that in the case of hardener/resin ratio of 0.6:1, after failure of the adhesive layer, it slides off prominently at the flange (Fig. 8.6(b)), as the base materials deform. This confirms that the adhesive layer with hardener/resin ratio of 0.6:1 is debonded during experimental cup drawing of adhesive bonded blanks. But in the case of adhesive bonded blanks with hardener/resin ratio of 1:1, the adhesive has failed at the wall of the cup at the end of maximum drawing or successful cup, and thinning of adhesive layer at the bottom corner of the cup is observed (Fig. 8.6(c)). The adhesive failure at the cup wall and thinning of adhesive indicates the plasticity of adhesive at 1:1 ratio during deep drawing. In the case of brittle adhesive (like 0.6:1 ratio), thinning is absent. From Fig. 8.6(d), it is clearly seen that the adhesive with hardener rich formulation (1:1) deform well with base materials. There is no adhesive failure at the wall as compared to experiment (Fig. 8.6(c)) after drawing full cup, but thinning is observed at the bottom corner of the cup.

Further, while comparing CB nano powder filled adhesive bonded blanks, the adhesive layer has not failed in the case of CB nano powder with its 2 wt.%. Also reduced thinning of adhesive layer is observed as compared to unfilled adhesive layer with hardener/resin ratio of 1:1 (Fig. 8.6(e, f)). In Fig. 8.6(f), increase in CB up to 2 wt.% in adhesive showing reduced thinning at the bottom corner of the cup of adhesive bonded blanks is clearly seen. From Fig. 8.6(g, h), it is noted that the adhesive fails at the bottom corner of cup at the end of drawing of successful cup in the case of 6 wt.% of CB filled adhesive bonded blanks. In the case of CB with 6 wt.%, the adhesive failure is observed, but there is no sliding of adhesive during drawing of adhesive bonded blanks (Fig. 8.6(h)).

This reveals that the adhesive has failed at the completion of drawing successful cup. From these results, it is perceived that the resin rich formulation which turns the adhesive layer brittle in nature imparts its validity or existence without failure in the deep drawing of adhesive bonded blanks up to a certain limit of drawing a cup (about 12 mm in the present work). In the case of hardener rich formulation (1:1) of adhesive layer, it exists without failure till drawing of a successful cup. In the case of CB nano powder filled adhesive, it reduces severe thinning, and delays the failure of in response to 2 wt.% and 6 wt.% as shown in Figs. 8.6(c-h).

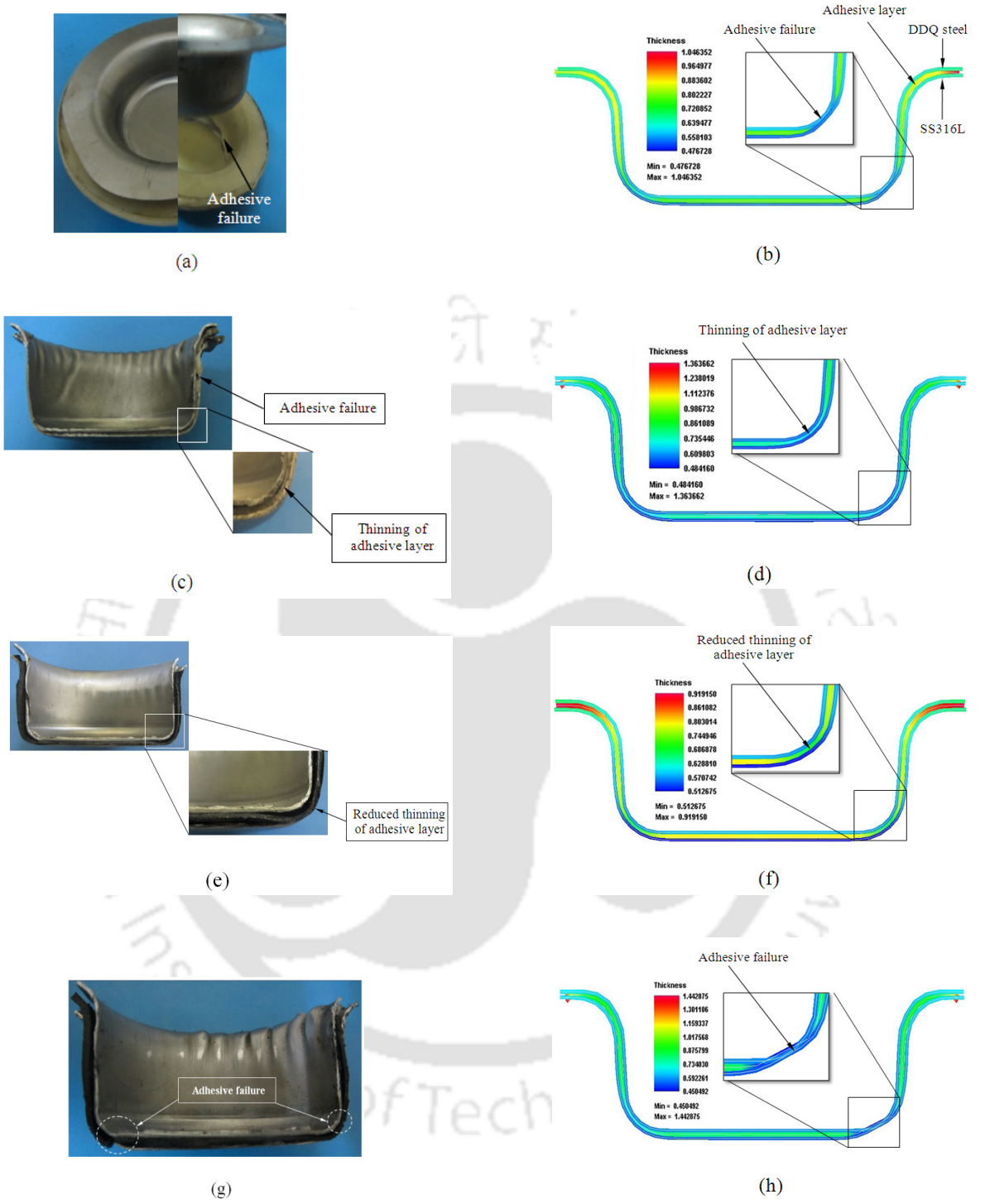

Fig. 8.6 Deformation pattern of adhesive layer constituting adhesive bonded blanks: (a) H/R = 0.6:1 (Experiment), (b) H/R = 0.6:1 (Prediction), (c) H/R = 1:1 (Experiment), (d) H/R = 1:1 (Prediction), (e) CB-2 wt.% (Experiment), (f) CB-2 wt.% (Prediction), (g) CB-6 wt.% (Experiment), and (h) CB-6 wt.% (Prediction)

8.7.2.2 Wrinkling behaviour of adhesive bonded blanks

The wrinkling behaviour of adhesive bonded blanks with different hardener/resin ratios, and with different CB wt.% during experiments is shown in Fig. 8.7(a-d). The predicted wrinkling behaviour is shown in Fig. 8.8(a-d). It is noted that the wrinkling in base materials constituting adhesive bonded blanks decreases considerably for increasing hardener/resin ratio (Fig. 8.7(a-b)). During cup drawing of adhesive bonded blanks, the resin rich formulated adhesive (0.6:1) has been failed before drawing successful cup (Fig. 8.6(a, b)). Further drawing of adhesive bonded blanks slides out the adhesive layer as the base materials deform. This instability and imperfections in the geometry of adhesive bonded blanks increases the wrinkling in base materials during deep drawing process (Fig. 8.7(a)). In the case of bonded blanks with hardener rich formulation (H/R = 1:1), the adhesive layer has been drawn along with base materials till completion of successful cup (Fig. 8.6(c, d)). The reduced instability and imperfection in the geometry of adhesive bonded blanks by adhesive layer reduces wrinkling in the base materials (Fig. 8.7(b)). While comparing the wrinkling behaviour of adhesive bonded blanks filled with CB (Fig. 8.7(c, d)), no wrinkling is observed in the case of adhesive bonded blanks filled with 2 wt.% of CB due to significant increase in plasticity of adhesive (Fig. 8.7(c)). The excessive addition of CB (6 wt.%) in the adhesive is entrapped in between the wrinkled region of base materials and failed (Fig. 8.7(d)) during deep drawing process. This reveals that the excessive formulation of CB makes softer the adhesive layer, which also imparts instability in base materials during cup drawing, and results in unwanted wrinkling.

When comparing the wrinkling pattern of adhesive bonded blanks during prediction (Figure 8.8(a-d)), the DDQ steel blanks positioned as the top layer is not wrinkled till drawing of successful cup in all the cases. While comparing Figs. 8.8(a) and 8.8(b), there is not much difference in the wrinkling pattern of adhesive and SS316L which is bottom layer. In the case of CB filled adhesive bonded blanks also; there is not much difference in the wrinkling pattern (Fig. 8.8(c, d)).

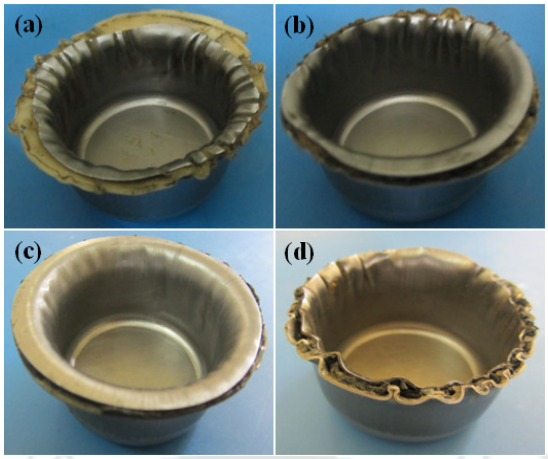

Fig. 8.7 Comparison of wrinkling of adhesive bonded blanks from experiment: (a) H/R = 0.6:1, (b) H/R = 1:1, (c) CB-2 wt.%, and (d) CB-6 wt.%

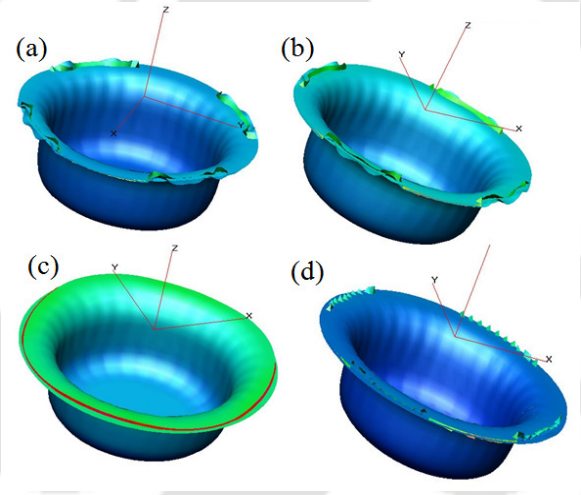

Fig. 8.8 Comparison of wrinkling of adhesive bonded blanks from FE simulation: (a) H/R = 0.6:1, (b) H/R = 1:1, (c) CB-2 wt.%, and (d) CB-6 wt.%

This reveals that the base materials have been deformed as like monolayer of base materials. The imperfection in the geometry of adhesive bonded blanks made by the adhesive layer during cup drawing results in some wrinkling pattern in the bottom layer of SS316L in the case of different hardener/resin ratios of adhesive. It is believed that these inaccuracies in wrinkling pattern during simulation are due to the (i) absence of interface bonding between adhesive and base materials, (ii) approximation in BHF applied during experiment and in simulations, and (iii) selection of yield function during modelling.

Fig. 8.9 shows the comparison of load-stroke behaviour of base materials (DDQ steel and SS 316L) deep drawn as monolayer between experiment and prediction. There is no significant

difference in load-stroke behaviour of base materials between experiment and prediction. Both the results are correlating well with each other.

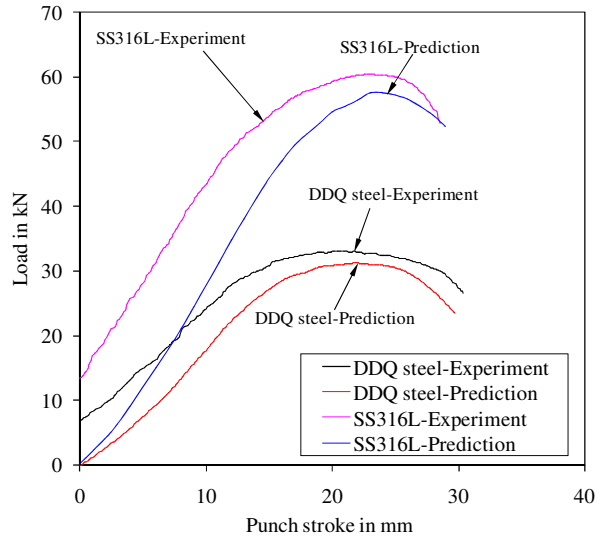

Variation in maximum load during experiment:
DDQ steel = 0.75 kN; SS 316L = 1.5 kN
Variation in punch stroke at maximum load duirng experiment :
DDQ steel = 1.5 mm ; SS 316L = 1 mm
Variation in maximum load between experiment and prediction:
DDQ steel = 2 kN; SS 316L = 2.8 kN
Variation in punch stroke at maximum load between experiment and prediction :
DDQ steel = 1 mm; SS 316L = 1.3 mm

Fig. 8.9 Comparison of load-progression behaviour of base materials between experiment and prediction

8.7.2.3 Deep drawability prediction of un-bonded and adhesive bonded blanks

The load-stroke behaviour of adhesive bonded blanks with different hardener/resin ratios and different CB wt.% is shown in Fig. 8.10(a, b). The load-stroke behaviour of monolayer of DDQ steel and SS316L blanks, and two base materials drawn together without any adhesive (called double blank) are also shown in Fig. 8.10(a). It is observed that the punch stroke of adhesive bonded blanks increases (an indication of increase in drawability) with increase in hardener/resin ratio in response to the maximum load from the deep drawing behaviour. This increase in punch stroke at maximum drawing load with increase in hardener/resin ratio is larger than the punch stroke at maximum load in deep drawing of double blank and monolayer of base materials. Similarly, from Fig. 8.10(b), it is noted that the punch stroke on adhesive bonded blanks increases with increase in CB up to 2 wt.% as compared to unfilled adhesive bonded blank with hardener/resin ratio of 1:1, and then decreases with excessive addition of CB wt.%.

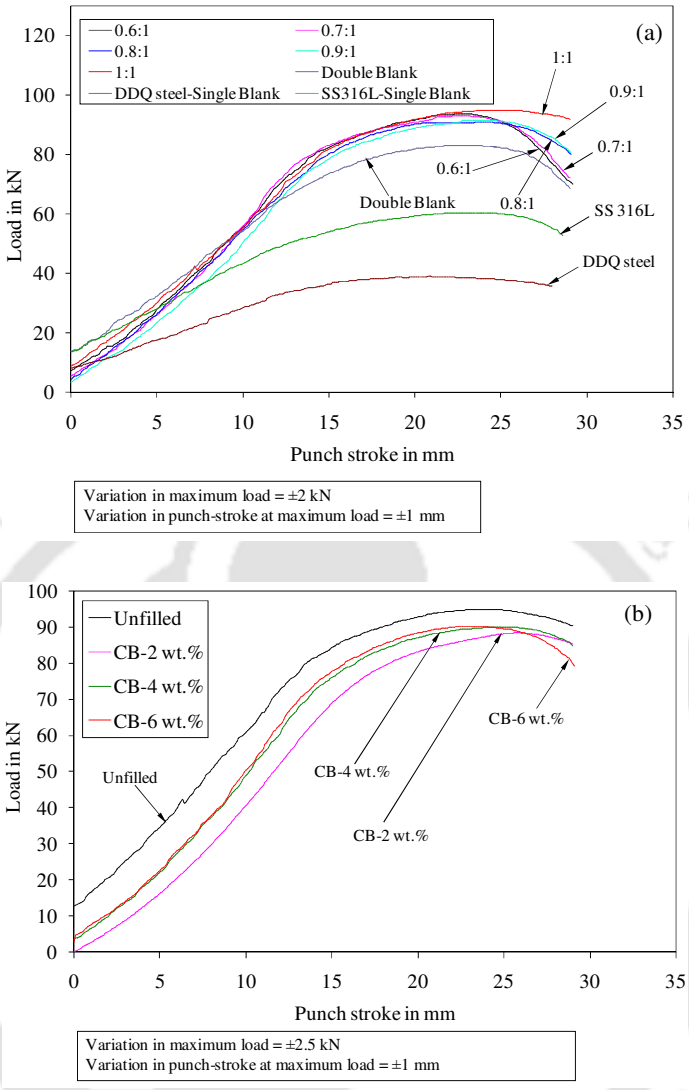

Fig. 8.10 Load-stroke behaviour of adhesive bonded blanks from experiment: (a) different hardener/resin ratios, and (b) different CB wt.%

Fig. 8.11(a-d) presents the comparison of load-stroke behaviour of adhesive bonded blanks between experiment and prediction by approach-1 and approach-2. There is not much difference in load-stroke behaviour predicted by approach-1 and approach-2. There is about 12 kN to 17 kN variations in maximum load, and from 2.7 mm to 6.2 mm difference in punch-stroke between experiment and prediction by approach-1. Similarly, from 5.42 kN to 18.3 kN variations in maximum load, and about 2.7 mm to 5.7 mm variations in punch-stroke between experiment and prediction by approach-2 are observed. Generally, it is observed that the initial load which has been exhibited to deform the blanks by punch varies from 2 kN to 15 kN in all the cases during experiment.

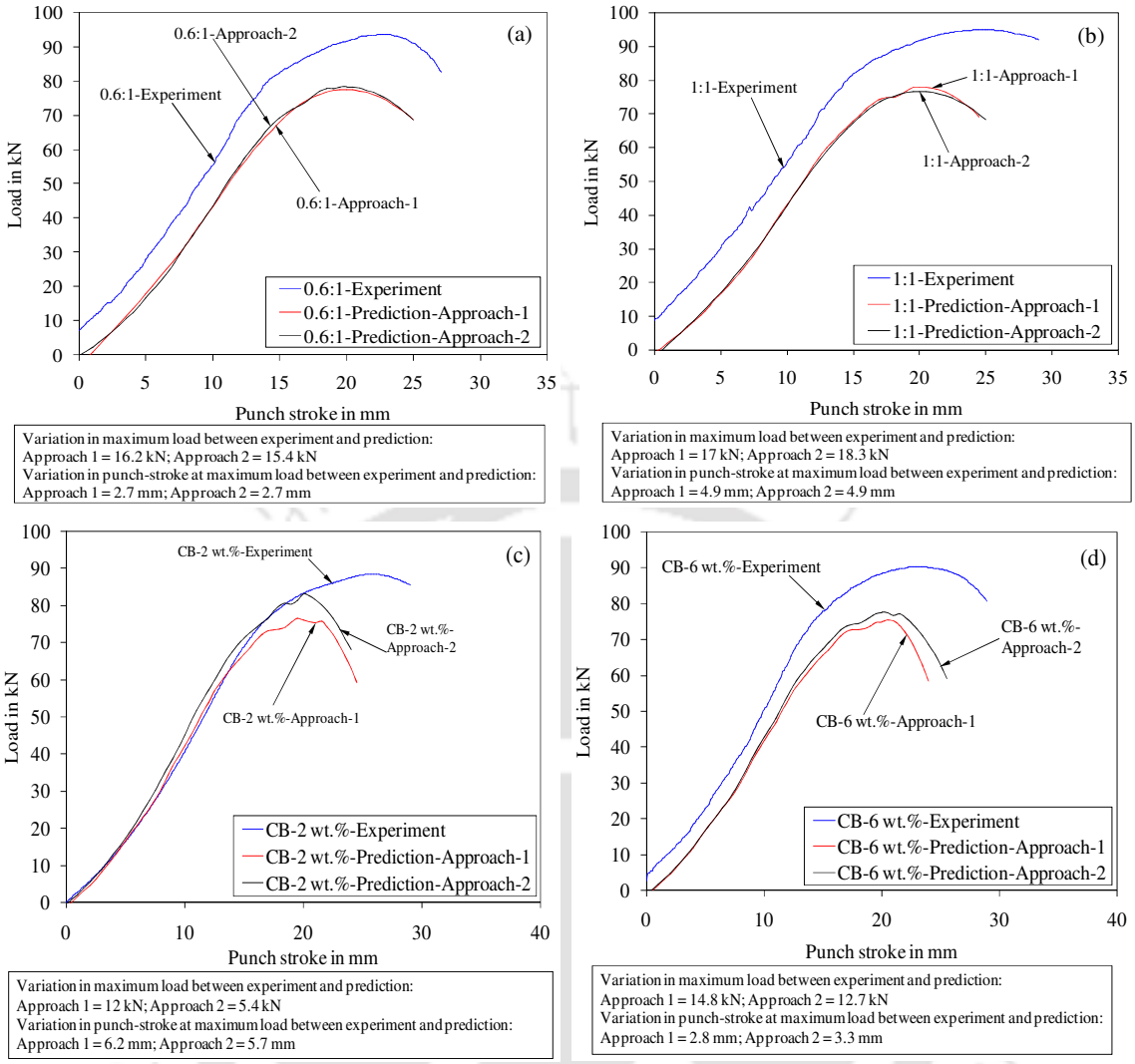

Fig. 8.11 Comparison of load-stroke behaviour of adhesive bonded blanks between experiment and prediction (a) H/R = 0.6:1, (b) H/R = 1:1, (c) CB – 2 wt.% and (d) CB – 6 wt.%

From these results, the cup height determined at maximum load with respect to base materials and double blank, adhesive bonded with different hardener/resin ratios, and with different CB wt.% are shown in Fig. 8.12(a), (b) and (c), respectively. There is not much difference in cup height between monolayer SS316L and double blank (Fig. 8.12(a)). The cup height increases with increase in hardener/resin ratio during experiment, and about 4.5% to 11.5% variation in cup height between experiment and prediction by both the approaches.

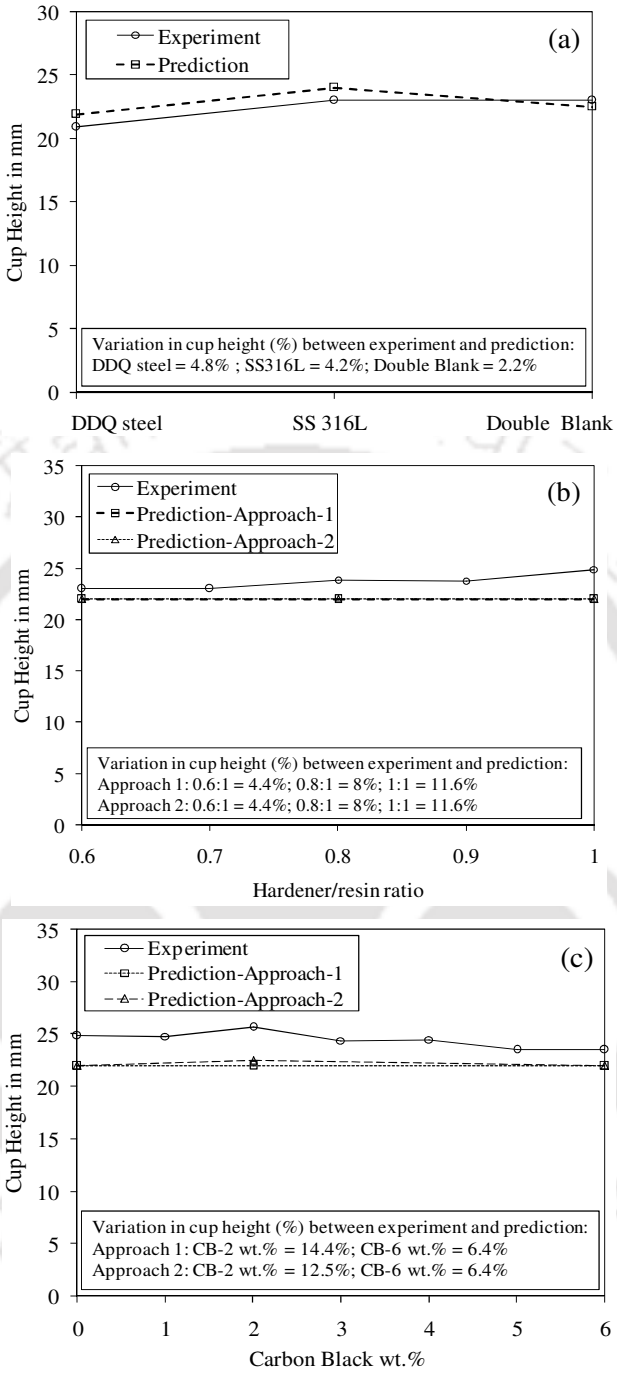

Fig. 8.12 Comparison of cup height at maximum load between experiment and prediction: (a) Monolayer of base materials and double blank, (b) Adhesive bonded blanks with different hardener/resin ratios, and (c) Adhesive bonded blanks with different CB wt.%

When comparing cup height with the effect of CB filled adhesive bonded blanks, the cup height increases with increase in CB up to 2 wt.%, and then decreases with excessive addition of CB. The trend in cup height of adhesive bonded blanks influenced by the adhesive properties

(different H/R ratios and CB wt.%) is not clearly captured during predictions by both the approaches as that of experimental results. About 6.5% to 14.5% difference in cup height between experiment and prediction by approach-1, and 6.5% to 12.5% between experiment and prediction by approach-2 are observed. It is believed that this inaccurate trend in cup height is due to the absence of interface bonding between adhesive and base materials, and incorporation of only the mechanical properties of adhesive behaviour during modelling. From these results, it is understood that the hardener rich formulation increases the plasticity of adhesive, thereby increases the drawability of constituting adhesive bonded blanks. Further, filling of CB nano powder to the optimum wt.% (up to 2 wt.% in the present work) in adhesive increases the drawability of adhesive bonded blanks. Though the effect of hardener/resin ratio and CB wt.% on adhesive is not captured accurately, the overall results from deep drawing behaviour of adhesive bonded blanks moderately correlate with the experimental results.

8.7.3 Comparison of estimated maximum drawing load from analytical equations

Fig. 8.13(a-c) shows the comparison of maximum drawing load (P_{max}) estimated by (i) empirical equation (8.13) and eqs. (8.15) and (8.16), (ii) experiment, and (iii) numerical predictions using adhesive properties from approach-1 and approach-2. It is observed that the estimated maximum drawing loads by empirical eq. (8.13) (Korhonen, 1982), eq. (8.15) (Leu, 1997) and eq. (8.16) (Leu and Wu, 2004) show good agreement with the experiments than numerically predicted results. Though there is not much difference in the maximum drawing load between estimations by eqs. (8.13), (8.15) and (8.16), and experiment, the eq. (8.16) developed by Leu and Wu, 2004 shows less difference of about 2.3 kN to 5.2 kN as compared to other eqs. (8.13) and (8.15). There is not much variation in the maximum drawing load between numerically predicted, estimated and experimental cup drawing of monolayer base materials. During deep drawing of adhesive bonded blanks, about 6 kN to 18 kN variation in maximum drawing load is observed between numerical prediction and experiment. Though the influencing parameters, such as strain hardening exponent (n), normal anisotropy (R), strength coefficient (K) and coefficient of friction (μ) are common in both the estimated and numerically predicted maximum drawing load, the factor of drawing efficiency (f) and coefficient of friction (μ) play a vital role in the estimation of maximum drawing load, improving the accuracy.

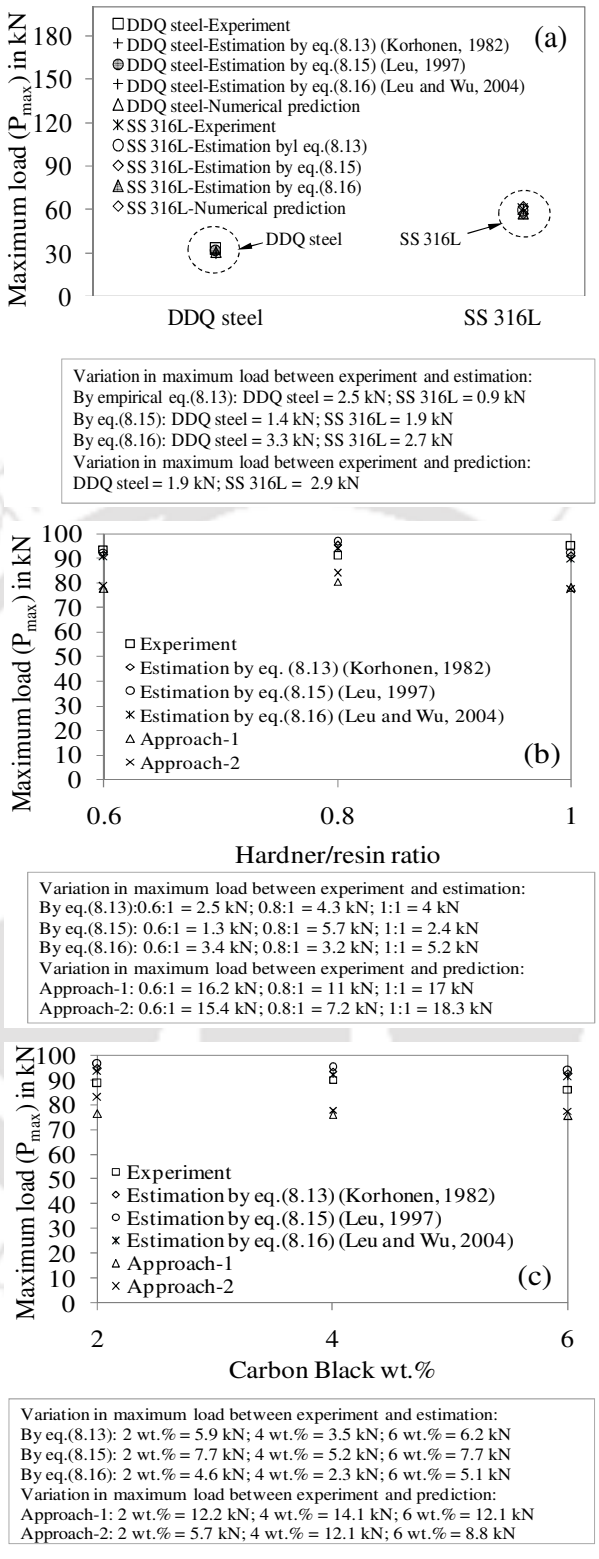

Fig. 8.13 Comparison of maximum drawing load between experiment, estimation and numerical simulation (During estimation by eqs.(8.13) (Korhonen, 1982), (8.15) (Leu, 1997), (8.16) (Leu and Wu, 2004), f = 0.98 and μ = 0.05): (a) Base materials, (b) adhesive bonded blanks with different hardener/resin ratio, and (c) adhesive bonded blanks with different CB wt.%

There is no considerable variation in maximum drawing load estimated between approach 1 and approach 2. It is checked that the eqs. (8.13), (8.15) and (8.16) are applicable for estimating the maximum drawing load during deep drawing of adhesive bonded blanks as well as monolayer base materials, and eq. (8.16) developed by Leu and Wu, 2004 shows more suitability for the estimation of maximum drawing load.

8.7.4 Prediction of load – progression behaviour through maximum load estimation

Fig. 8.14(a-h) shows the comparison of deep drawing behaviour of monolayer base materials and adhesive bonded blanks obtained from experiments and predicted by the proposed system of equations (8.17) and (8.18) for drawing load. The deep drawing behaviour of monolayer and adhesive bonded blanks was predicted by proposed model (eqs. (8.17 and 8.18)) with maximum load from experiment, numerical prediction (approach 1 in the case of adhesive bonded blanks), and by eq.(8.16) (Leu and Wu, 2004).

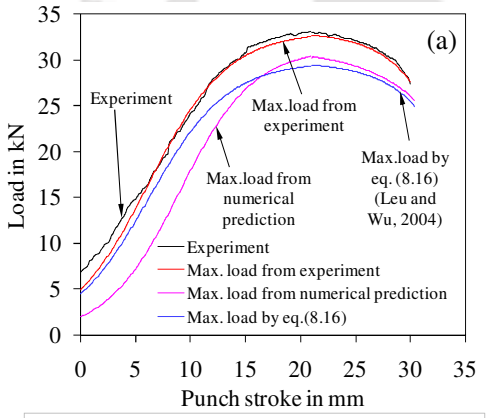

Variation in max. load between experiment and predicted by proposed model with max.load from experiment = 0.35 kN; numerical prediction = 2.7 kN; by eq. (8.16) = 3.7 kN

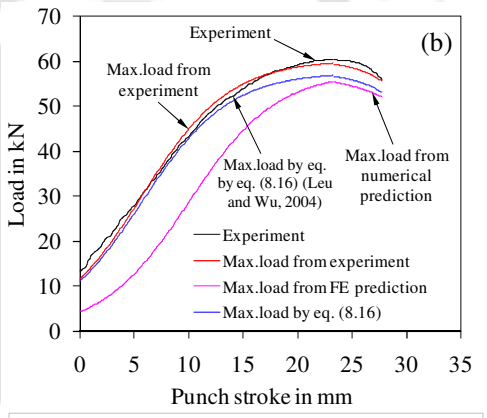

Variation in maximum load between experiment and predicted by proposed model with max.load from experiment = 0.75 kN; numerical prediction = 5 kN; by eq.(8.16) = 3.5 kN

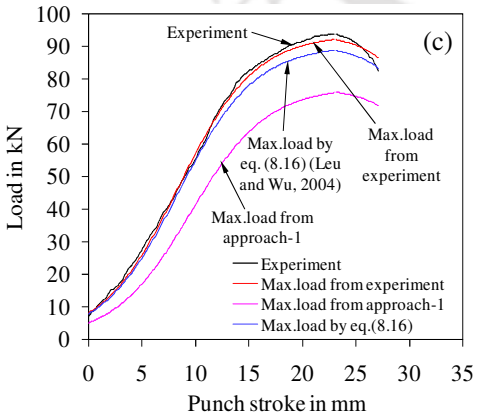

Variation in maximum load between experiment and predicted by proposed model with max.load from experiment = 1.6 kN; approach-1 = 18 kN; by eq.(8.16) = 5 kN

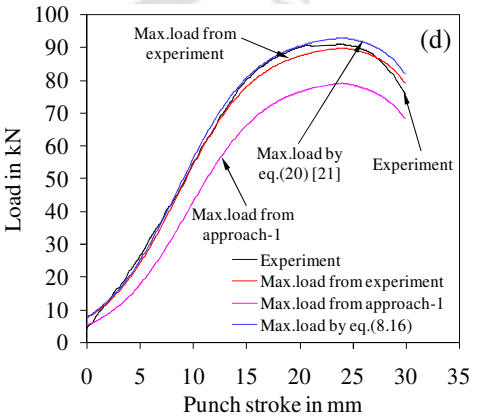

Variation in maximum load between experiment and predicted by proposed model with max.load from experiment = 1 kN; approach-1 = 12 kN; by eq.(8.16) = 2 kN

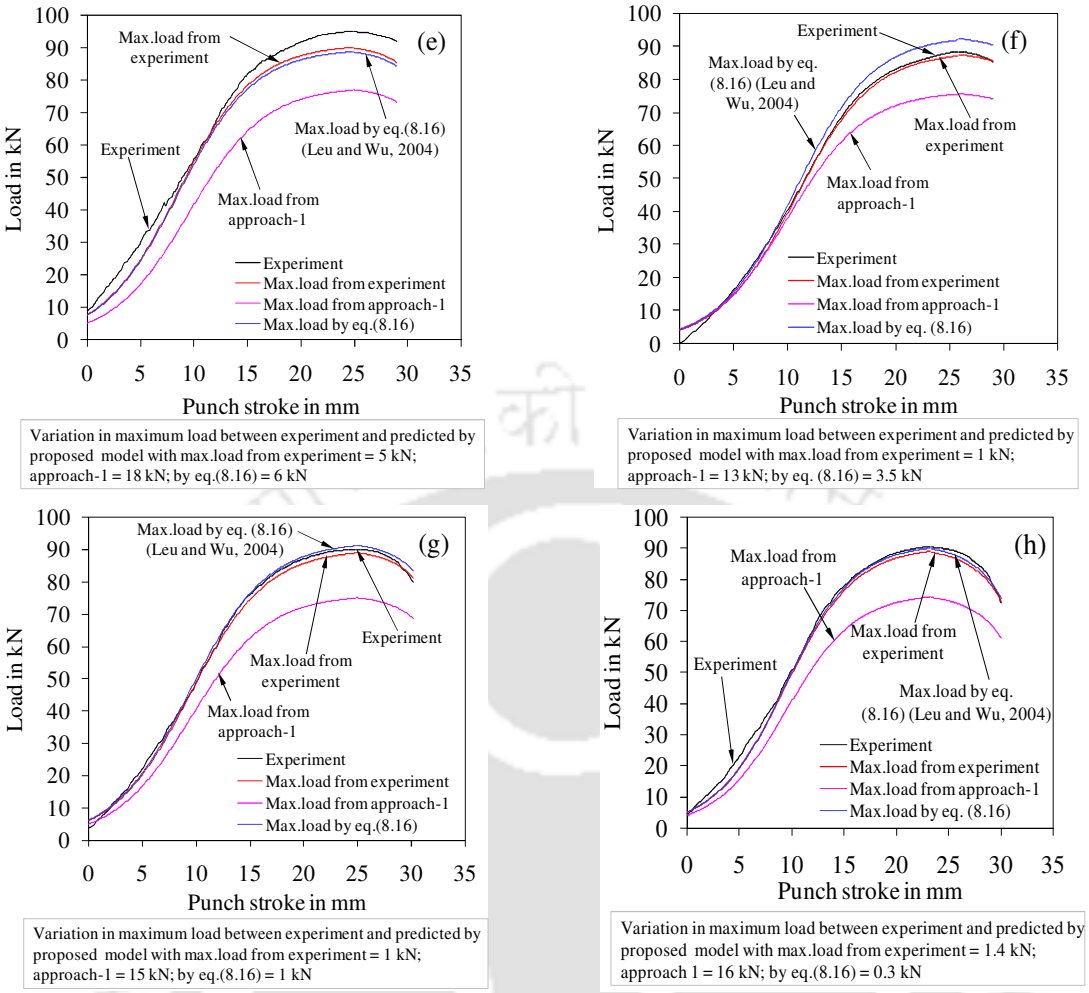

Fig. 8.14 Comparison of deep drawing behaviour between experiment and proposed model by eqs. (8.17 and 8.18) with max. load from experiment, numerical prediction and by eq.(8.16): (a) DDQ steel, (b) SS 316L, (c) ABB with H/R = 0.6:1, (d) ABB with H/R = 0.8:1, (e) ABB with H/R = 1:1, (f) ABB with CB = 2 wt.%, (g) ABB with CB = 4 wt.% and (h) ABB with CB = 6 wt.% (ABB-Adhesive bonded blanks)

The predicted results show a good correlation with the maximum load obtained from experiment and by eq. (8.16) (Leu and Wu, 2004) with the experimental results. But there is a considerable variation in maximum load about 2.7 kN to 18 kN between prediction by proposed model (eqs. (8.17 and 8.18)) and experiment with the maximum load from numerical prediction.

Since the proposed system of equations does not include material properties, yield criteria, geometry details, friction conditions, anisotropy properties for predicting deep drawing behaviour, this could be applicable for all types of monolithic and multilayered sheets. Particularly, for adhesive bonded blanks that constitute three different layers, this system of equations could be a simple approach to predict the deep drawing behaviour without bothering about interface bonding and yield criteria. The main advantage of the proposed system of

equations is that the history of drawing load could be captured by relating only the maximum drawing load obtained by anyone of the methods, such as experiment, numerical simulations (or) theoretical estimation, and the punch-stroke quickly for the industrial applications.

8.8 Conclusions

The following conclusions are derived from the present work.

- The resin rich formulation of adhesive reduces the deep drawability of adhesive bonded blanks; whereas the hardener rich formulation of adhesive improves the deep drawability of adhesive bonded blanks due to the increased plasticity of adhesive layer.
- Filling of carbon black in adhesive to the optimum level reduces the thinning of adhesive layer without any failure of constituting adhesive bonded blanks and improves the drawability. This is due to increased plasticity of adhesive by carbon black up to an appropriate level (up to 2 wt.% in the present study).
- The wrinkling of adhesive bonded blanks decreases with increase in hardener/resin ratio, and there is no wrinkling in adhesive bonded blanks by filling carbon black up to 2 wt.%.
- The deep drawability of adhesive bonded blanks predicted by approach-1 and approach-2 shows moderate variations in load-stroke behaviour and cup height results between experimental results. The predicted failure pattern of adhesive bonded blanks shows good agreement with experimental results.
- There is a considerable difference in wrinkling pattern between experiment and prediction by both the approaches.
- There is not much difference in the predictions by approach-1 and approach-2. It is suggested that the adhesive properties could be incorporated either by approach-1 or approach-2 during prediction of deep drawing of adhesive bonded blanks. It is believed that the inaccuracies in the predictions as compared to experiments may be due to the absence of interface bonding between adhesive and base materials.
- It is recommended that taking average normal anisotropy of base materials constituting adhesive bonded blanks, and average strain hardening exponent in all the deforming regions (A, B and C) into account during estimation of maximum drawing load by eqs. (8.13) (Korhonen, 1982), (8.15) (Leu, 1997) and (8.16) (Leu and Wu, 2004) which provides good agreement with the experimental results.
- It is suggested from the present work that the maximum drawing load could be estimated by using anyone of the simple equations, such as eq. (8.13) (Korhonen, 1982), eq.(8.15)

developed by Leu, 1997 or eq. (8.16) developed by Leu and Wu, 2004 and the deep drawing behaviour could be predicted by the proposed system of eqs. (8.17) and (8.18), instead of modelling adhesive and its interface bonding between base materials. This method of approach is not only applicable for adhesive bonded blanks, but also for all types of sheets for predicting their deep drawing behaviour. This method could be applicable for industrial purpose for sorting out quick decisions.

Chapter 9

Estimation of formability and deep drawability of adhesive bonded sheets using equivalent geometrical heterogeneities

9.1 Methodology

The mechanical properties of base materials and epoxy adhesive are already discussed in Chapter 2 in Sections 2.1.1 and 2.4.1, respectively. The fabrication methodology of adhesive bonded blanks, tensile testing, and evaluation of limit strains of base materials constituting adhesive bonded blanks are already discussed in Chapter 2 in Section 2.3. The fabrication of adhesive bonded circular blanks is already discussed in Chapter 8 in Section 8.3. The deep drawing process and evaluation of final cup height of adhesive bonded blanks are carried out as discussed in Chapter 7 in Section 7.2.

9.2 Prediction of forming behaviour of adhesive bonded blanks using geometrical heterogeneities

In the prediction of forming behaviour of base materials constituting adhesive bonded blanks with the effect of different hardener/resin ratios of adhesive, different initial geometrical heterogeneities were adapted. The initial geometrical heterogeneities adapted in the present work are broadly classified into two types namely infinite geometrical heterogeneity and finite geometrical heterogeneity. In the present analysis, the initial finite geometrical heterogeneities are surrounded by the bulk material in all the directions, whereas the initial infinite geometrical heterogeneities are not surrounded by the bulk material in one of the directions.

In the finite element (FE) simulation, the average mesh size of 0.5 mm was used in the tensile specimen during tensile test, and 2 mm was chosen in the circular blanks during deep drawing process. Considering the tensile test sample or circular shape blank having homogeneous material properties but varying thickness in two regions, 'a' and 'b', the heterogeneity factor is given as $f = t_a/t_b$ (where t_a – thickness in the groove region, and t_b – thickness in the bulk region). For the fully homogeneous sheet material, $f = 1$, the limit strain attains a large value. Different types of infinite

and finite initial geometrical heterogeneities were used during tensile tests, and finite geometrical heterogeneity was used during deep drawing process. In the present work, the geometrical heterogeneity refers to thickness heterogeneity in the base materials in all the cases.

9.2.1 Prediction of forming behaviour of adhesive bonded blanks during tensile test

During tensile test, one of the base materials constituting adhesive bonded blanks, i.e., DDQ steel was selected for the present demonstration. The initial infinite geometrical heterogeneities like (i) rectangular-infinite groove (Fig. 9.1(a)) running along the width or transverse direction of the tensile sample was analysed with different widths, w = 0.5, 1, 1.5, 2, 2.5, and 3 at various heterogeneity factor 'f' during prediction of limit strains, (ii) square hole (no material in the thickness direction of the sheet) (Fig. 9.1(b)) at different size with a side of 'w' was analysed, and the limit strains were predicted. In the case of initial finite geometrical heterogeneity, square-finite groove (Fig. 9.1(c)) was analysed at different size with a side, w = 0.5, 1, 1.5, 2, 2.5, 3, and 3.5 at various heterogeneity factor 'f'. The properties of SS 316L were incorporated as given in Table 2.2 (Chapter 2). The thickness of DDQ steel sheet was chosen as 2.2 mm, which is equivalent to the thickness of whole adhesive bonded blanks in experiments. The total number of elements was 5302. The limit strains were predicted using effective strain rate criterion (ESRC) as discussed in Chapter 4 in Section 4.3.2.

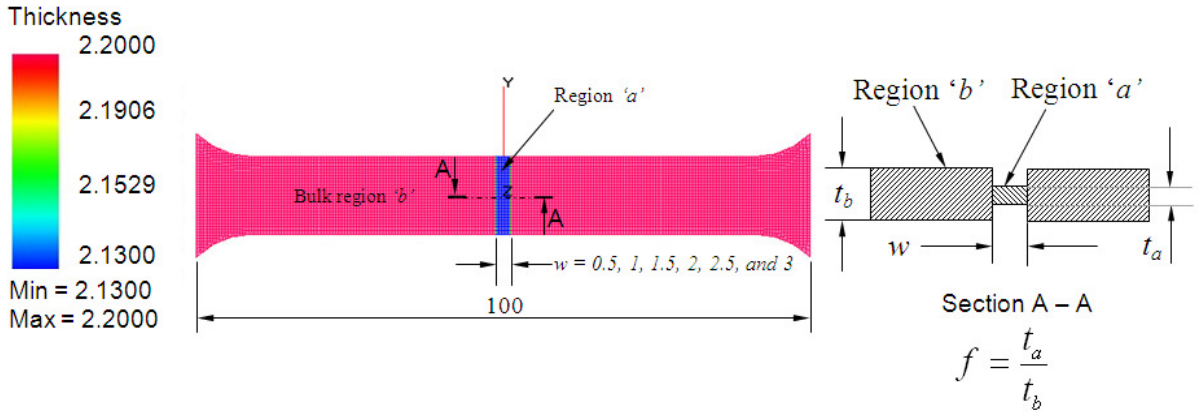

(a)

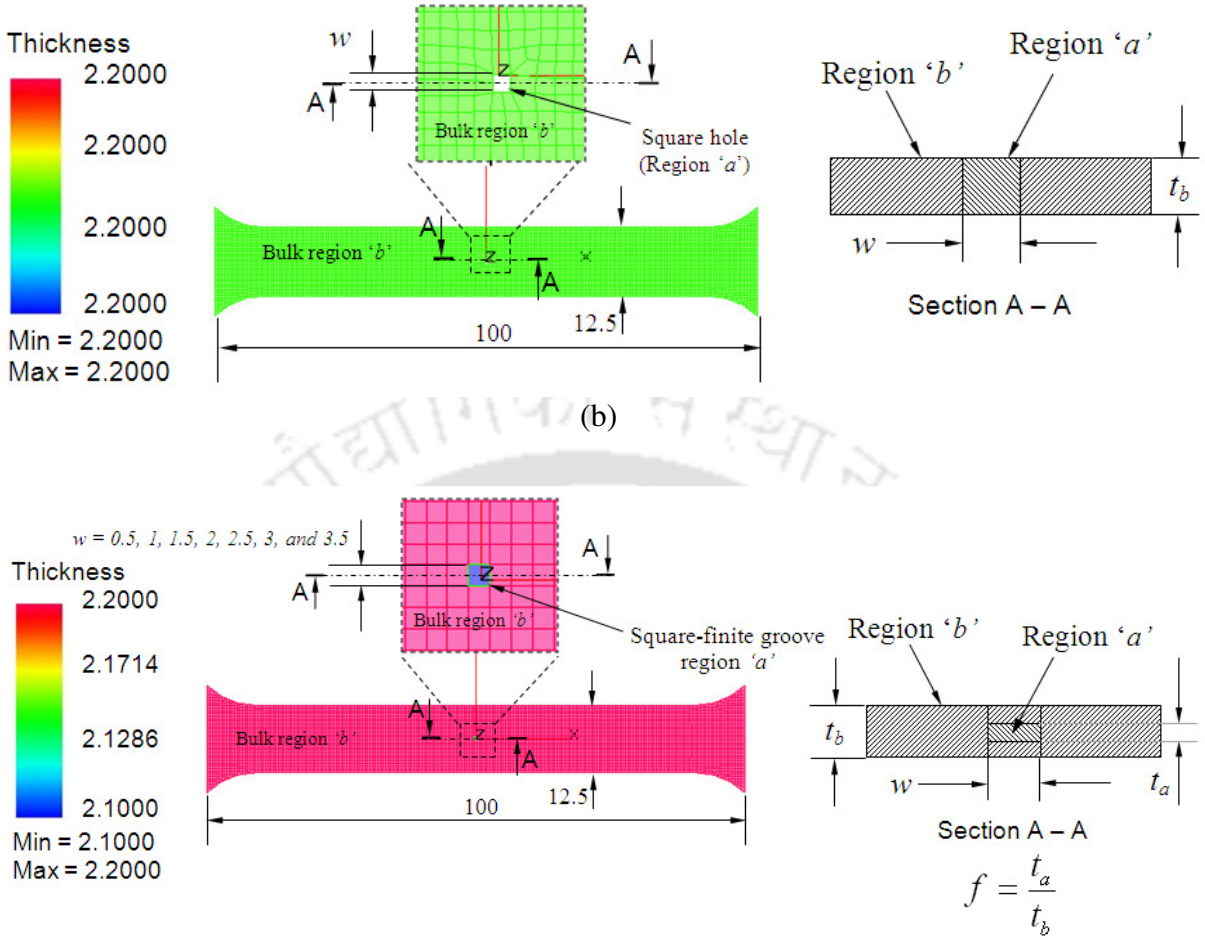

Fig. 9.1 FE models with (a) rectangular-infinite groove in region *'a'* (initial infinite geometrical heterogeneity), (b) square hole in region *'a'* (initial infinite geometrical heterogeneity), and (c) square-finite groove in region *'a'*, (initial finite geometrical heterogeneity) (All dimensions in 'mm')

9.2.2 Deep drawability prediction of adhesive bonded blanks

During deep drawing process, one of the base materials constituting adhesive bonded blanks i.e., the SS 316L was chosen for the demonstration. In the prediction, initial finite geometrical heterogeneity in the circular blank of SS 316L was considered. The circular-finite groove (Fig. 9.2) in region *'a'* with different diameters, d_1 = 50, 60, and 70 during deep drawing process were analysed at various *'f'* values to predict the cup height that is equivalent to the effect of hardener/resin ratio of adhesive. The thickness of SS 316L sheet was chosen as 2.1 mm, which is equivalent to the thickness of whole adhesive bonded blanks. The total number of elements was

3552. The properties of SS 316L were incorporated as given in Table 2.3 (Chapter 2). The imposed force on blank holder was 5 kgf, and coefficient of friction between contact surfaces was 0.12 simulating dry friction condition. The cup height was evaluated at the maximum load in the load-stroke behaviour.

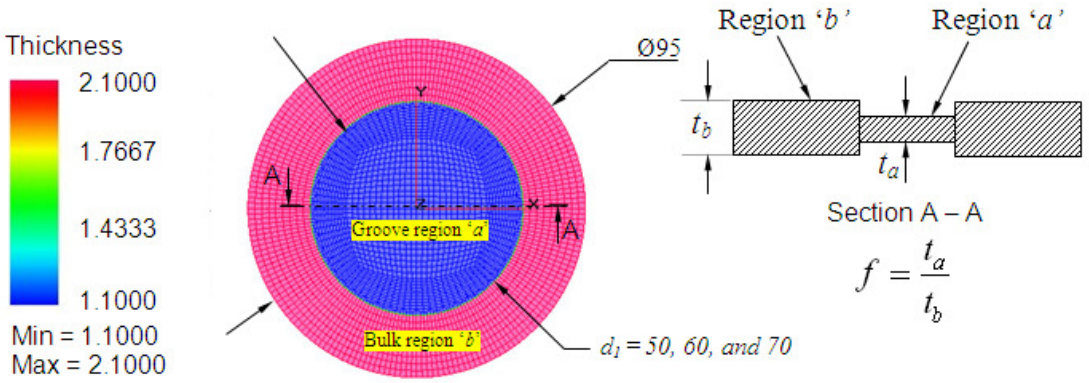

(d)

Fig. 9.2 FE model of circular blank showing the initial finite heterogeneity (circular-finite groove) in region *'a'* (All dimensions in 'mm')

In the tensile test and the deep drawing process, the strain-hardening behaviour description, and plasticity model selection for DDQ steel and SS 316L sheet materials were done as discussed in Chapter 4 in Section 4.3. The predicted results were validated with the experimental results. Fig. 9.3 describes the methodology of predicting the forming behaviour of base materials constituting adhesive bonded blanks with different initial geometrical heterogeneities equivalent to the effect of hardener/resin ratio of adhesive.

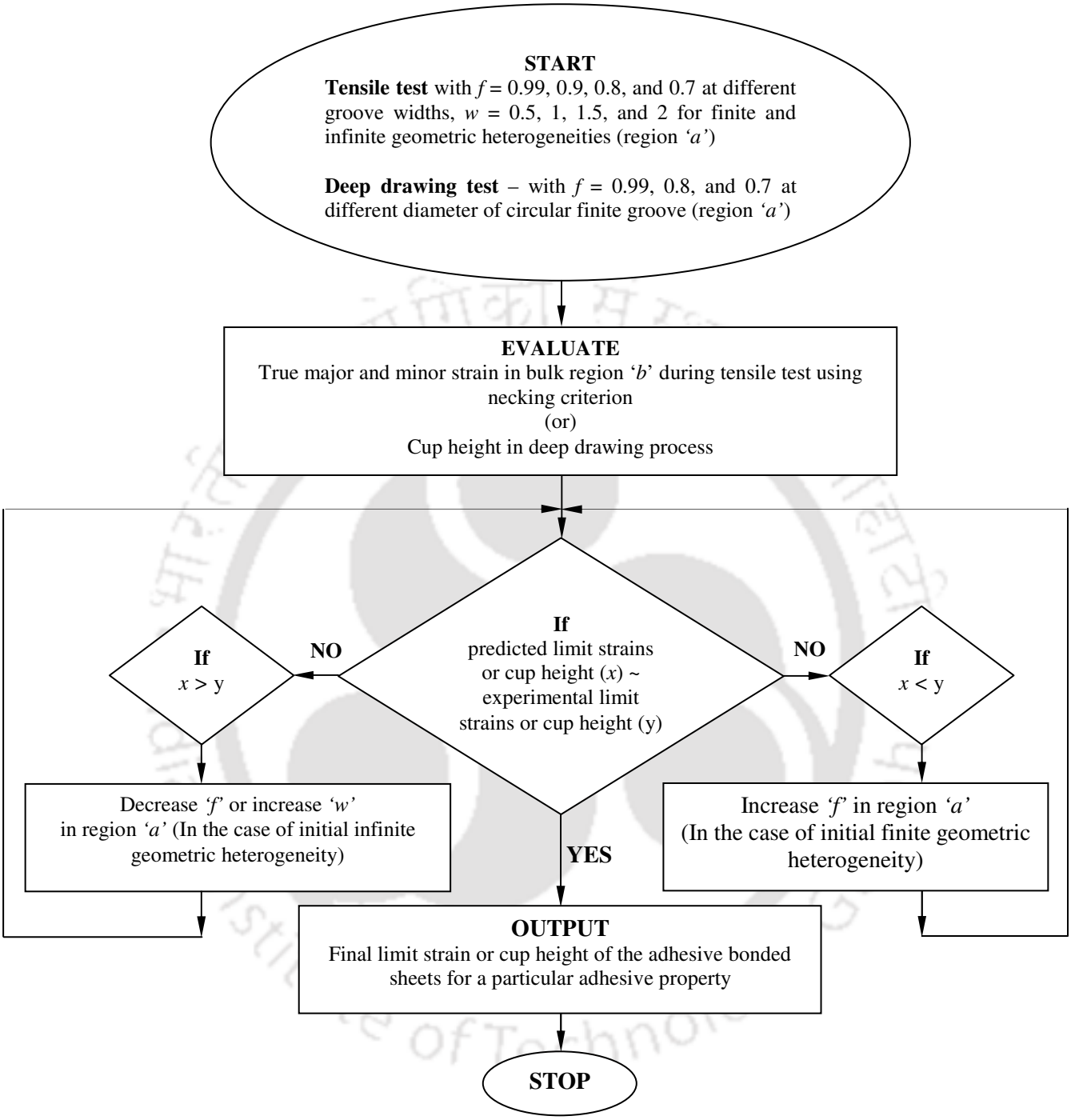

Fig. 9.3 Methodology followed during prediction of forming behaviour of adhesive bonded blanks using geometrical heterogeneities

9.3 Results and discussion

In this section, the predicted results of the effect of different hardener/resin ratios of adhesive on the forming behaviour of adhesive bonded blanks evaluated in the tensile and deep drawing tests through finite element simulations using geometrical heterogeneities are discussed. In tensile test, the forming limit strains with rectangular-infinite groove (Fig. 9.1(a)), square-hole (Fig. 9.1(b)), and square-finite groove (Fig. 9.1(c)) in the DDQ steel sheet were predicted by effective strain rate based criterion (ESRC) and validated with the experiment results. In the deep drawing process, the cup height with circular-finite thickness heterogeneity (or groove) in the SS 316L blank (Fig. 9.2) was predicted and validated with the experiment results.

9.3.1 Prediction of limit strains of base materials constituting the adhesive bonded sheets

The experimental limit strain results of DDQ steel and SS 316L constituting adhesive bonded blanks with different hardener/resin ratios are already discussed in Chapter 2 in Section 2.4.4. It observed that the limit strains in the base materials increase with increase in hardener/resin ratios of adhesive. It is noted that the forming limit strains significantly increase in the low formable sheet (DDQ steel), which is similar to the results of Aghchai *et al.,* 2008, and moderate improvement is observed in the high formable sheet (SS 316L) constituting adhesive bonded blanks. Elsewhere, Aghchai *et al.,* 2008 results showed that the formability of two-layer metallic sheet is better than its lower formability component. Since there is an improvement in the limit strains of SS 316L which is high formable sheet in the present work, it is perceived that the adhesive layer compensates positively the micro inhomogeneities in the as-received sheet metals due to the presence of interfacial bonding, and improves their formability due to improved plasticity by hardener rich formulation of adhesive. This causes delay in the localised necking due to plastic instability, and thereby improving the forming limit strains of base materials.

In the present work, the DDQ steel sheet is chosen for demonstrating limit strain prediction with geometrical heterogeneities due to the significant improvement in limit strains with the effect of different hardener/resin ratios of adhesive than SS 316L during experimental tensile test.

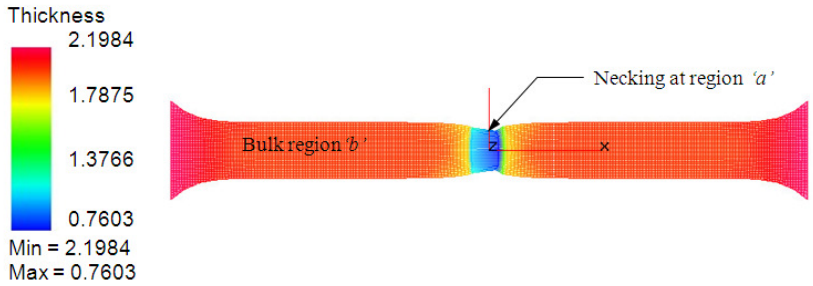

(a)

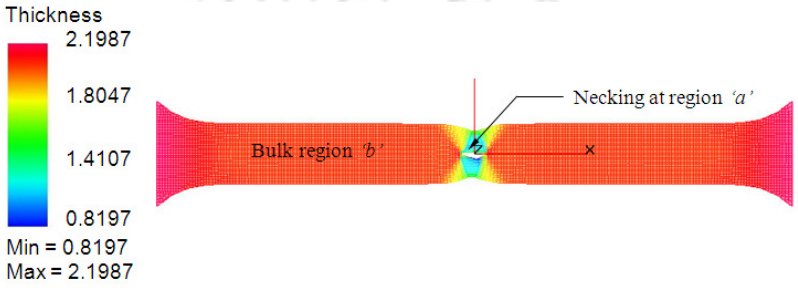

(b)

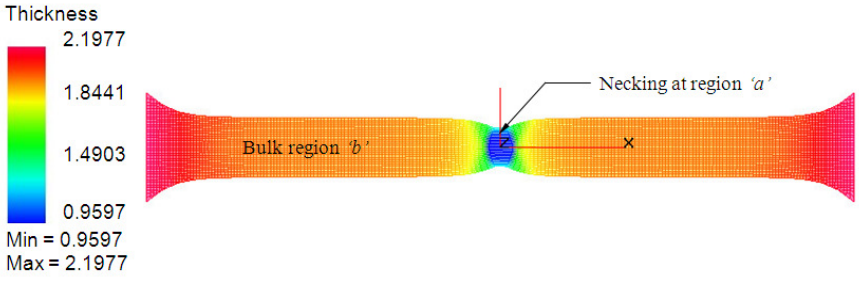

(c)

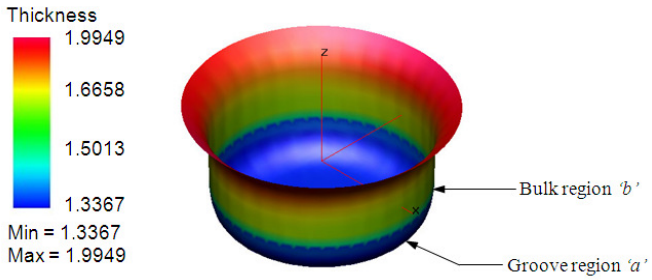

(d)

Fig. 9.4 FE models with different geometrical heterogeneities in the base materials showing necking at region *'a'* after deformation: (a) Rectangular-infinite groove (Tensile test), (b) Square hole (Tensile test), (c) Square-finite groove (Tensile test), and (d) Circular-finite groove (deep drawing test)

Fig. 9.4(a-d) shows the FE models with different geometrical heterogeneities in the base materials such as DDQ steel and SS 316L after deformation. It is observed that the necking occurs at the location of geometric heterogeneities (region *'a'*) in the base materials in all cases during tensile test. The thickness distributions in all cases reveal that there is a severe plastic deformation at the location of geometric heterogeneities (region *'a'*) than in the bulk region (region *'b'*) during tensile and deep drawing tests.

Fig. 9.5 demonstrates the variation of effective strain rate ratio with true major strain in the bulk region of DDQ steel sheet with different geometric heterogeneities during simulation. It is understood that the effective strain rate ratio increases unstably once the criterion is reached, which is the indication for the occurrence of necking. The corresponding major strain and minor strain in the bulk element indicate the limit strain in that strain path. It should be noted that the ratios shown in the figure is arbitrary numbers that are less than or equal to ESRC above which a sudden increase in ratio is seen. The true major strain in bulk saturates when the criterion is satisfied. Hence, the criterion is not modified, and original criterion of ESRC ≥ 4 for failure to occur is used for prediction. In the case of square-hole present in the tensile specimen, the true major strain in bulk was very low, since the strain is rather concentrated at the groove. In this case, the limit strains were evaluated in the necked element by following the same ESRC.

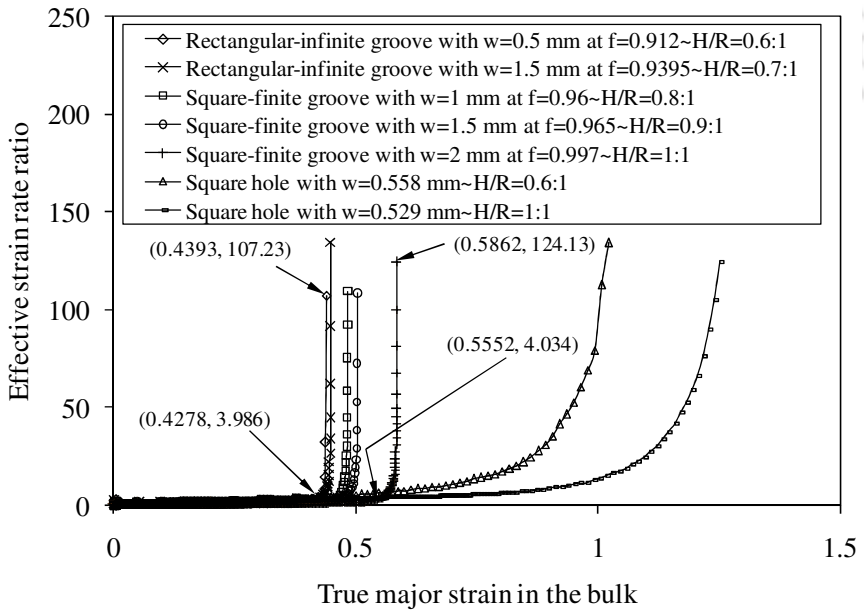

Fig. 9.5 Variation of effective strain rate ratio with true major strain in bulk in DDQ steel sheet different initial geometric heterogeneities during tensile test

During prediction of limit strains of DDQ steel with the effect of different hardener/resin ratios of adhesive, the range of *'f'* in which the limit strains lie, and the range of different heterogeneities size were analysed with reference to the experimental limit strain results following the standardized methodology as described in Fig. 9.3. Fig. 9.6(a, b) shows the range of *'f'* in which the limit strains of DDQ steel are predicted, with the effect of hardener/resin ratios of adhesive at different width (*w*) of rectangular-infinite groove. In the case of rectangular-infinite groove with '*w*' of 0.5 mm (Fig. 9.6(a)), the two values of *'f',* 0.99 and 0.9, in between which the experimental limit strains of DDQ steel lie. But in the case of *'w'* of 3 mm (Fig. 9.6(b)), the '*f*' value, 0.99, which could predict the limit strain is only equivalent to the limit strain of DDQ steel with the effect of hardener/resin ratio of 0.7:1. From this analysis, the width *'w'* of the rectangular-infinite groove has been considered as 0.5 mm, 1 mm, 1.5 mm, 2 mm and 2.5 mm, and the *'f'* value equivalent to the effect of different hardener/resin ratios of adhesive on DDQ steel limit strains are found.

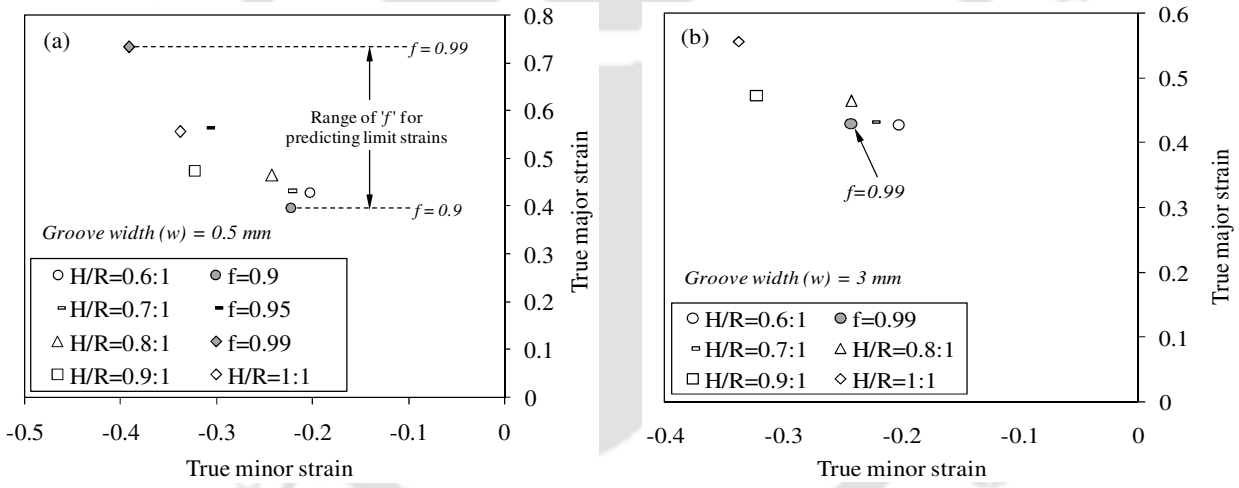

Fig. 9.6 The range of *'f'* for predicting the limit strains with different rectangular-infinite groove widths (*w*) during tensile test: (a) *w*= 0.5 mm, and (b) *w*= 3 mm

Fig. 9.7(a-e) shows the comparison between the predicted limit strains of DDQ steel with different *'f'* values at different width dimensions of rectangular-infinite groove which are equivalent to the effect of hardener/resin ratio of adhesive on DDQ steel sheet. It is observed that the limit strain of DDQ steel increases with increase in *'f'* value, which is similar to the trend of the effect of hardener/resin ratio of adhesive during experiment. There is about 0.01 to 3.5% variation in true major strains and about 1.6 to 6.3% variation in true minor strain between experiment and predicted results.

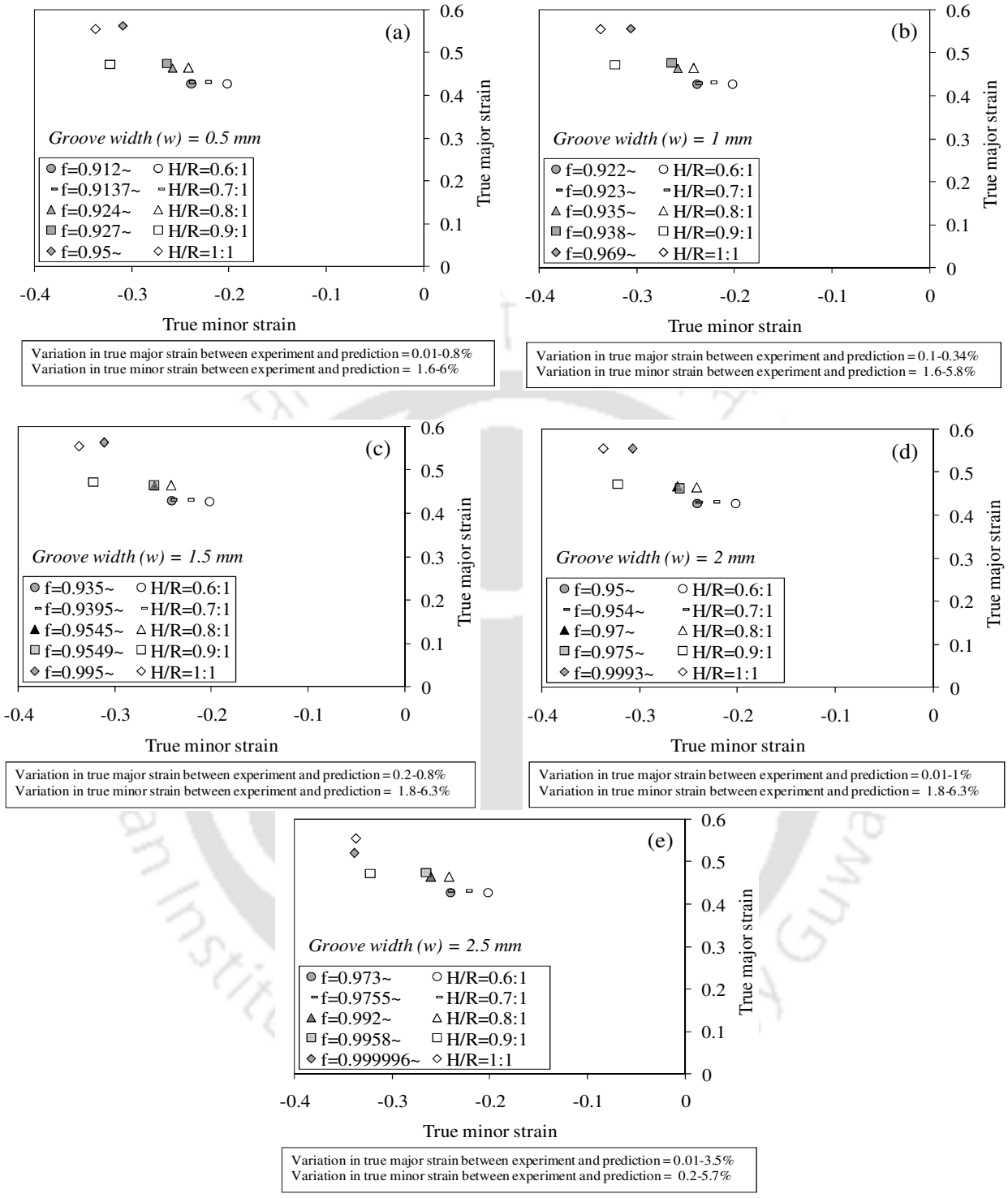

Fig. 9.7 Predicted limit strains of DDQ steel with the effect of different hardener/resin ratios of adhesive with the equivalent *'f'* at different rectangular-infinite groove width (*w*) in tensile test: (a) *w* = 0.5 mm, (b) *w* = 1 mm, (c) *w* = 1.5 mm, (d) *w*= 2 mm, and (e) *w*= 2.5 mm

In the case of rectangular-infinite groove with w = 0.5 mm (Fig. 9.7(a)), the limit strains of DDQ steel evaluated at f = 0.912, f = 0.9137, f = 0.924, f = 0.927, and f = 0.95 are equivalent to the H/R ratios of 0.6:1, 0.7:1, 0.8:1, 0.9:1, and 1:1 of adhesive, respectively. Similarly, the other cases of rectangular-infinite groove with different 'w' and 'f' values that are equivalent to the effect of different H/R ratios of adhesive are shown in Fig. 9.7(b-e).

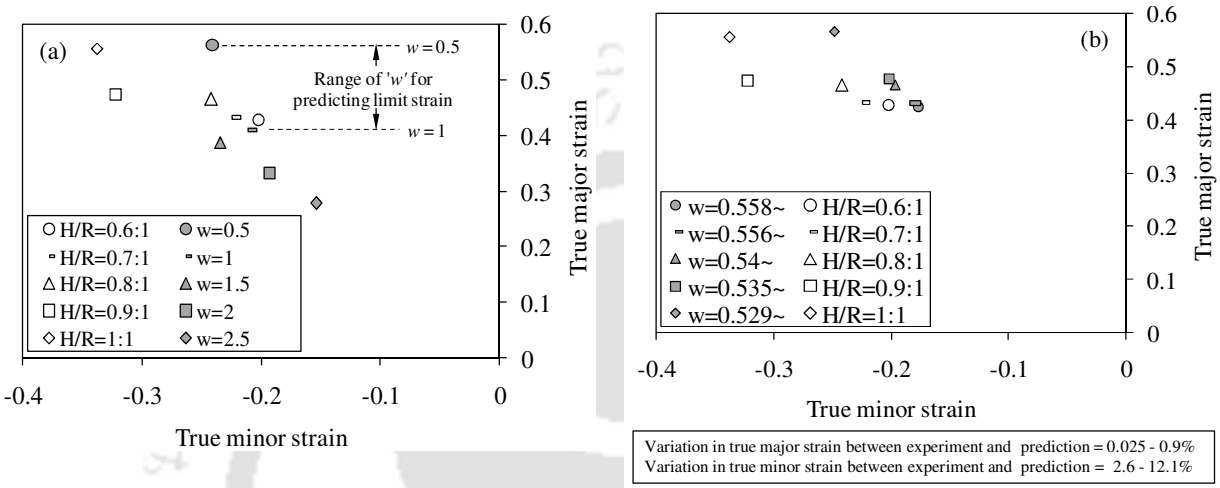

Fig. 9.8 (a) The range of 'w' of square hole for predicting the limit strains, and (b) Predicted limit strains of DDQ steel with the effect of different hardener/resin ratios of adhesive with the equivalent 'w' of square hole

Fig. 9.8(a) shows the range of square hole size 'w' in which the limit strains of DDQ steel are predicted with the effect of hardener/resin ratios of adhesive. The square hole size 'w' of 0.5 mm to 1 mm is the range within which the limit strain predictions are focused. Fig. 9.8(b) shows the comparison between the predicted limit strains of DDQ steel with different 'w' of square infinite groove which are equivalent to hardener/resin ratios of adhesive. It is noted that the limit strain of DDQ steel increases with decrease in size of square hole that is similar to the trend of the effect of hardener/resin ratio of adhesive during experiments. There is a maximum of about 0.9% variation in true major strain and about 12.1% variation in true minor strain between experiment and predicted results. In the case of square hole (Fig. 9.8(b)), the limit strains of DDQ steel evaluated at w = 0.558, w = 0.556, w = 0.54, w = 0.535, and w = 0.529 are equivalent to the effect of *H/R* ratios of 0.6:1, 0.7:1, 0.8:1, 0.9:1, and 1:1 of adhesive, respectively.

In the case of square-finite thickness heterogeneity (or groove) in the DDQ steel sheet, the two values of 'f', within which the limit strain prediction are focused for w = 0.5 mm (Fig. 9.9(a)) are

0.99 and 0.8. But in the case of *'w'* of 3.5 mm (Fig. 9.9(b)), the *'f'* value of 0.99 which could predict the limit strain is only equivalent to the limit strain of DDQ steel at H/R = 0.6:1. From this study, the size *'w'* of the square-finite heterogeneity has been considered as 0.5 mm, 1 mm, 1.5 mm, 2 mm, 2.5 mm, and 3 mm. Further, the *'f'* values which are equivalent to different hardener/resin ratios of adhesive on DDQ steel limit strains are found.

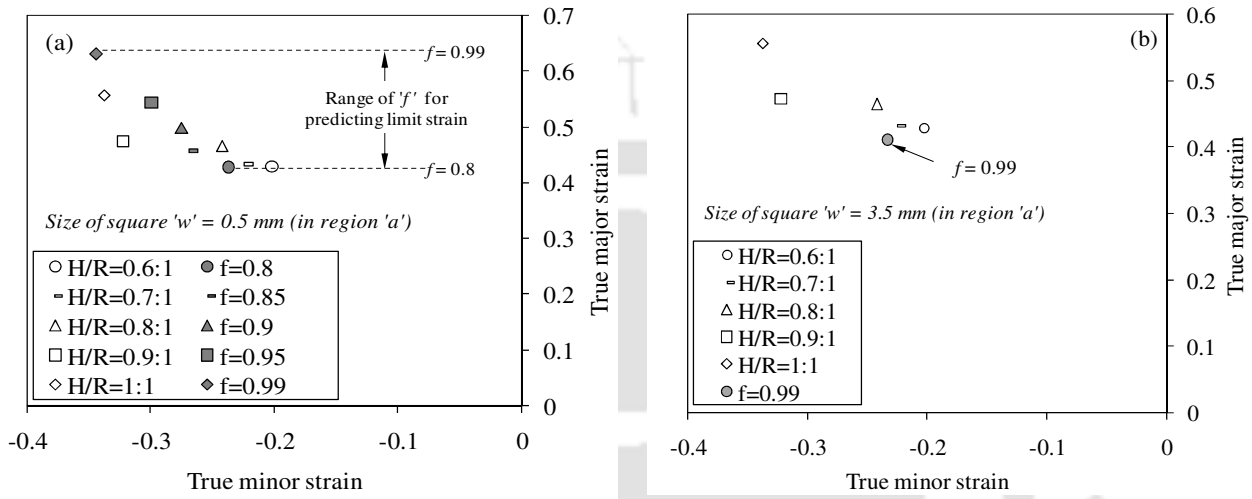

Fig. 9.9 The range of *'f'* for predicting the limit strains with different square-finite groove size (*w*): (a) *w*= 0.5 mm, and (b) *w*= 3.5 mm

Fig. 9.10(a-f) shows the comparison between the predicted limit strains of DDQ steel with different *'f'* values at different widths of square-finite thickness heterogeneity (or groove), which are equivalent to the effect of hardener/resin ratio of adhesive. It is seen that the limit strain of DDQ steel increases with increase in *'f'* values at different size of square-finite thickness heterogeneity which is similar to the effect of hardener/resin ratio of adhesive during experiment. There is about 0.01 to 3.5% variation in true major strain and about 1.6 to 8% variation in true minor strain between experiment and predicted results. In the case of square-finite groove with w = 0.5 mm (Fig. 9.10(a)), the limit strains of DDQ steel evaluated at $f = 0.8$, $f = 0.81$, $f = 0.85999$, $f = 0.87$, and $f = 0.96$ are equivalent to H/R ratios of 0.6:1, 0.7:1, 0.8:1, 0.9:1, and 1:1 of adhesive, respectively. Similarly, the other cases of square-finite groove with different '*w*' and *'f'* values that are equivalent to the effect of different H/R ratios of adhesive are shown in Fig. 9.10(b-f).

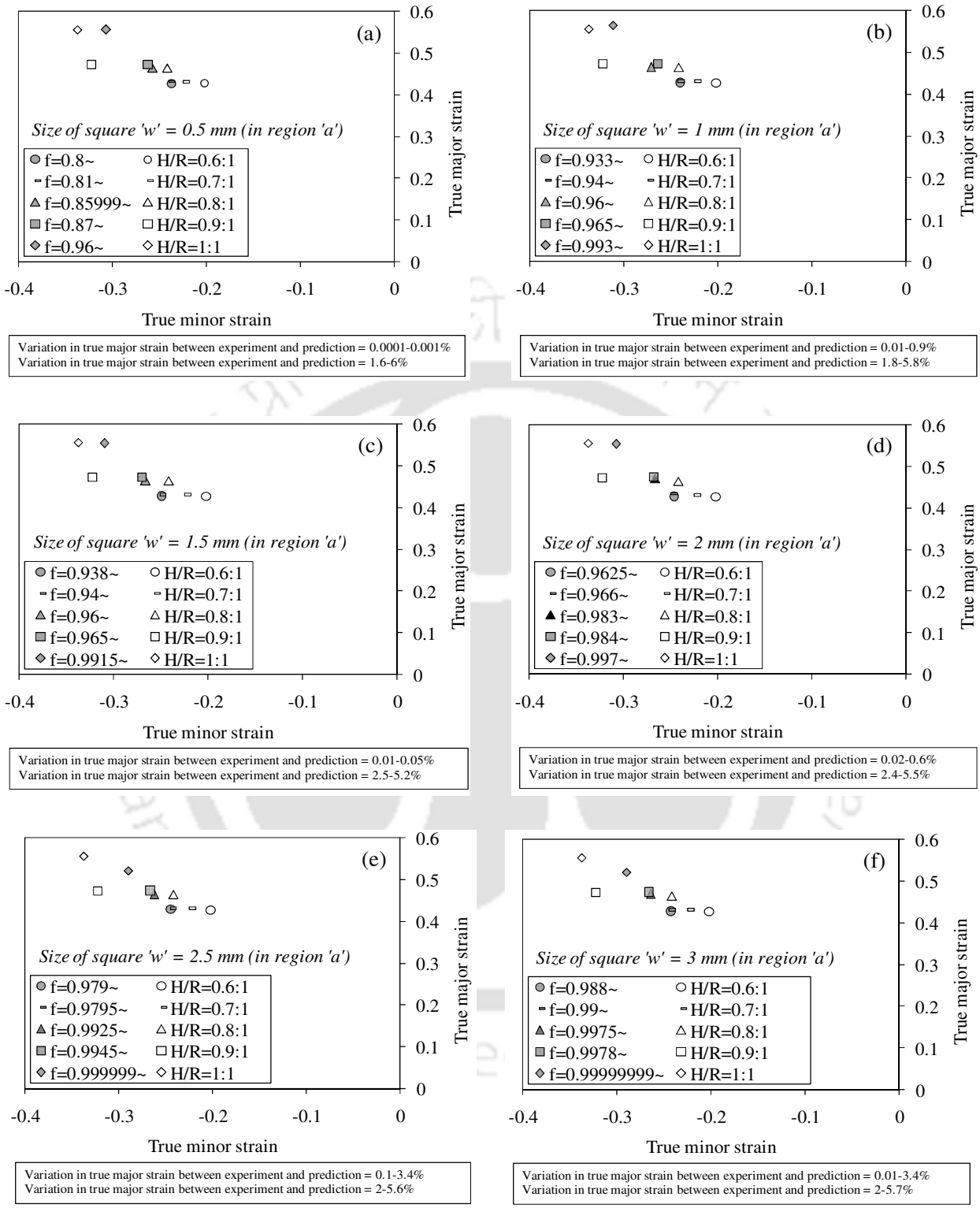

Fig. 9.10 Predicted limit strains of DDQ steel with the effect of different hardener/resin ratios of adhesive with the equivalent *'f'* at different square-finite groove size (*w*): (a) *w* = 0.5 mm, (b) *w* = 1 mm, (c) *w* = 1.5 mm, (d) *w*= 2 mm, (e) *w*= 2.5 mm, and (f) *w*= 3 mm

It is observed from these results that the forming limit strains are significantly influenced by the geometric heterogeneities in the base material. The forming limit strain decreases with increase in the size of the geometric heterogeneities, or increase in the localised reduction of homogeneous sheet materials, where the strain is localised due to the plastic instability. Though the true major strain prediction shows good agreement with the experimental true major strain results, there is a large difference in the true minor strain in some of the cases. But these variations are falling in the standard deviation evaluated in the experimental limit strains. It is perceived from these results that the adhesive in the bonded blanks compensates positively the micro and macro defects in the as-received sheet metals due to interfacial bonding between adhesive and base materials during experiments. In the presence of interfacial bonding, the forming limits are improved by the plasticity of the adhesive, which could be improved by the hardener rich formulation.

Just to summarize, it has been demonstrated that the effect of hardener/resin ratio of adhesive on the forming limit strains of base materials constituting adhesive bonded sheets could be predicted well using initial geometrical heterogeneity in the base materials. It has been demonstrated that using initial geometrical heterogeneity is not only to predict the collective effect of the micro defects present in the as-received sheet materials on their formability, but also the formability of adhesive bonded sheets. The major issues related to the adhesive bonded sheets are delamination, defects in the adhesive, appropriate selection of adhesive properties, degree of adhesive curing, surface treatments of base material constituents, environmental influence on adhesive properties, adapting appropriate adhesion condition, and selection of instability condition during modeling of adhesive. All these issues could be overcome by designing the base material components using initial geometric heterogeneities during formability prediction with the effect of adhesive properties, which is practically simple. The present method of prediction of formability of bonded sheets can also be extended to study the effects of factors like adhesive thickness, bond width, reinforcements in adhesive, and other functional properties. Though this is the case, the direct relationship between geometrical heterogeneities and few instability phenomena like delamination etc. is not straight forward and one should evolve a strategy to predict the same during modeling simulation.

9.3.2 Deep drawability prediction of adhesive bonded blanks

The present investigation is not only limited to the coupon level analysis but also extended to the industrial applications similar to deep drawing process. In this section, the deep drawability of

adhesive bonded blanks is predicted with SS 316L blank. During experimental deep drawing of adhesive bonded blanks, the cup height was evaluated at the maximum load in the load-stroke behaviour. Among DDQ steel and SS 316L sheets constituting adhesive bonded blanks during deep drawing experiment, the cup height of DDQ steel blank (low formable material) would not increase beyond the cup height of SS 316L blank (high formable material). The main aim is to predict the final cup height of adhesive bonded blanks, and not to analyse the cup height of base materials constituents. That is why, SS 316L material was chosen during prediction of cup height with the effect of different hardener/resin ratios of adhesive.

Fig. 9.11 presents the comparison of predicted cup height with varied radius of circular finite groove (region *'a'*) (in Fig. 9.2) in the SS 316L circular blank for different *'f'* values. There is not much difference (only about 0.5%) in the cup height with different radius of circular groove (region *'a'*), for various *'f'* values. From this result, the diameter (d_1) of region *'a'* has been kept constant as 60 mm, further, the *'f'* value has been varied to predict the cup height of SS 316L to predict the effect of different hardener/resin ratios of adhesive.

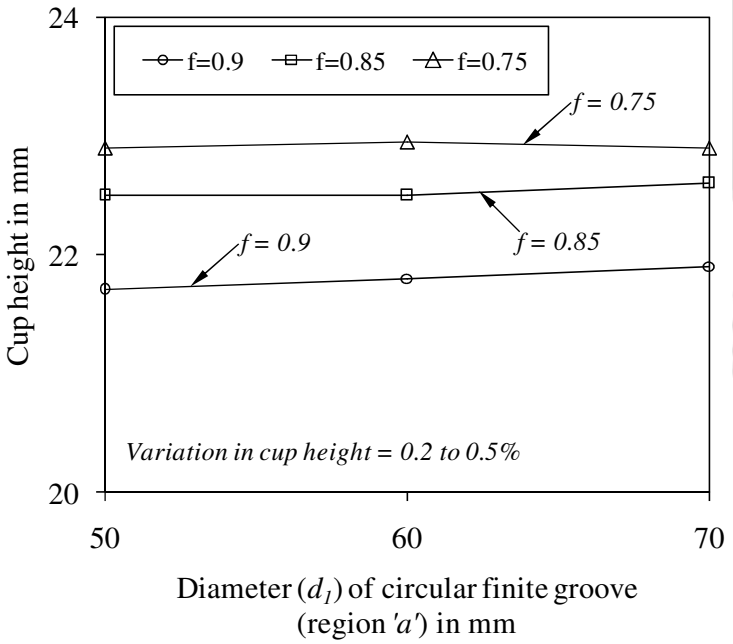

Fig. 9.11 Comparison of cup height result with different radius at region '*a*' in circular blank at different *'f'* values

The experimental cup height results of adhesive bonded blanks with different hardener/resin ratios of adhesive evaluated at the maximum load in the load-stroke behaviour during experiment is

already discussed in Chapter 8 in scetion 8.7.2.3. Fig. 9.12(b) shows the range of *'f'* values, between 0.58 and 0.74, that is considered for predicting the cup height of SS 316L blank with the effect of different hardener/resin ratios of adhesive.

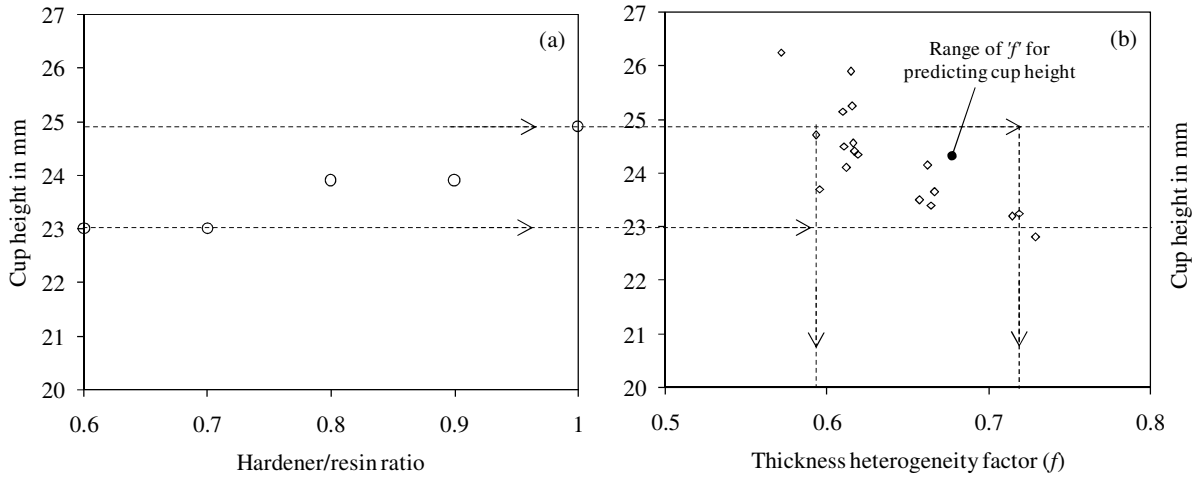

Fig. 9.12 (a) Cup height of adhesive bonded blanks with different hardener/resin ratios during experiment (Experimental variation in cup height data = ±0.5 mm), and (b) The range of *'f'* for predicting the cup height at d_1 = 60 mm in the region *'a'* (circular-finite groove)

The load-stroke behaviour at different *'f'* values is shown in Fig. 9.13 as an evidence from which the maximum load is evaluated. The predicted cup height result of SS 316L blank with different *'f'* values that is equivalent to the cup height of adhesive bonded blanks with the effect of hardener/resin ratio of adhesive is shown in Fig. 9.14. It is seen that the cup height increases with decrease in *'f'* values. There is about 0.6% variation in cup height between experiment and prediction. Here this out-of-plane test results are fully contradictory to the in-plane test results, wherein the limit strains are reduced by the increase in size of the geometric heterogeneities. This is due to the increase in severity of deformation in region *'a'* in the SS 316L circular blank increases the overall cup height during deep drawing process. The failure tendency of circular blank due to severe deformation is compensated by the continuous flow of bulk region *'b'* in to the die during deformation. However, it does not mean that further decrease in *'f'* value would increase the cup height. The optimized thickness heterogeneity factor *'f'* predicts the cup of the SS 316L with effect of hardener/resin ratio of adhesive.

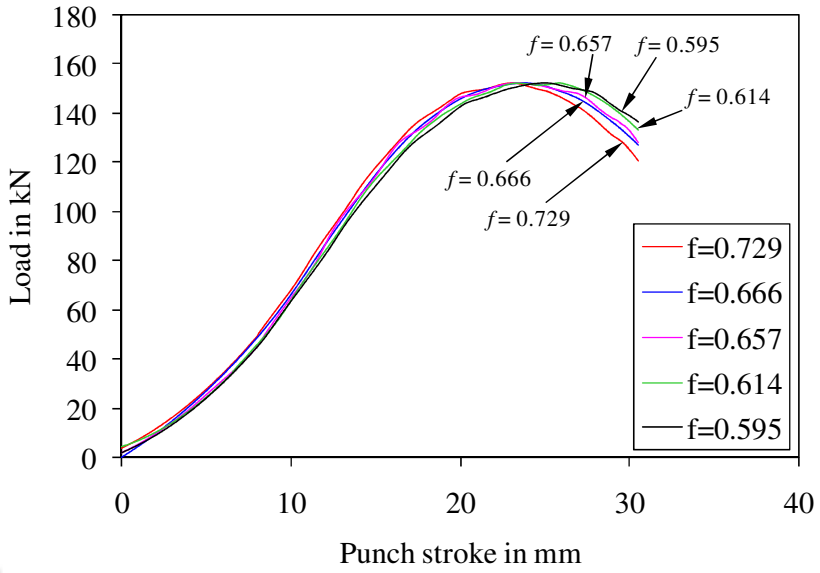

Fig. 9.13 Load-stroke behaviour at different *'f'* values during deep drawing process

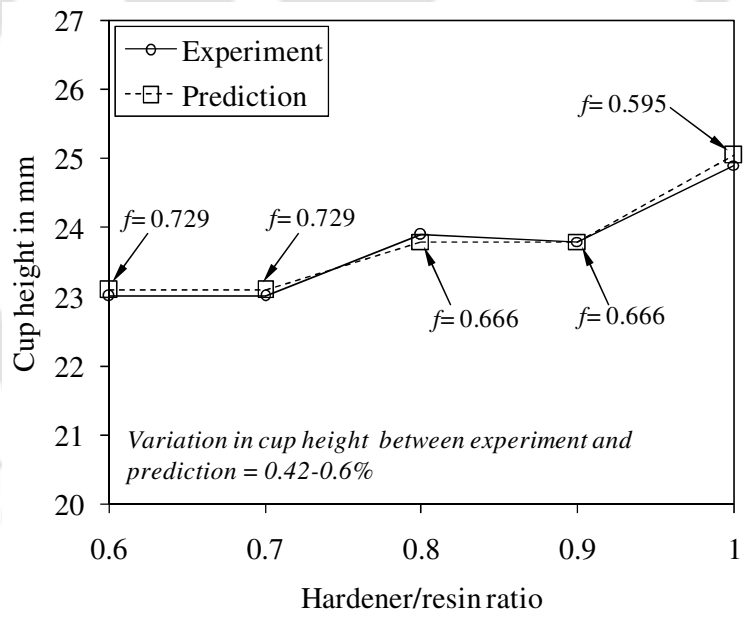

Fig. 9.14 Predicted cup height results by circular-finite groove in region '*a*' of SS 316L circular blank with the effect of different hardener/resin ratios of adhesive with equivalent *'f'* values

In summary, since the severe deformation of region *'a'* than the bulk region *'b'* is the main cause in the improvement of cup height during prediction, it is suggested to design the sheet components with any type of finite geometric heterogeneity with optimized *'f'* during prediction of formability with the effect of adhesive properties in the deep drawing process. It is also suggested not to use any type of infinite groove in the blanks during deep drawing process, wherein the

influence infinite geometrical heterogeneities in region '*a*' would be suppressed by the bulk region 'b' with which the tools are in contact during deformation. Even if the initial finite geometrical heterogeneities are not desired, it is suggested to design the sheet material components with finite geometrical heterogeneity aesthetically so that the formability of base materials constituents can be improved for automotive and other applications, and also it would not be perceived as defect in the formed components.

9.4 Conclusions

From the above analysis, the following conclusions are drawn.

- It has been hypothesized and later demonstrated that with a simple thickness heterogeneity factor *'f'*, the forming limit of adhesive bonded sheets can be predicted efficiently and accurately, without incorporating adhesive layer and properties during simulations.
- The effect of hardener/resin ratio on the forming limit of adhesive bonded sheets is well predicted by the thickness heterogeneity *'f'* and size of such defect. This has been shown with evidence from tensile tests. In the case of rectangular-infinite groove with $w = 0.5$ mm, the limit strains of DDQ steel evaluated at $f = 0.912$, $f = 0.9137$, $f = 0.924$, $f = 0.927$, and $f = 0.95$ are equivalent to the H/R ratios of 0.6:1, 0.7:1, 0.8:1, 0.9:1, and 1:1 of adhesive, respectively. Similarly, the other cases of rectangular-infinite groove with different '*w*' and *'f'* values that are equivalent to the effect of different H/R ratios of adhesive were evaluated. In the case of square hole, the limit strains of DDQ steel evaluated at $w = 0.558$, $w = 0.556$, $w = 0.54$, $w = 0.535$, and $w = 0.529$ are equivalent to the effect of H/R ratios of 0.6:1, 0.7:1, 0.8:1, 0.9:1, and 1:1 of adhesive, respectively. In the case of square-finite groove with $w = 0.5$ mm, the limit strains of DDQ steel evaluated at $f = 0.8$, $f = 0.81$, $f = 0.85999$, $f = 0.87$, and $f = 0.96$ are equivalent to H/R ratios of 0.6:1, 0.7:1, 0.8:1, 0.9:1, and 1:1 of adhesive, respectively. Similarly, the other cases of square-finite groove with different '*w*' and *'f'* values that are equivalent to the effect of different H/R ratios of adhesive were evaluated.
- It is recommended to avoid adapting hole types of geometrical heterogeneities like square-infinite groove in the base materials to predict limit strains with the effect of hardener/resin ratio of adhesive, wherein the strain is severely localised, which could predict inaccurately.

- In the deep drawing process, the equivalent initial geometrical heterogeneities proposed to predict the cup height with the effect of hardener/resin ratios of adhesive on the base material (SS 316L) is more dependent on thickness heterogeneity factor *'f'*. It is very important to optimize the thickness heterogeneity factor *'f'* which could predict the cup of the base materials with the effect of hardener/resin ratio of adhesive, avoiding cup failure. In the case of circular-finite groove with d_1 = 60 mm, the cup height of SS 316L evaluated at f = 0.729, f = 0.729, f = 0.666, f = 0.666, and f = 0.595 are equivalent to H/R ratios of 0.6:1, 0.7:1, 0.8:1, 0.9:1, and 1:1 of adhesive, respectively.
- The main disadvantages of such a defect representation is the difficulty in predicting the delamination, wrinkling etc. during forming, which can be taken care by evaluating a strategy as there are not related in a straight forward manner.

Chapter 10

Prediction of formability of adhesive bonded sheets by neural network and its validation

10.1 Methodology

In this section, the evaluation of adhesive bonded sheets forming behaviour by experiment, neural network prediction, and numerical prediction is discussed. The mechanical properties of base materials and epoxy adhesive are already discussed in Chapter 2 in Section 2.1.1 and Section 2.4.1, respectively. The mechanical properties of CB filled adhesive properties are already discussed in Chapter 6 in Section 6.5.1.

10.2 Tensile test and forming limit strain evaluation

The limit strains of base material constituting adhesive bonded blanks evaluated during experimental tensile test with different hardener/resin ratios like 0.6:1, 0.7:1, 0.8:1, 0.9:1 and 1:1 (as discussed in Chapter 2 in Section 2.3), with different aspect ratios of adhesive finite defect (as discussed in Chapter 3 in Section 3.3.3), with different orientations of adhesive infinite defect (as discussed in Chapter 3 in Section 3.3.15), with different CB wt.% in adhesive (as discussed in Chapter 6 in Section 6.5.4), with different numbers of longitudinal reinforcement of Cu wires in adhesive (as discussed in Chapter 7 in Section 7.4.3) are utilized for ANN prediction.

10.3 Deep drawability and cup height evaluation

In the experimental deep drawing process, the cup height results of adhesive bonded blanks with the influence of hardener/resin ratios (as discussed in Chapter 8 in Section 8.7.2.3), CB wt.% (as discussed in Chapter 8 in Section 8.7.2.3), and Cu wire reinforcements in the adhesive with different levels (as discussed in Chapter 7 in Section 7.7) are utilized for ANN prediction.

10.4 Artificial Neural Network (ANN) modelling

In this work, a code was developed in the Matlab R2013a® environment for modelling the neural network to predict the forming behaviour of adhesive bonded blanks. Different ANN models were developed for tensile test and deep drawing process of adhesive bonded blanks. The forming behaviour of adhesive bonded blanks is predicted by feed forward network in which a sequence of layers consisting of a number of nodes or neurons in each layer is interconnected. Generally, the network comprises input layer, hidden layers, and output layer. The output of neurons of one layer becomes input to neurons of the succeeding layer. The output of a typical neuron which receives one or more input signals is transferred to connected neurons in varying intensities, the signal intensity decided by the weights (Robi and Dixit, 2003). The input layer receives input data of the influencing factors such as hardener/resin ratio of adhesive, aspect ratios of finite adhesive defects, orientations of infinite adhesive defects, CB wt.%, and number of wire reinforcements on the forming behaviour of adhesive bonded blanks that is the output response. Each input connection is associated with weight and a bias value (representing an internal resting level of the neuron (Rumelhart *et al.,* 1994), or simply it is difference between the expected value and the true value). The neural network can adjust the weights by itself through the learning process, and represents the nonlinear relationship between the input and output, that is occurring in the hidden layers, which is difficult to express in mathematical modeling (Moon and Na, 1997).

After developing the network architecture defining connections between the layers associated with weights and bias values, the network was trained by providing data in the form of several input such as different levels of above mentioned influencing factors of adhesive bonded blanks, and output data like true major strains and true minor strains of DDQ steel and SS 316L sheets constituting adhesive bonded blanks in the case of tensile test, and final cup height of adhesive bonded blanks in the case of deep drawing process. For training the network, three set of input data and corresponding target data were used. During the training process, the network adjusts its weights to minimize the error between the predicted and experimental results. Most common algorithm for adjusting the weights is back propagation algorithm in which the training process involves forward and backward passes. In the forward pass, the input signals propagate from the network input to the output. In the reverse pass, the calculated error signals propagate backwards through the network where they are used to adjust the weights (Robi and Dixit, 2003). The performance of the neural network was judged in order to optimize the network. The trained neural

network was tested by supplying test data. In the prediction, all the levels of data and intermediate levels of input data were used to predict the output response and validated with the experimental results. If the testing error is much more compared to training error, the network is said to over-fit the data (Robi and Dixit, 2003). In the optimization of appropriate network topology, nearly equal training and testing error values were monitored. During optimization of network, the models of many parameters could fit with the response data in many different ways. In order to fit the function, in such a way that the network was generalized for predicting the unseen collection of data by following two strategies like varying the number of neurons in the hidden layer in order to vary the number of weights and bias values, and training the network with different back propagation algorithms (Rumelhart *et al.,* 1994).

10.4.1 Learning rule

The learning rules such as gradient descent weight and bias learning function (GD), and gradient descent with momentum weight and bias learning function (GDM) were used during development of neural network (The MathWorks, 1994-2013). Here the GD function calculates the weight change (dw) for a given neuron from the neuron's input and error, and the weight (or bias) learning rate (μ), according to the gradient descent.

$$dw = \mu \times gw \tag{10.1}$$

where gw – gradient with respect to performance.

The GDM function calculates the weight change (dw) for a given neuron from the neuron's input and error, the weight (w) (or bias (b)), learning rate (μ), and momentum constant (α), according to gradient descent with momentum.

$$dw = \alpha \times dw_{prev} + (1-\alpha) \times \mu \times gw \tag{10.2}$$

where dw_{prev} is the previous weight change that is stored and read from the learning state. Here the training rate (μ) is a constant ranging between 0 and 1 which fixes the training speed of the network. The moment coefficient (α), generally takes a value ranging between 0.1 and 1, and makes possible to accelerate the convergence of the algorithm (Abbassi *et al.,* 2013). During analysis, learning rate and moment coefficient were started with the values 0.9 and 0.35, respectively (Pal *et al.,* 2008). After analysing with these two learning rules, the GDM function was selected based on the better network performance.

10.4.2 Activation function

In the network structure, each input is weighted with an appropriate weight. The sum of the weighted inputs and the bias forms the input to the transfer function or activation function (*f*). There are three major types of transfer functions such as linear, tan-sigmoid ((The MathWorks, 1994-2013), and log-sigmoid (Robi and Dixit, 2003) used in the hidden layer and output layer. Further, Nguyen-Widrow initialization algorithm was used to initialize the layer's weights and biases (Nguyen and Widrow, 1990). This algorithm chooses values in order to distribute the active region of each neuron in the layer approximately evenly across the layer's input space based on the degree of randomness. This algorithm was used only for log-sigmoid and tan-sigmoid transfer functions whose active input range is the finite interval (The MathWorks, 1994-2013).

Linear transfer function: $f = x$ (10.3)

Log-sigmoid transfer function (Robi and Dixit, 2003): $f = \frac{1}{(1+e^{-x})}$ (10.4)

Tan-sigmoid transfer function (The MathWorks, 1994-2013): $f = \frac{2}{(1+e^{(-2x)})-1}$ (10.5)

where *'x'* represents net input. Different combinations of these activation functions were used in the hidden layer and output layer during development of neural network. Finally, log-sigmoid function in the hidden layer, and tan-sigmoid function in the output layer were adapted for calculating outputs (Table 10.1).

10.4.3 Data selection

While training the networks, the target data was divided into three sets using random indices such as training, validation, and testing, which is general in practice. During network modelling, 70% of target data was used for training, 15% data was used for validation, and remaining 15% was used for testing. The training set is used for computing the gradient and updating the network weights and biases. The validation set error was monitored during the training process. The network weights and biases were saved at the minimum of the validation set error. More care was taken during dividing data by monitoring the test set error not reaching minimum at a different iteration number than the validation set error (The MathWorks, 1994-2013).

10.4.4 Back propagation algorithm

Though Levenberg-Marquardt (LM) back propagation algorithm is popular and widely used for training the neural network (Abbassi *et al.,* 2013; Veera Babu *et al.,* 2009; Patel *et al.,* 2012; Tiryaki *et al.,* 2014; Robi and Dixit, 2003), the other back propagation algorithms such as Bayesian Regularization (BR) (MacKay, 1992), BFGS Quasi-Newton (BFG) (Gill *et al.,* 1981), Resilient Back propagation (RP) (Riedmiller, 1993), Scaled Conjugate Gradient (SCG) (Moller, 1993), One Step Secant (OSS) (Battiti, 1992), and Gradient Descent with Momentum (GDM) (The MathWorks, 1994-2013.) were used for training network. Finally, Levenberg-Marquardt back propagation algorithm was chosen as a suitable back propagation algorithm for present ANN modelling (Table 9.2).

10.4.5 Network performance

The mean square error (MSE) was used to judge the performance of the ANN model. MSE was computed using eq. (10.6) (Tiryaki *et al.,* 2014; Pal *et al.,* 2008).

$$MSE=\frac{1}{N}\sum_{i=1}^{N}(y_i-y_p)^2 \qquad (10.6)$$

where y_i is the measured value of the experimental samples, y_p is the predicted value, and N is the total number of samples. By judging the MSE during training and then testing with the intermediate input data for which the output data to be predicted, the neural network was optimized with different combinations of activation functions in the hidden layer and output layer (Table 10.1), different ANN structures, different learning results with different learning rates and momentum coefficients, and different training algorithms (Table 10.2) for tensile test. Table 10.3 shows the optimization of neural network for deep drawing process of adhesive bonded blanks.

Table 10.1 Optimization of network with different activation functions in the hidden layer and output layer for tensile test (Learning rule: GDM, μ = 0.5; α = 1; Training Algorithm: LM)

S.No.	ANN Structure (*x*-*y*-*z*)	Training algorithm	Activation Function		MSE training×10^{-4}	MSE testing×10^{-4}
			Hidden Layer	Output Layer		
1	5-10-5	LM	logsigmoid	logsigmoid	14.000	16.000
2*	**5-10-5**	**LM**	**logsigmoid**	**tansigmoid**	**2.5004**	**7.8808**
3	5-10-5	LM	tansigmoid	tansigmoid	2.9245	14.000
4	5-10-5	LM	tansigmoid	logsigmoid	12.000	14.000
5	5-10-5	LM	logsigmoid	linear	2.7804	19.000
6	5-10-5	LM	linear	logsigmoid	15.000	23.000
7	5-10-5	LM	tansigmoid	linear	2.8430	24.000
8	5-10-5	LM	linear	tansigmoid	3.1510	20.000
9	5-10-5	LM	linear	linear	2.3225	27.000

Note: * indicates optimized network; ANN Structure (*x*-*y*-*z*) → (number of neurons in input layer-hidden layer-output layer)

Table 10.2 Optimization of network with different ANN structures, learning rules with different μ and α, and different training algorithms for tensile test (Transfer functions: Hidden layer – log-sigmoid and Output layer – tan-sigmoid)

S.No.	ANN Structure	Learning rule	Learning rate	Momentum coefficient	Training algorithm	MSE training×10^{-4}	MSE testing×10^{-4}
1	5-10-5	GD	0.9	-	LM	3.1487	21.000
2	5-10-5	GDM	0.9	0.35	LM	2.7943	13.000
3	5-15-5	GDM	0.9	0.35	LM	2.7054	13.000
4	5-20-5	GDM	0.9	0.35	LM	2.7832	14.000
5	5-5-5	GDM	0.9	0.35	LM	2.6657	27.000
6	5-10-5	GDM	0.8	0.35	LM	3.0160	11.000
7	5-10-5	GDM	0.7	0.35	LM	2.7703	17.000
8	5-10-5	GDM	0.6	0.35	LM	4.9384	21.000
9	5-10-5	GDM	0.5	0.35	LM	2.5687	13.000
10	5-10-5	GDM	0.4	0.35	LM	3.1475	9.5341
11	5-10-5	GDM	0.3	0.35	LM	3.095	16.000
12	5-10-5	GDM	0.2	0.35	LM	2.8992	22.000
13	5-10-5	GDM	0.1	0.35	LM	3.3568	15.000
14	5-10-5	GDM	0.2	0.4	LM	2.9449	20.000
15	5-10-5	GDM	0.2	0.5	LM	2.9288	12.000
16	5-10-5	GDM	0.2	0.6	LM	3.0376	11.000
17	5-10-5	GDM	0.2	0.7	LM	2.8518	13.000
18	5-10-5	GDM	0.2	0.8	LM	2.9657	11.000
19*	**5-10-5**	**GDM**	**0.2**	**0.9**	**LM**	**2.4995**	**8.4541**
20	5-10-5	GDM	0.2	1	LM	2.4337	15.000
21	5-10-5	GDM	0.2	0.9	BR	2.5874	9.3467
22	5-10-5	GDM	0.2	0.9	BFG	32.000	23.000
23	5-10-5	GDM	0.2	0.9	RP	5.4624	11.000
24	5-10-5	GDM	0.2	0.9	SCG	12.000	19.000
25	5-10-5	GDM	0.2	0.9	OSS	31.000	37.000
26	5-10-5	GDM	0.2	0.9	GDM	59.000	55.000

Note: * indicates optimized network; ANN Structure (*x*-*y*-*z*) → (number of neurons in input layer-hidden layer-output layer)

Table 10.3 Optimization of network with different ANN structures for deep drawing test (Transfer functions: Hidden layer – log-sigmoid and Output layer – tan-sigmoid)

S.No.	ANN Structure	Learning rule	Learning rate	Momentum coefficient	Training algorithm	MSE training	MSE testing
1	3-5-3	GDM	0.2	0.9	LM	0.0155	0.5219
2	3-10-3	GDM	0.2	0.9	LM	0.0160	0.3509
3*	**3-15-3**	**GDM**	**0.2**	**0.9**	**LM**	**0.0148**	**0.2997**
4	3-20-3	GDM	0.2	0.9	LM	0.0161	0.3805

Note: * indicates optimized network; ANN Structure (*x*-*y*-*z*) → (number of neurons in input layer-hidden layer-output layer)

10.5 Neural network model

Fig. 10.1 shows the optimized architecture of neural network model developed for predicting the forming behaviour of base materials constituting adhesive bonded blanks in the tensile test with the influencing parameters of hardener/resin ratios of adhesive, aspect ratios of adhesive infinite defects, orientations of adhesive infinite defects, CB wt.% filled in adhesive, and high ductile wire reinforcements in the adhesive which is correspondingly taken as 5 number of neurons in the input layer. The number neurons used in the hidden layer is 10, and the output is activated by log-sigmoid function. The input weights and bias values are associated with the output of hidden layer. The limit strains corresponding to the effect of the above mentioned influencing parameters of adhesive bonded blanks are predicted as output response of the network that holds 5 neurons in the output layer. The output of output layer is activated by tan-sigmoid function associated with the layer weights and bias values.

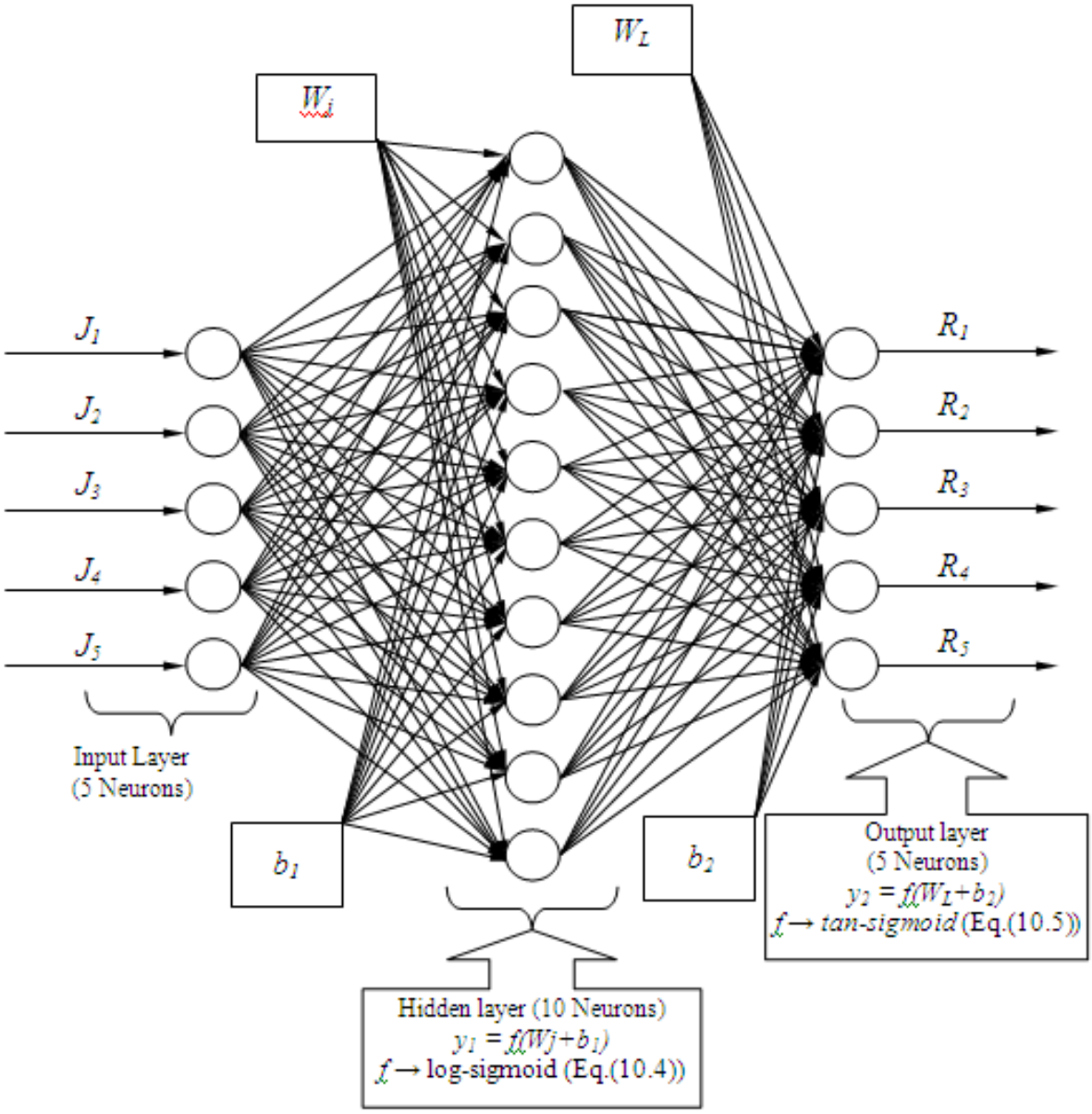

where J_1 – *H/R ratios* of adhesive, J_2 – *a/b ratios of* adhesive finite defect, J_3 – Orientations of adhesive infinite defect, J_4 – wt.% of CB in adhesive, and J_5 – number of reinforcement of *Cu* wire,
W_j *and* W_L – input weight and layer weight,
b_1 and b_2 – bias values associated with hidden layer and output layer,
y_1 and y_2 – output of hidden layer and output layer,
f – transfer or activation function,
R_1, R_2, R_3, R_4,and R_5 – predicted limit strains of DDQ steel and SS 316L sheets constituting adhesive bonded blanks corresponding to the effect of *H/R* ratios of adhesive, *a/b ratios of* adhesive finite defect, orientations of adhesive infinite defect, wt.% of CB in adhesive, and number of reinforcement of *Cu* wire.

Fig. 10.1 Neural network architecture developed for predicting the forming behaviour of adhesive bonded blanks in tensile test

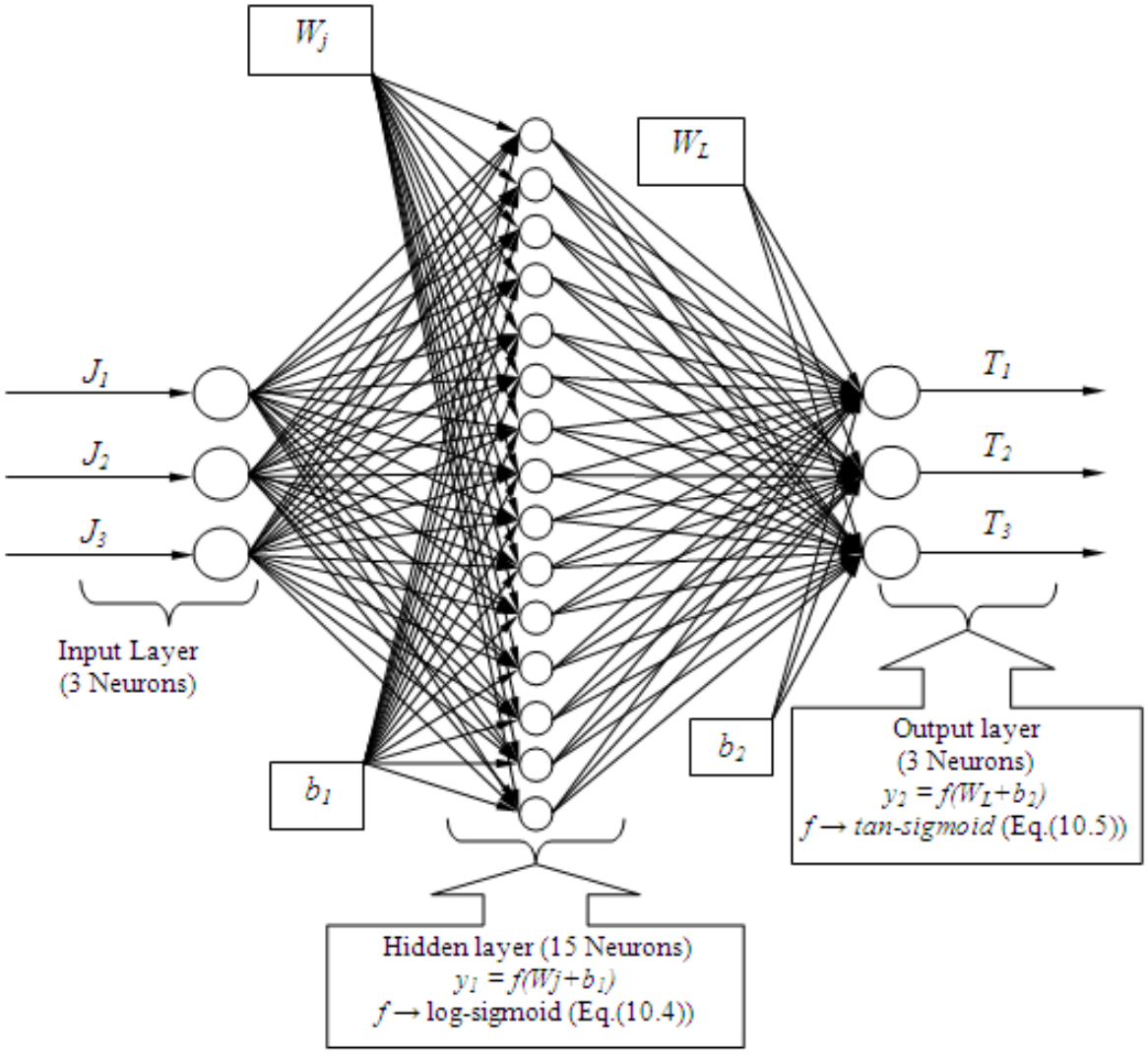

Fig. 10.2 Neural network architecture developed for predicting the forming behaviour of adhesive bonded blanks in deep drawing process

Fig. 10.2 shows the optimized architecture of neural network model developed for predicting the deep drawability of adhesive bonded blanks with the influencing parameters of hardener/resin ratios of adhesive, CB wt.% filled in adhesive, and high ductile wire reinforcements in the adhesive which is correspondingly taken as 3 number of neurons in the input layer. The number neurons used in the hidden layer is 15, and the output is activated by log-sigmoid function. The input weights and bias values are associated with the output of hidden layer. The limit strains corresponding to the effect of the above mentioned influencing parameters of adhesive bonded blanks are predicted as output response of the network that holds 3 neurons in the output layer. The output of output layer is activated by tan-sigmoid function associated with the layer weights and bias values.

10.6 Prediction of formability of adhesive bonded sheets using geometrical heterogeneities

The prediction of equivalent forming limit strains of base materials with the effect of hardener/resin ratio of adhesive using geometrical heterogeneities are already discussed in Chapter 9. In this work, the limits strains of base materials constituting adhesive bonded blanks in the tensile test, and the cup height results of adhesive bonded blanks predicted by ANN are validated with experimental results and the predicted results by using geometrical heterogeneities like finite and infinite heterogeneities.

10.6.1 Prediction of forming behaviour during tensile test and deep drawing process

As discussed in Chapter 9 in Section 9.4.1, the initial infinite geometrical heterogeneity, rectangular-infinite groove (Fig. 9.1(a)) in the tensile sample made of DDQ steel at 0.5 mm width (w), and square-finite groove (Fig. 9.1(c)) with side (w) of 0.5 mm for various heterogeneity factor *'f'* during prediction of forming limit strains were considered. In the case of deep drawing process (as discussed in Chapter 9 in Section 9.4.2), the circular-finite groove (Fig. 9.2) in region *'a'* with diameter, d_1 = 60 mm considered during prediction of cup height results.

10.7 Results and discussion

In this section, the predicted results with the effect of different adhesive properties on the forming behaviour of adhesive bonded blanks evaluated in the tensile and deep drawing tests through ANN model and finite element simulations using geometrical heterogeneities are discussed.

10.7.1 Prediction of forming behaviour of adhesive bonded blanks by ANN

10.7.1.1 Prediction of limit strains of base materials constituting adhesive bonded blanks in tensile test

Here the prediction of limit strains of DDQ steel and SS 316L sheets constituting adhesive bonded blanks are performed in two modes. In the first mode, all the important levels of input parameters are trained with three set of input data (Table 10.4) and corresponding target data that is limit strains of DDQ steel and SS 316L sheets in each case. Then output is predicted for one set of input parameters. In the second mode, the limit strains are predicted corresponding to the intermediate levels of unseen input data. Both modes of predicted results are validated with the experimental results.

Table 10.4 Input parameters and different levels during training of network corresponding to the target data

Input Parameter	Levels			
	1	2	3	4
Hardener/Resin (H/R) ratio	0.6	0.8	0.9	1.0
Adhesive finite defect *a/b* ratio	0 (No defect)	0.5	1	1.5
Adhesive infinite defect orientation	0º (No defect)	45º	90º (Transverse)	180º (Longitudinal)
CB wt.% in adhesive	0 (Unreinforced)	2	4	6
No.of reinforcements of *Cu* wire in adhesive	0 (Unfilled)	2	4	5

Fig. 10.3(a–j) shows the comparison between experimental and ANN predicted limit strain results of DDQ steel and SS 316L sheets constituting adhesive bonded blanks with the effect of different hardener/resin ratios (Fig. 10.3(a, b)), different aspect ratios of adhesive finite defect (Fig. 10.3(c, d)), different orientations of adhesive infinite defect (Fig. 10.3(e, f)), different CB wt.% filled in adhesive (Fig. 10.3(g, h)), various number of wire reinforcements (Fig. 10.3(i, j)). In the experimental results, it is observed that the limit strains in both the base materials increase with increase in hardener/resin ratio of adhesive. The limit strains of base materials decrease with increase in aspect (*a/b*) ratio of adhesive finite defects. There is a significant reduction in limit strains base materials in the case of transverse oriented adhesive infinite defect, and moderate reduction in limit strains in the case of longitudinal and 45º oriented adhesive infinite defects. The limit strains increase with increase in CB nano powder up to 2 wt.%, and then decreases with

excessive addition of CB powder in the adhesive. In the wire reinforcement case, the limit strains increase with increase in number reinforcements up to 2 wires, and then decrease with excessive reinforcements. The trend is observed in the predicted results by ANN model. There is a good agreement between experimental and predicted results, except in few cases. Table 10.5 shows the percentage of absolute error range in limit strains between experiment and ANN prediction. Table 10.6 shows the input parameters and different levels chosen during training of network corresponding to the target data during prediction of the limit strains corresponding to the intermediate levels of input data.

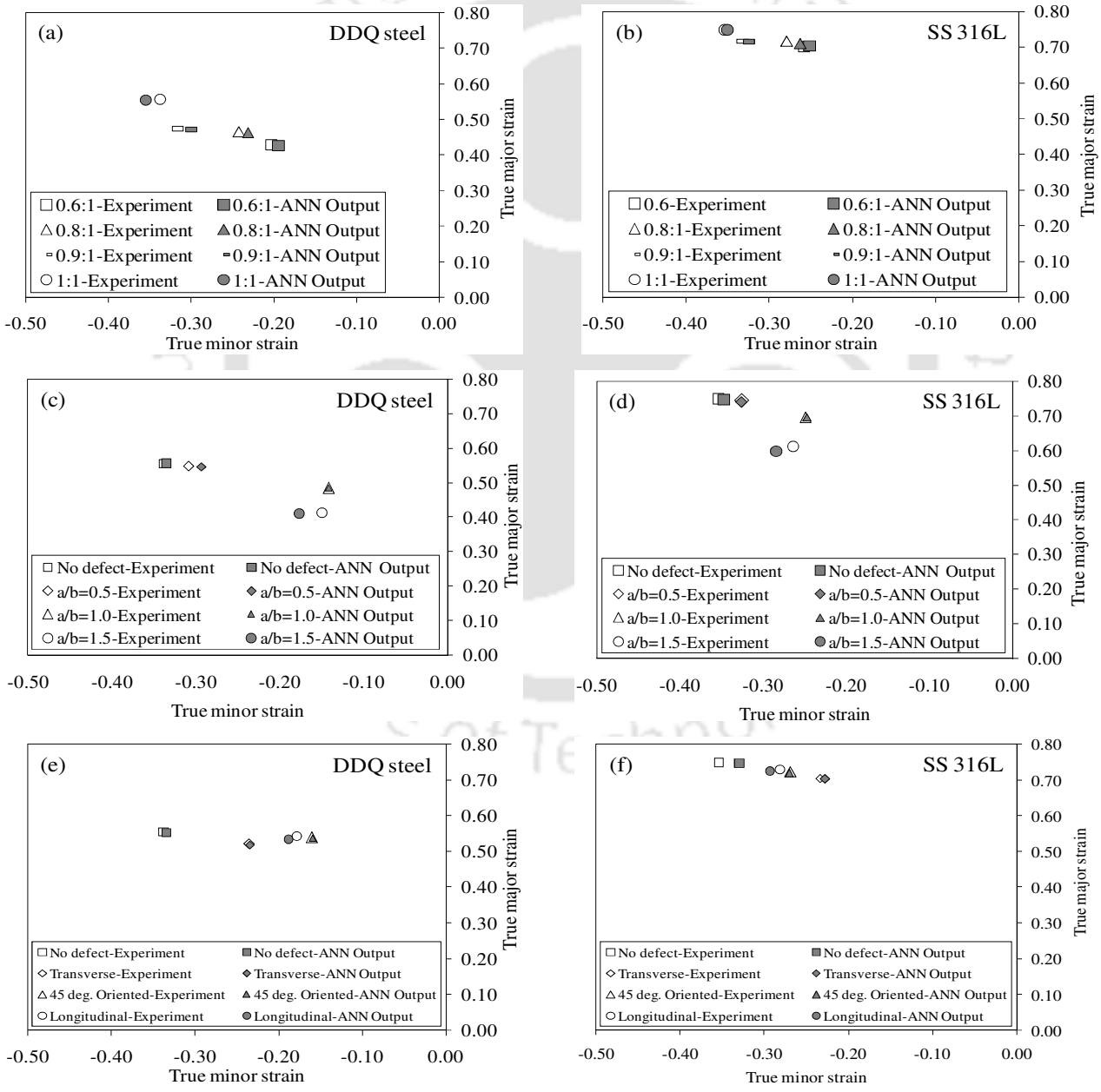

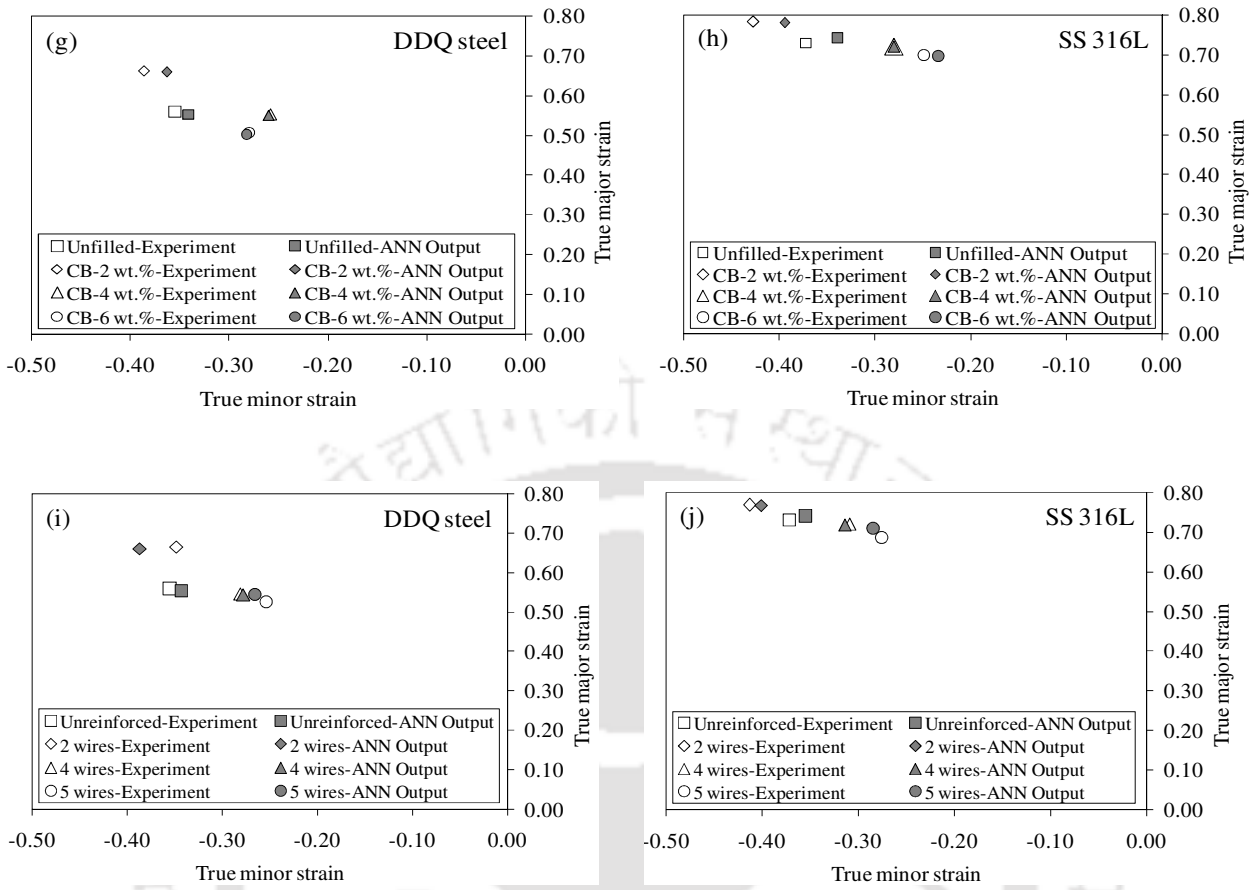

Fig. 10.3 Comparison of limit strains of base materials of adhesive bonded blanks between experiment and ANN output: (a) different H/R ratios of adhesive-DDQ steel, (b) different H/R ratios of adhesive-SS 316L, (c) different a/b ratios of adhesive finite defect-DDQ steel, (d) different a/b ratios of adhesive finite defect-SS 316L, (e) different orientations of adhesive infinite defect-DDQ steel, (f) different orientations of adhesive infinite defect-SS 316L, (g) different CB wt.% in adhesive –DDQ steel, (h) different CB wt.% in adhesive-SS 316L, (i) different numbers of wire reinforcements in adhesive-DDQ steel, and (j) different numbers of wire reinforcements in adhesive-SS 316L

Table 10.5 Percentage of error range of limit strains

Influencing parameters	True major strain		True minor strain	
	Error % between experiment and ANN prediction		Error % between experiment and ANN prediction	
	DDQ steel	SS 316L	DDQ steel	SS 316L
Hardener/resin (H/R) ratio	0.16 – 0.21	0.1 –0.5	0.8 – 1.7	0.4 – 1.6
Adhesive finite defect *a/b* ratio	0.001 –0.3	0.01 –1.5	0.01–2.7	0.1 – 2.01
Adhesive infinite defect orientation	0.1 –0.9	0.13 –0.5	0.1 –1.1	0.1 – 2.4
CB wt.% in adhesive	0.2 –0.6	0.03 –1.1	0.2 –2.3	0.1 – 3.4
No.of wire reinforcements	0.1 –2.3	0.1 –2.3	0.3 –3.9	0.5 – 1.7

Table 10.6 Input parameters and different levels used during intermediate level prediction

Input Parameter	Levels		
	1	2	3
Hardener/Resin (H/R) ratio	0.6	0.8	1.0
Adhesive finite defect *a/b* ratio	0 (No defect)	1	1.5
Adhesive infinite defect orientation	0º (No defect)	90º	180º
CB wt.% in adhesive	0 (Unfilled)	2	4
No.of reinforcements of *Cu* wire in adhesive	0 (Unreinforced)	2	4

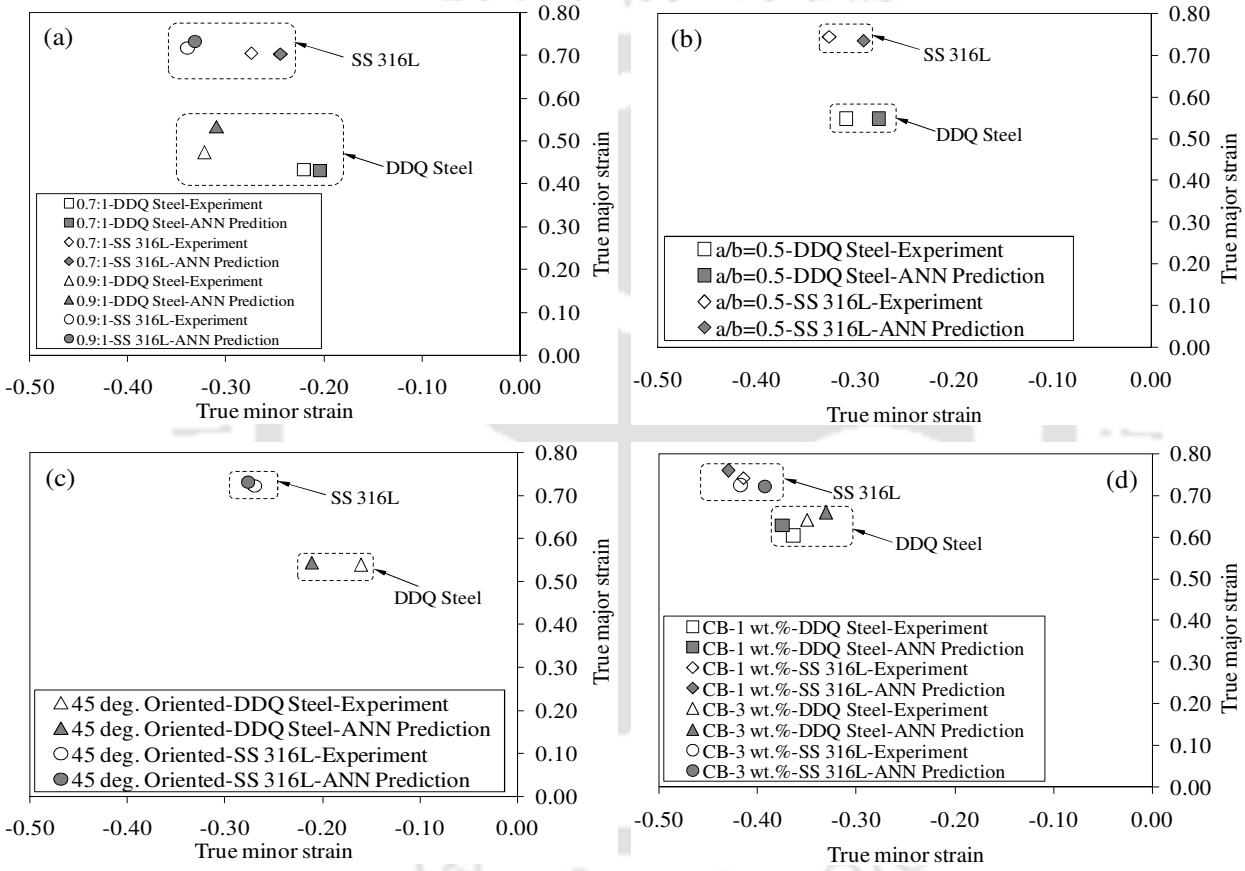

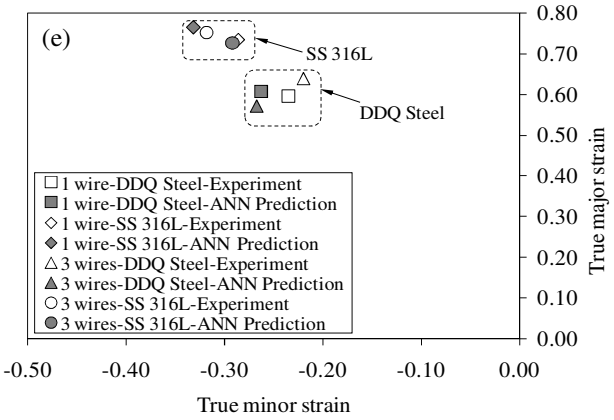

Fig. 10.4 Comparison of intermediate levels of limit strains of base materials of adhesive bonded blanks between experiment and ANN output: (a) different H/R ratios of adhesive-DDQ steel, (b) different H/R ratios of adhesive-SS 316L, (c) different a/b ratios of adhesive finite defect-DDQ steel, (d) different a/b ratios of adhesive finite defect-SS 316L, (e) different orientations of adhesive infinite defect-DDQ steel, (f) different orientations of adhesive infinite defect-SS 316L, (g) different CB wt.% in adhesive –DDQ steel, (h) different CB wt.% in adhesive -SS 316L, (i) different numbers of wire reinforcements in adhesive-DDQ steel, and (j) different numbers of wire reinforcements in adhesive-SS 316L

Fig. 10.4 (a-e) shows the comparison between experiment and ANN predicted limit strains of DDQ steel and SS 316L predicted for the intermediate levels of different input parameters. It is observed there is a good agreement between experimental results and ANN model predicted results except some of the cases. Table 10.7 shows the percentage of absolute error range in limit strains for intermediate input levels between experiment and ANN prediction.

Table 10.7 Percentage of error range in limit strains

Influencing parameters	True major strain	True minor strain
	Error % between experiment and ANN prediction	Error % between experiment and ANN prediction
Hardener/resin (H/R) ratio	0.2 – 6.0	0.7 – 3.0
Adhesive finite defect *a/b* ratio	0.1 – 1.0	3.3 – 3.5
Adhesive infinite defect orientation	0.5 – 0.9	0.7 – 5.0
CB wt.% in adhesive	0.3 – 2.4	1.0 – 2.5
No.of wire reinforcements	1.0 – 6.5	2.6 – 4.8

10.7.1.2 Prediction of deep drawability of adhesive bonded blanks

Table 10.8 shows the different levels of input parameters chosen for predicting the cup height of adhesive bonded blanks in the first mode of prediction. Fig. 10.5(a–j) shows the comparison of experimental and ANN predicted cup height adhesive bonded blanks with the effect of different hardener/resin ratios (Fig. 10.5(a)), different CB wt.% filled in adhesive (Fig. 10.5(b)), various number of wire reinforcements (Fig. 10.5(c)). In the experimental results, it is observed that the cup height increases with increase in hardener/resin ratio of adhesive. The cup height of adhesive bonded blanks increases with increase in CB nano powder up to 2 wt.% and then decreases with excessive addition of CB powder in the adhesive. In the wire reinforcement case, the cup height increases with increase in number reinforcements up to 16 wires, and then decrease with excessive reinforcements. The same trend is observed in the predicted results by ANN model. There is a good agreement between experimental and predicted results. Table 10.8 shows the percentage of absolute error range in cup height results between experiment and ANN prediction. Table 10.9 shows the different levels of input parameters chosen for predicting the cup height of adhesive bonded blanks intermediate levels of input parameters in the second mode of prediction. Fig. 10.6(a-c) shows the comparison between experiment and ANN predicted cup height adhesive bonded blanks with the intermediate levels of different input parameters. It is observed there is a good agreement between experimental results and ANN model predicted results. During intermediate level prediction, the absolute error % range in cup heights results between experiment and ANN prediction is 1.3 – 2.5%.

Table 10.8 Input parameters and different levels during training of network corresponding to the target data

Input Parameter	Levels				
	1	2	3	4	5
Hardener/Resin (H/R) ratio	0.6	0.7	0.8	0.9	1.0
CB wt.% in adhesive	0 (Unreinforced)	1	2	4	6
No.of reinforcements of *Cu* wire in adhesive	0 (Unfilled)	8	16	24	40

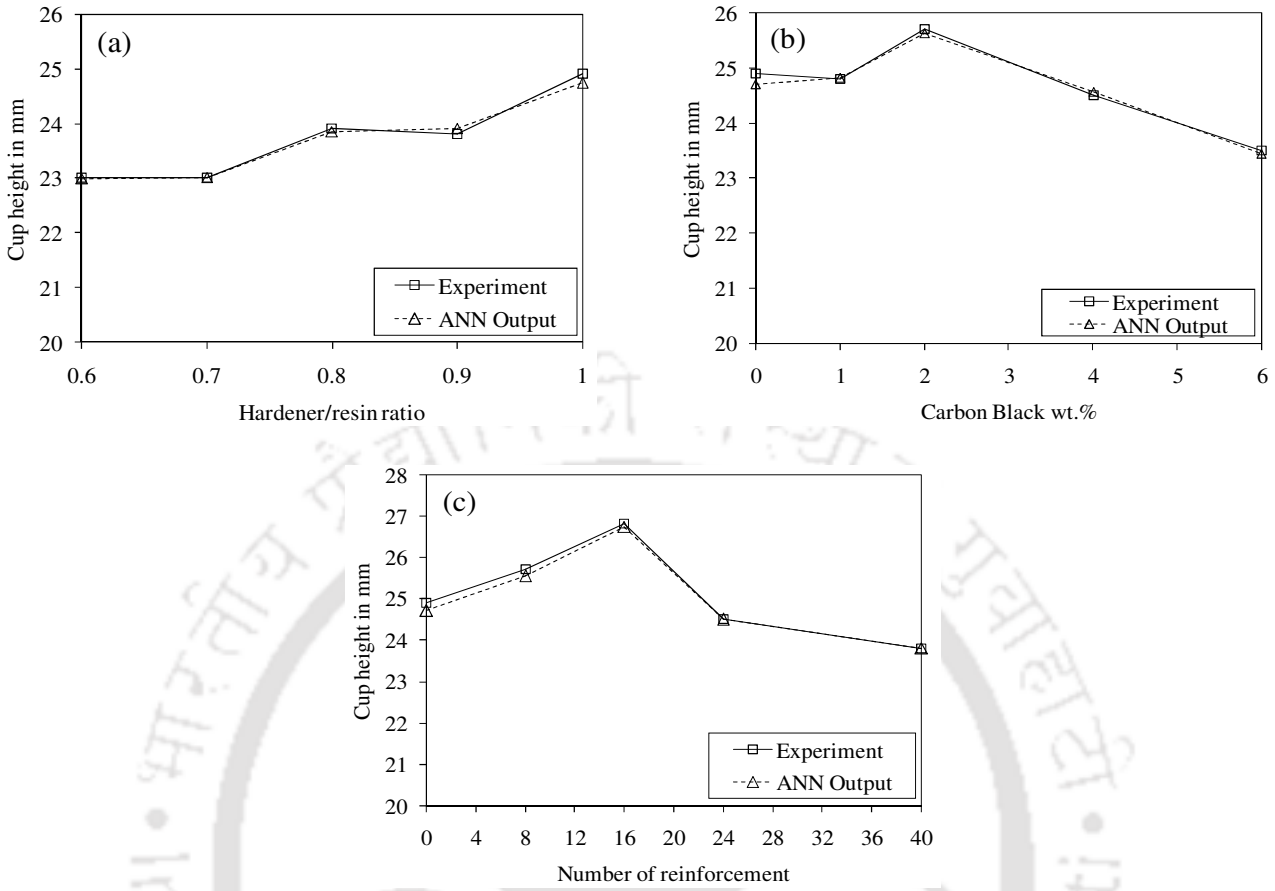

Fig. 10.5 Comparison of cup height results of adhesive bonded blanks: (a) different H/R ratios of adhesive, (b) different CB wt.% in adhesive, and (c) various numbers of wire reinforcement

Table 10.9 Percentage of error range in cup height results

Influencing parameters	Cup height
	Error % between experiment and ANN prediction
Hardener/resin (H/R) ratio	0.02 – 0.7
CB wt.% in adhesive	0.02 – 0.8
No.of wire reinforcements	0.01 – 0.8

Table 10.10 Input parameters and different levels used during intermediate level prediction

Input Parameter	Levels		
	1	2	3
Hardener/Resin (H/R) ratio	0.6	0.8	1.0
CB wt.% in adhesive	0 (Unfilled)	2	5
No.of reinforcements of *Cu* wire in adhesive	0 (Unreinforced)	16	32

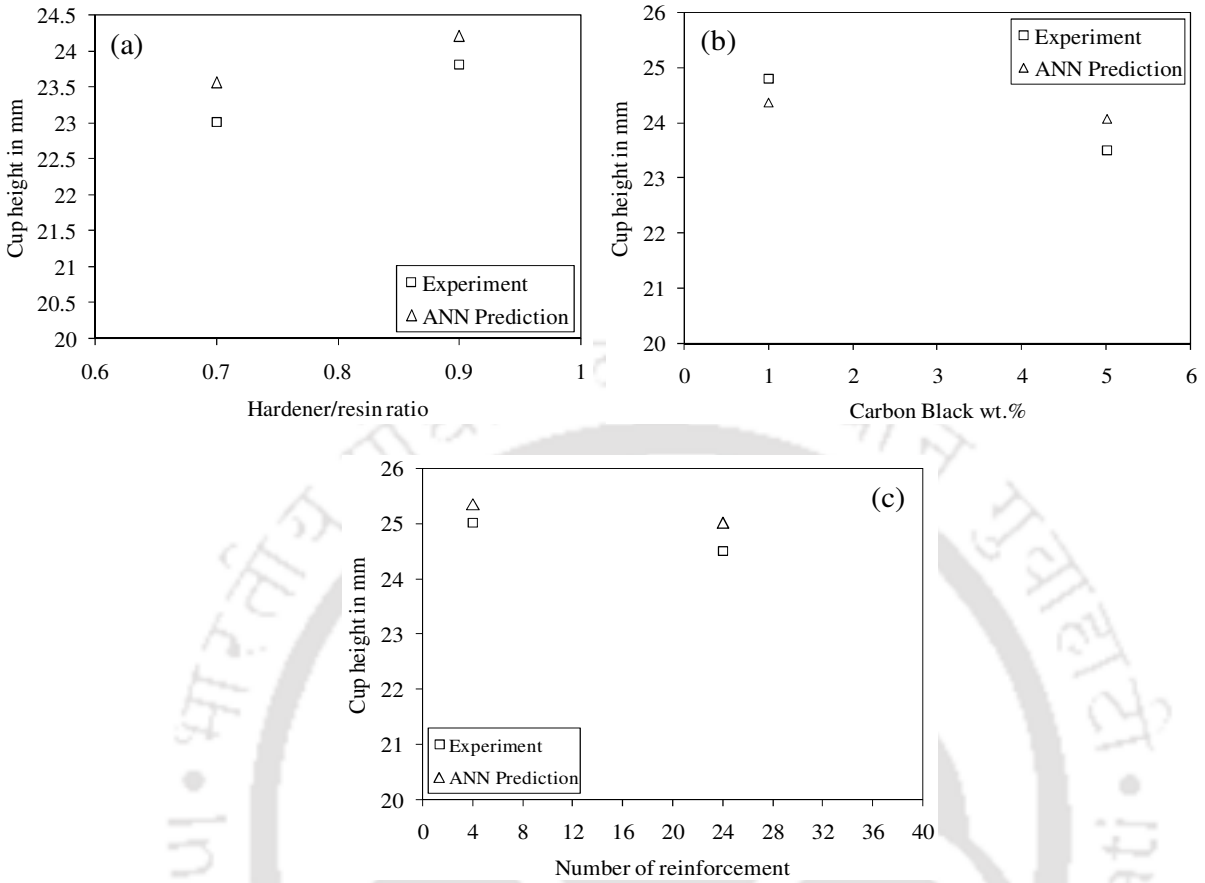

Fig. 10.6 Comparison of cup height results of adhesive bonded blanks for intermediate levels: (a) different H/R ratios of adhesive, (b) different CB wt.% in adhesive, and (c) various numbers of wire reinforcement

10.7.2 Validation of tensile test results with numerical prediction and experimental data

Fig. 10.7(a, b) shows the comparison of limit strains of DDQ steel between experiment, ANN prediction, and geometrical heterogeneity (infinite and finite) prediction equivalent to the effect of hardener/resin ratio of adhesive. From Fig. 10.7(a), it is observed that the limit strain of DDQ steel increases with increase in *'f'* value, which is similar to the trend of the effect of hardener/resin ratio of adhesive during experiment. There is about 0.01 to 3.5% variation in true major strains and about 1.6 to 6.3% variation in true minor strain between experiment and predicted results. There is about 0.02 to 13.7% variation in true major strain and about 1.8 to 11.4% in true minor strain between thickness heterogeneity with square finite-groove and ANN prediction.

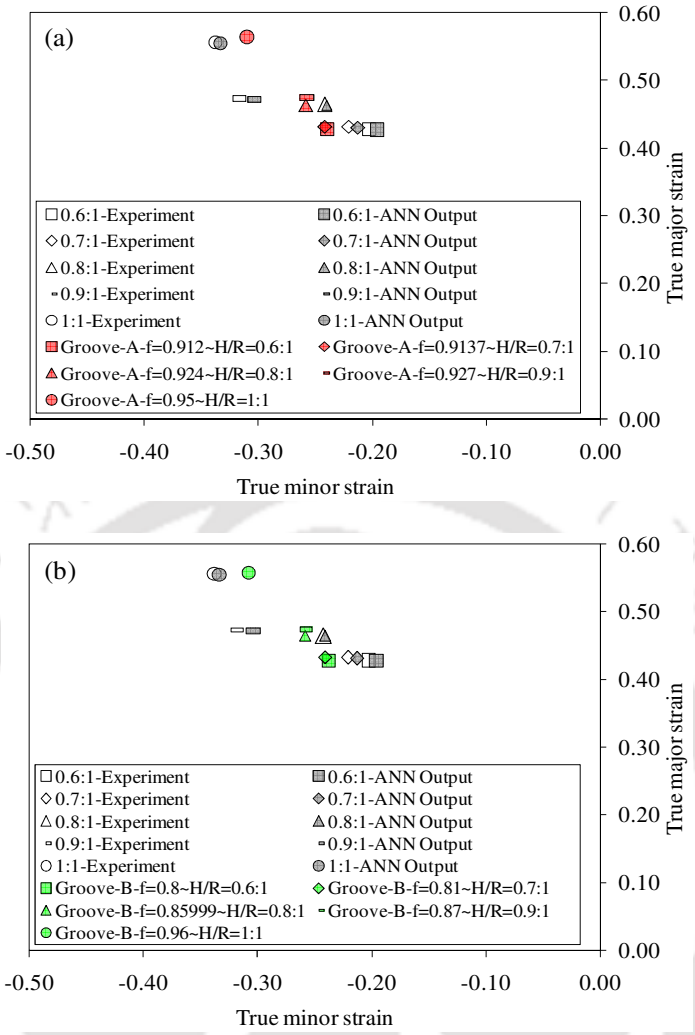

Fig. 10.7 Comparison of limit strains between experiment, ANN prediction and geometrical heterogeneity prediction during tensile test: (a) rectangular infinite-groove (Groove-A), and (b) square finite-groove (Groove-B)

Similarly, it is seen that the limit strain of DDQ steel increases with increase in *'f'* values in the case of square-finite thickness heterogeneity which is similar to the effect of hardener/resin ratio of adhesive during experiment (Fig. 10.7(b)). There is about 0.01 to 3.5% variation in true major strain and about 1.6 to 8% variation in true minor strain between experiment and predicted results. There is about 0.1 to 13.0% variation in true major strain and about 1.7 to 11.2% in true minor strain between thickness heterogeneity with square finite-groove and ANN prediction.

10.7.3 Validation of deep drawability with numerical prediction and experimental data

The predicted cup height result of SS 316L blank with different *'f'* values that is equivalent to the cup height of adhesive bonded blanks with the effect of hardener/resin ratio of adhesive is shown in Fig. 17. It is seen that the cup height increases with decrease in *'f'* values. There is about 0.6% variation in cup height between experiment and prediction. There is about 1.3% variation in cup height between ANN prediction and geometrical heterogeneity prediction.

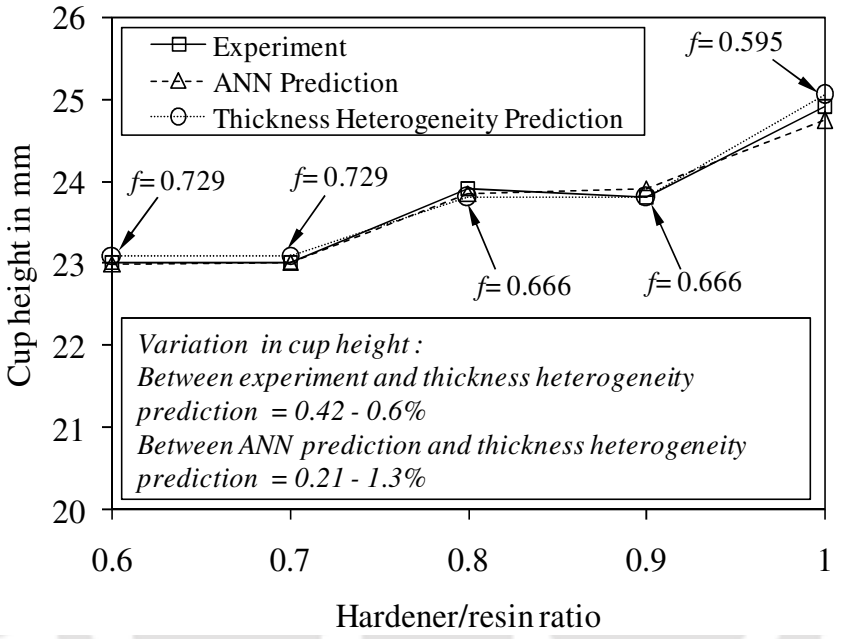

Fig. 10.8 Comparison of cup height results between experiment, ANN prediction, and geometric heterogeneity prediction

10.8 Proposed expert system

From the overall analyses carried out in the thesis work, an expert system for predicting the forming behaviour of adhesive bonded blanks (Fig. 10.9) is proposed. This approach is expected to overcome the difficulties of incorporation of adhesion properties of adhesive, selection of appropriate instability condition of adhesive during, and predicting the forming behaviour at varying adhesive properties.

During deformation of adhesive bonded blanks in tensile test and in-plane plane-strain (IPPS) formability test, the adhesive layer fails at first which is low ductile material, the low formable sheet DDQ steel fails after failure of adhesive layer, and then SS 316L at last which high formable

material. In this case, the overall formability of adhesive bonded blanks is decided by the ductility of the adhesive layer during deformation. Further, the limit strains of base materials constituting adhesive bonded blanks vary with adhesive properties in the presence of interface bonding as discussed in Chapter 1. Based on these results, the forming behaviour of adhesive bonded blanks can be divided into two categories like overall forming behaviour of adhesive bonded blanks, and forming behaviour of base materials constituting adhesive bonded blanks.

During experiment, the forming behaviour of adhesive bonded blanks is evaluated by monitoring the failure pattern, stress-strain behaviour of whole adhesive bonded blanks, forming limit strains of base materials constituting adhesive bonded blanks through tensile and IPPS formability tests. In the proposed predictive approach, the failure pattern of adhesive bonded blanks and stress-strain behaviour are obtained through finite element simulation by incorporating mechanical properties and materials models of base materials, and mechanical properties of adhesive as discussed in Chapter 4. The forming limit strains of base materials constituting adhesive bonded blanks are evaluated by two different approaches such as geometrical heterogeneities concept and ANN models. Using the geometrical heterogeneities concept, the equivalent forming behaviour of base materials constituting adhesive bonded blanks with the effect of varying adhesive properties could be predicted which simply involves knowledge based design of sheet metals. Generally, the forming limit strain results of base material constituents of adhesive bonded blanks are very much concerned with repeatability of the experiments. Using ANN models, the forming limit strains could be optimized, and the unknown forming limits corresponding to the intermediate levels of input data could also be predicted using the important levels of target data obtained through experiment. In the experimental deep drawing process of adhesive bonded blanks as discussed in Chapter 8, deformation pattern, load-stroke behaviour, final cup height at the maximum load in load-stroke behaviour, wrinkling pattern were monitored. In the proposed approach, the deformation pattern, approximated load-stroke behaviour, and wrinkling pattern of adhesive bonded blanks could be predicted by FE simulations by incorporating mechanical properties and materials models of base materials, and mechanical properties of adhesive. The cup height results of adhesive bonded blanks are evaluated by two different approaches such as geometrical heterogeneities concept and ANN models. Using the geometrical heterogeneities concept, the equivalent forming behaviour of the whole adhesive bonded blanks with the effect of varying adhesive properties could be predicted through knowledge based design of sheet metals.

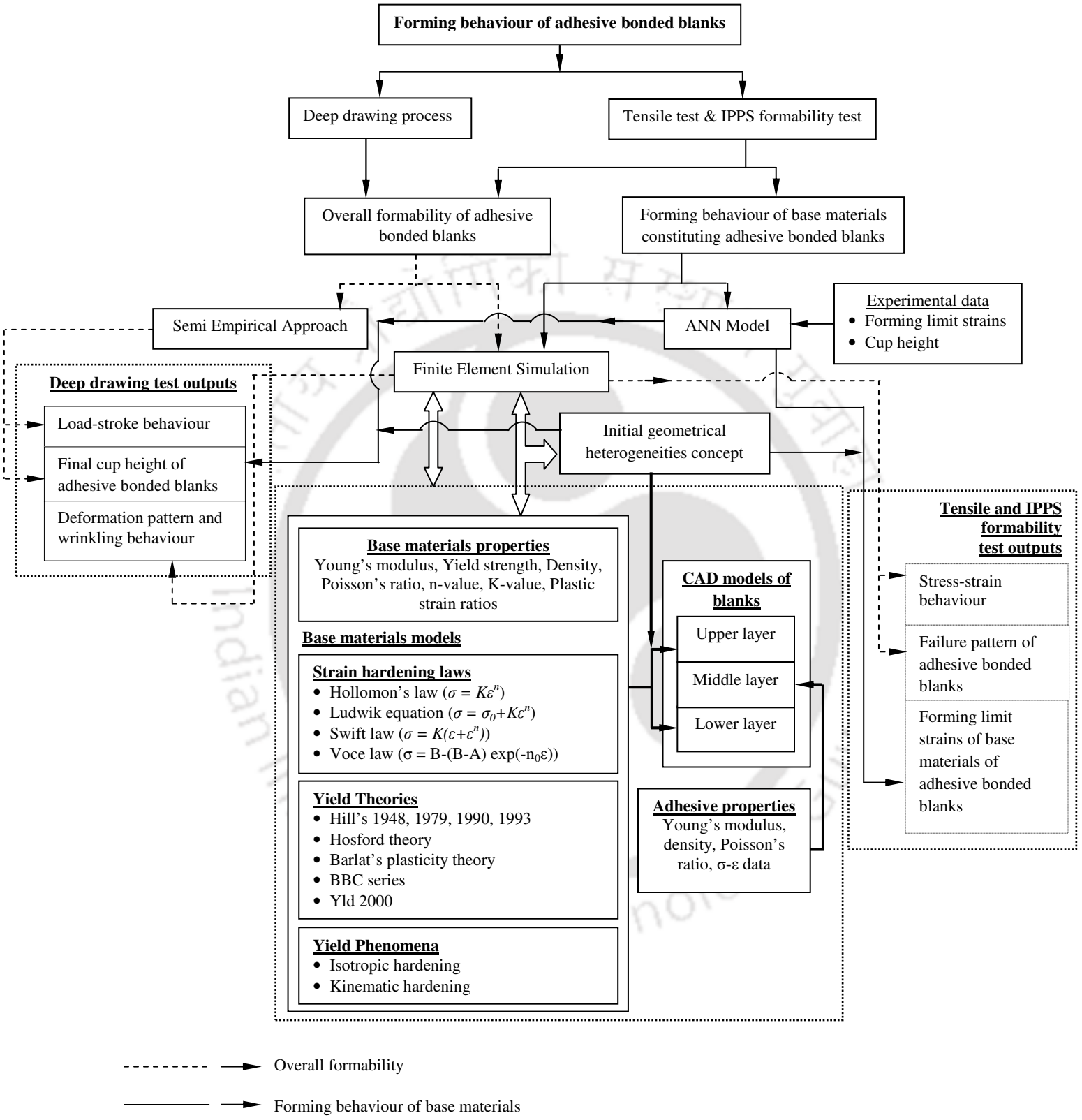

Fig. 10.9 Proposed expert system for prediction of formability of adhesive bonded sheets

Using ANN models, the cup height of adhesive bonded blanks could be optimized from different trails of experimental results, and the unknown cup height results corresponding to the intermediate levels of input data could be predicted. The entire load-stroke behaviour and the cup height of adhesive bonded blanks at the maximum load in load-stroke behaviour could also be predicted by semi-empirical approach which was attempted in our previous investigations.

10.9 Conclusions

The following conclusions are drawn from this work.

- It has been demonstrated that neural network can be used as an effective approach to predict the formability of adhesive bonded sheets, with no concern about incorporation of adhesive properties and bonding between the sheets, as observed during numerical simulations. On the other hand, the geometrical heterogeneity based concept is also equally effective in predicting the formability.
- The ANN models predict the influence of adhesive properties like hardener/resin ratios of adhesive, artificially generated adhesive defects, CB wt.% in adhesive, and wire reinforcement of adhesive very well and is comparable with experimental results.
- An expert system has been proposed to predict the formability of adhesive bonded blanks. This system involves neural network modeling, finite element simulations, and material modeling that show significant influence on the accuracy of final predicted results.

Chapter 11

Conclusions and scope of future work

11.1 Conclusions

The following major conclusions are drawn from the present work

- The overall formability of adhesive bonded blanks and the forming limits strains of base materials constituting adhesive bonded blanks improved with increase in hardener/resin ratio of adhesives. This is mainly due to the changeover of resin rich formulation to hardener rich formulation turning the sample more ductile. The improvement in ductility of adhesive with hardener rich formulation improves the plasticity of base materials constituting adhesive bonded sheets which results in improvement of forming limits due to presence of interface bonding.
- The formability of adhesive bonded blanks is significantly affected by adhesive defects. This is due to early failure caused by the adhesive layer in the bonded sheets at the defect location where strain is concentrated critically. This early failure of adhesive causes reduction in ductility of adhesive, and thereby the formability of adhesive bonded blanks and the limit strains of base materials decrease as compared to the formability of adhesive bonded blanks without defect. From these results, it is understood that the ductility of adhesive layer depends on the functional group, hardener/resin ratio, and the defect volume. The presence of micro-voids of volume less than or equal to $a/b = 0.5$ in the adhesive may not affect the formability of adhesive bonded blanks significantly. Since the formability of adhesive bonded blanks is influenced by volume of an adhesive defect; not number of adhesive defects and the reasonable numbers of equi-volume adhesive defects can be present in the adhesive bonded blanks.
- The ductility of adhesive bonded sheets increases with increase in wt.% of carbon black nano powder in the adhesive layer up to 2 wt.%, and then decreases excessive addition of

carbon black. This means that the ductility of adhesive and overall formability of adhesive bonded blanks could be improved by filling the carbon black powder in the adhesive up to an appropriate level (2 wt.% in this work) at constant hardener/resin ratio, without compromising the bondability of adhesive. This is not limited to improvement in formability, but also with aim of utilizing adhesive layer as a conductive polymer layer in adhesive bonded blanks.

- The ductility of adhesive bonded sheets and the forming limits of base material constituents improve when a low ductile adhesive is reinforced with high ductile wires along the loading direction up to an appropriate level. This is due to the optimum level of reinforcement of high ductile wires improves ductility of adhesive layer. But more replacement of adhesive with high ductile wire reduces the ductility of adhesive bonded sheets as compared to unreinforced adhesive bonded sheets. The orientation of wire reinforcement also affects the formability of adhesive bonded sheets. Since there is not much difference in the limit strains in the case of transverse reinforcement to the loading direction, it is suggested that replacement of adhesive layer (Ø0.3 mm in this work) with metal wires could be utilized as conductive adhesive bonded blanks (since adhesive is non-conductive polymer) without affecting the formability.
- The hardener rich formulation of adhesive improves the deep drawability of adhesive bonded blanks due to the improved ductility of adhesive layer. Further, filling of carbon black nano powder and reinforcement of high ductile wire in the low ductile adhesive to the optimum level improves the drawability, and also reduces the thinning of adhesive layer without any failure of constituting adhesive bonded blanks. This is due to increased ductility of adhesive by filling of carbon black or high ductile wire reinforcements up to an appropriate level.
- It is suggested that the true stress-strain behaviour of adhesive obtained either from rule of mixtures approach or from direct testing of adhesive could be followed in the forming limit strains and deep drawability predictions of adhesive bonded sheets. Limit strains and deep drawability results predicted through these approaches are almost same.
- From the finite element numerical prediction of adhesive bonded sheets forming behaviour, it is understood that the formability is mainly affected by interfacial bonding between

adhesive and the base materials constituting adhesive bonded sheets. On the whole, in tensile test and IPPS formability test at varying hardener/resin ratio and wt.% carbon black nano powder in the adhesive during finite element simulation, there is about 0.5 to 23.5% variation in true major strain, and about 1.7 to 13.4% variation in true minor strain of base materials constituting adhesive bonded sheets by thickness gradient based necking criterion prediction as compared to experimental results. Similarly, there is about 2.3 to 35.2% variation in true major strain, and about 2.1 to 20.9% variation in true minor strain of base material constituents of adhesive bonded sheets by effective strain based necking criterion prediction as compared to experimental results. There is about 4.5 to 14.5% variation in cup height of adhesive bonded blanks at varying hardener/resin ratio of adhesive, and wt.% of carbon black nano powder in the adhesive between experiment and finite element simulation.

- It is suggested from the present work that the maximum drawing load could be estimated by using anyone of the simple equations, such as equation (8.13) (Korhonen, 1982), equation (8.15) developed by Leu, 1997 or equation (8.16) developed by Leu and Wu, 2004 and the deep drawing behaviour could be predicted by the proposed equations (8.17) and (8.18), instead of modelling the adhesive and its interface bonding between base materials. This method of approach is not only applicable for adhesive bonded blanks, but also for all types of sheets for predicting their deep drawing behaviour.
- It has been hypothesized and demonstrated that with simple thickness heterogeneity factor the forming limits and deep drawability of adhesive bonded sheets could be predicted efficiently and accurately, without incorporating adhesive layer and properties during simulations. The effect of hardener/resin ratio on the forming limit of adhesive bonded sheets is well predicted by the thickness heterogeneity factor *'f'* and size of such defect. This has been shown with evidence from tensile tests. In the case of rectangular-infinite groove with $w = 0.5$ mm, the limit strains of DDQ steel evaluated at $f = 0.912$, $f = 0.9137$, $f = 0.924$, $f = 0.927$, and $f = 0.95$ are equivalent to the hardener/resin ratios of 0.6:1, 0.7:1, 0.8:1, 0.9:1, and 1:1 of adhesive, respectively. Similarly, the other cases of infinite and finite grooves with different dimensions and *'f'* values that are equivalent to the effect of different hardener/resin ratios of adhesive were evaluated.

- It has been demonstrated that neural network could be used as an effective approach to predict the formability of adhesive bonded sheets, with no concern about incorporation of adhesive properties and bonding between the sheets, as observed during numerical simulations. On the other hand, the geometrical heterogeneity based concept is also equally effective in predicting the formability.
- Finally, an expert system has been proposed to predict the formability of adhesive bonded blanks. This system involves neural network modeling, finite element simulations, and material modeling that shows significant influence on the accuracy of final predicted results.

11.2 Scope of future work

The following recommendations can be applied in the future works of this field.

- In the forming prediction of adhesive bonded sheets forming behaviour during finite element simulation, interfacial bond between adhesive and the base materials can be modelled at varying adhesive properties, and the accuracy of prediction can be analysed.
- The formability of adhesive bonded sheets can be investigated by limiting dome height (biaxial stretching) and the forming limits can be analysed at different strain paths.
- The formability of adhesive bonded sheets can be investigated with different filler materials and different reinforcements at varying orientations with the aim of improving forming limits.
- The hybrid joining processes of sheets metals like combination of adhesive bonding and conventional welding methods like spot welding and friction bit joining with the aim of avoiding delamination issue, minimising the effect of adhesive defects etc., and the forming behaviour can be investigated.
- The influence of adhesive properties on the tube bending process can be studied. The results such as bend ability of tubes and wrinkling at the bent region can be analysed with the effect of adhesive properties.
- In the prediction of equivalent forming behaviour of adhesive bonded sheets using geometrical heterogeneities with the effect of varying adhesive properties, a definite relationship between adhesive properties and thickness heterogeneity factor through some formulation with the common information of adhesive can be explored with the aim of quick prediction. Further, some kind of damage criterion that could predict failure without the need for extensive trial and error fitting can be derived.

References

Abbassi F., Belhadj T., Mistou S., Zghal A., Parameter identification of a mechanical ductile damage using artificial neural networks in sheet metal forming, Materials and Design, 45 (2013) 605–615.

Abdullah K., Wild P.M., Jesweit J.J., Ghasempoor A., Tensile testing for weld deformation properties in similar gage tailor welded blanks using the rule of mixtures, Journal of Materials Processing Technology, 112 (2001) 91–97.

Aboubakr S.H., Kandil U.F., Taha M.R., Creep of epoxy–clay nano composite adhesive at the FRP interface: A multi-scale investigation, International Journal of Adhesion and Adhesives, 54 (2014) 1–12.

Adams R.D., Adhesive bonding-science, technology and applications, Woodhead Publishing limited and Press LLC, UK, (2010).

Aghchai A.J., Shakeri M., Dariani B.M., Theoretical and experimental formability study of two–layer metallic sheet (Al1100/St12), Proc. IMechE Part B: Journal of Engineering Manufacture, 222 (2008) 1131–1138.

Allen K.W., Hatzinikolaou T., Armstrong K.B., A comparison of acrylic adhesives for bonding aluminium alloys after using various surface preparation methods, International Journal of Adhesion and Adhesives, 4(3) (1984) 133–136.

Allen K.W., Greenwood L., Armstrong K.B., A comparison of different grades of an acrylic adhesive for bonding an aluminium alloy, International Journal of adhesion and adhesives, 5(3) (1985) 149–152.

Al–Qureshi H.A., Klein A.N., Fredel M.C., Grain size and surface roughness effect on the instability strains in sheet metal stretching, Journal of Materials Processing Technology, 170 (2005) 204–210.

ASTM E646–07e1: Standard test method for tensile strain–hardening exponents (n–Values) of metallic sheet materials, ASTM International, West Conshohocken, PA, 2007.

ASTME 517–00(2010): Standard test method for plastic strain ratio (r) for sheet metal, ASTM International, West Conshohocken, PA, 2010.

ASTM D638–10: Standard test method for tensile properties of plastics, ASTM International, West Conshohocken, PA, 2010.

ASTM D1505–10: Standard test method for density of plastics by the density–gradient technique, ASTM International, West Conshohocken, PA, 2010.

ASTM A931–08(2013): Standard test method for tension testing of wire ropes and strand, ASTM International, West Conshohocken, PA; 2013.

Banabic D., Limit strains in the sheet metals by using the new Hill's yield criterion (1993), Journal of Materials Processing Technology, 92–93 (1999) 429–432.

Banabic D., Dannenmann E., Prediction of the influence of yield locus on the limit strains in sheet metals, Journal of Materials Processing Technology, 109 (2001) 9–12.

Banabic D., Sheet metal forming processes constitutive modeling and numerical simulation, Springer–Verlag, Heidelberg, (2010).

Bate P., Wilson D.V., Strain localisation in biaxial stretched sheets containing compact defects – II analysis using a finite element model, International Journal of Mechanical Sciences, 26(5) (1984) 363–372.

Battiti R., First and second order methods for learning: Between steepest descent and Newton's method, Neural Computation, 4(2) (1992) 141–166.

Behrens B.A., Dilger K., Wisner G., Rosenberger J., Locally reinforced hydro bonded blanks, Journal for Technology of Plasticity, 35(1-2) (2010) 1–11.

Berry N.G., d'Almeida J.R.M., The influence of circular centered defects on the performance of carbon–epoxy single lap joints, Polymer Testing, 21 (2002) 373–379.

Borsellinoa C., Bellab G. D., Ruisi V.F., Adhesive joining of aluminium AA6082: The effects of resin and surface treatment, International Journal of Adhesion and Adhesives, 29 (2009) 36–44.

Branco R., Antunes F.V., Costa J.D., Notched M(T) specimen for plane strain studies, International Journal of Fatigue, 58 (2014) 28–39.

Brockmann W., Hennemann O.D., Kollek H., Surface properties and adhesion in bonding aluminium alloys by adhesives, International Journal of Adhesion and Adhesives, 2(1) (1982) 33–40.

Butuc M.C., Barlat F., Gracio J.J., Study on plastic flow localization prediction using a physically–based hardening model, Computational Materials Science, 50 (2011) 2688–2697.

Chadegani A., Batra R.C., Analysis of adhesive–bonded single–lap joint with an interfacial crack and a void, International Journal of Adhesion and Adhesives, 31 (2011) 455–465.

Cheng J., Wu X., Li G., Pang S.S., Taheri F., Analysis of an adhesively bonded single–strap joint integrated with shape memory alloy (SMA) reinforced layers, International Journal of Solids and Structures, 44 (2007) 3557–3574.

Cherouat H., Borouchakic H., Present state of the art of composite fabric forming: geometrical and mechanical approaches, Materials, 2 (2009) 1835–1857.

Crocombe A.D., Global yielding as a failure criterion for bonded joints, International Journal of Adhesion and Adhesives, 9(3) (1989) 145–153.

Czamocki P., Piekarski K., Fracture strength of an adhesive–bonded joint, International Journal of Adhesion and Adhesives, 6 (1986) 93–95.

d'Almeida J.R.M., Monteiro S.N., The effect of the resin/hardener ratio on the compressive behaviour of an epoxy system, Polymer Testing, 15 (1996) 329–339.

d'Almeida J.R.M., Monteiro S.N., The role of the resin matrix/hardener ratio on the mechanical properties of low volume fraction epoxy composites, Advanced Performance Materials, 4 (1997) 285–295.

d'Almeida J.R.M, de Menezes G.W., Monteiro S.N., Ageing of the DGEBA/ TETA epoxy system with off-stoichiometric compositions, Materials Research, 6 (2003) 415–420.

da Silva L.F.M., Adams R.D., Gibbs M., Manufacture of adhesive joints and bulk specimens with high–temperature adhesives, International Journal of Adhesion and Adhesives, 24 (2004) 69–83.

de Moura M.F.S.F., Daniaud R., Magalhaes A.G., Simulation of mechanical behaviour of composite bonded joints containing strip defects, International Journal of Adhesion and Adhesives, 26 (2006) 464–473.

Deb A., Malvade I., Biswas P., Schroeder J., An experimental and analytical study of the mechanical behaviour of adhesively bonded joints for variable extension rates and temperatures, International Journal of Adhesion and Adhesives, 28 (2007) 1–15.

Detwiler A.T., Lesser A.J., Aspects of network formation in glassy thermosets, Journal of Applied Polymer Science, 117 (2010) 1021–1034.

D'Urso G., Maccarini G., The formability of aluminum foam sandwich panels, International Journal of Materials Forming, 5 (2012) 243–257.

Ebnesajjad S, Adhesives technology handbook, William Andrew Inc., New York, (2008).

Elangovan K., Sathiya Narayanan C., Narayanasamy R., Modelling of forming limit diagram of perforated commercial pure aluminium sheets using artificial neural network, Computational Materials Science, 47 (2010) 1072–1078.

Evangelista S.H., Lirani J., Al–Qureshi H.A., Implementing a modified Marciniak–Kuczynski model using the finite element method for the simulation of sheet metal deep drawing, Journal of Materials Processing Technology, 130–131 (2002) 135–144.

Floresa P., Tuninettia V., Gilles G., Gonry P., Duchene L., Habraken A.N., Accurate stress computation in plane strain tensile tests for sheet metal using experimental data, Journal of Materials Processing Technology, 201 (2010) 1772–1779.

Forte M.S., Whitney J.M., Schoeppner G.A., The influence of adhesive reinforcement on the Mode–I fracture toughness of a bonded joint, Composites Science and Technology, 60 (2000) 2389–2405.

Ghazanfari A., Assempour A., Calibration of forming limit diagrams using a modified Marciniak–Kuczynski model and an empirical law, Materials and Design, 34 (2012) 185–191.

Gill P.E., Murray W., Wright M.H., Practical Optimization, Academic Press Inc., London, (1981).

Gisario A, Barlett M., Conti C., Guarino S., Springback control in sheet metal bending by laser–assisted bending: Experimental analysis, empirical and neural network modelling, Optics and Lasers in Engineering, 49 (2011) 1372–1383.

Goodwin G.M., Application of strain analysis to sheet metal forming in the press shop, SAE Technical Paper, 680093, 1968.

Grant L.D.R., Adams R.D., da Silva L.F.M., Effect of the temperature on the strength of adhesively bonded single lap and T joints for the automotive industry, International Journal of Adhesion and Adhesives, 29 (2009) 405–413.

Gutowski W., The relationship between the strength of an adhesive bond and the thermodynamic properties of its components, International Journal of Adhesion and Adhesives, 7(4) (1987) 189–198.

Hasan R., Kasikci T., Tsukrov I., Kinsey B.L., Numerical and experimental investigations of key assumptions in analytical failure models for sheet metal forming, Journal of Manufacturing Science and Engineering, 136 (2014) 011013-1–011013-9.

Heslehurst R.B., Observations in the structural response of adhesive bondline defects, International Journal of Adhesion and Adhesives, 19 (1999) 133–154.

Holmberg S., Enquist B., Thilderkvist P., Evaluation of sheet metal formability by tensile tests, Journal of Materials Processing Technology, 145 (2004) 72–83.

Hufenbach W., Ullrich H., Gude M., Czulak A., Malczykn P., Geske V., Manufacture studies and impact behaviour of light metal matrix composites reinforced by steel wires, Archives of Civil and Mechanical Engineering, 12 (2012) 265 – 272.

Huntsman Advanced Materials (India) Private Ltd., Test report of Araldite AW106 (Batch No: 1011GOA16) and HV 953 IN (Batch No: 1011GOA17), (Standard Epoxy Structural Adhesive), 2012.

Johnson D.A., Metals and Chemical Change, Open University, Royal Society of Chemistry, Great Britain, (2002).

Karachalios E.F., Adams R.D., da Silva L.F.M., Strength of single lap joints with artificial defects, International Journal of Adhesion and Adhesives, 45 (2013) 69–76.

Karlsson K.F., Astrom B.T., Manufacturing and applications of structural sandwich components, Composites Part A, 28A (1997) 97–111.

Katsiropoulos Ch.V., Chamos A.N., Tserpes K.I., Pantelakis Sp.G., Fracture toughness and shear behavior of composite bonded joints based on a novel aerospace adhesive, Composites: Part B, 43 (2012) 240–248.

Kee K.J., Rhee M.H., Choi B.I., Kim C.W., Sung C.W., Han C.P., Kang K.W., Won S.T., Development of application technique of aluminum sandwich sheets for automotive hood, International Journal of Precision Engineering and Manufacturing, 10 (2009) 71–75.

Keeler S.P., Backhofen W.A., Plastic instability and fracture in sheet stretched over rigid punches, ASM Transactions Quarterly, 56 (1964) 25–48.

Khalili S.M.R., Shokuhfar A., Hoseini S.D., Bidkhori M., Khalili S., Mittal R.K., Experimental study of the influence of adhesive reinforcement in lap joints for composite structures subjected to mechanical loads, International Journal of Adhesion and Adhesives, 28(8) (2008) 436–444.

Kim K.J., Kim D., Choi S.H., Chung K., Shin K.S., Barlat F., Oh K.H., Youn J.R., Formability of AA5182/polypropylene/AA5182 sandwich sheets, Journal of Materials Processing Technology 139 (2003) 1–7.

Kim K.J., Rhee M.H., Choi B., Kim C.W., Sung C.W., Han C.P., Kang K.W., Won S.T., Development of application technique of aluminum sandwich sheets for automotive hood, International Journal of Precision Engineering and Manufacturing, 10(4) (2010) 71–75.

Kim Y.T., Lee M.J., Lee B.C., Simulation of adhesive joints using the superimposed finite element method and a cohesive zone model, International Journal of Adhesion and Adhesives, 31 (2011) 357–362.

Korhonen A.S., Drawing force in deep drawing of cylindrical cup with flat–nosed punch, Journal of Engineering for Industry, 104 (1982) 29–37.

Kotkunde N., Deole A.D., Gupta A.K., Prediction of forming limit diagram for Ti–6Al–4V alloy using artificial neural network, Procedia Materials Science, 6 (2014) 341–346.

Leu D.K., Prediction of the limiting drawing ratio and the maximum drawing load in cup drawing, International Journal of Machine Tool Manufacturing, 37(2) (1997) 201–213.

Leu D.K., Wu J.Y., A simplified approach to estimate limiting drawing ratio and maximum drawing load in cup drawing, Journal of Engineering Materials and Technology, 126 (2004) 116–122.

Lin Y.Y., Hui C.Y., Cavity growth from crack–like defects in soft materials, International Journal of Fracture, 126 (2004) 205–221.

Liu J., Xue W., Formability of AA5052/polyethylene/AA5052 sandwich sheets, Transactions of Nonferrous Metals Society of China, 23 (2013) 964−969.

Liu J.G., Wei L., Wang J., Influence of interfacial adhesion strength on formability of AA5052/polyethylene/AA5052 sandwich sheet, Transactions of Nonferrous Metals Society of China, 22 (2012) s395–s401.

Llopart L.P., Tserpes K.I., Labeas G.N., Experimental and numerical investigation of the influence of imperfect bonding on the strength of NCF double–lap shear joints, Composite Structures, 92 (2010) 1673–1682.

Ma A.J., Chen W., Hou Y., Zhang G., Dispersion, Mechanical and thermal properties of epoxy resin composites filled with the nanometer carbon black, Polymer-Plastics Technology and Engineering, 49 (2010) 916 – 920.

MacKay D.J.C., Bayesian interpolation, Neural Computation, 4(3) (1992) 415–447.

Marciniak Z., Kuczyinski K., Pokora T., Influence of the plastic properties of a material on the forming limit diagram for sheet metal in tension, International Journal of Mechanical Sciences, 15 (1973) 789–805.

Marciniak Z., Kuczynski K., Limit strains in the processes of stretch–forming sheet metal, International Journal of Mechanical Sciences, 9 (1967) 609–620.

May M., Vob H., Hiermaier S., Predictive modelling of damage and failure in adhesively bonded metallic joints using cohesive interface elements, International Journal of Adhesion and Adhesives, 49 (2014) 7–17.

Melander A., Linder J., Stensio H., Larsson M., Gustavsson A., Bjorkman G., How defects in an adhesive layer influence the fatigue strength of bonded steel–sheet specimens, Fatigue and Fracture of Engineering Materials and Structures, 22 (1999) 421–426.

Metlok private Ltd., Test report of My–T–Bond 1001 (Structural Acrylic Adhesive), 2012.

Moller M., A scaled conjugate gradient algorithm for fast supervised learning, Neural Networks, 6 (1993) 525–533.

Monaco A., Sinke J., Benedictus R., Experimental and numerical analysis of a beam made of adhesively bonded tailor–made blanks, International Journal of Adhesion and Adhesives, 44 (2009) 766–780.

Moon H.S., Na S.J., Optimum design based on mathematical model and neural network to predict weld parameters for fillet joints, Journal of Manufacturing Systems, 16(1) (1997) 13–23.

Morovvati M.R., Dariani B. M., Ardakani M.H.A., A theoretical, numerical, and experimental investigation of plastic wrinkling of circular two–layer sheet metal in the deep drawing, Journal of Materials Processing Technology, 210 (2010) 1738–1747.

Morovvati M.R., Fatemi A., Sadighi M., Experimental and finite element investigation on wrinkling of circular single layer and two–layer sheet metals in deep drawing process, International Journal of Advanced Manufacturing Technology, 54 (2011) 113–121.

MTLS – Metallurgical testing laboratory services, Certificate of analysis of SS 316L, No. K/6951, 2012.

Mukesh K., Kailas S.V., Ganesh Narayanan R., Influence of external flash on the in–plane plane–strain formability of friction stir welded sheets, The Journal of Strain Analysis for Engineering Design, 48(6) (2013a) 376–385.

Mukesh K., Kailas S.V., Ganesh Narayanan R., In–plane plane–strain formability investigation of friction stir welded sheets made of dissimilar Aluminium alloys, Applied Mechanics and Materials, 446–447 (2013b) 301–305.

Nakamura R., Goda K., Noda J., Ohgi J., High temperature tensile properties and deep drawing of fully green composites, eXPRESS Polymer Letters, 3(1) (2009) 19–24.

Nam S., Yu Y.H., Choi I., Bang C.S., Lee D.G., Fracture toughness improvement of polyurethane adhesive joints with chopped glass fibers at cryogenic temperatures, Composite Structures, 107 (2014) 522–527.

Narasimhan K., Wagoner R.H., Finite element modeling simulation of in–plane forming limit diagrams of sheets containing finite defects, Metallurgical Transactions A, 22(11) (1991) 2655–2665.

Nassar S.A., Mao J., Yang X., A damage model for adhesively bonded single–lap thick composite joints. Journal of Engineering Materials and Technology 134 (2012) 041004-1–041004-6.

Nguyen A., Widrow B., Improving the learning speed of 2–layer neural networks by choosing initial values of the adaptive weights, Proceedings of the International Joint Conference on Neural Networks (IJCNN), San Diego, CA, 3 (1990) 21–26.

Ning S., Mackie R.I., Harvey W.D., The effects of ageing and environment on the fatigue life of adhesive joints, International Journal of Adhesion and Adhesives, 12(2) (1992) 85–93.

Nishimura T., Stress intensity factors for multiple cracks in an adhesively bonded sandwich sheet, Journal of Engineering Materials and Technology, 115 (1993) 134–139.

Novak I., Krupa I., Chodak I., Analysis of correlation between percolation concentration and elongation at break in filled electroconductive epoxy–based adhesives, European Polymer Journal, 39 (2003) 585– 592.

Olia M., Rossettos J.N., Analysis of adhesively bonded joints, with gaps subjected to bending International Journal of Solids Structure, 33(18) (1996) 2681–2693.

Oya T., Tiesler N., Kawanishi S., Yanagimoto J., Koseki T., Experimental and numerical analysis of multilayered steel sheets upon bending, Journal of Materials Processing Technology, 210 (2010) 1926–1933.

Pal S., Pal S.K., Samantaray A.K., Artificial neural network modeling of weld joint strength prediction of a pulsed metal inert gas welding process using arc signals, Journal of Materials Processing Technology, 202 (2008) 464–474.

Parmar A., Mellor P. B., Predictions of limit strains in sheet metal using a more general yield criterion, International Journal of Mechanical Sciences, 20 (1978) 385–391.

Parmar A., Mellor P.B., Chakrabarty J., A new model for the prediction of instability and limit strains in thin sheet metal, International Journal of Mechanical Sciences, 19 (1977) 389–398.

Parsa M.H., Ahkami S.N.A, Ettehad M., Experimental and finite element study on the spring back of double curved aluminum/polypropylene/aluminum sandwich sheet, Materials and Design 31 (2010) 4174–4183.

Parsa M.H., Ettehad M., Matin P.H., Nasher S., Ahkami A., Experimental and numerical determination of limiting drawing ratio of Al3105– polypropylene–Al3105 sandwich sheets, Journal of Engineering Materials and Technology, 132 (2010) 031004-1–031004-11.

Patel A., Das S., Ganesh Narayanan R., CAFE modeling, neural network modeling, and experimental investigation of friction stir welding, Proc IMechE Part C: Journal of Mechanical Engineering Science, 227(6) (2012) 1164–1176.

Pereira A.M., Ferreira J.M., Antunes F.V., Bartolo P.J., Analysis of manufacturing parameters on the shear strength of aluminium adhesive single–lap joints, Journal of Materials Processing Technology, 210 (2010) 610–617.

Perton M., Blouin A., Monchalin J.P., Adhesive bond testing of carbon–epoxy composites by laser shockwave, Journal of Physics D: Applied Physics, (2011) doi:10.1088/0022–3727/44/3/034012.

Pertrie E.M., Handbook of adhesives and sealants, The McGraw-hill companies, New York, (2000).

Pocius A.V., Adhesion and adhesive technology–An introduction, 2nd Edition, Hanser, Germany, (2002).

Potocnik D., Pesan B., Balic J., Ulbin M., Intelligent system for the automatic calculation of stamping parameters, Advances in Production Engineering and Management, 6(2) (2011) 129–137.

Prasse T., Schwarz M.K., Schulte K., Bauhofer W., The interaction of epoxy resin and an additional electrolyte with non-oxidised carbon black in colloidal dispersions, Colloids and Surfaces A: Physicochemical and Engineering Aspects, 189 (2010) 183–188.

Ragab A.R., Saleh Ch.A.R., Effect of void growth on predicting forming limit strains for planar isotropic sheet metals, Mechanics of Materials, 32 (2000) 71–84.

Ravi K., Ganesh Narayanan R., In–plane testing behaviour of adhesive–bonded steel sheets: influence of sheet surface roughness, adhesive thickness, and bonding width, Journal of Testing and Evaluation, 40(2) (2012) 97–106.

Riedmiller M., Braun H., A direct adaptive method for faster backpropagation learning: The RPROP algorithm, Proceedings of the IEEE International Conference on Neural Networks (ICNN), San Francisco, (1993) 586–591.

Robi P.S., Dixit U.S., Application of neural networks in generating processing map for hot working, Journal of Materials Processing Technology, 142 (2003) 289–294.

Rocha A.B.D., Barlat F., Jalinier J.M., Prediction of the forming limit diagrams of anisotropic sheets in linear and non–linear loading, Materials Science and Engineering, 68 (1984–1985) 151–164.

Rossettos J.N., Lin P., Nayeb–Hashemi H., Comparison of the effects of debonds and voids in adhesive joints, Journal of Engineering Materials and Technology, 116 (1994) 533–538.

Rumelhart D.E., Widrow B., Lehr M.A., The basic ideas in neural networks, Communications of the ACM, 37(3) (1994) 87–92.

Saleh N.J., Adnan A., Abdul Razak, Tooma M.A., Aziz M.E., A study mechanical properties of epoxy resin cured at constant curing time and temperature with different hardeners, Engineering and Technology Journal, 29 (2011) 1804–1818.

Shahin M., Elchalakani M., Neural networks for modelling ultimate pure bending of steel circular tubes, Journal of Constructional Steel Research, 64 (2008) 624–633.

Shin K.S., Kim K.J., Choi S.W., Rhee M.H., Mechanical Properties of Aluminum/Polypropylene/Aluminum Sandwich Sheets, Metals and Materials, 5 (1999) 613–618.

Sokolovan O.A., Kuhn M., Palkowski H., Deep drawing properties of lightweight steel/polymer/steel sandwich composites, Archives of Civil and Mechanical Engineering, 12 (2012) 105–112.

Srivatsan T.S., Lam P.C., Krause J., The impact toughness characteristics of steel wire–reinforced polymer composites. Materials Letters, 39 (1999) 324–328.

Stoughton T.B., Yoon J.W., Path independent forming limits in strain and stress spaces, International Journal of Solids and Structures, 49 (2012) 3616–3625.

Sujit Kumar, Date P.P., Narasimhan K., A new criterion to predict necking failure under biaxial stretching, Journal of Materials Processing Technology, 45(1–4) (1994) 583–588.

Sumfleth J., Buschhorn S.T., Schulte K., Comparison of rheological and electrical percolation phenomena in carbon black and carbon nanotube filled epoxy polymers, Journal of Material Science, 46 (2011) 659–669.

Taib A., Boukhili R., Achiou S., Gordon S., Boukehili H., Bonded joints with composite adherends. Part I. Effect of specimen configuration, adhesive thickness, spew fillet and adherend stiffness on fracture, International Journal of Adhesion and Adhesives, 26(4) (2006) 226–36.

Takano N., Ohnishi Y., Zako M., Nishiyabu K., Microstructure-based deep-drawing simulation of knitted fabric reinforced thermoplastics by homogenization theory, International Journal of Solids and Structures, 38 (2001) 6333–6356.

Takiguchi M., Yoshida F., Plastic bonding adhesive bonding of sheet metals, Journal of Materials Processing Technology, 113 (2001) 743–748.

Takiguchi M., Yoshida F., Analysis of plastic bending of adhesive–bonded sheet metals taking account of viscoplasticity of adhesive, Journal of Materials Processing Technology, 140 (2003) 441–446.

Tang C.Y., Tai W.H., Material damage and forming limits of textured sheet metals, Journal of Materials Processing Technology, 99 (2000) 135–140.

Tata steel, Test certificate – IS 513 Grade–CR1, Licence No. CM/L–51524, 2012.

The MathWorks, Inc., 1994–2013.

Tiryaki S., Ozsahin S., Yildirima I., Comparison of artificial neural network and multiple linear regression models to predict optimum bonding strength of heat treated woods, International Journal of Adhesion and Adhesives, 55 (2014) 29–36.

Uehara K., Sakurai M., Bonding strength of adhesives and surface roughness of joined parts, Journal of Materials Processing Technology, 127 (2002) 178–181.

Ungar T., Gubicza J., Ribarik G., Pantea C., Zerda T.W., Microstructure of carbon blacks determined by X–ray diffraction profile analysis, Carbon, 40 (2002) 929–937.

Veera Babu K., Ganesh Narayanan R., Saravana Kumar G., An expert system based on artificial neural network for predicting the tensile behavior of tailor welded blanks, Expert Systems with Applications, 36 (2009) 10683–10695.

Vietri U., Guadagno L., Raimondo M., Vertuccio L., Lafdi K., Nanofilled epoxy adhesive for structural aeronautic materials. Composites: Part B, 61 (2014) 73–83.

Wagoner R.H., Comparison of plane–strain and tensile work hardening in two sheet steel alloys, Metallurgical Transactions A, 12 (1981) 877–882.

Wagoner R.H., Measurement and analysis of plane–strain work hardening, Metallurgical Transactions A, 11 (1980) 165–175.

Wake W.C., Theories of adhesion and uses of adhesives: a review, Polymer, 19 (1978) 291–308.

Wang J., Wu X., Thomson P.F., Flitman A., A neural networks approach to investigating the geometrical influence on wrinkling in sheet metal forming, Journal of Materials Processing Technology, 105 (2000) 215 – 220.

Wang T.J., Kuang Z.B., Stress, deformation and damage fields near the tip of a crack in a damaged nonlinear material, International Journal of Fracture, 79 (1996) 1–26.

Weiss M., Dingle M.E., Rolfe B.F., Hodgson P.D., The influence of temperature on the forming behaviour of metal/polymer laminates in sheet metal forming, Journal of Engineering Materials and Technology, 129 (2007) 530–537.

Zadpoor A.A., Sinke J., Benedictus R., The mechanical behaviour of adhesively bonded tailor–made blanks, International Journal of Adhesion and Adhesives, 29 (2009) 558–571.

Zadpoor A.A., Sinke J., Benedictus Rinze., Elastoplastic deformation of dissimilar–alloy adhesively–bonded tailor–made blanks. Materials and Design, 31 (2010) 4611–4620.

Zhang Y., Luo R., Zhang J., Xiang Q., The reinforcing mechanism of carbon fiber in composite adhesive for bonding carbon/carbon composites, Journal of Materials Processing Technology, 211 (2011) 167–173.

Publications from the present work

Refereed Journals

[1] **Satheeshkumar V**, Ganesh Narayanan R, "Experimental evaluation and prediction of formability of adhesive bonded steel sheets at different adhesive properties", Journal of Testing and Evaluation. (Accepted)

[2] **Satheeshkumar V,** Ganesh Narayanan R, "Prediction of formability of adhesive bonded steel sheets and experimental validation", Archives of Civil and Mechanical Engineering, 15 (2015) 30 – 41.

[3] **Satheeshkumar V**, Ganesh Narayanan R, "In-plane plane-strain formability of adhesive bonded steel sheets: Influence of adhesive properties", International Journal of Advanced Manufacturing Technology, DOI 10.1007/s00170-014-6335-0.

[4] **Satheeshkumar V**, Ganesh Narayanan R, "Formability of adhesive bonded steel sheets with artificial finite adhesive defects", Journal of Strain Analysis for Engineering Design, Vol. 49(5) (2014) 286–300.

[5] **Satheeshkumar V**, Ganesh Narayanan R, "Investigation on the influence of adhesive properties on the formability of adhesive bonded steel sheets", Proc. of the Institution of Mechanical Engineers, Part C, Journal of Mechanical Engineering Science, Proc IMechE Part C: J Mechanical Engineering Science, Vol. 228(3) (2014) 405–425.

[6] **V. Satheeshkumar**, R. Ganesh Narayanan, "Influence of pre-generated infinite adhesive defects on the forming behaviour of adhesive bonded steel sheets", Advanced Materials Research, Vol. 939 (2014) pp. 328-335.

Book Chapters

[1] **Satheeshkumar V**, Avinash Kumar Yadav and Ganesh Narayanan R., "Formability prediction and springback evaluation of adhesive-bonded steel sheets", Advances in Material Forming and Joining, Springer India, DOI: 10.1007/978-81-322-2355-9, pp. 61-80.

Refereed Conferences

[1] **Satheeshkumar V.**, Ganesh Narayanan R., "Experimental evaluation of deep drawability of adhesive bonded steel sheets", 23rd International conference on Processing and Fabrication of Advanced Materials, IIT Roorkee, India. pp. 1026–1032.

[2] **Satheeshkumar V.**, Ganesh Narayanan R., "Forming behaviour of adhesive bonded steel sheets: Influence of finite defects in the adhesive layer", Proceedings of 16th International conference on Advances in Materials and Processing Technologies, 2013, Taipei, Taiwan. (Paper ID: 257).

[3] **Satheeshkumar V.**, Ganesh Narayanan R., "Influence of pre-generated infinite adhesive defects on the forming behaviour of adhesive bonded steel sheets", Proceedings of 16th International conference on Advances in Materials and Processing Technologies, 2013, Taipei, Taiwan. (Paper ID: 258).

[4] **Satheeshkumar V.**, Ganesh Narayanan R., "Experimental investigation on the influence of adhesive properties on forming behaviour of adhesive bonded steel sheets", Proceedings of IDDRG, 2012, Mumbai, Part II: pp.508-513.